IRD 64-36

2 of 3

256 p #6.00

Research programme on magnetoplasmadynamic power generation. Technical summary report 1 December 1962 to 31 March 1964 Part 1: MPD closed loop

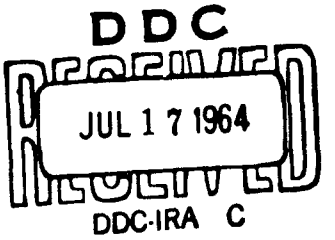

INTERNATIONAL RESEARCH & DEVELOPMENT CO LTD

Fossway, Newcastle upon Tyne 6, England

RESEARCH PROGRAMME ON

MAGNETOPLASMADYNAMIC POWER GENERATION

Contract N62558-3127

TECHNICAL SUMMARY REPORT

1 December 1962 to 31 March 1964

PART 1 : MPD CLOSED-LOOP

Advanced Research Projects Agency
Order No. 209-62, Amendment No. 2
Contract period : 1 December 1961 to 31 July 1964
Contract amount : $382,500
Contractor : International Research & Development Co Ltd
Principal Investigator : Dr. B.C. Lindley

International Research & Development Co Ltd
Newcastle upon Tyne 6
England

RESEARCH PROGRAMME ON MAGNETOPLASMADYNAMIC POWER GENERATION

TECHNICAL SUMMARY REPORT

1 December 1962 to 31 March 1964

SUMMARY

SUMMARY

Research programme

The research programme on MPD power generation at International Research & Development Co Ltd (IRD) is closely associated with the possibility of utilizing a high temperature nuclear reactor heat source in conjunction with an MPD generator and steam cycle, the overall thermal efficiency of such a system being estimated as up to 60 per cent.

One of the most important aspects of closed-cycle MPD electrical power generation now being studied is the possibility of using non-equilibrium enhanced ionization produced by elevated electron temperature. Under these conditions high specific powers may be obtained at gas temperatures of 1800°K or even lower. Apart from the obvious use for large-scale electricity production, nuclear MPD plant has attractive features for space power units in the 10 to 100 kWe and multi-megawatt ranges, and for compact 10 to 50 MWe units in surface ship, submarine and other applications.

Progress details of the IRD MPD energy conversion programme from August 1960 to November 1962 were presented in a previous Technical Summary Report (IRD 63-1). The programme covers three main aspects: MPD closed-loop; plasma physics; and theoretical.

MPD closed-loop

High temperature commissioning of the closed-cycle helium-cesium MPD loop occupied about twelve months (January 1963 to January 1964), with a total of about 2000 hours of circuit operation, of which 300 hours have been at temperatures up to 2500°K with unseeded helium. The difficulties associated with achieving operation at such high temperatures, and the relatively long time scale involved in finding solutions to the various problems, reflect the current state-of-the-art in ultra-high-temperature loop technology. The IRD loop is unique in that there is no comparable facility anywhere in which gas temperatures approaching 2500°K can regularly be maintained for periods of hours under exceptional conditions of purity. Extremely low content of molecular gases in the circulating helium is important both in attaining high plasma electrical conductivity and in minimizing attack of refractory materials at high temperatures.

The commissioning phase of the loop development programme culminated on 19 March 1964 in cesium-seeded operation and electric power generation. In these initial experiments the loop was operated continuously for fifteen hours with indicated gas temperatures up to 2020°K. Twenty series of measurements were made, with varying temperature, cesium content and applied magnetic field, extracting a

maximum power output of 0.46 We from a five-electrode-pair constant-area generator. Electrical conductivities of about 0.5 mho/m were obtained at static gas temperatures below 1500°K and there are reasons to expect a considerable improvement on this level. The main success is that the loop technology and operation has been proved, and the future detailed programme to elucidate MPD power processes under a wide range of conditions can now be undertaken with confidence.

Plasma physics

It became evident early on in planning the research programme that, in assessing the potential performance of MPD generators and in the interpretation of experimental results, there were virtually no basic data on the factors which govern behaviour of the plasma regimes under investigation. In particular, at the particle energies which apply (usually less than 1 eV) data on thermal ionization and on the corresponding charged particle concentrations, collision cross-sections for electrons, ions, atoms and molecules, and ionization, recombination, and attachment coefficients are either non-existent or conflicting.

A series of experiments was designed for measurement of these parameters in static plasmas, both under thermal equilibrium and non-equilibrium conditions, and to establish diagnostic techniques which could also be applied to the closed-cycle loop. The four principal plasma physics investigations are:

microwave measurements, in thermally-excited plasmas, of electron concentrations and collision frequencies;

atom-atom and ion-atom collision cross-sections by atomic beam techniques;

photon cross-sections and recombination coefficients in photoionized plasmas; and

plasma electrical conductivity and breakdown.

All experiments are now functional and a number of measurements are already completed.

Theoretical

In addition to providing direct analytical support to the experimental programme, the theoretical work on closed-cycle systems is mainly related to MPD power generation from a non-equilibrium plasma flow. Present and future aspects involve:

studies of MPD interactions in supersonic, transonic, and subsonic plasma flows, including boundary layer effects and the optimization of generator duct and electrode geometry;

solution of rate equations for ionization, radiation, recombination and other atomic and molecular processes in an accelerating plasma;

optimization of atomic seeding fraction, under non-equilibrium conditions;

heat loss by radiation from seeded monatomic plasmas, requiring an investigation of the transitions between atomic levels;

effect of molecular impurity gases;

electrode processes and boundary layer effects in the presence of elevated electron temperature and high magnetic field;

study of metal foam and other multi-phase MPD systems for space and other applications; and,

an extension of the work on transport properties of MPD plasmas.

CONTENTS TO PART 1

CHAPTER 1

INTRODUCTION : ENERGY CONVERSION PROGRAMME

by

B.C. Lindley

1.1 GENERAL

The present research programme on MPD power generation at International Research & Development Co. Ltd. (IRD)[2,12,20], initiated by C.A. Parsons & Co. Ltd. in 1960, is closely associated with the possibility of utilizing a high temperature nuclear reactor heat source in conjunction with an MPD generator and steam cycle, the overall efficiency of such a system being estimated as up to 60 per cent[11]. The research is relevant, however, to both open and closed-cycle MPD concepts, since the power extraction processes have common features. Inert gas-alkali metal vapour plasmas, under controlled conditions, are ideal for such studies, their behaviour being much more amenable to theoretical and experimental analysis than that of multi-species combustion plasmas derived from burning coal, oil or gas.

One of the most important aspects of closed-cycle MPD electrical power generation now being studied is the possibility of using non-equilibrium enchanced ionization, particularly when this effect is due to elevated electron temperature. For thermal equilibrium ionization, temperatures of about 2500°K are considered necessary for useful electrical conductivity and specific power[11]; under non-equilibrium conditions, high specific powers may be obtained at 1800°K or even lower. Projected performance from very high temperature nuclear reactors of the OECD Dragon type (including the Peach Bottom HTGR, UHTREX and the 'pebble bed' reactors studied both in Germany and in the United States) indicates that gas temperatures of 1500° to 1800°K may eventually be achieved. This type of reactor will operate with purified helium as the coolant, as in the helium-cesium MPD loop at IRD. Apart from the obvious use for large-scale electric power production, nuclear MPD power plant has attractive features for space power units in the 10 to 100 kWe[30] and multi-megawatt ranges, and for compact 10 to 50 MWe units for marine propulsion and other applications.

Details of the IRD MPD energy conversion programme have been presented in a previous Technical Summary Report[24], in which progress from August 1960 to November 1962 was reviewed. During the period covered by the present Technical Summary Report (from 1 December 1962 to 31 March 1964) the financial support received from C.A. Parsons and Company has been increased to a total of £150,000 ($420,000), while a further contract has been gained from the Advanced Research Projects Agency (ARPA) for £35,000 ($100,000) to cover the period 1 December 1963 to 31 July 1964, bringing the total contribution by ARPA to £135,000 ($382,500).

For convenience, so as to present information on the programme in sufficient detail consistent with clarity, the present report is divided into three parts covering the main aspects: MPD closed-loop; plasma physics; and theoretical. Further subdivision is into separate chapters, each intended to be self-contained. The MPD closed-loop programme is described in thirteen chapters, 2 to 5 being related to the several stages of commissioning and operation, 6 to 12 dealing with associated engineering and materials development problems, and in 13 a review of the intended future programme is given. Full details of basic equipment for the four plasma physics experiments were given in the previous Technical Summary Report[24], and chapters 14 to 17 deal with the further developments which have been required in each case to reach satisfactory operation; results are mainly presented in 18 to 20. Full reports on the main areas of study in the theoretical programme are presented in 21 to 29, 21 to 24 dealing with important fundamental aspects, with presentation in 25 to 29 of advanced studies of performance and operational aspects of MPD generators in a number of applications. Further technical reports will be issued on aspects which have not been fully described in the present report. A bibliography of the main technical reports and publications by IRD staff on MPD power generation follows this chapter (1).

1.2 THE MPD CLOSED-CYCLE LOOP

In the MPD closed-cycle loop (Figs. 1.1 and 1.2), continuously filtered and purified helium is heated in passage through an electrical resistance heater (to simulate the nuclear reactor) which is capable of producing gas temperatures up to 2500°K. A metered flow of cesium vapour is introduced before the mixture expands to a high velocity through a rectangular-section nozzle. In the present arrangement a supersonic flow of helium and ionized cesium passes through the MPD generator duct and a subsonic diffuser to a recuperative heat exchanger and final cooler. Cesium is removed in a cold trap before the helium re-enters the circulator.

The power generation experiment is designed to yield date on MPD power processes for a wide range of experimental variables. In particular, closed-cycle steady-state operation allows the investigation of different working fluids (e.g. the various inert gas-alkali metal vapour combinations) under controlled purity conditions, and should establish conclusive evidence whether non-equilibrium ionization can be promoted by field-induced elevation of the electron temperature and by other techniques (such as by photoionization, r.f., electron or ion injection, etc.). Additional major variables in the experiment are pressure, pressure ratio, temperature, Mach number, fractional seed concentration, controlled concentration of other gases, generator duct configuration and magnetic field.

High temperature commissioning of the loop occupied a period of about 12 months (January 1963 to January 1964), with a total of about 2000 hours of circuit operation, of which 300 hours have been at temperatures up to 2500°K with unseeded helium. The difficulties associated with achieving operation at this high level of temperature, and the relatively long time scale involved in finding solutions to the various problems, reflect the current state-of-the-art in ultra-high temperature loop technology. The IRD loop is unique in that there is no comparable facility anywhere in which gas temperatures approaching 2500°K can regularly be maintained for periods of hours under exceptional conditions of purity. Extremely low content in the circulating helium of molecular gases is important not only in minimizing attack of refractory materials at high temperatures but, more significantly, in assuring conditions in the plasma suitable for the attainment of elevated electron temperature and extra-thermal ionization, since even small concentrations of molecular gases serve to dissipate enhanced electron energy because of high collision cross sections, non-elastic collisions and propensity for electron attachment.

The commissioning phase of the loop development programme culminated on 19 March 1964 in cesium-seeded operation and electric power generation. In these initial experiments the loop was operated continuously for fifteen hours with indicated gas temperatures up to 2020°K. Twenty series of measurements were made, with varying temperature, cesium content and applied magnetic field, with maximum power outputs of 0.46 We for the 5-electrode-pair constant-area generator. Electrical conductivities of about 0.5 mho/m were obtained at static gas temperatures below 1500°K and there are reasons to expect a considerable improvement on this level. The main success of this operation is that the loop technology and operation has been proved and the future detailed programme to elucidate MPD power processes under a wide range of

conditions can now be undertaken with confidence.

In the next series of power runs the inlet pressure and seeding fraction at the nozzle are being kept constant at approximately 1 atm. and 0.5 per cent respectively. The inlet temperature will be varied to provide a wide band of thermal ionization levels, and measurements (including end losses) will be made with 10-electrode and 36-electrode constant-area ducts. Power generation experiments will take place for a range of nozzle inlet pressure (0.5 to 1.2 atm), nozzle inlet temperature (1500° to 2500°K), cesium seed fraction (up to 3 atomic per cent), electrical load and magnetic field (up to 2T). Profiled generator ducts and alternative electrode arrangements are planned, and several expansion nozzles will be used to vary the flow Mach number from the present level of 2.3 to subsonic values of 0.5 (or possibly less). Pressure levels will be increased towards those anticipated for a full-scale system and seeding levels will be in the region shown theoretically (Chapter 23) and by experiment to produce optimum specific power.

Two non-equilibrium ionization effects are anticipated: the first due to 'frozen flow' of electron concentration in rapid acceleration through the nozzle[9,29,31]; and the second to field-induced ionization in the generator duct[28]. The latter effect has been demonstrated theoretically to be possible and the present programme is aimed at producing experimental evidence in support.

Microwave and spectroscopic techniques, developed in the plasma physics studies (Part 2), are to be used in obtaining electron temperatures, concentrations and collision frequencies at the window station upstream of the accelerating nozzle; it is proposed to extend such measurements within the generator duct itself. Later in the programme controlled additions of molecular gases (which inhibit electron motion) and other noble gases (which may assist non-equilibrium ionization), within limits imposed by constructional materials, will be made to assess the effect on ionization and electrical conductivity.

Although the low-field magnet (at present being modified to increase the maximum field from 1.2 T up to about 2T) will be sufficient for the purpose of the early stages of the experimental programmes, there is a strong incentive to operate at very much higher applied magnetic fields to increase the specific power (which is proportional to the square of the magnetic field) and field-induced non-equilibrium ionization effects; in addition, the surface-to-volume ratio of the generator decreases with a consequent lower heat loss through the walls. The Hall number (to which is related the angle by which the electric field and current vectors are displaced from the transverse direction in the plane

perpendicular to the magnetic field) increases directly with the magnetic field. The axial pressure gradient in the duct increases with the magnetic field, which may be a disadvantage, and ion slip (which gives a reduction in power output) can occur at very high fields. Other problems which may be encountered at high fields are electrical breakdown due to the high electric field in the plasma, inability of electrodes to support the very high current densities which are demanded and transverse pressure gradients in the duct. which could lead to fluid flow instability. In a large-scale system, the fraction of the output power which must be used in conventional copper coils to provide the magnetic field is substantial, so that superconducting field coils (which have no resistive loss and only a small power demand for refrigeration) are attractive. The technical feasibility and capital cost of building large superconducting magnets are uncertain; however, the 5 T superconducting Helmholtz pair, which the UK Department of Scientific and Industrial Research has nominated IRD to construct for operation with this MPD experiment, should contribute significantly to the technology.

1.3 PLASMA PHYSICS

It became evident early on in planning the research programme that, in assessing the potential performance of MPD generators and in the interpretation of experimental results, there was virtually no basic data on the factors which govern behaviour of the plasma regimes under investigation[4]. In particular, at the particle energies which apply (usually less than 1eV) data on thermal ionization and the corresponding charged particle concentrations, collision cross-sections for electrons, ions, atoms and molecules, and ionization, recombination, and attachment coefficients are either non-existent or conflicting.

A series of experiments were designed for measurement of these parameters in static plasmas, both under thermal equilibrium and non-equilibrium conditions, and to establish diagnostic techniques which could also be applied to the closed-cycle loop. The four principal plasma physics experiments are now functional and a number of measurements already completed.

Thermally-excited plasmas are being studied using microwave techniques to measure electron concentrations and collision frequencies in helium-cesium mixtures at pressures ranging from 1 to 760 torr and temperatures ranging from 1000° to 2300°K to establish basic data at the appropriate particle energies. The programme will be extended to include mixtures containing from zero to 100 per cent of cesium, sodium or potassium in krypton argon, neon, helium or hydrogen. It is hoped to establish the optimum seeding fraction for each

mixture under thermal equilibrium conditions, and to derive the effective collision cross-sections; in particular, the regions in which electron-ion collisions become important may be obtained.

In an atomic beam experiment[37], cesium atom-helium atom and cesium ion-helium atom collision cross-sections are being measured, with similar measurements on other alkali metal-inert gas combinations at a later stage. The data are important in assessing viscosity, heat transfer coefficients and coupling factors, all of which are significant in boundary layer effects and energy transfer mechanisms in an MPD generator. It is believed that surface effects may constitute one of the main limitations on specific power in a practical system operating at very high magnetic fields. No published experimental data exists for the regimes being studied.

Photon cross-sections and recombination coefficients in plasma irradiated with light energy are being studied[36]. The technique is significant both in the energy balance of the ion-electron pairs produced (as compared with, say, microwave energy pulses), making it very convenient for experimental investigations of ionization and recombination, and also as a possible technique for producing non-equilibrium ionization in a large-scale system[22,36].

Very little information is available on the electrical conductivity of helium-cesium and other inert gas-alkali metal vapour mixtures. In one published investigation, the results are limited to a few volts; experience at the University of Sydney has indicated that, above 20 volts, breakdown occurred irrespective of electrode separation. Some indication of this behaviour has been verified at IRD[38]. As a possible and severe limitation on MPD generator performance this breakdown problem is being investigated in detail (including electrode materials, surface finish, magnetic field effects, etc.).

1.4 THEORETICAL

In addition to providing direct analytical support on the experimental programme, the theoretical work on closed-cycle systems is mainly related to MPD power generation from a non-equilibrium plasma flow. A large proportion of the papers listed in the bibliography are related to these studies. Present and future aspects involve: studies of MPD interactions at supersonic, transonic and subsonic plasma flows, including boundary layer effects and the optimization of generator duct and electrode geometry; solution of rate equations for ionization, radiation, recombination and other atomic and molecular processes in an accelerating plasma; optimization of atomic

seeding fraction under non-equilibrium conditions; heat loss by radiation from seeded monatomic plasmas, requiring an investigation of the transitions between atomic levels; effect of molecular impurity gases; electrode processes and boundary layer effects in the presence of elevated electron temperature and high magnetic field; study of metal foam and other multi-phase MPD systems for space and other applications; and an extension of the work on transport properties of MPD plasmas.

BIBLIOGRAPHY OF TECHNICAL REPORTS AND PUBLICATIONS BY IRD STAFF ON MPD POWER GENERATION

1 LINDLEY, B.C. The direct conversion of thermal to electrical energy by ionized gas streams NRC 60-7 January 1960

2 LINDLEY, B.C. The direct conversion of thermal to electrical energy NRC 60-8 January 1960

3 LINDLEY, B.C. The direct generation of electricity Parts 1 and 2 Nuclear Power Vol 5, no. 50, p 100, 1960; Vol 5, no. 51, p 80, 1960

4 McNAB, I.R. The electrical properties of cesium-helium mixtures NRC 61-12 March 1961

5 LINDLEY, B.C. and McNAB, I.R. Microwave diagnostics for helium-cesium plasmas Proceedings of the Fifth International Conference on Ionization Phenomena in Gases North-Holland 1961

6 LINDLEY, B.C. Magnetoplasmadynamic electrical power generation British Power Engineering October 1961

7 LINDLEY, B.C. An investigation into the characteristics of pebble bed reactor cores Report NRC 62-4 February 1962

8 MAITLAND, A. Some consequences of ion slip in a plasma flowing through a magnetic field Nature Vol 194, p 670-1 May 1962

9 McNAB, I.R. and LINDLEY, B.C. Electron temperature in the rapid expansion of a plasma flow NRC 61-122 May 1962

10 McNAB, I.R. and ROBINSON, C.A. Electron-ion recombination in magnetoplasmadynamic power generators Report NRC 62-90 1962

11 LINDLEY, B.C. Closed-cycle magnetoplasmadynamic electric power generation Proceedings of the International Conference on Gas Discharges and the Electricity Supply Industry Butterworths 1962

12 LINDLEY, B.C. A magnetoplasmadynamic power generation experiment using helium-cesium 3rd Symposium on Engineering Aspects of Mangetohydrodynamics University of Rochester 1962

13 DUNN, M.H. and MAITLAND, A. Energy obtainable from a Carnot engine with a thermally ionized gas as the working fluid J.Appl.Phys. Vol. 33, no 12, p 3598-9 December 1962

14 McNAB, I.R. and ROBINSON, C.A. The viscosity of gaseous cesium at temperatures up to 3000°K IRD 63-10 February 1963

15 MAITLAND, A. and DUNN, M.H. Thermal ionization in a system with a distribution of ionization potentials Phys. of Fluids Vol 6, no 4, p 586-9 April 1963

16 McNAB, I.R. and ROBINSON, C.A. Electron-ion recombination in MPD generators Magnetoplasmadynamic Electrical Power Generation IEE Conference Report Series No.4 1963

17 ARTHUR, G. and HEPWORTH, M.A. Ceramic materials for MPD power generation Magnetoplasmadynamic Electrical Power Generation IEE Conference Report Series No.4 1963

18 LINDLEY, B.C. Some economic and design considerations of large-scale MPD generators Magnetoplasmadynamic Electrical Power Generation IEE Conference Report Series No.4 1963

19 CRAMPTON, F.J.P. and WILKINSON, T.S. An open-cycle MPD generator optimization study Magnetoplasmadynamic Electrical Power Generation IEE Conference Report Series No.4 1963

20 LINDLEY, B.C. A magnetoplasmadynamic power generation experiment Advances in Magnetohydrodynamics Pergamon Press 1963

21 LINDLEY, B.C. A closed-cycle MPD experiment Magnetoplasmadynamic Electrical Power Generation IEE Conference Report Series No.4 1963

22 MAITLAND, A. A criterion for assessing methods of producing non-equilibrium ionization Magnetoplasmadynamic Electrical Power Generation IEE Conference Report Series No.4 1963

23 WILSON, G.W. and ROBERTS, D.C Superconducting magnets for magnetoplasmadynamic power generation Magnetoplasmadynamic Electrical Power Generation IEE Conference Report Series No.4 1963

24 Research programme on magnetoplasmadynamic power generation Technical summary report for 1 December 1961 to 30 November 1962 IRD 63-1 June 1963

25 LINDLEY, B.C. Oil-fired MPD power generation Paper 29 Section VI World Petroleum Congress June 1963 (also IRD 63-45)

26 McNAB, I.R. The viscosity of helium-cesium mixtures IRD 63-59 July 1963

27 McNAB, I.R. and McNEILL, P.C. Density-time profiles for an electric propulsion unit efflux. 5th AGARD Combustion and Propulsion Colloquium, Athens. July 1963 (also IRD 63-63)

28 McNAB, I.R. and COOPER, N.A. Flow processes in MPD generators. IRD 63-82 October 1963

29 McNAB, I.R. and LINDLEY, B.C. Electron temperature in the rapid expansion of a plasma flow. Advances in Magnetohydrodynamics Pergamon Press 1963

30 McNAB, I.R. Power conversion in space I.E.E. Conference on Electric Propulsion (to be published) February 1964

31 McNAB, I.R. A non-equilibrium electron mode for kilowatt-range MPD space power. Sixth AGARD Combustion and Propulsion Colloquium, Cannes March 1964 (to be published)

32 FINNISTON, H.M. and THRING, M.W. Basic research aspects of MPD power generation (prepared for the Advisory Council on Research and Development of the Ministry of Power) April 1964

33 FINNISTON, H.M. Industrial collaborative programme on MHD generation (prepared for the Advisory Council on Research and Development of the Ministry of Power) April 1964

34 LINDLEY, B.C. Magnetoplasmadynamic generation. II The future power plant. I.Mech.E. Fluid Mechanics Convention, Cambridge. April 1964 (to be published)

35 ROBINSON, C.A. and McNAB, I.R. Viscosity of partially-ionized gaseous cesium. J.App.Phys. June 1964

36 BALFOUR, D. and HARRIS, J.H. Photoionization in MPD generators. International Symposium on Magnetohydrodynamic Electrical Power Generation. Paris, July 1964

37 JOLLY, A.B. and NEWCOMBE, J. Cross section measurements and transport properties in seeded inert gas MPD generators. International Symposium on Magnetohydrodynamic Electrical Power Generation. Paris, July 1964

38 SANDS, A. and BALFOUR, D. Electrical conductivity and breakdown in cesium vapour. International Symposium on Magnetohydrodynamic Electrical Power Generation. Paris, July 1964

39 ARTHUR, G. Compatibility studies of some refractory materials with cesium vapour. International Symposium on Magnetohydrodynamic Electrical Power Generation. Paris, July 1964

40 CRAMPTON, F.J.P. and WILKINSON, T.J. Liquefied natural gas applied to oxygen-enrichment and magnet cooling in open-cycle MPD generators. International Symposium on Magnetohydrodynamic Electrical Power Generation. Paris, July 1964

41 LINDLEY, B.C., BROWN, R. and McNAB, I.R. MPD experiments with a helium-cesium loop. International Symposium on Magnetohydrodynamic Electrical Power Generation. Paris, July 1964

42 LINDLEY, B.C. and McNAB, I.R. Optimization of large-scale nuclear MPD systems. International Symposium on Magnetohydrodynamic Electrical Power Generation. Paris, July 1964

43 LINDLEY, B.C. Nuclear magnetoplasmadynamic energy conversion. Third Geneva Conference on the Peaceful Uses of Atomic Energy September 1964 (to be published)

DUNN, P.D., LINDLEY, B.C. and WRIGHT, J.K. A survey of MHD research in the United Kingdom. World Power Conference, Lausanne, September 1964 (to be published).

FLOW DIAGRAM FOR MPD POWER GENERATION EXPERIMENT

FIG 1·1

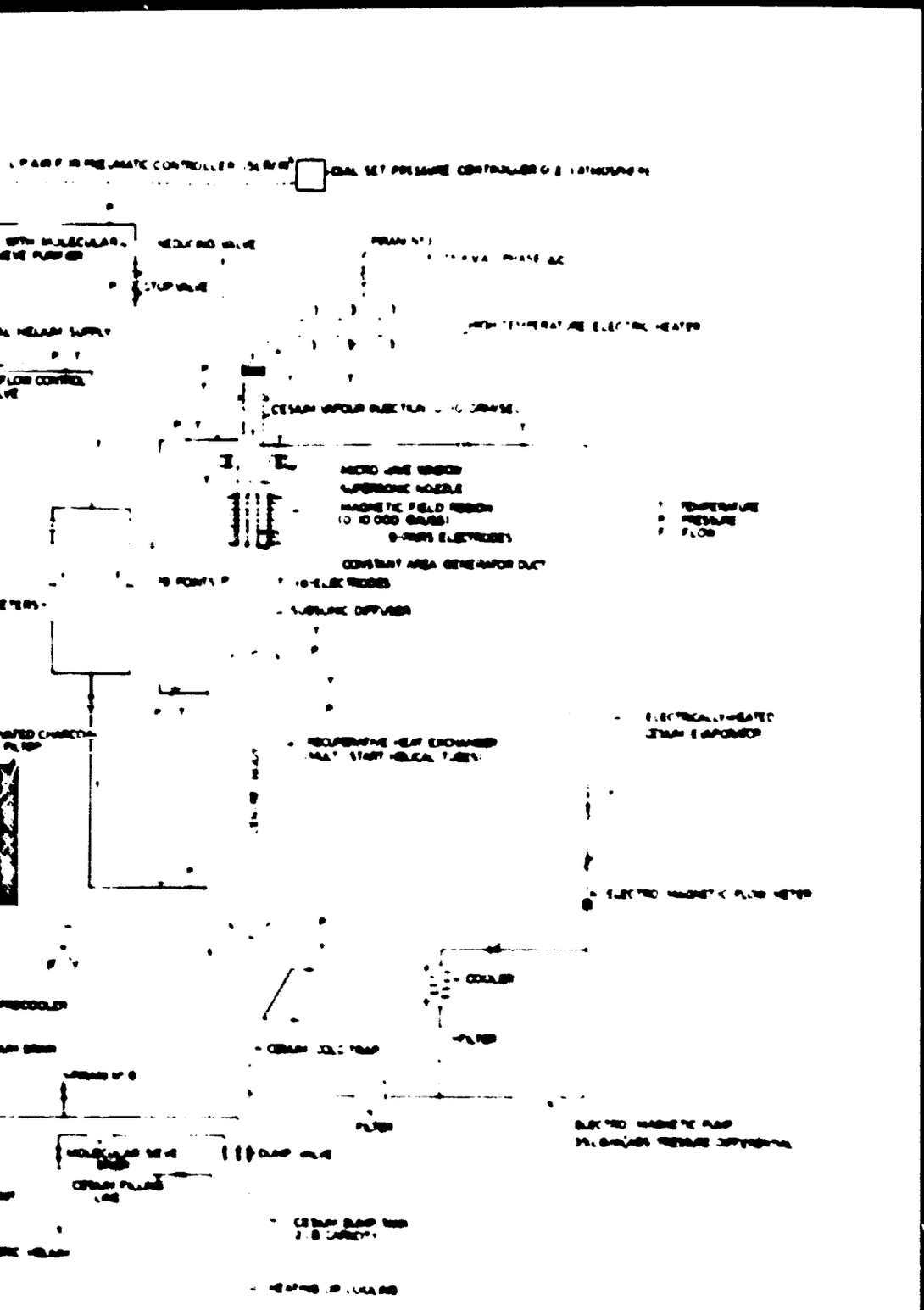

MPD POWER GENERATION EXPERIMENT

FIG 1·2

CHAPTER 2

DEVELOPMENT OF CLOSED LOOP

by

R. Brown, W.J. Slator, W. Morrison, J. Davidson, K. Cass and V. Brown

2.1 GENERAL

Basic design details, manufacture and test of the individual loop components have been described in the previous Technical Summary Report (IRD 63-1). In the period under review, much of the effort was devoted to commissioning the complete loop, at first without the main generator section, so as to prove the mechanical and thermal performance and a capability for extended operation at high temperature, and with extremely low impurity content in the helium. Quantitatively, one of the objectives was to operate the complete loop at steady-state gas temperatures of over 2200°K for more than 1 hr with <10 ppm content in the helium of molecular gases other than hydrogen. Fig. 2.1 summarizes development as far as 31 March 1964.

A brief description of the main aspects of development will be given here, followed in Chapter 3 by consecutive reports on the features of each run at high gas temperatures, and in subsequent chapters with details of particular development problems on main components.

2.2 HELIUM PURIFICATION

A number of cold runs were carried out early in the period (December 1962 to January 1963) to characterize and develop the helium purification and analysis plant. In these, the high temperature heater was in position and a temporary tantalum-stainless steel transfer duct was mounted between the heater and diffuser, allowing closure of the loop. The original 0.25 per cent bypass purification plant supplied by Linde had proved inadequate and unsatisfactory. A redesigned molecular sieve bed was introduced, giving an increased bypass rate of 1½ to 2 per cent of the main helium flow. The early procedure of analysing gas samples in the Applied Chemistry Laboratory of IRD introduced prohibitive errors, and an improved helium chromatographic analysis plant was developed and integrated in the loop. The equipment provides for continuous sample circulation from various loop stations, and semi-continuous analysis with minimum detectable content of each of

several gases of about 1 ppm.

The running time for 'clean up' to acceptable impurity levels (<100 ppm) was approximately 70-100 hr with inconsistent clean up rates. Outgassing of the loop and graphite in the heater element and oil filter was considered to be significant, and nitrogen purging of the CECA carbon used for circulator oil removal was discontinued to prevent desorption of nitrogen gas into the loop. Purification efficiency appeared low but exhaustive leak detection indicated the loop to be tight to $<10^{-5}$ μl/sec. A typical curve for rates of impurity removal is shown in Fig. 2.2.

Considerable modification of purification plant components during the high temperature development running, based on increased residence times, a bypass rate of up to 6 per cent of the main mass flow, and other features eventually gave a capability for purification cold to about 5 ppm within 1 hr from start up and about 10 to 15 hr to operation at full temperature.

During high temperature development runs valuable information was gained on maximum tolerable gaseous impurity levels for long life operation of the tantalum transfer duct, bellows, sapphire window assembly, and supersonic nozzle. Temporary tantalum transfer ducts (0.015 in. material) were loaded with sample strips and afterwards subjected to metallographic examination. In this way outgassing techniques, purification bypass rates, acceptable leakage and rate of temperature rise were optimized.

2.3 HIGH TEMPERATURE OPERATION

In February 1963 high temperature runs were begun using a temporary tantalum transfer duct between the high temperature heater and subsonic diffuser, that is, without a generator section in the loop.

The first heater system employed 1 molybdenum and 4 stainless steel radiation shields concentrically distributed around a single graphite element (Figs. 22 and 23 of previous Technical Summary Report), and arranged for radial inward flow of helium through the shields. The highest helium temperature achieved with this system was 1190°C. Problems included mismatching of the element electrical resistance, control of radiant heat losses, distribution of helium flow through the shields and behaviour of electrical end connections (overheating and arcing). Subsequently, 18 high temperature runs were carried out employing temporary transfer systems, successively increasing the helium outlet temperature level to about 2400°K. Many configurations of radiation shield systems were tested, the most satisfactory being a multi-pass axial flow concentric system with radial flow through the graphite element. Electrical connection problems were experienced

at the hot (upper) end of the heater. Modifications to the heater necessitated longer lengths of graphite for manufacture. Poor delivery dates (5 months) from suppliers for extended lengths of suitable graphite led to the adoption of temporary extension graphite pin/copper connectors, which eventually allowed operation at currents of up to 3000 amp.

In an early run, during which the total impurity level was maintained below 50 ppm, the maximum gas temperature was increased in stages up to 1450°K with 5 gm/sec mass flow and 33 kW heater power input; the high temperature heater centre (maximum) temperature was then almost 1900°K. The loop was shut down after about ½ hr at this temperature level owing to failure of the temporary tantalum duct (2 in. diameter) between the heater and diffuser. This failure emphasizes the need to obtain specified impurity levels.

In August 1963, using a graphite pin/copper cone extension on the heater, and a temporary tantalum transfer duct, a proving hot cycle was carried out under conditions envisaged for loop operation. A helium temperature of 2250°K was attained and held steady for 1 hr. All units operated satisfactorily with negligible deterioration of refractory metal and other critical components.

In September 1963, a 2-electrode recrystallized alumina generator system was installed in loop with the complete tantalum transfer duct (bellows, cesium vapourizer, window and supersonic expansion nozzle). After careful vacuum-outgassing a hot run was carried out. Thermal stress in the generator duct system was minimized by limiting the rate of temperature rise to ~200°K/hr up to a maximum nozzle inlet temperature of 2000°K. On dissembly, the generator alumina sections were all found to be severely fractured and cracked, although maintaining a smooth gas channel. The failure was attributed to axial misalignment due to the mounting and support arrangement and excessive compressive and axial stress from differential expansion during the thermal cycle. Other problems at this stage included overheating of the single skin stainless steel subsonic diffuser throat section and thermal insulation of the high temperature transfer duct and generator duct assembly.

Following this first operation with a generator duct, a new assembly and mounting system was adopted, entailing considerable modifications of this section of the loop. In the new arrangement the tantalum transfer duct generator and diffuser entry sections are mounted to provide strain-free axial movement on a massive stainless steel backbone and the complete sub-assembly (including thermal insulation and instrumentation) can be racked into the accepting outer case.

During these modifications to the duct system availability of graphite in

longer lengths allowed the manufacture of a one-piece heater element, thus dispensing with the graphite pin and high temperature graphite-graphite interface which had been subject to arcing. The electrical end connection design, which had previously passed currents of up to 3000 amp, was retained. Molybdenum radiation shields had presented a problem of vaporization and carry-over to cooler sections, and these were replaced by tungsten.

From late September to mid-November 1963, a series of prolonged vacuum-outgassing procedures proved necessary to rid the high temperature heater system of mineral oil contamination. The contaminant origin is unknown but it is possible that oil pick up occurred during the manufacture of the material or element prior to delivery at IRD. A full hot run was carried out on 17 November 1963, using a temporary high temperature transfer to clean the system under flow conditions. The new high temperature heater operated satisfactorily and a helium temperature of 1940°K was attained. To minimize overheating of the high temperature heater core an additional thermal shield employing pure zirconia fibre was fitted.

Owing to the initial problems with the recrystallized alumina duct sections, a survey was carried out for other suitable high temperature insulating ceramics. Since the original conception of the loop, the envisaged operating temperatures in the generator region have significantly lowered and boron nitride was considered attractive for use as a duct wall material below 2000°K. Test generator sections were manufactured in boron nitride and comprehensive compatibility studies for its use with cesium at elevated temperatures were initiated.

After initial outgassing, the system was closed on 30 November to 4 December 1963, using the redesigned high temperature transfer and generator support system. The generator section consisted of (slip-cast, hot pressed) sections of recrystallized alumina and a boron nitride top wall. High temperature runs were carried out attaining gas temperatures of about 1600°K, the rate of temperature rise in the generator region being limited to 200°K/hr. It was apparent that gas leakage was occurring into the central high temperature region, bypassing the heater and reducing the gas temperature, and the runs were discontinued. Inspection showed no damage to the generator ceramics and the locations of leakage proved to be a fractured tantalum pressure pipe on the high temperature transfer and at the diffuser sliding seal. Appreciable sodium contamination, and deposition on lower temperature sections of the loop was found to originate from the zirconia fibre and its use was temporarily suspended, pending investigation by the manufacturers and suppliers of "sodium-free" zirconia fibre (Hitco Corporation).

On 10 December 1963 a further run was carried out with the previous system, with the zirconia insulation removed and the tantalum pressure pipe repaired. On the up-cycle at approximately 1720°K helium temperature manual blow-off was in operation to accommodate pressure rise from expansion. At this stage during blow-off an extremely violent pressure rise was accommodated with helium loop mass flow being maintained. Electrical power to the high temperature heater was switched off immediately and component temperatures fell at approximately 200°K/min. Flow conditions appeared steady but after circulation for a further 30 min the circulator was stopped and the loop opened up for inspection.

20 gallons of water were drained from the loop, mainly from the high temperature heater (Fig. 2.3). The copper/graphite upper electrical connection to the element had arced through the copper allowing high pressure water to enter the loop. Inspection revealed the following conditions.

heater element and shields:	corroded but intact
high temperature tantalum transfer duct:	bellows, cesium vaporizer tube and window sections disintegrated, heavy section supersonic nozzle unharmed
recrystallized alumina duct sections:	minor cracking but otherwise excellent condition
boron nitride duct sections:	unharmed
purification plant ice trap:	blocked
oil filter (CECA carbon):	saturated
remainder of loop:	no damage

By 24 December 1963, the loop was again in the closed condition. Modifications included: a temporary heater to nozzle graphite tube transfer duct; a spherical-profile graphite/copper electrical interface connector; thermocouple inserts on interface; an arcing warning device with oscilloscope display integrated in heater power control system; and cooled glass windows to view the copper/graphite interface. Heater vacuum-outgassing was carried out to a maximum centre element temperature of about 2300°K, requiring 1470 amp and with no evidence of arcing. However, with gas circulation, arcing occurred on the hot interface at 1950 amp. Power was reduced, but arc instability persisted and the run was discontinued with switch off from this power level. Inspection showed serious pitting of the graphite interface, but no deterioration of the generator sections. Similar arcing behaviour was apparent on subsequent runs (7 and 12 January 1964) in which modifications to the end connections were tested. Owing to

the uncertainties and inherent dangers of arcing at the hot electrical power connection of the high temperature heater the graphite/copper cone connection was abandoned. Throughout the whole of the tedious and expensive series of runs where prohibitive arcing occurred no conclusive mechanism was established for the electrical breakdown.

Flow data from earlier runs and a flow check with the high temperature heater bypassed demonstrated that the recuperative heat exchanger was bypassing up to 25 per cent of the helium mass flow. The unit was removed, cleaned and the leaking sliding seal and centrebody repaired.

On 5 March 1964 a proving run showed that a redesigned hot end electrical connection was satisfactory. The pitted interface of the element was removed and the head extended with a screwed graphite collar and rod connector. A copper clamp electrical connector was arranged to pass cold helium (1 gm/sec) from the circulator outlet through cooling channels in the graphite head system.

At this stage a segmented 5 electrode-pair generator duct was completed. The main tantalum transfer duct was undergoing repair at Murex Ltd. To allow build-up of the initial power generator system a glove box welding facility was set up at IRD and a transfer duct-cesium injection-nozzle system fabricated from 0.020 in. tantalum.

On 12 March 1963, with the outgassed heater, transfer and 5 electrode-pair generator in position, the loop was closed and a high temperature run begun. Severe arcing and a total loss of heater power occurred at 2000 amp and the run was discontinued. Inspection showed fracture of the element at the extreme upper end of the perforated section. It appeared the previous corrosion with water and steam in the loop had severely stressed and weakened the element at the point of fracture. All components of the new electrical connection were satisfactory.

2.4 POWER GENERATION

On 18 March 1964, with a repaired element fully outgassed, the loop was closed once again. It was expected that the heater performance would be satisfactory and a simple intermittent-flow cesium injection system was attached to the loop; all other preparations were carried out for seeded power generation. Loop operation commenced on 19 March 1964, heater power being gradually increased while maintaining $\frac{1}{2}$30 ppm total impurity level in circuit. 20 short-duration cesium-seeded runs were carried out at indicated nozzle inlet temperatures between 1910° and 2020°K and 1 atm pressure, and with magnetic fields from 0.2 to 1.0 T. Consistent power readings up to $\frac{1}{2}$ watt were measured from the generator delivering to five isolated electrical loads. Seeded operation over a period of 5 hr and a

total cesium injection of 380 gm resulted in no problems of loop operation although indications were that carry-over of cesium into cold sections of loop had occurred.

The rig was run down and circulation stopped, and main sections of the loop - high temperature heater - generator assembly removed using a helium blow-off and isolation technique. The performance of the high temperature heater had been entirely satisfactory and inspection of the components and electrical end connections showed no significant deterioration. The generator duct showed a single fracture and minor cracking in the lower and one side wall. Deposits on the inner surfaces were found in parts to be electrically-conducting. This surface deposition material is being subjected to intensive metallographic and chemical analysis to determine its nature and origin. The cesium drains on the heat exchanger and precooler were blown off but only minor quantities of cesium were recovered. With oxidation and alcohol dissolution techniques and due caution, the circuit was completely stripped. Approximately one-third (100 gm) of the cesium throughput was found in the precooler outlet, the remainder apparently being dissolved in lubricating oil in the main helium circulator and aftercooler. No deterioration of any component owing to the presence of cesium was apparent.

2.5 SUMMARY OF CLOSED LOOP DEVELOPMENT

The sequence of operating conditions during loop development is summarized in the Tables which follow this Chapter; the final Table is related to the power generation run (RHT32).

TABLE 2.1

MPD POWER GENERATION EXPERIMENT

SUMMARY OF HIGH TEMPERATURE OPERATION (FEB. 1963 - MARCH 1964)

Date	Graphite element	Resistance (hot), ohm	Radiation shield system	Helium mass flow, gm/sec	Heater power, volt amp kW	Heater temp (max), °C	Max. gas temp (uncorrected), °C	Max. gas temp (corrected), °C	Regenerative He outlet temp, °C	Helium purification: max. impurity level during run, ppm H_2	N	O_2	NOTES
RHT 1 2-2-63	CS 20(1)		1 Molybdenum 4 stainless steel radial flow	5.0		1050 950	960	915	260	2900	140	10	Test abandoned due to cooling water failure. Previously 100 hours cold clean up with 2% by-pass. Fig.3.2 shows the last 15 hours of the run RHT 1
RHT 2 10-2-63	CS 20(1)		As above	5.0		1615 1430	1080	1100	250	600	300	60	Overheating of heater body. Rapid build up of impurities during hot run (mol sieve blocked). Tantalum transfer section disintegrated. Final impurities too high for analysis plant.
RHT 3 23-2-63	CS 20(1)		As above Baffled half way on outer	5.5		1375 1100	960	975	245	1400	175	50	New tantalum transfer section incorporating bellows unit. O_2 and N_2 maintained at 425ppm by a snap rise in N impurity (Fig.3.6). No apparent damage to tantalum after 12 hours hot running.
RHT 4 5-3-63	CS 20(1)		Baffled to give axial flow through shields	5.1		1615 1540	1220	1250	350	500	30	35	Overheating of heater body, 20 hours hot running at varying impurity levels (Fig.3.7). Molybdenum inner shields failed suddenly
RHT 5 18-3-63	CS 20(1) Thinned	0.0096	2 graphite 2 Molybdenum 6 stainless steel (axial flow)	5.4		1575 1620	1220	1240	340		290	90	Larger diameter heater body installed and small intermittent air leak cured. Purification (Fig.3-9) from 3500 ppm to 10ppm in four hours. 3 hours hot running, no indication of H_2 impurity. The inner stainless steel shield melted
RHT 6 23-3-63	CS 20(1) Thinned		2 graphite 2 Molybdenum 2 stainless steel	5.25			1430	1550	355	1500	65	10	Overheating of heater body. Element thinned to match impedance of electrical power supply
RHT 7 10-4-63	EY 9(1)	0.0160	2 graphite 2 molybdenum	5.6	18.6 1820 33.8	1425 1575 1460	1430	1480	370	200	30	8	Leaking Dowty valve cured. Helium gas temperature thermocouple failed, lower end of heater casing red hot, stainless steel support block melted, inner graphite shield cracked, and H_2 held at 200ppm during hot run.
RHT 8 18-4-63	Ey 9(1)	0.0160		7.0	21.8 2460 61.0	1530 1790 1880 1400	1630 1740	1710 1830	355	500	20	6	Lower support block made in graphite. During hot run, short circuit to earth (external) causing heater element to fracture

TABLE 2.2 MPD POWER GENERATION EXPERIME[illegible]

SUMMARY OF HIGH TEMPERATURE OPERATION (FEB. [illegible] - [illegible]

Date	Graphite element	Resistance (hot) ohm	Radiation shield system	Helium mass flow gm/sec	Heater power Volt	amp	kW	Heater temps. °C	Max. gas temp. (indicated) °C	°C correct[illegible]
HHT 9 [illegible].4.63	CS [illegible]	[illegible]9		[illegible]	[illegible]	[illegible]	5[illegible]	1450 [illegible] 1750 [illegible]	156[illegible]	[illegible]
HHT 10 [illegible].4.63	CS 20 [illegible]	[illegible]9		6.3	25.4	[illegible]	61.3	[illegible] [illegible] 1930	[illegible] 1740	[illegible]
HHT 11 3.5.63	CS [illegible] ([illegible]) thinned	[illegible]106		6.3	27.6	[illegible]	56.8	1860 2100 2550 1675	1[illegible]5	[illegible]
HHT 12 5.5.63	CS 20 ([illegible])	[illegible]		6.7	28.2	[illegible].80	67	[illegible] [illegible]150 2450	1560	2[illegible]0
HHT 13 [illegible].5.63	[illegible]	[illegible]	[illegible] graphite [illegible] molybdenum [illegible] molybdenum (dimpled) [illegible] stainless steel	[illegible]	[illegible]	[illegible]	[illegible]	1[illegible]	15[illegible]	[illegible]
HHT 1[illegible] [illegible].6.63 to 26.6.[illegible]	AT[illegible] with [illegible] extension zone	[illegible]	as above	[illegible]	[illegible]	[illegible]	[illegible]	1175 1465 [illegible] [illegible]	[illegible]	15[illegible]
HHT 15 1.7.63	AT[illegible] with [illegible] [illegible] extension zone	[illegible]	as above	[illegible]	[illegible]	[illegible]	[illegible]	[illegible] [illegible] 12[illegible] [illegible]	[illegible]	[illegible]

[illegible]MENT

– MARCH 1[illegible]

°C Tested	[illegible] °C	[illegible]			Notes
		[illegible]	[illegible]	[illegible]	
550	[illegible]	[illegible]	[illegible]	[illegible]	[illegible] operati[illegible], [illegible] temperature was [illegible] failed
[illegible] 5	3[illegible]	[illegible]	[illegible]	[illegible]	[illegible] greater [illegible], [illegible] no apparent damage
[illegible]00	3[illegible]	1500	[illegible]		[illegible] high temperature [illegible] thermocouple failed
[illegible]00	350	[illegible]	[illegible]	2	[illegible] even [illegible] air cool[illegible]. [illegible] shield [illegible] stainless steel. [illegible] transfer section [illegible]. Tungsten [illegible] welded to heater outlet, [illegible]denum [illegible] damaged, and [illegible] ring [illegible] heater outlet [illegible] damaged
[illegible]	3[illegible]	[illegible]	[illegible]	[illegible]	[illegible] due to [illegible] impurit[illegible] [illegible] element. [illegible] and fracture of [illegible] element
[illegible]	[illegible]	[illegible]	[illegible]	[illegible]	Copper connection with [illegible] and bellows made to graphite heater extension. High impurity levels and failure of [illegible] temperature thermocouples. Excessive heat loss at top of the element. Heater [illegible] at [illegible] at max pressure of [illegible] torr
[illegible]	[illegible]	[illegible]	[illegible]	[illegible]	[illegible] of [illegible] tion, [illegible] of analysis [illegible]

TABLE 2.3

MPD POWER DEGRADATION EXPERIMENT

SUMMARY OF HIGH TEMPERATURE OPERATION (PER. 1

Date	Graphite element	Resistance (hot), ohm	Radiation shield system	Helium mass flow, gm/sec	Heater power volt amp kW	Heater Temps, °C	Max. gas temp (indicated), °C	Ma
RHT 16 [illegible]	EY 9 EY 110 pin connector	.007	as above					
RHT 17 [illegible]	As above	.0063	as above	5.8	13.2 1580 20.9	955 1085 1085	985	
RHT 18 [illegible]	As above	.008	as above	6.1	24.3 2920 71.0	1750 1810 1850 1850	1370	
RHT 19 [illegible]	As above	.0084	as above	6.4	24.6 3040 [illegible]	1830 2040 2070 1580	[illegible]	
RHT 20 [illegible]	EY 9 pin connector	.0094	as above	6.2	21.6 2580 55.7	1850 2090 2150 2000	1560	
RHT 21 23-11-63 to 15-11-63	EYX 94		as above then altered to graphite tungsten molybdenum stainless steel					
RHT 22 12-11-63	EYX 94	.0094	Graphite tungsten molybdenum stainless steel	5.4	22.8 2580 54.4	2175 2150 1750	1480	
RHT 23 22-11-63	EYX 94	.0167	as above					

INENT

3. 1963 - MARCH 1964)

Max. gas temp. (Corrected) °C	Recuperative He outlet temp. °C	Helium purification max. impurity level during run, ppm			NOTES
		H_2	N	O_2	
					Several outgassing procedures. New graphite pin connection checked, mineral oil contamination on optical windows. Repeated cleaning of all components removed the contamination. Max temperature 2400°C at less than 27μ. New pumping line attached to base of heater.
1050	376	800	50	12	Analysis plant failure, the element thinner another .060in. on diameter.
1540	405	320	70	12	Short circuits between, heater shields, tantalum transfer section and heater head. Failure of gas temperature measurement.
2070	440	260	50	10	Graphite pin system spring loaded 300lbs thrust held at 2070°C for one hour. Pin and heater head bonded and cracked signs of molybdenum vapourization, deposited on heater head.
1770	352	30	25	10	Two CuO beds used to increase the efficient of H_2 removal. Alumina duct shattered due to thermal and mechanical shock.
					New single length element, molybdenum shields found to be dirty and were replaced with tungsten shields. Max element temperature of 2200°C achieved during outgassing. No over heating of case.
1670	430	80	44	20	Temporary transfer duct fitted
					Outgassing run

TABLE 2.4 MPD POWER GENERATION RAP

SUMMARY OF HIGH TEMPERATURE OPERATION (FEB. 1

Date	Graphite element	Resistance (hot) ohm	Radiation shield system	Helium mass flow gm/sec	Heater power Volt	amp	kW	Heater temps., °C	Max. gas T, (indicated) °C	cor
RHT 4 30.1.63	EYX 94	.0099	Graphite Tungsten Molybdenum Zirconia wool Stainless steel	6.75	17.8	1800	32	1810 1870	1260	1
RHT 25 4.12.63	EYX 94	.0097	as above with no Zirconia	6.2	18.5	1900	35	2000 1940 1760	1200 on T-piece	1
RHT 26 10.12.63	EYX 94	.0097	as above with no Zirconia	6.4	18.9	1950	37	2000 1960 1950	1200 on T-piece	1
RHT 27 24.12.63	EYX 94	.0116	as above with no Zirconia	14.3	20.8	1800	37.5	1990 1740 1700	1250 on T-piece	18
RHT 28 7.1.64	EYX 94	.0129	as above with no Zirconia	7.5	24.4	1900	46.5	1870 1720	1165 on T-piece	17
RHT 29 14.1.64	EY 9	.0098	as above with no Zirconia	11.3	27.1	2760	75.0	2000 1900	1475 on T-piece	18
RHT 30 .3.64	EYX 94	.0126	as above with no Zirconia	7.3	24	1900	45.5	1660 1700	1260 on T-piece	17
RHT 31 12.3.64	EYX 94	.0108	as above with no Zirconia	6.35	21.6	2010	43.5	1800	1280 on T-piece	16
RHT 32 18.3.64	EY 9	.0094	as above with no Zirconia	9.1	25.8	2750	71.0	2100	1750 on nozzle	20

EXPERIMENT

R, 1963 - MARCH 1964)

°C corrected	Recuperative He outlet, °C	Helium purification max. impurity level during run, ppm					Notes
		H_2	N	O_2	CO	CH_4	
1370	410	2[illegible]	90	25			Gas contamination by Na released from Zirconia fibre. Several integral leaks in the circuit, not all the flow in passing through the heater
1700	160	10	25	16			Low recuperative helium outlet showed large flow bypass on heater, transfer and duct. The duct walls were found cracked
1700	180	90	66	34			Still a large bypass flow across the generator section, failure of joint in water cooled Cu conductor allowed water into loop, causing errosion of heater. Major damage to tantalum transfer section
1820	260	120	38	17			Tantalum tungsten diffuser split down both walls and across base, allowing helium to bypass heater and duct
1730	300	170	5	-			Severe arcing and sharp rise of impurity (Fig. 3.38). Simple flow test showed a 25% bypass of helium flow across heat exchanger
1800	400	800	20	12			Arcing at 2700 amps, caused the heater head to crack on the interface, and severe pitting of interface of pin. H_2 impurity high and fluctuating (Fig. 3.41)
1700	350	80	-	-			New electrical hot connection not entirely satisfactory, arcing between graphite and interference fitting copper connector
1600	360	60	-	-			At 2000 amps, heater lost power, on dessembly the element was found to have fractured across top end of heater section
2000	406	100	10	5			Seeded power generation Run. Five electrode duct with simple loading. Twenty seeded runs, with 0.2 - 1.0 Nm^2 and choked and unchoked conditions. Max. power output was $\frac{1}{2}$ watt

PURIFICATION PLANT DEVELOPMENT
HEATER DEVELOPMENT
MPD CLOSED LOOP : PROGRESS SUMMARY
TEMPERATURE, °K
2500
2000
1500
1000
500
0
JAN
FEB
MAR
APRIL
MAY
JUNE
JULY
AUG
1963
PROV

FIG 2.1

CESIUM RECOVERY

HEATER ARCING PROBLEMS

GENERATOR DUCT DEVELOPMENT

OVING RUN

CESIUM SEEDED POWER GENERATION *

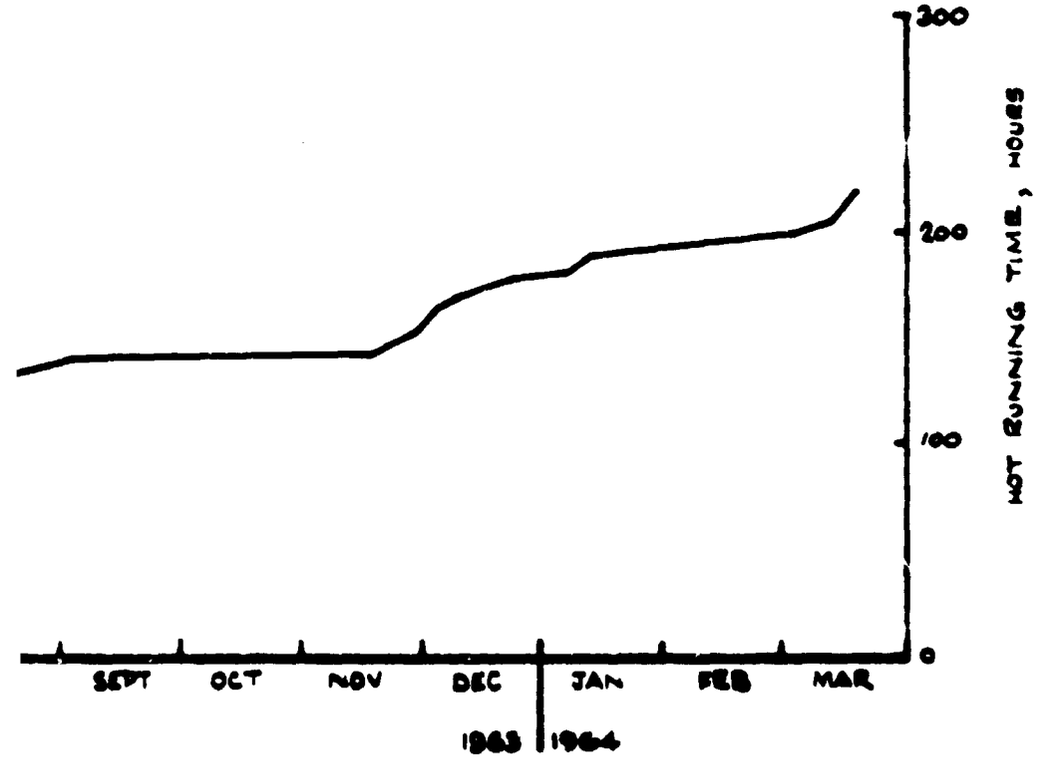

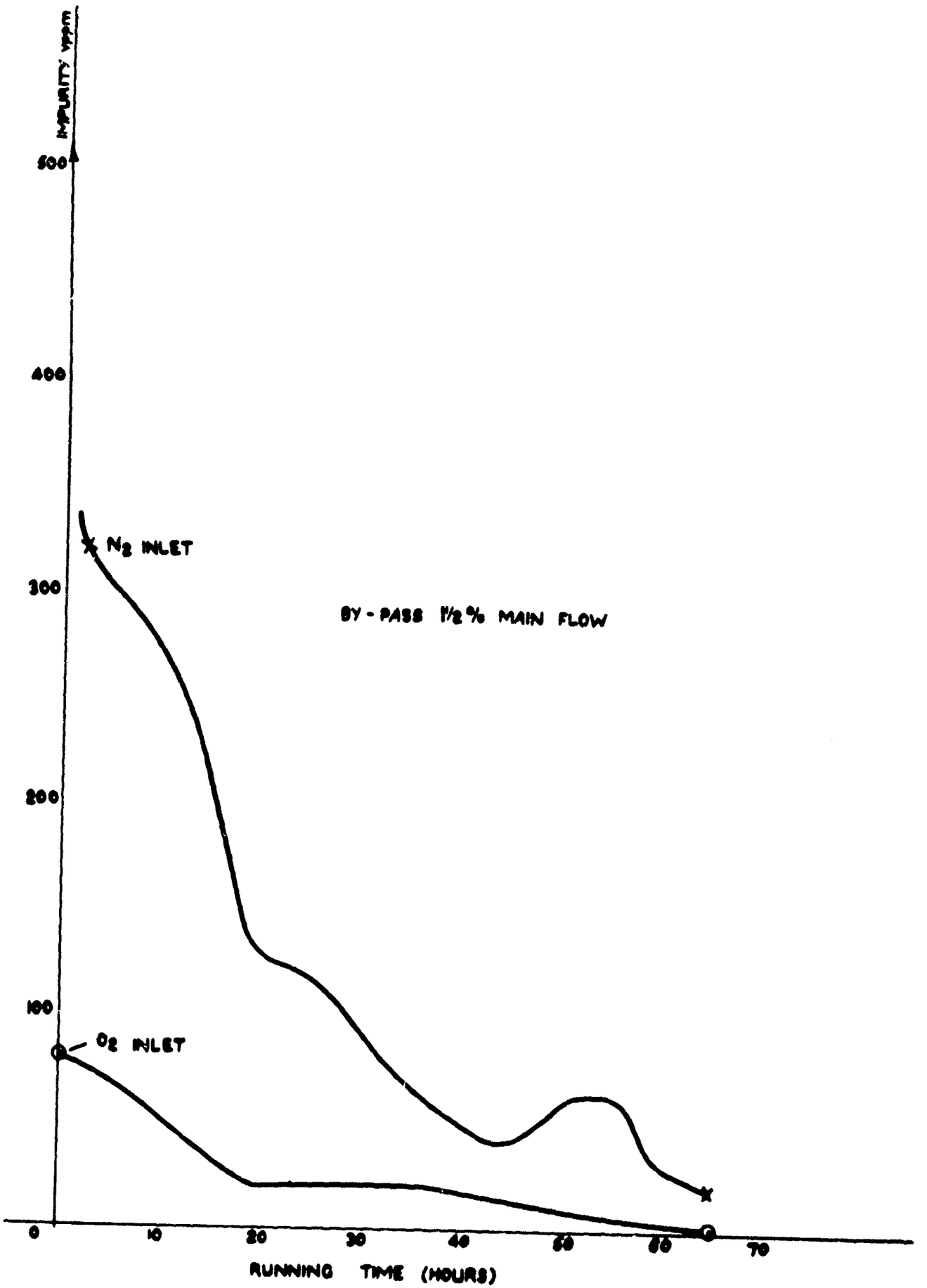

HELIUM PURITY COLD RUN

FIG 2·2

WATER DRAINING FROM HEATER AFTER END CONNECTION FAILURE

FIG 2·3

CHAPTER 3

HIGH TEMPERATURE GAS CIRCULATION

by

R. Brown, W.J. Slator, V. Brown, K. Cass and J. Davidson

3.1 HEATER OUTGASSING

During the period February 1962 to March 1963 a large number of high temperature runs (Tables 2.1 to 2.4) have been undertaken with various heater-transfer duct - generator duct configurations. Before each run it has been necessary to establish vacuum-outgassing techniques for the heater unit previous to gas circulation. Throughout the programme the requirement has been for lower gaseous impurity levels and the degree of vacuum-outgassing of the heater graphite components has become increasingly important. The procedure adopted throughout the latter part of the programme has been to achieve a heater core temperature greater than 2500°K with pressures read at four loop stations and at the heater core of less than 30 torr, and then holding at this temperature to attain an ultimate base pressure of less than 5 torr and pressure rise in this isolated loop of less than 1 torr/min.

A change in temperature profile of the element from outgassing to gas circulation is inevitable and produces further desorption of gaseous impurities. With the adopted procedure and present purification capacity the only short holding conditions necessary during thermal cycling from 1600° to 2200°K are for hydrogen removal.

RHT 1 : 2 February 1963

Operation

The loop had been closed during cold runs from December 1962 to January 1963. The high temperature heater assembly (Fig. 3.1) has been discussed previously (Technical Summary Report ERD 63-1) A simple high temperature tantalum/stainless steel transfer duct arrangement connected the heater outlet to the subsonic diffuser inlet. Heater power was steadily increased to give 1200°K indicated outlet temperature with 5 gm/sec helium flow. Some difficulty was experienced in reducing gaseous impurities (Fig. 3.2). Failure of a rubber heater cooling water supply pipe necessitated rig shut down.

Inspection and modification

Inspection showed a faulty seam and the pipe was replaced.

RHT 2 : 10 February 1963

Operation

With the rig condition unchanged from RHT 1 a further thermal cycle under flow conditions was undertaken. At a helium mass flow of 5.0 gm/sec a maximum indicated heater outlet temperature of 1350°K was achieved. An undetermined amount of air leaked into loop from a cracked joint on the sub-atmospheric purification return line. Temporary sealing was effected but a rapid increase in impurity levels (Fig. 3.3), the blockage of the H_2O and CO_2 trap in the purification system, and serious overheating (~1250°K) of the lower part of the heater case caused the run to be discontinued.

Inspection

Inspection showed overheating of the heater core as a result of poor axial flow distribution. The tantalum transfer duct (0.015 in. material) had partially disintegrated (Fig. 3.4), allowing helium to bypass the heater and thus aggravate the stagnation condition in the heater.

Modifications

The leaking section in purification outlet was repaired.

The temporary tantalum transfer duct was replaced with a further unit fabricated from 0.020 in material and incorporating a 0.015 in. material bellows (Fig. 3.5). A stainless steel baffle was fitted over the upper half of the outer radiation screen in the high temperature heater core to improve the helium distribution to the element.

RHT 3 : 23 February 1963

Operation

The run duration was 26 hr with 12 hr hot running. A helium outlet temperature of 1230°K was attained and held for 4 hr. Progressive blockage of a molecular sieve bed in the purification plant reduced the bypass flow to about 0.3 per cent and some difficulty was experienced in maintaining low gaseous impurity levels (Fig. 3.6). Overheating of the high temperature heater body again became evident and the run was discontinued.

Inspection

The purification plant molecular sieve blockage was due to carry-over of ice from the H_2O and CO_2 trap. No significant embrittlement or damage to the tantalum transfer duct was apparent. The copper flexible head connection to the high temperature heater showed signs of overheating and relaxation.

Modifications

The H_2O and CO_2 helium purification trap was redesigned, manufactured and fitted. The new unit comprised a small stainless steel tube heat exchanger with stainless steel wool packing for even distribution of solids. The concentric shield heater radiation system was sectioned and the individual shields baffled with stainless steel inserts to improve the axial temperature distribution of the graphite heating element. The inner molybdenum shield baffles were increased to 5 layers of dimpled molybdenum sheet. Dimpled transverse molybdenum radiation shields were fitted below the heater top connection to reduce radiation on the copper clamp.

RHT 4 : 5 March 1963

Operation

The run duration was 30 hr with 20 hr hot running time. A maximum heater outlet temperature of 1490°K was indicated at 5.5 gm/sec helium mass flow. At this temperature level with a heater core temperature of ~ 1850°K overheating of the heater outer case occurred. A rapid increase in the case temperature dictated loop shut-down. Mismatching of the graphite element electrical resistance was pronounced at high temperature, 0.0075 ohm compared with a required value of 0.012 ohm. The run was carried out with impurity levels of less than 30 ppm (Fig. 3.7), the performance of the redesigned purification cold trap satisfactorily overcoming blockage of the molecular sieve.

Inspection

Melting of the lower end of the inner molybdenum radiation shield at high temperature had occurred (Fig. 3.8). Although a 260°K improvement in gas temperature had been achieved the modified shield system had resulted in poor helium distribution into the element, and temperatures at the lower end of the element greater than 3000°K.

Modifications

A heater body of larger diameter was manufactured to allow multi-axial flow radiation shields to be fitted. These comprised: inner, 2 graphite; outer, 2 molybdenum, 7 dimpled molybdenum and 6 electro-polished stainless steel. The wall thickness of the CS20 graphite element was reduced by 0.030 in.

RHT 5 : 18 March 1963

Operation

Before helium circulation a large leak (>1μ/sec) was detected in the helium circulator. The leak proved to be through an oilway into the subatmospheric section of the circulator, and had not been capable of detection during leak-checking. In the static state the circulator rotor end face stopped in close contact with the main housing cover face and with lubricating oil at the interface no leak was detectable. After sealing, on cold helium circulation rapid clean-up ensued and throughout the run excellent helium purities were maintained (Fig.3.9).

An indicated helium outlet gas temperature of 1490°K was achieved at 5.4 gm/sec helium mass flow. Overheating of the inner stainless steel radiation shields dictated loop shut-down. During running the element electrical resistance hot had improved to 0.0096 ohm.

Inspection

Melting of the inner two electropolished stainless steel radiation shields had taken place.

Modifications

The inner four stainless steel radiation shields were removed from the heater assembly.

The CS20 graphite heater element wall thickness was further reduced by 0.060 in.

RHT 6 : 23 March 1963

Operation

A further hot run was carried out and with the improved helium clean up rate (Fig. 3.10) the complete thermal cycle was undertaken in under 12 hr.

The maximum indicated helium outlet temperature was 1760°K for a helium mass flow of 5.25 gm/sec. The thinned CS20 graphite element hot electrical resistance of 0.0099 ohm was again lower than ideal. Overheating of the

heater outer case became evident and the run was discontinued.

Modifications

With repeated thinning of the CS20 graphite element to approach electrical resistance matching of 0.012 ohm, the transverse strength of the heater was becoming intolerably weak. The reduced passage length of the 2500 $\frac{1}{8}$ in. diameter holes in the element wall was resulting in poorer heat transfer to the helium, a larger temperature difference between surface and gas and a higher radiant loss.

Fine-grained Morgan grade EY9 graphite (resistivity 2000 μohm. cm. CS20 800 μohm. cm.) was obtained and a replacement element with a $\frac{3}{8}$ in. wall thickness produced.

In the event of molecular sieve blockage or saturation in the purification plant shut-down of the loop is imperative and, to overcome this a second molecular sieve system was added in parallel in the purification circuit.

RHT 7 : 10 April 1963

Operation

Modifications to the purification plant enabled by-pass flow rates to be increased to about 4 per cent of the main helium flow. An intermittent leak on a Dowty helium circulator oil control valve was located and cured. (This leak was difficult to locate since in isolation the valve appeared leak-tight but with oil flow under dynamic conditions and helium circulation air was being drawn into the sub-atmospheric section of the circulator.) Because of these improvements excellent ($<$10 ppm) impurity levels were maintained (Fig. 3.11).

At an indicated helium outlet temperature of 1700^{o}K the tantalum-sheathed high temperature thermocouple failed and the run was discontinued.

Inspection

Melting of the stainless steel radiation shield support block in the heater (Fig. 3.12) had occurred, and the inner graphite shield had cracked. The stainless steel balls used as a radiation screen in the lower hollow end of the element had fused together.

Modifications

A replacement graphite radiation shield support block was manufactured and a new inner shield fitted to the heater. Alumina balls were used to

replace the melted stainless steel balls.

A 0.015 in. thickness tantalum sheath was fitted to the replacement high temperature tantalum-sheathed thermocouple.

RHT 8 : 18 April 1963

Operation

A further hot cycle was carried out over a period of 4 hr with impurity levels maintained at <5 ppm (Fig. 3.13). An indicated helium outlet temperature of 2010°K was attained but a direct short circuit to earth of the bottom electrical connection on the high temperature heater at a power level of 61 kW caused the element to fracture (apparently from thermal shock). The run was discontinued.

Inspection

Fracture of the graphite element had occurred in the thinned section.

Modifications

As a hold up was inevitable for replacement of the graphite element, the thinned CS20 element was refitted.

RHT 9 : 22 April 1963

Operation

After 80 minutes total operation with controlled purities (Fig. 3.14) at an indicated helium outlet temperature of 1850°K failure of the high temperature heater outlet thermocouple caused shutdown.

Inspection

The tantalum sheathed thermocouple had no significant impurity attack and the reason for failure of the grounded junction was not apparent.

Modifications

Replacement high temperature thermocouple fitted.

RHT 10 : 23 April 1963

Operation

The indicated helium outlet temperature was raised to 2070°K, holding between 2070° and 2010°K at 6.3 gm/sec for 20 min. (Fig. 3.15). Slight overheating of the heater body became evident. Electrical mismatching of the heater element restricted further power increase and the run was discontinued.

Inspection

The high temperature heater and tantalum transfer duct had suffered no significant damage.

Modification

The CS20 graphite element wall thickness was further reduced by 0.030 in.

RHT 11 : 3 May 1963

With helium impurity levels maintained below 5 ppm (Fig. 3.16) 45 min of high temperature (2140°K indicated helium outlet) was carried out under steady conditions. Considering that the heater wall thickness was only 3/16 in. the heat transfer performance was impressive; a contributory factor was preheating in the multi-pass axial flow between shields. A temperature profile of the graphite element is given in Fig. 3.19. After 45 min at the top temperature failure of the high temperature couple ensued and the run was discontinued.

Inspection

No significant damage of any section was apparent.

Modification

The high temperature tantalum-sheathed thermocouple pocket wall thickness was increased to 0.020 in.

RHT 12 : 5 May 1963

In under 2 hr an indicated helium temperature of 2130°K was achieved under low impurity conditions (Fig. 3.17). Significant overheating (to > 1000°K) of the heater case around the outlet section occurred over the last 15 min. of operation. A sudden rise in core temperatures and evidence of bypass leakage around the heater dictated the rapid shut down of power and loop circulation.

Inspection

Melting had taken place at the helium outlet section. The tungsten bush, molybdenum head radiation screens, graphite heater head and inner tantalum and outer stainless steel transfer duct had fused together and bonded into the graphite head section. It was necessary to fracture the graphite head to dissemble the system (Fig. 3.18). The presence of molybdenum in contact with graphite was thought to have initiated the melting process; since concentrations of carbon in molybdenum are known to lower its melting point to about 2500°K.

The heater head temperature measured optically with a Leeds-Northrup pyrometer was 2520 K (viewing by 3/16 in. in-line holes through the radiation shields) at the maximum gas temperature. From the degree of melting, temperatures in the region of 2500°K must have been attained indicating that temperatures at head were low by more than 180°K. Emissivity, solid angles and transmission adsorption in the viewing window are contributory factors.

Modifications

A replacement element, in EY9 grade graphite with $\frac{3}{8}$ in. wall thickness, was fitted. All radiation shielding in contact with the graphite heater head section was fabricated from 0.010 in. tantalum sheet. A replacement 0.020 in. tantalum transfer duct with 0.015 in. bellows was fitted.

RHT 13 : 31 May 1963

Operation

The new EY9 element proved to have a resistance of 0.0064 ohm, compared with the matched value of 0.012 ohm. After reaching a gas temperature of about 1750°K the run was discontinued due to mismatching which prevented the power input being increased above 41 kW. High impurity levels were experienced (Fig. 3.20).

Inspection

The rod upper end connection to the element had fractured evidently on cooling; no further deterioration was apparent.

Modifications

The rod and clamp end connection, which had been successful with CS20 graphite, appeared to be unsatisfactory with EY9 which has a lower transverse strength, although other factors were change in section at the copper plating and possible deterioration by ingress of electrolyte. Consequently, it was decided to abandon this type of end connection. Preferred configurations required longer lengths of graphite, but a 5-month delivery on graphite of suitable properties (EY110 with a resistivity of 2000 ohm cm) led to a tapered cone heater extension (not an ideal arrangement in graphite). The $\frac{1}{2}$ in. thickness cone cracked during assembly. The element wall thickness was reduced by 0.060 in.

Tantalum test strips were introduced in the high temperature transfer duct to monitor attack in individual runs.

RHT 14 : 21-26 June 1963

Operation

An indicated gas temperature of 1650°K was attained but considerably increased heat losses (~10-12 kW higher input) at heater upper end led to shut-down. The top end of the heater was 200°K cooler than usual. Impurity levels were high (Fig. 3.21).

Inspection

The cone extension was cracked (Fig. 3.22).

Modification

The cone wall thickness was reduced to $\frac{3}{8}$ in.

RHT 15 : 1 July 1963

Operation

A temperature of 1480°K was reached before the cone section begar to collapse. Difficulties were experienced with the helium analysis plant (Fig. 3.23) and the run was discontinued for reactivation.

Inspection

The cone had disintegrated (Fig. 3.24).

Modifications

The heater element wall thickness was reduced by a further 0.060 in. Although no information was available on this type of electrical connection for design temperatures and electric currents a connecting pin with flat graphite interface was adopted, with connection to a copper core at the upper end. Colloidal graphite was introduced at interfaces in an attempt to improve the connection. Fig. 3.25 shows components of the complete heater assembly.

RHT 16 : 5 to 17 July 1963

Operation

5 outgassing procedures were carried out and the current capacity of the pin connector checked to 3000 amp. No gas flow run was attempted.

RHT 17 : 18 July 1963

Operation

The helium analysis equipment failed, and full reactivation of the analysis and purification plants was completed.

RHT 18 : 19 July 1963

Operation

Purification (apart from hydrogen removal) was very good (Fig. 3.26). Electrical short-circuiting due to leakage through transfer duct and insulation caused thermocouple failure.

Inspection

Components showed signs of arcing and short-circuiting. The graphite pin/element interface was in satisfactory condition.

Modification

An insulated and spring-loaded pin connection was arranged.

RHT 19 : 26 July 1963

Operation

Apart from hydrogen removal purification was good (Fig. 3.27).

Inspection

Cracking and bonding had occurred at the heater interface (Fig. 3.28). There was evidence of molybdenum evaporation and deposition in cooler areas.

Modifications

The 2-electrode-pair generator duct (Thermal Syndicate recrystallized alumina) was installed with some difficulty due to the mounting arrangement. Alignment and the spring-loading arrangement was unsatisfactory and mechanical strain probable. Alumina chip thermal insulation was adopted, with dimpled tantalum sheet on the main tantalum transfer duct. The sapphire windows had provision for gas cooling. A T-piece was mounted for gas temperature measurement. A micrometer dial gauge was fitted on the heater to check growth. An extremely careful vacuum-outgassing procedure was followed.

Hydrogen removel was proving troublesome, reactivation occupying about 4 hr, and a second copper oxide bed was installed in parallel with the existing unit, thereby eliminating the need for shut-down. The analysis for hydrogen was re-checked and a factor of 400 change in the calibration constant was found.

RHT 20 : 3 and 4 September 1963

Operation

The gas (nozzle inlet) temperature was increased at about 150° to 200°K/hr, hot running occupying 20 hr. Loud cracks, at first attributed to strips of

alumina mounted against the nozzle for thermal insulation, were noticed at a temperature level of ~700°K. The heater resistance was still mismatched (~0.0084 ohm). Helium purification curves are shown in Fig. 3.29; hydrogen was held below 600 ppm. Filming of the sapphire windows was noticed, and a duct thermocouple failed. Some helium bypass and leakage was apparent between the heater inlet and outlet gas. The temperature cycle was immediately repeated in a second hot run.

Inspection

The generator duct had failed by multi-cracking (see Chapter 9). Molybdenum deposition on the element had occurred. A dark gray non-electrically-conducting deposit was found on the generator duct walls.

Modifications

The generator duct assembly was arranged on a mounting backbone (Chapter 9). Molybdenum radiation shields were replaced by two 0.030 in. tungsten units. A single-piece graphite heater became available, eliminating the connector interface. The material for this (Morgan Link EYX94 of resistivity 2200 ohm cm) was limited to $3\frac{1}{4}$ in. o.d., necessitating a reduced core connection at the lower end. Boron nitride insulation was adopted.

RHT 21 : 23 September to 15 November 1963

Operation

More stringent outgassing procedures were developed with an additional vacuum system on the heater base. A temporary transfer duct was fitted, to eliminate damage of the main duct.

RHT 22 : 17 November 1963

Operation

The graphite element was mismatched electrically; gas leakage between heater inlet and outlet was severe. Purification gave much lower hydrogen content (Fig. 3.30).

Modifications

The element wall thickness was reduced by 0.060 in. Zirconia E fibre (1 in. thickness on 10 in. diameter) was introduced between outer stainless steel and outermost molybdenum shields.

RHT 23 : 22 November 1963

Operation

Outgassing runs: viewing ports were blocked by a crystalline deposit

between element temperatures of 1500° and 2000°K.

RHT 24 : 30 November 1963

Operation

Hydrogen was maintained at less than 20 ppm (Fig. 3.31). Viewing parts were blocked by sodium deposition, preventing temperature measurement which, with evidence of severe heater bypass flow, caused shut-down. Effectiveness of the zirconia insulation was apparent.

Inspection

Sodium-containing deposition had occurred at the base of the heater as well as in the region of the viewing parts.

Modification

The zirconia insulation was removed. (The as-received material had 2 per cent sodium content, which the manufacturers were subsequently able to reduce to 0.5 per cent; treatment of the material at IRD produced a sodium content of less than 2 ppm).

A further 0.030 in. was removed from the element wall. A 9-electrode-pair duct assembly was built up with one side wall of hot-pressed alumina, the second of slip-cast alumina and the top wall of boron nitride, in which was set a strip electrode under a sapphire window. A tantalum-tungsten alloy diffuser inlet section was adopted. The duct was thermally-insulated with sodium-free zirconia fibre.

RHT 25 : 4 December 1963

Operation

A hydrogen level of less than 10 ppm was attained (Fig. 3.32). Considerable heater bypass leakage was evident, with a delivery temperature from the heat exchanger of only 430°K. The maximum duct sidewall temperature approached 1600°K.

Inspection

Gas was leaking at the tantalum-tungsten diffuser sliding seal, and the fracture of a pressure pipe in the transfer duct.

Modifications

Leakage was minimized.

RHT 26 : 10 December 1963

Operation

8 hr hot running was accomplished; hydrogen levels were high ~ 90 ppm (Fig. 3.33). While maintaining temperature for hydrogen removal, catastrophic arcing took place at the upper end of the heater allowing entry of water.

Inspection

Fig. 3.34 shows the heater interface. The tantalum transfer duct was severely damaged, the bellows being shown in Fig. 3.35. High temperature thermocouples were lost and the heater was considerably eroded but intact. Heavy deposits of tungsten oxide were evident as far as the diffuser. Slight damage to the alumina duct components occurred but the boron-nitride was unharmed.

Modifications

The loop was re-assembled with a temporary transfer duct. A monitor, with oscilloscope display, on electric power input was developed to discriminate arcing, and several thermocouples were mounted in the graphite and copper near the interface. The end connection was modified to a spheroid, allowing for some angular misalignment. Several viewing parts were added for critical sections. The heater assembly was separately outgassed to 2500°K.

RHT 27 : 24 December 1963

Operation

High hydrogen levels (~120 ppm) were evident (Fig. 3.36). Arcing again occurred at 1800 amp, and there was evidence of heater bypass. Fig. 3.37 shows initiation of arc behaviour which was also indicated by temperature assessments near the graphite/copper interface. The minimum indicated window T-piece temperature was 1520°K (corrected, 2090°K heater gas outlet).

Inspection

The tantalum-tungsten diffuser section was severely cracked, giving direct leakage of low temperature helium bypassing the heater, tantalum transfer section and generator duct.

Modification

A finned stainless steel (EN58B) diffuser section was fabricated and fitted to generator section. Viewing parts were added to the generator

case so the diffuser throat temperature could be maintained.

RHT 28 : 7 January 1964

Operation

The run duration was 8 hr with 5 hr hot running. The purification curve (Fig. 3.38) shows a sharp rise in H_2 impurity (>170 ppm) at the same time severe arcing occurred causing the run to be discontinued.

Inspection

Substantial areas of arcing (Fig. 3.39) were found on the interfaces. It also became evident that the heat exchanger was bypassing helium flow. A simple flow test proved this to be as high as 25 per cent of main helium gas flow.

Modification

The heat exchanger was removed from the loop and dissembled (Fig. 3.40). The coils, centre body and case were chemically-cleaned of impurities resulting from 1800 hr of cold and hot running. The sliding seal between the case and coils, and the damaged centre-body were repaired, reducing the bypass flow to less than 1 per cent.

RHT 29 : 12 January 1964

Operation

High H_2 impurity levels (~800 ppm) during run (Fig. 3.41) were evident. Seven hours hot running times followed one hour cold clean up. New finned pin connection used (Fig. 3.42), which demonstrated slight arcing at 1900 amp; severe arcing at 2700 amp caused run to be discontinued. The maximum indicated T-piece temperature was 1750°K which corresponded to 2070°K gas temperature at heater outlet.

Inspection

Severe arcing had occurred between interfaces with pitting of the finned pin face and serious cracking of the heater head.

Modification

The electrical hot end connection was redesigned making use of screwed connections and interference fits. The design also incorporated helium cooling channels in the copper connection leading through to the graphite head system.

Operation

The full assembly comprised a temporary transfer system, five-electrode pair duct, finned diffuser and new hot end connection on heater. Heater previously outgassed at 9μ and 2475°K top element core temperature. Fourteen hours running followed one hour cold clean up; the maximum hydrogen level was 80 ppm (Fig. 3.43). Shut-down was due to arcing between graphite head piece and copper connection. The maximum indicated temperature on T-piece was 1530°K which when corrected gave 1970°K gas temperature at outlet of heater.

Inspection

On inspection, it was decided that the interference fit between the graphite and copper was insufficient and with increase in temperature the copper expanded free of the graphite.

Modifications

Interference fit adjusted on the electrical hot end connection. The simplified cesium injection system was also attached to the loop.

RHT 31 : 12 March 1964

Operation

The total running time was 7 hr with 1 hr cold clean up of loop; the maximum impurity (Fig. 3.44) at any time was 60 ppm (99 per cent H_2). Heavy arcing and loss of heater power occurred at 2000 amp and 1970°K element core temperature. The maximum indicated gas temperature at the T-piece was 1550°K which gave 1870°K heater gas outlet temperature. Before arcing the gas temperatures were rising steadily.

Inspection

The element had fractured across the upper section of the heating element (Fig. 3.45). The weakness appears to be related to water corrosion effects on the element in RHT 26.

Modification

The element was replaced by the cracked interface element of RHT 29. The head of the element was screw cut with slight modifications to the system of RHT 31, components of high temperature heater are shown in Fig. 6.1 and the assemble of heater head in Fig. 6.2.

The loop was closed with all components attached necessary for a seeded power generation run. All joints were leak checked and the heater outgassed at 2350°K.

RHT 32 : 18 March 1964

Details of RHT 32, in which cesium-seeded operation was achieved, are given in Chapter 4; Fig. 3.46 shows the purification curves.

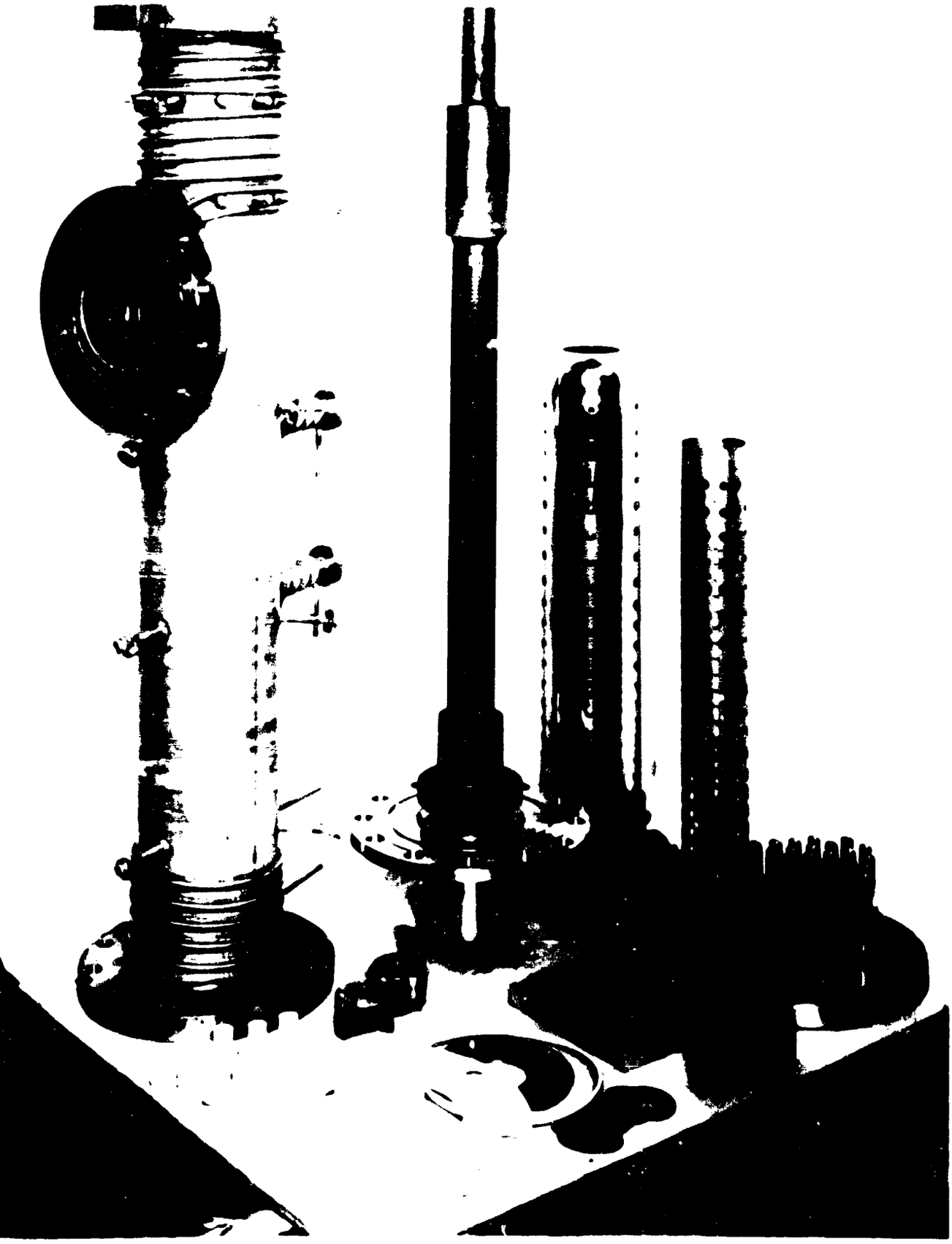

HIGH TEMPERATURE HEATER

FIG 3·1

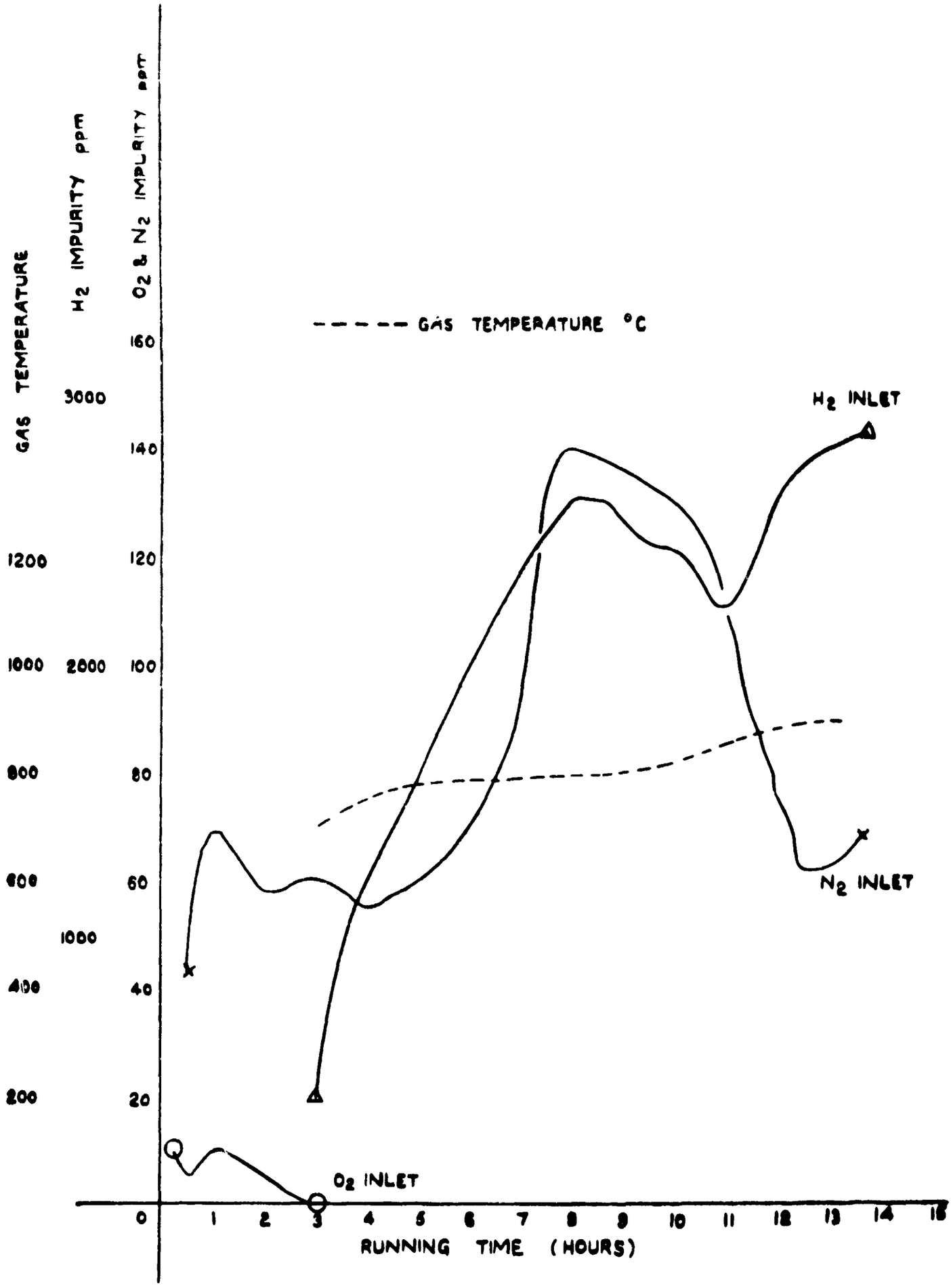

HELIUM PURITY RHT I

FIG 32

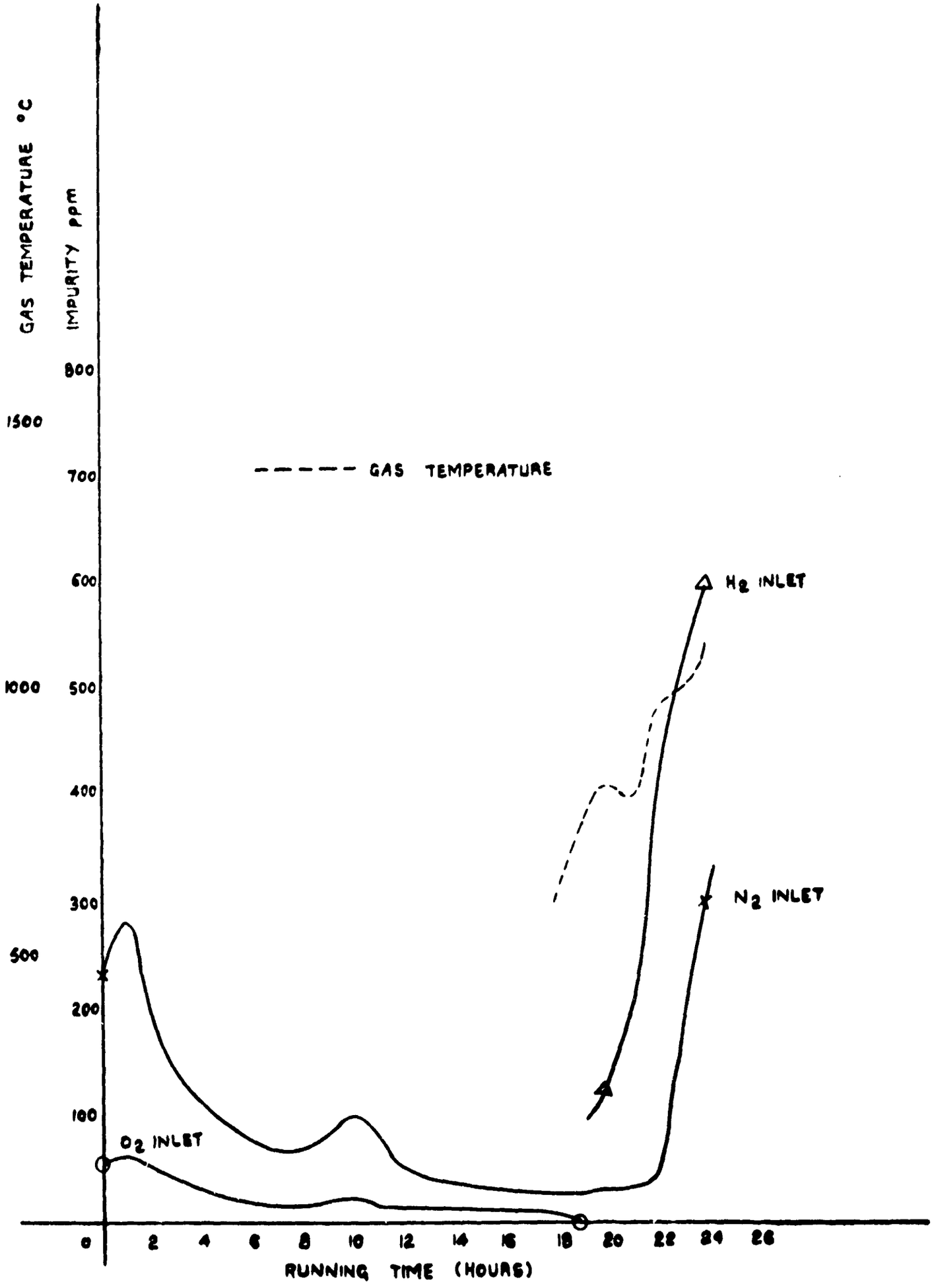

HELIUM PURITY RHT 2

FIG 32

FIG 3·4 EMBRITTLED TEMPORARY TANTALUM (0·015 in SECTION) TRANSFER SYSTEM

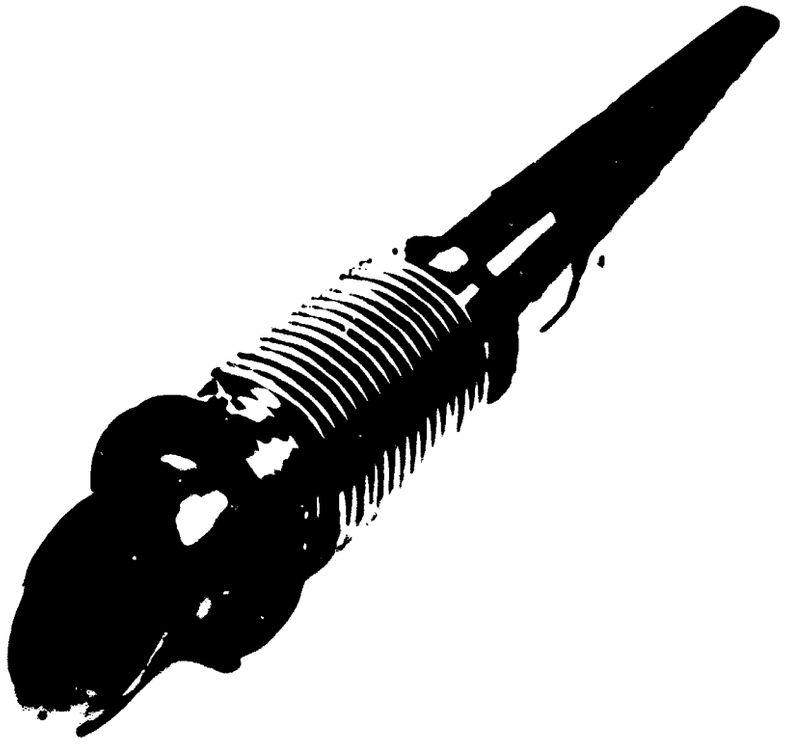

FIG 3·5 TEMPORARY TANTALUM (0·020 in. SECTION) TRANSFER SYSTEM WITH TANTALUM (0·015 in SECTION) EXPANSION BELLOWS

FIGS 3·4 &3·5

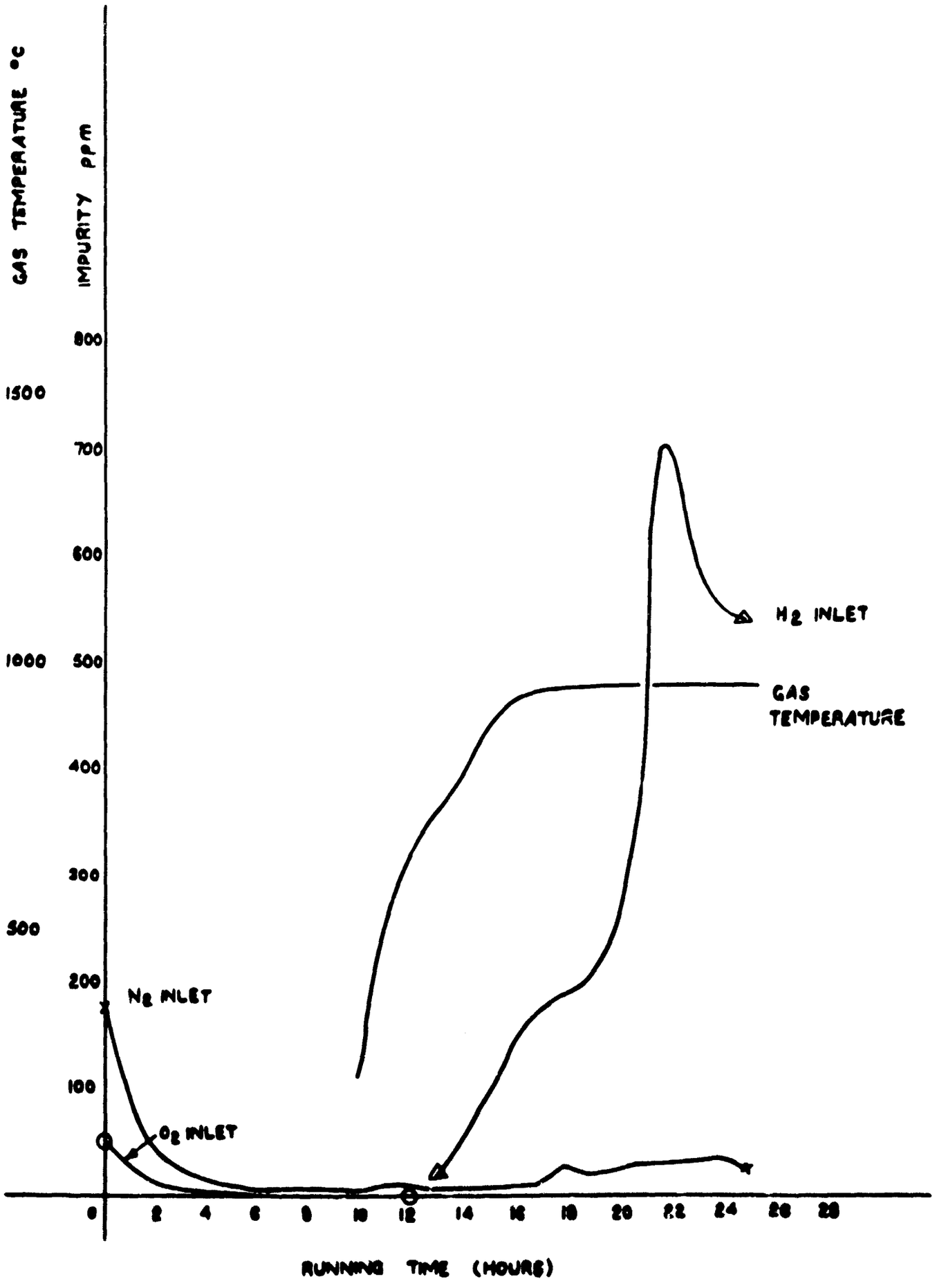

HELIUM PURITY RHT 3

FIG 2.4

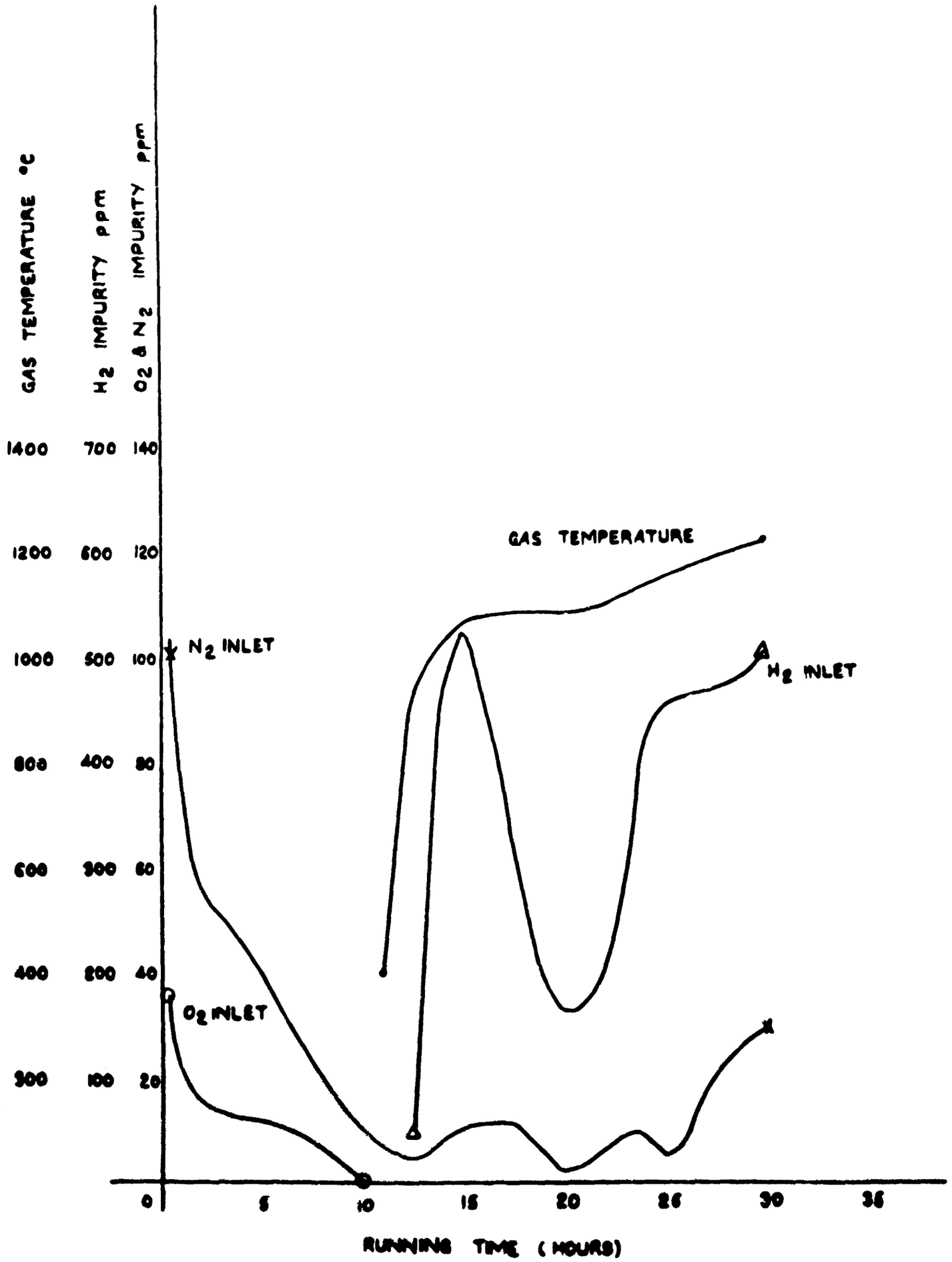

HELIUM PURITY RHT 4

MELTED INNER MOLYBDENUM RADIATION SCREEN

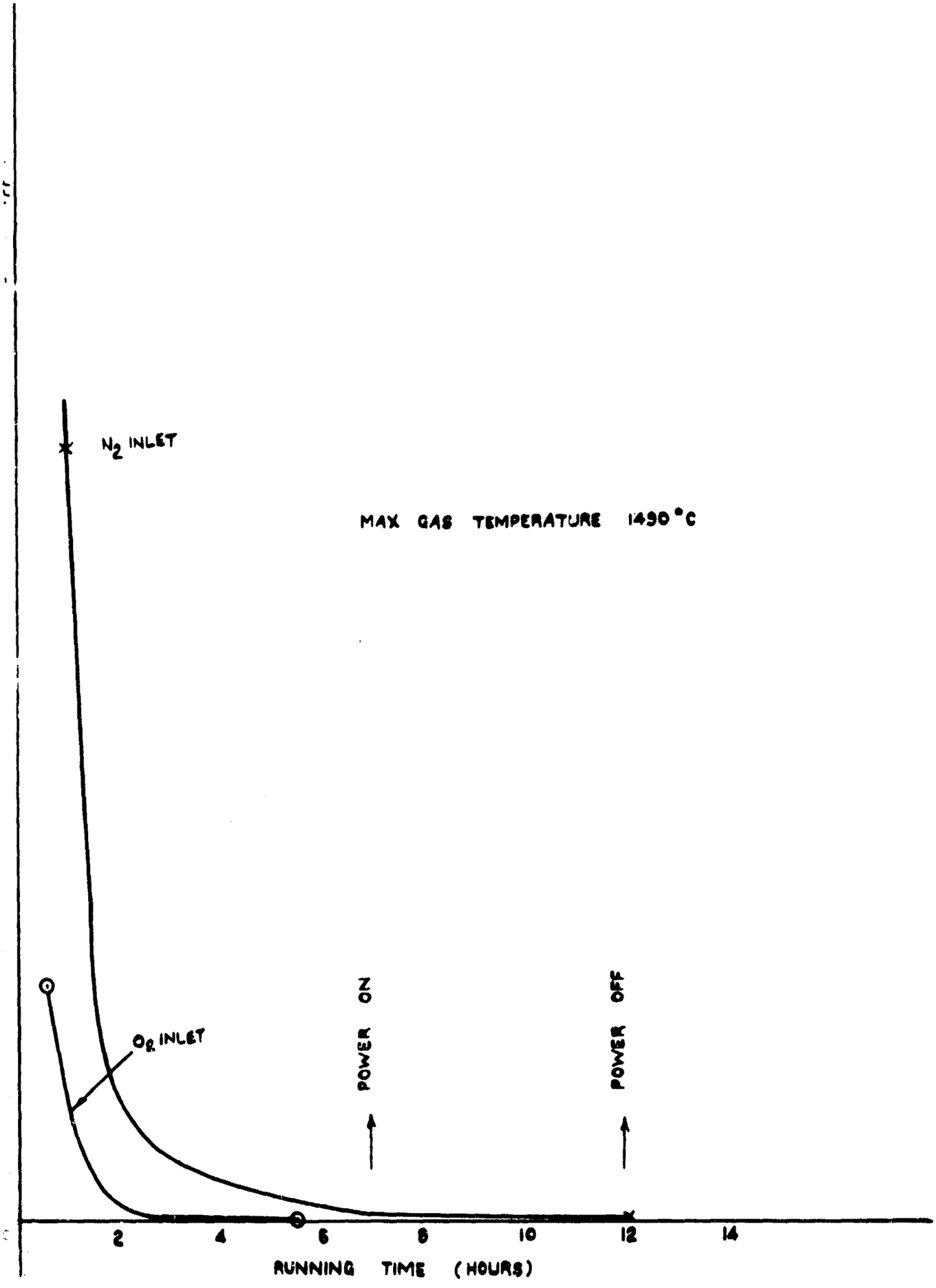

HELIUM PURITY RHT 5

FIG 3·9

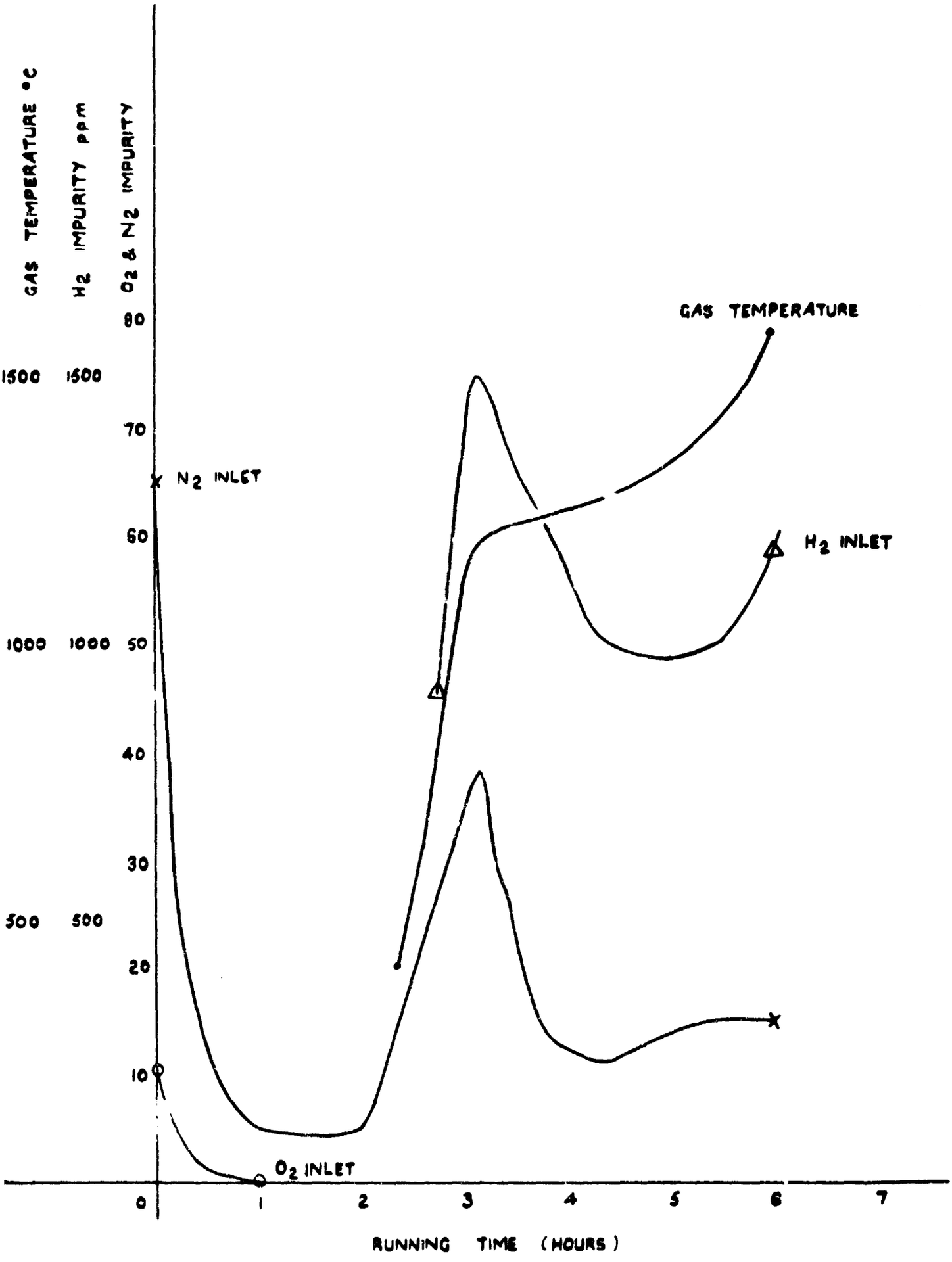

HELIUM PURITY PHT 6

FIG 3·10

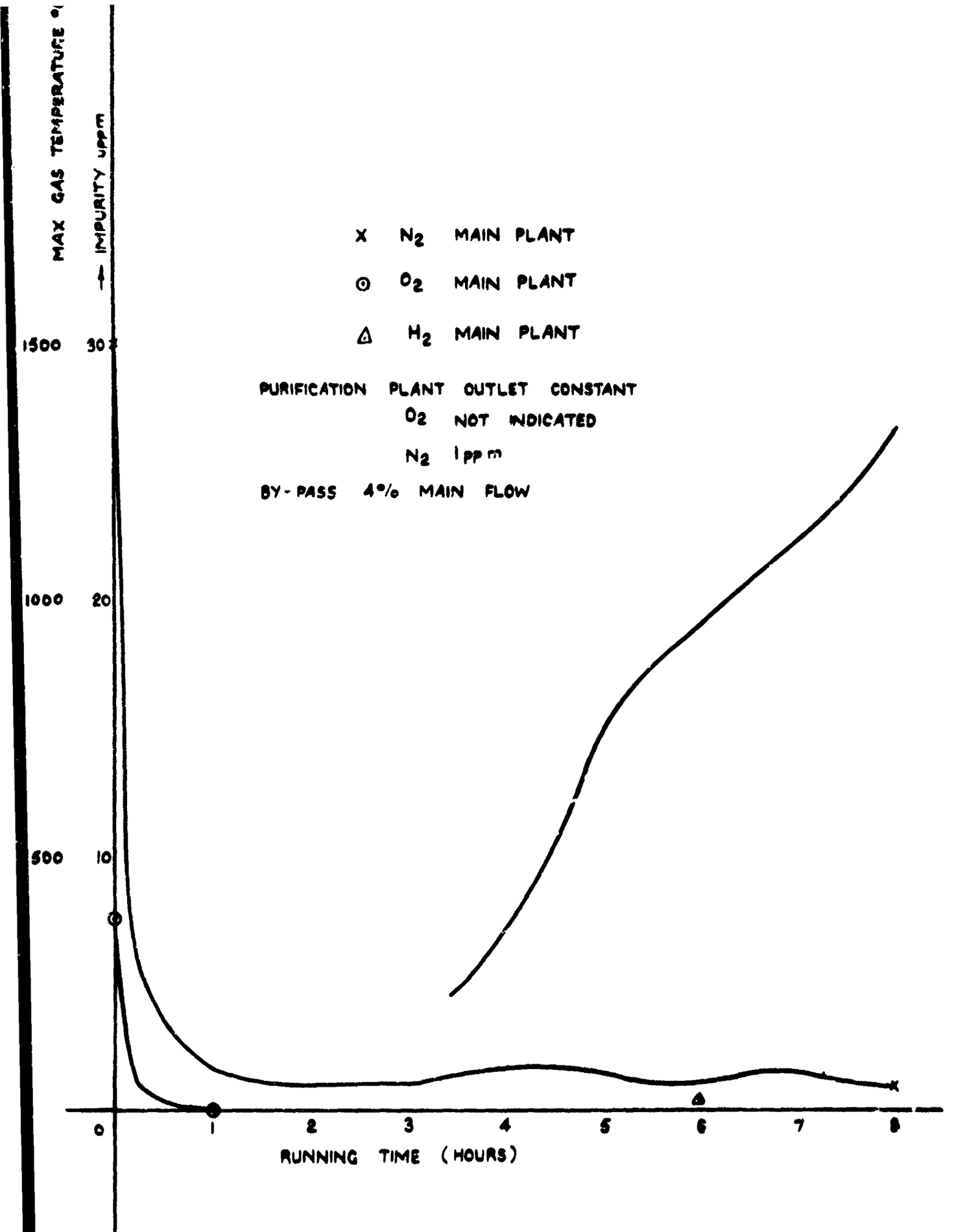

HELIUM PURITY RHT 7

FIG 3·11

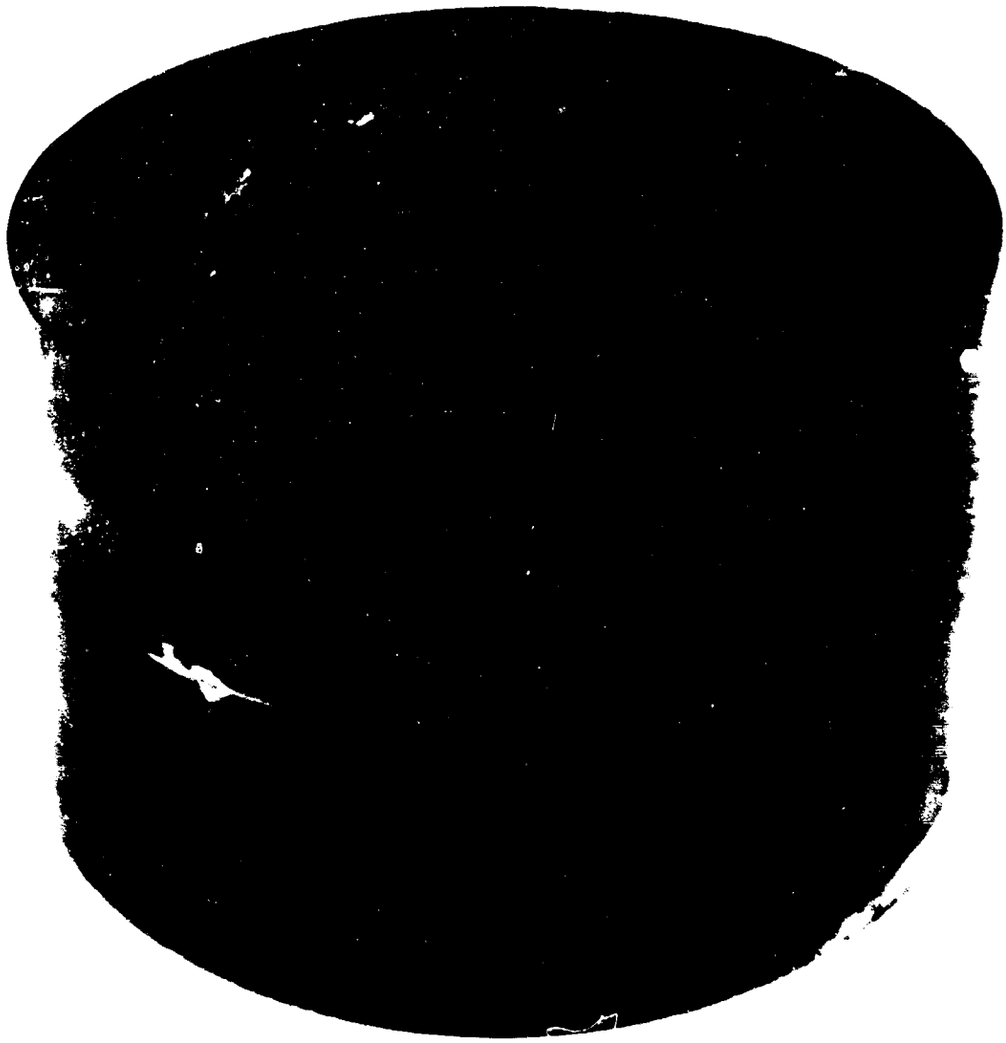

MELTED STAINLESS STEEL RADIATION SHIELD SUPPORT BLOCK

FIG 3·12

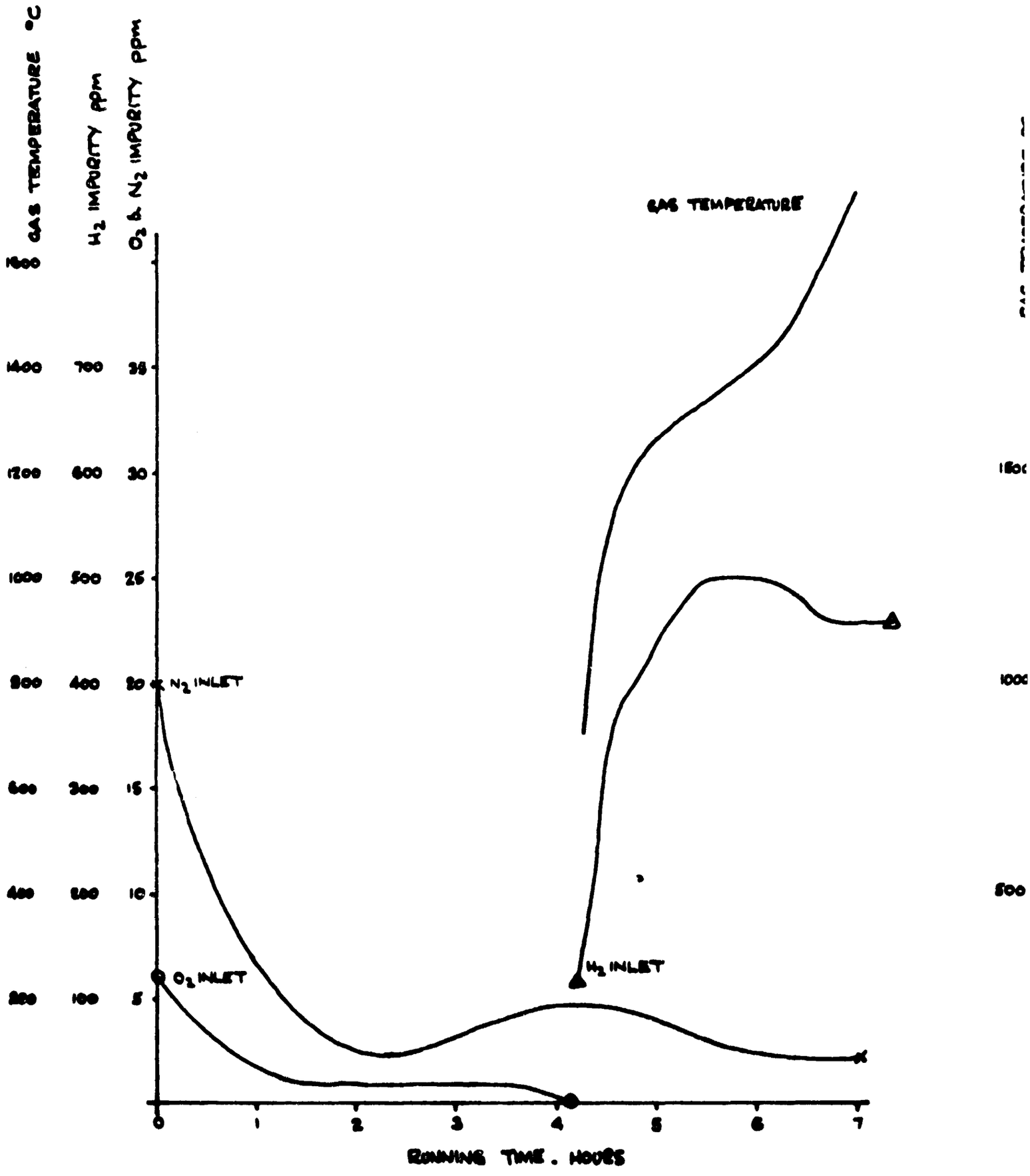

HELIUM PURITY RHTB

FIG 3.13

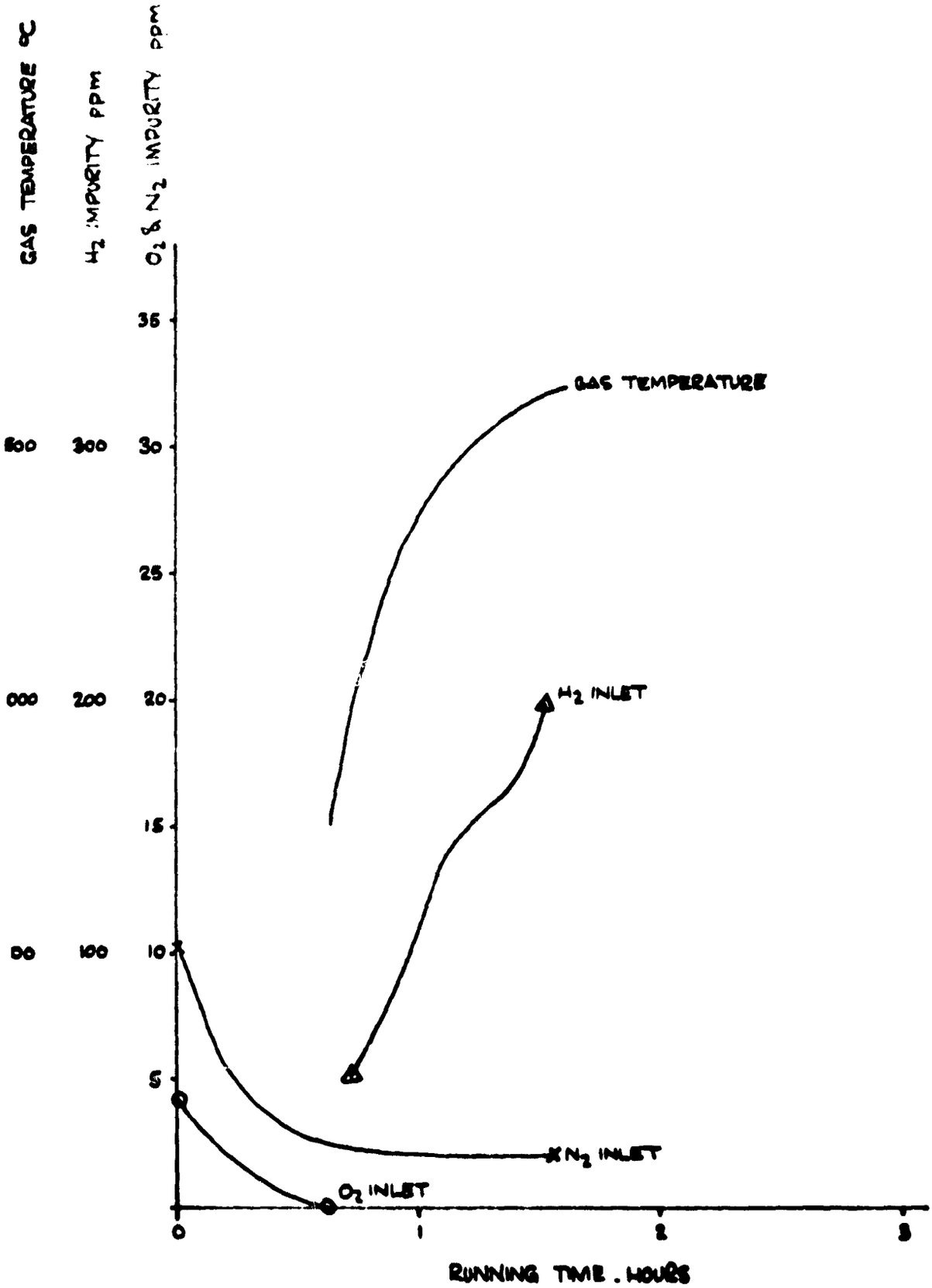

HELIUM PURITY RHT9

FIG 3.14

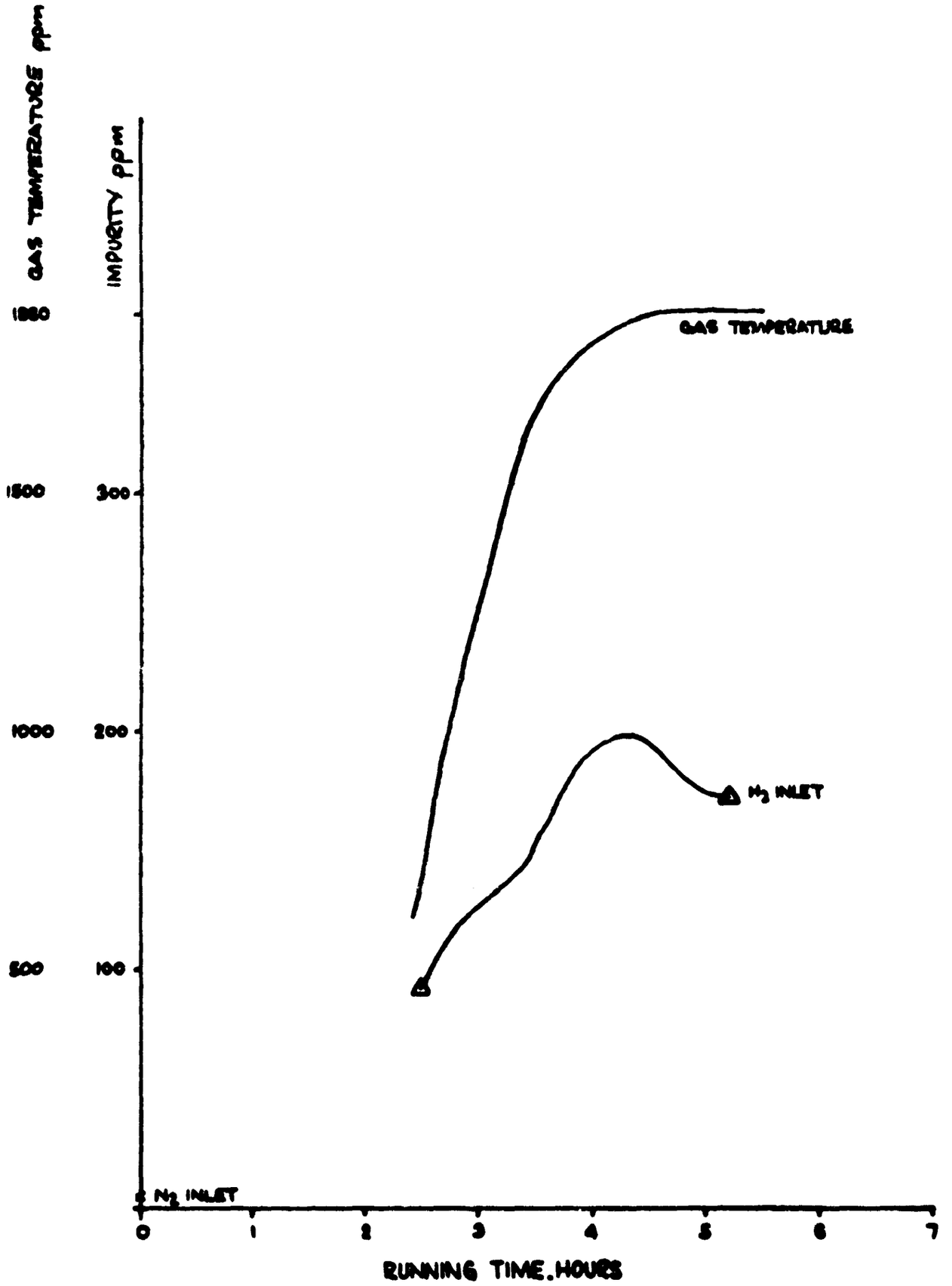

HELIUM PURITY RHT 10

FIG 3.15

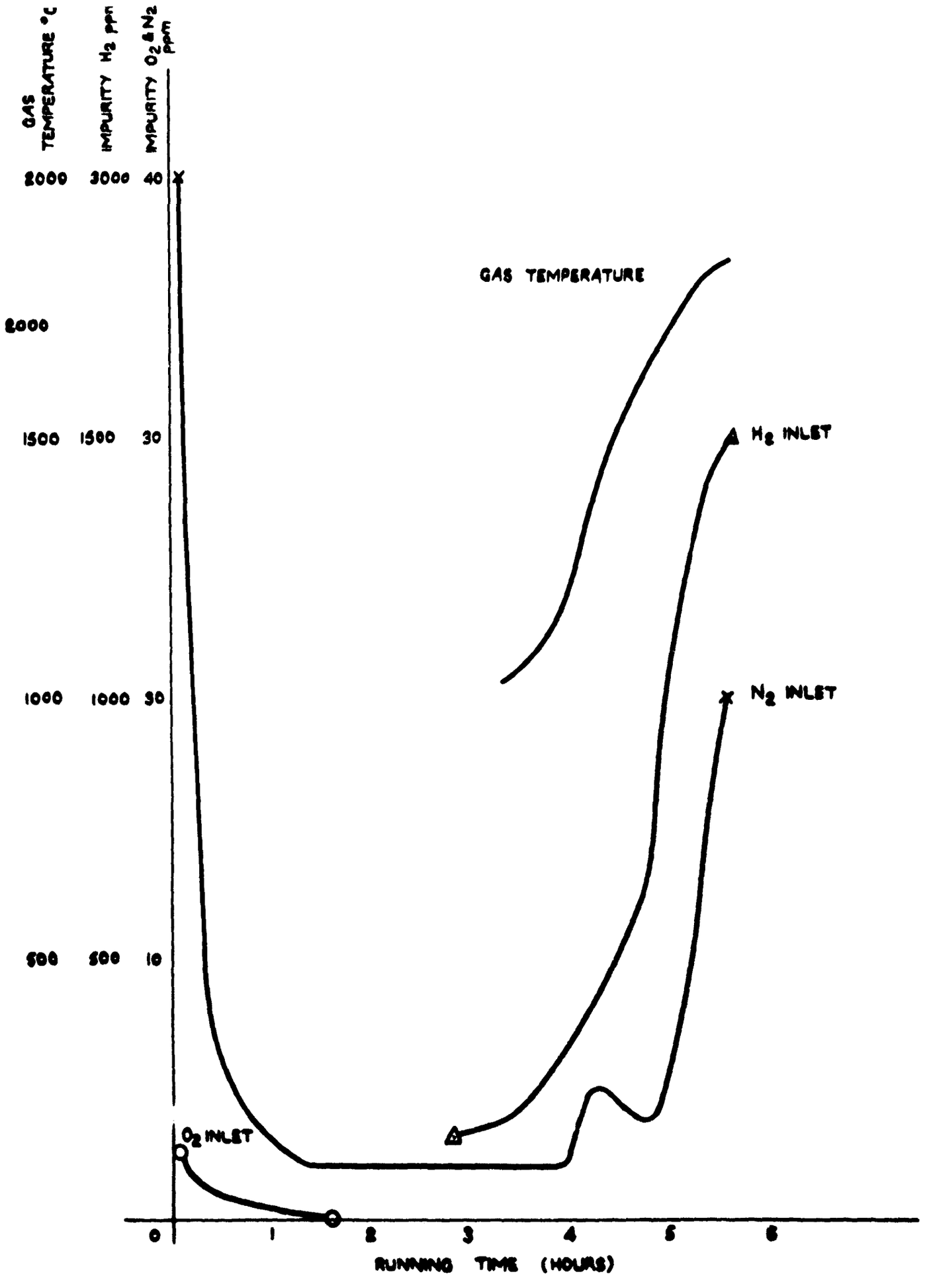

HELIUM PURITY RHT II

FIG3·16

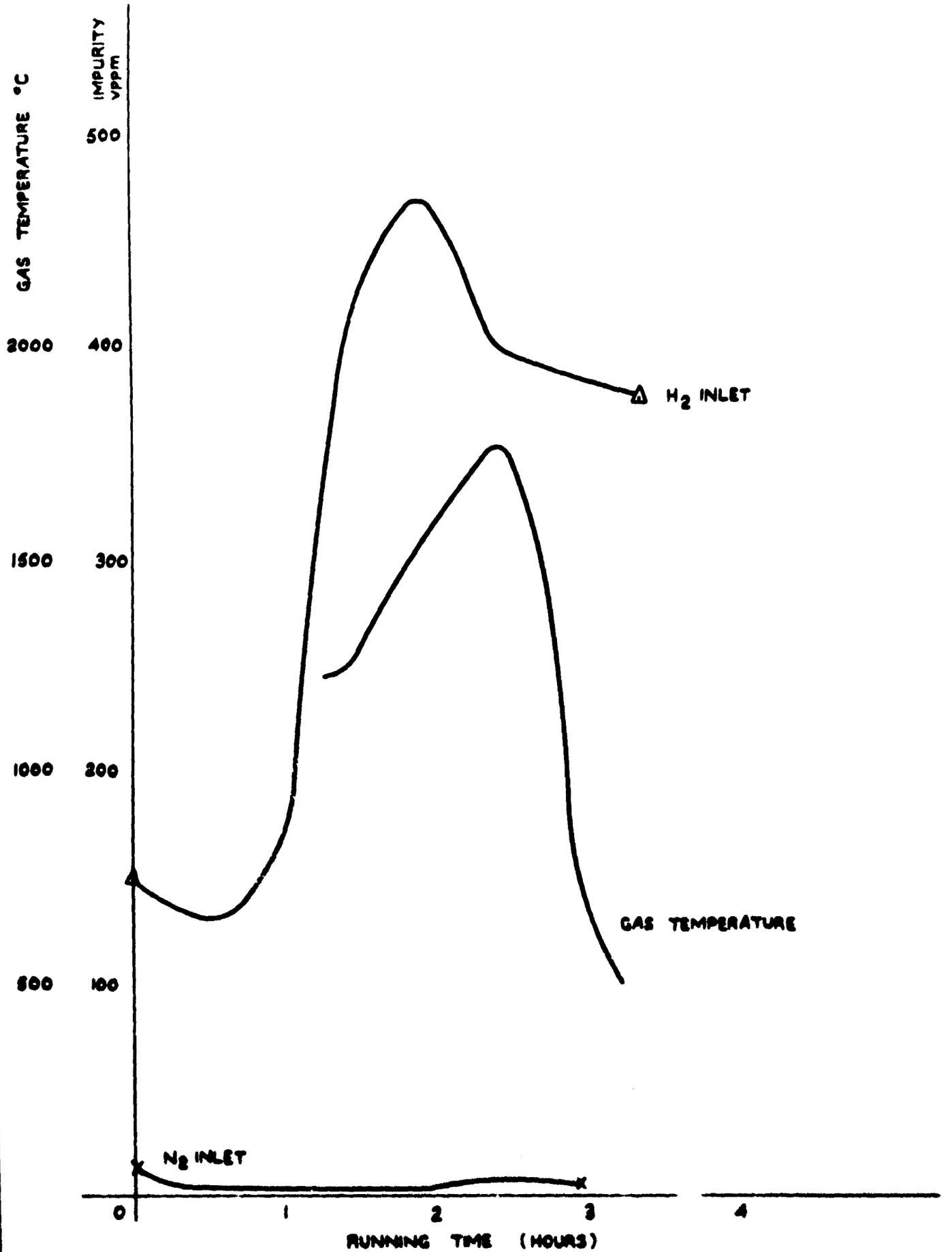

HELIUM PURITY RHT 12

FIG 3·17

CS 20 HIGH TEMPERATURE ELEMENT HEAD FRACTURE
AFTER DISSEMBLY

FIG 3.18

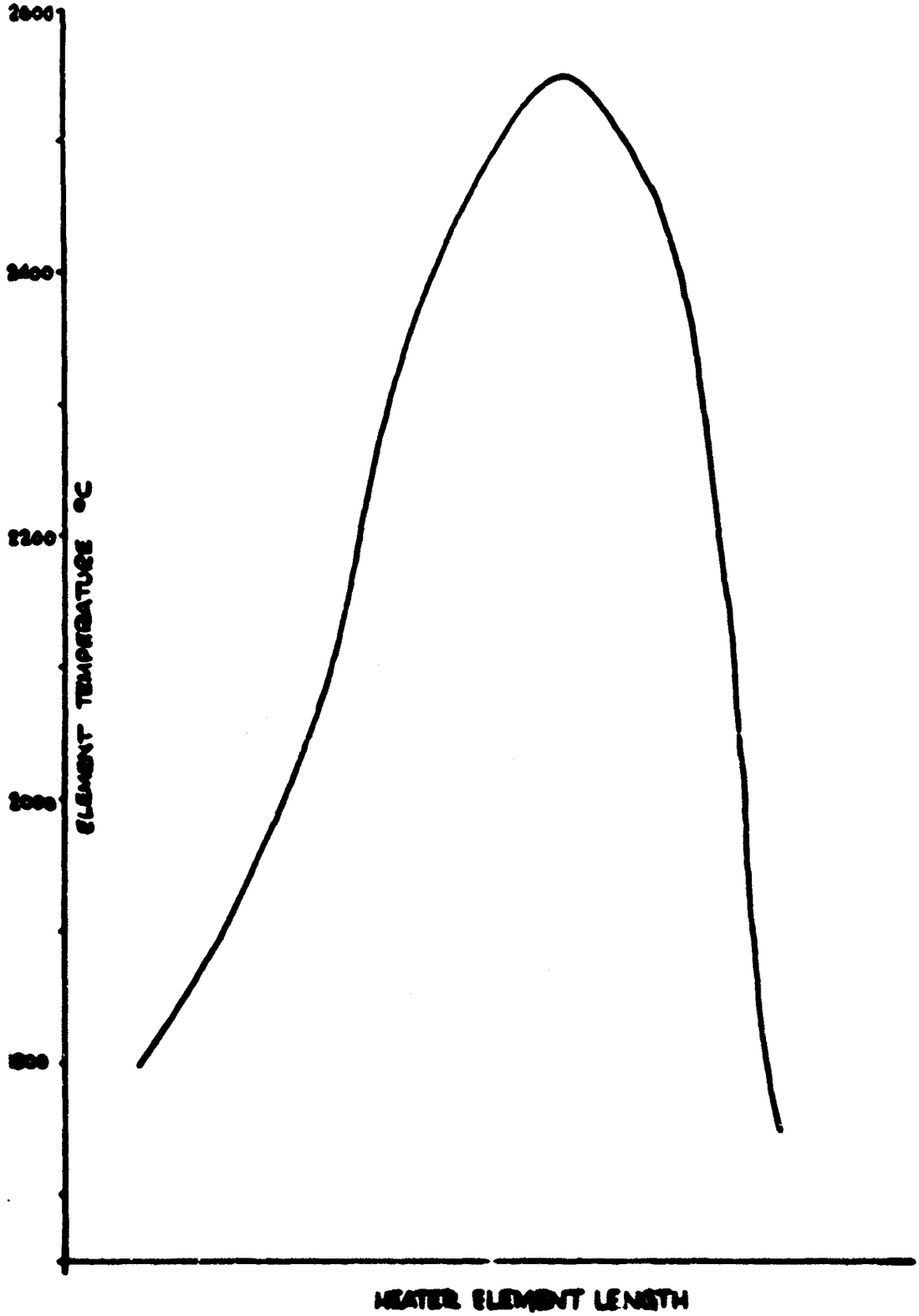

TEMPERATURE PROFILE OF CS 20(2) ELEMENT IN RHT II

FIG 3.19

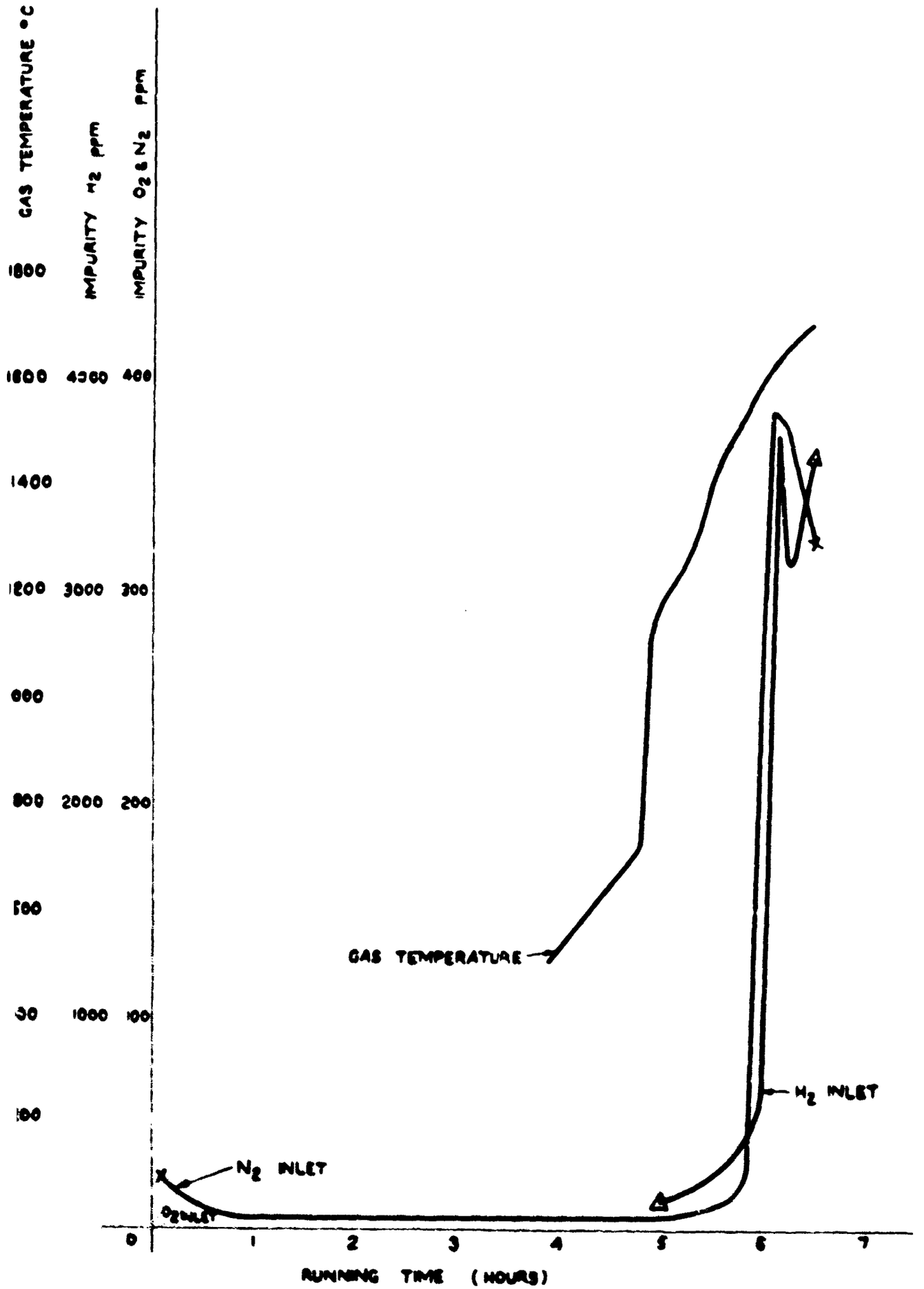

HELIUM PURITY RHT 13

FIG 3·20

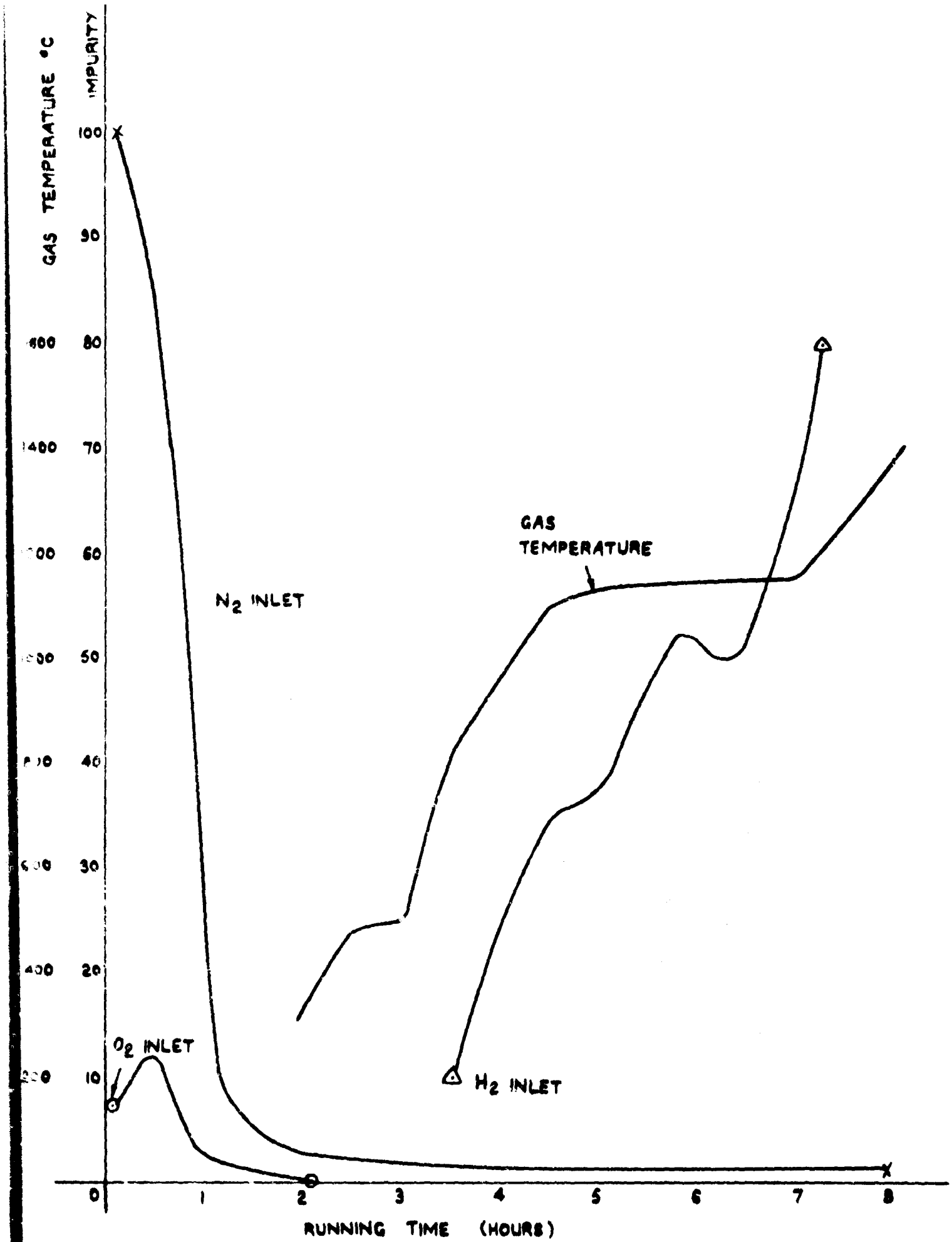

HELIUM PURITY RHT 14

FIG3·21

CRACKED GRAPHITE CONE EXTENSION

FIG 3.22

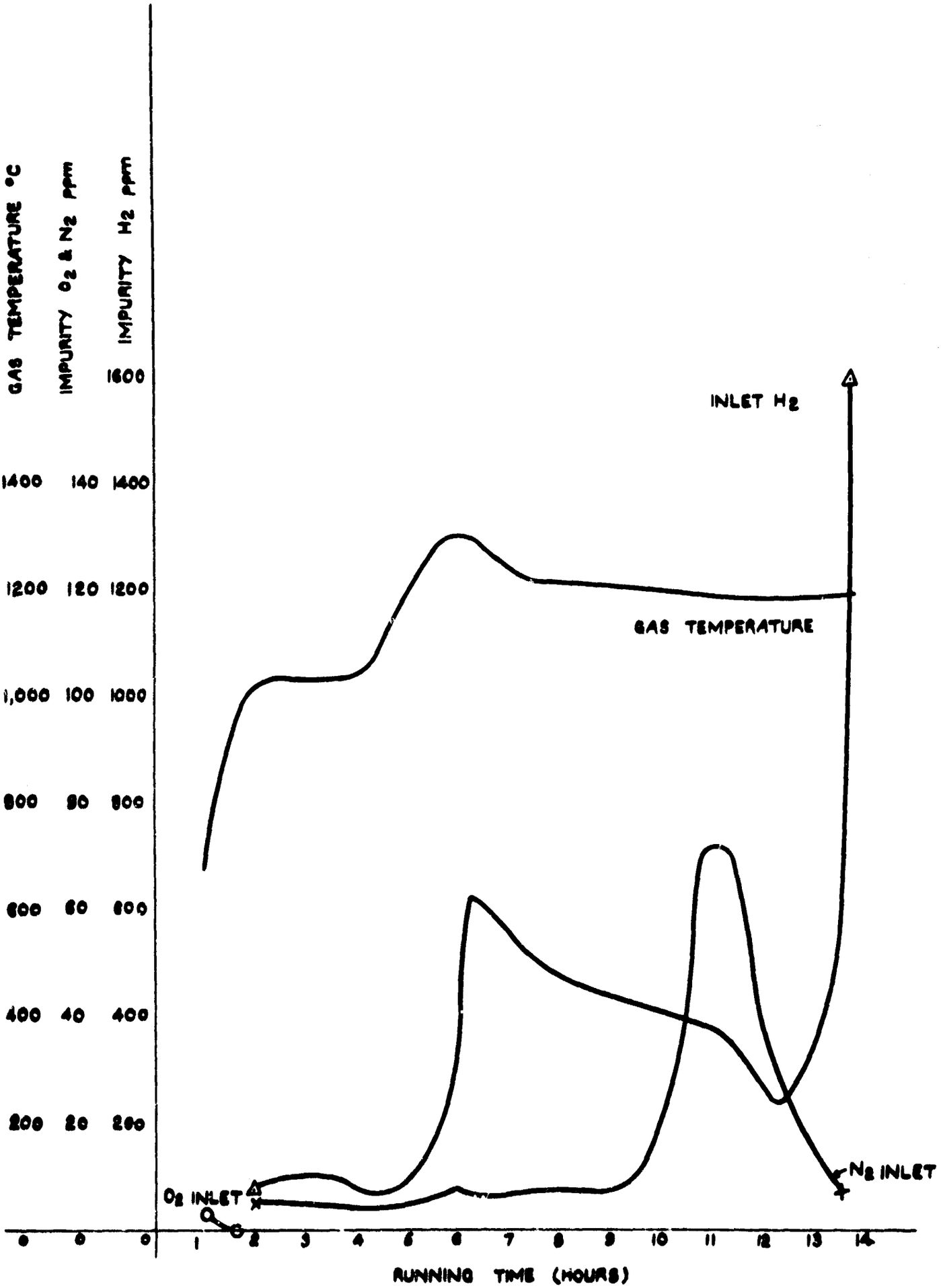

HELIUM PURITY RHT 15

FIG 3-23

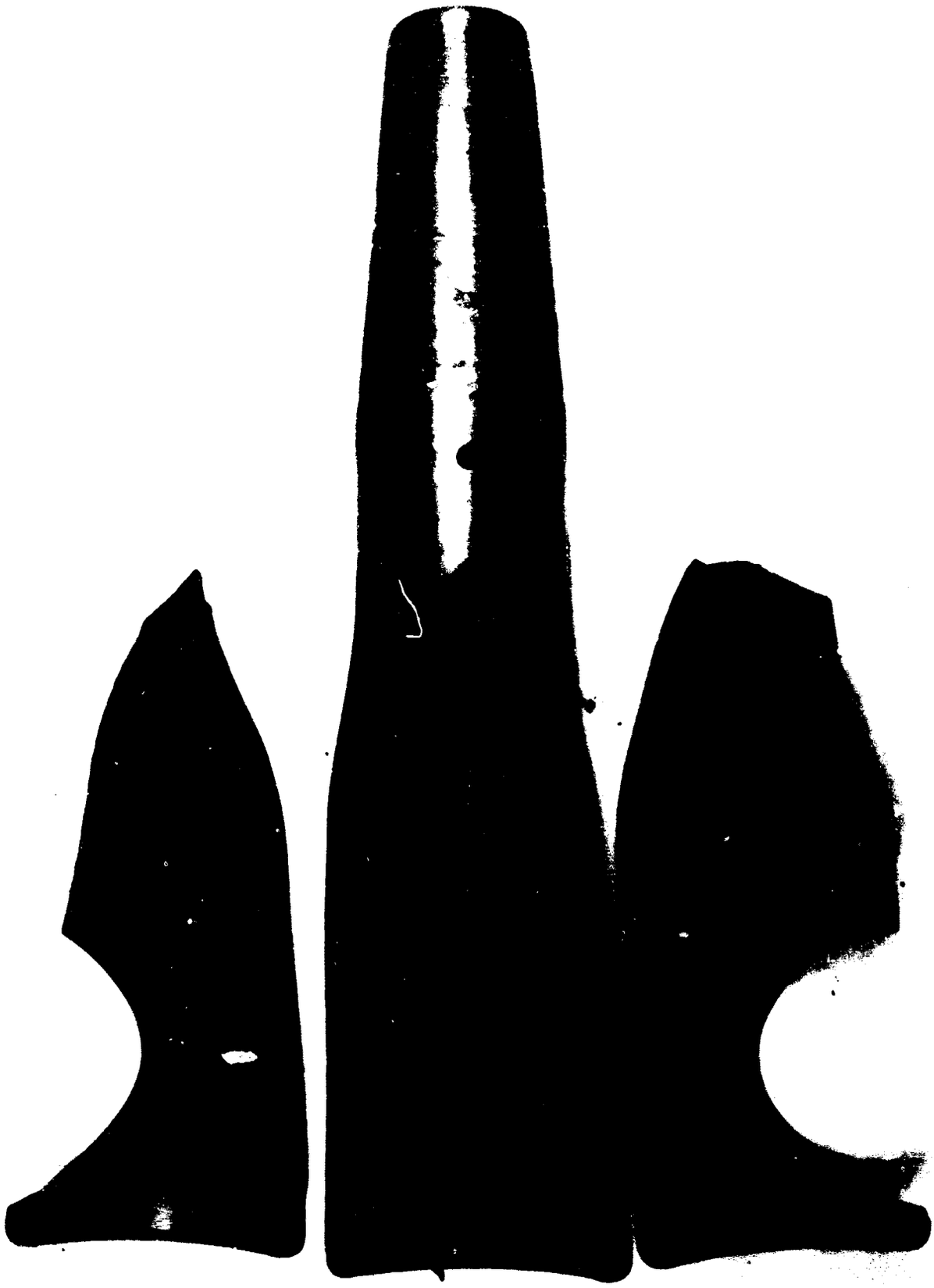

FRACTURED GRAPHITE CONE EXTENSION

FIG 3-24

GAS TEMPERATURE °C

1600

1400

1200

1000

800

600

400

200

0

HIGH TEMPERATURE HEATER COMPONENTS SHOWING
REVISED HEAD CONNECTION

FIG 3·25

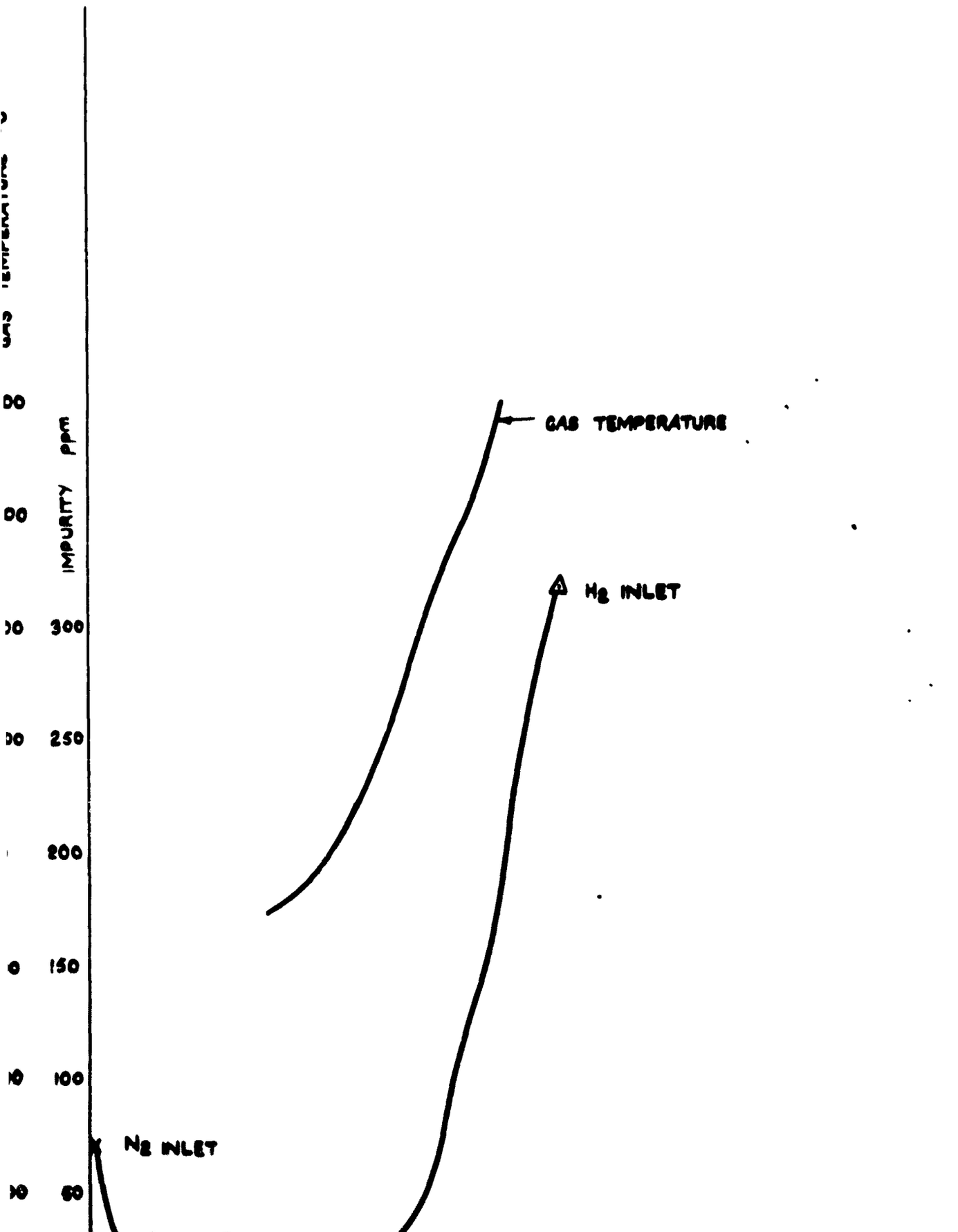

HELIUM PURITY RHT 18

FIG 3-26

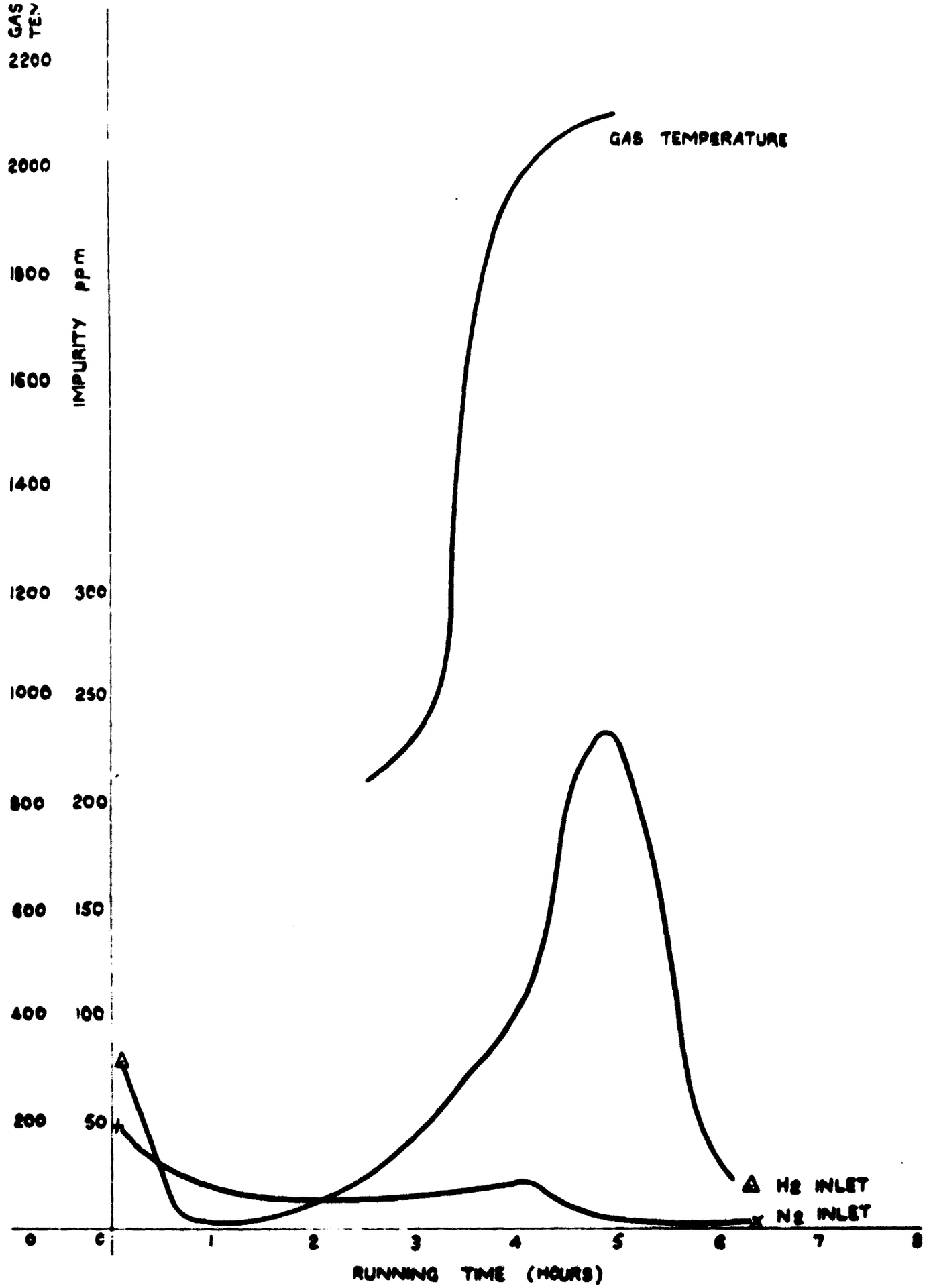

HELIUM PURITY RHT 19

FIG327

CRACKED GRAPHITE INTERFACE

FIG 3·28

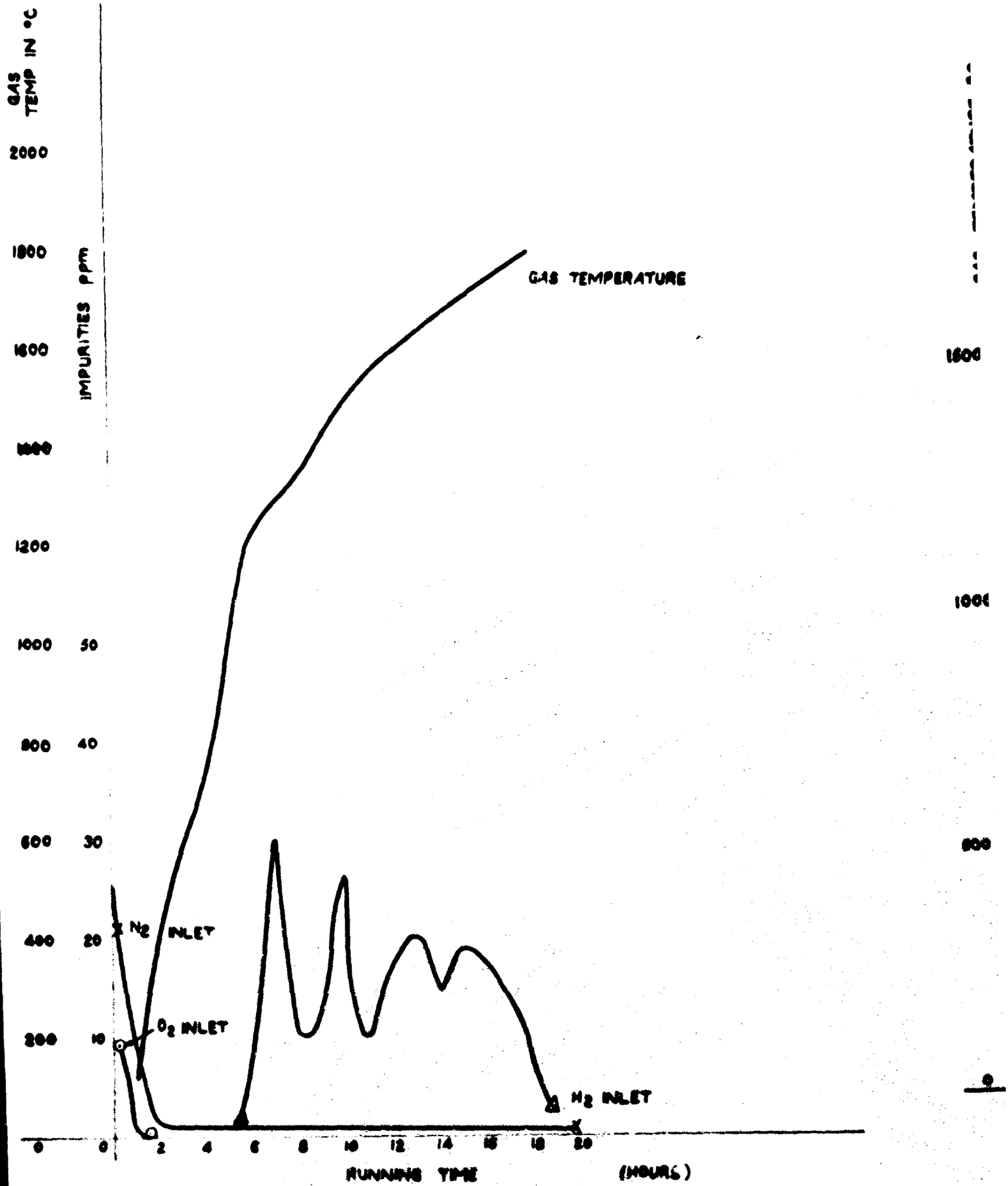

HELIUM PURITY RHT 20

FIG 329

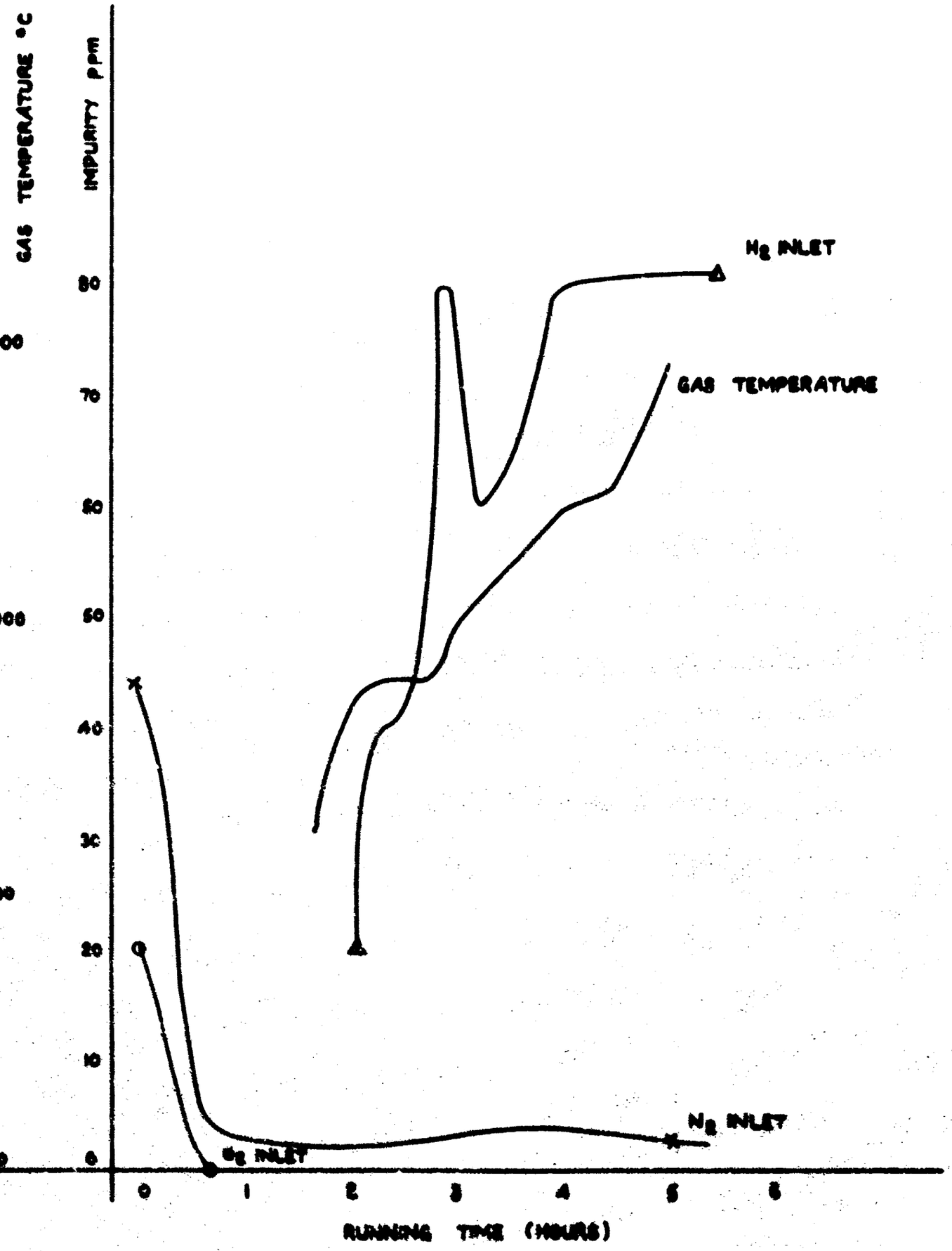

HELIUM PURITY RHT 22

FIG 3·30

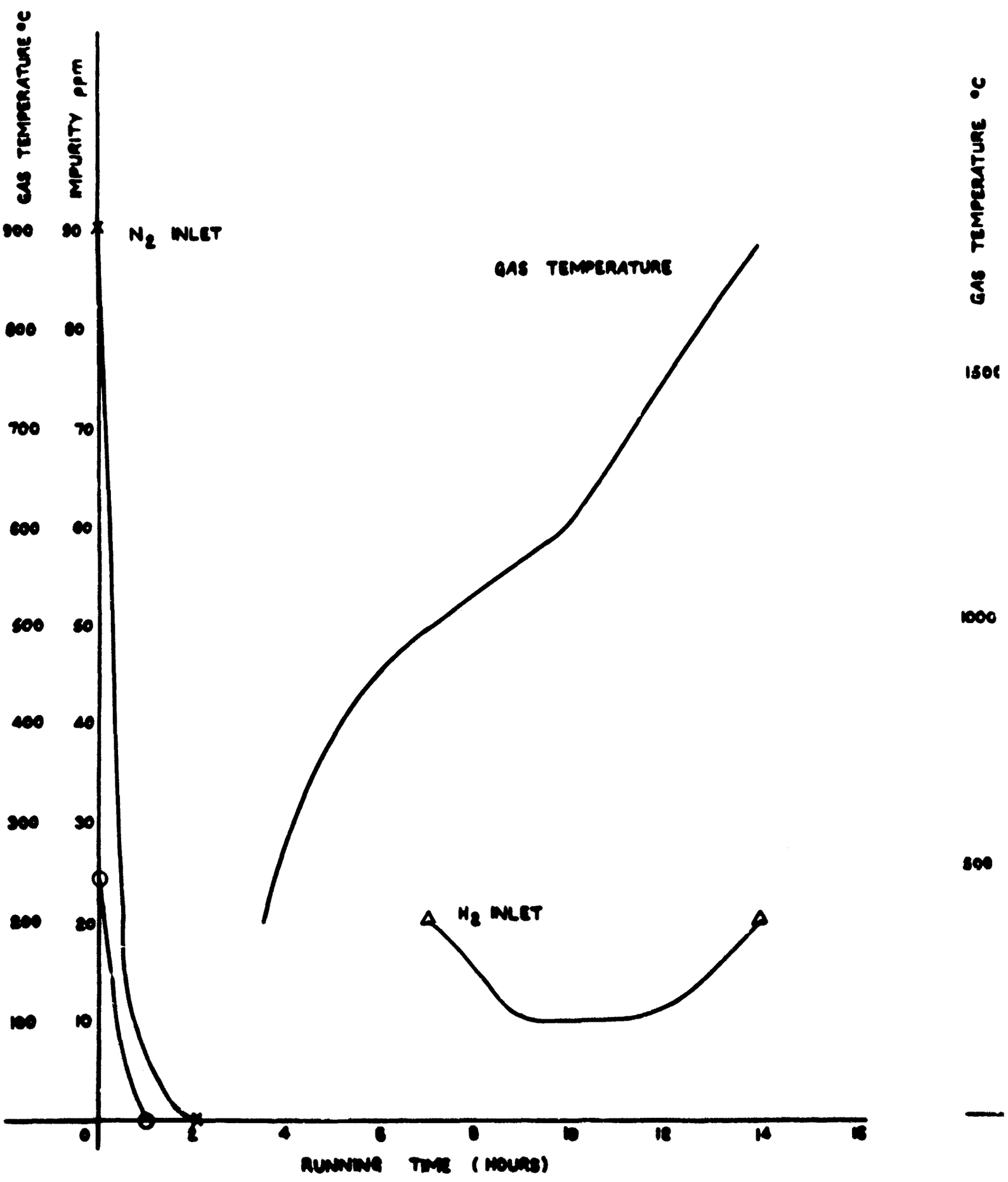

HELIUM PURITY RHT 24

FIG 3·31

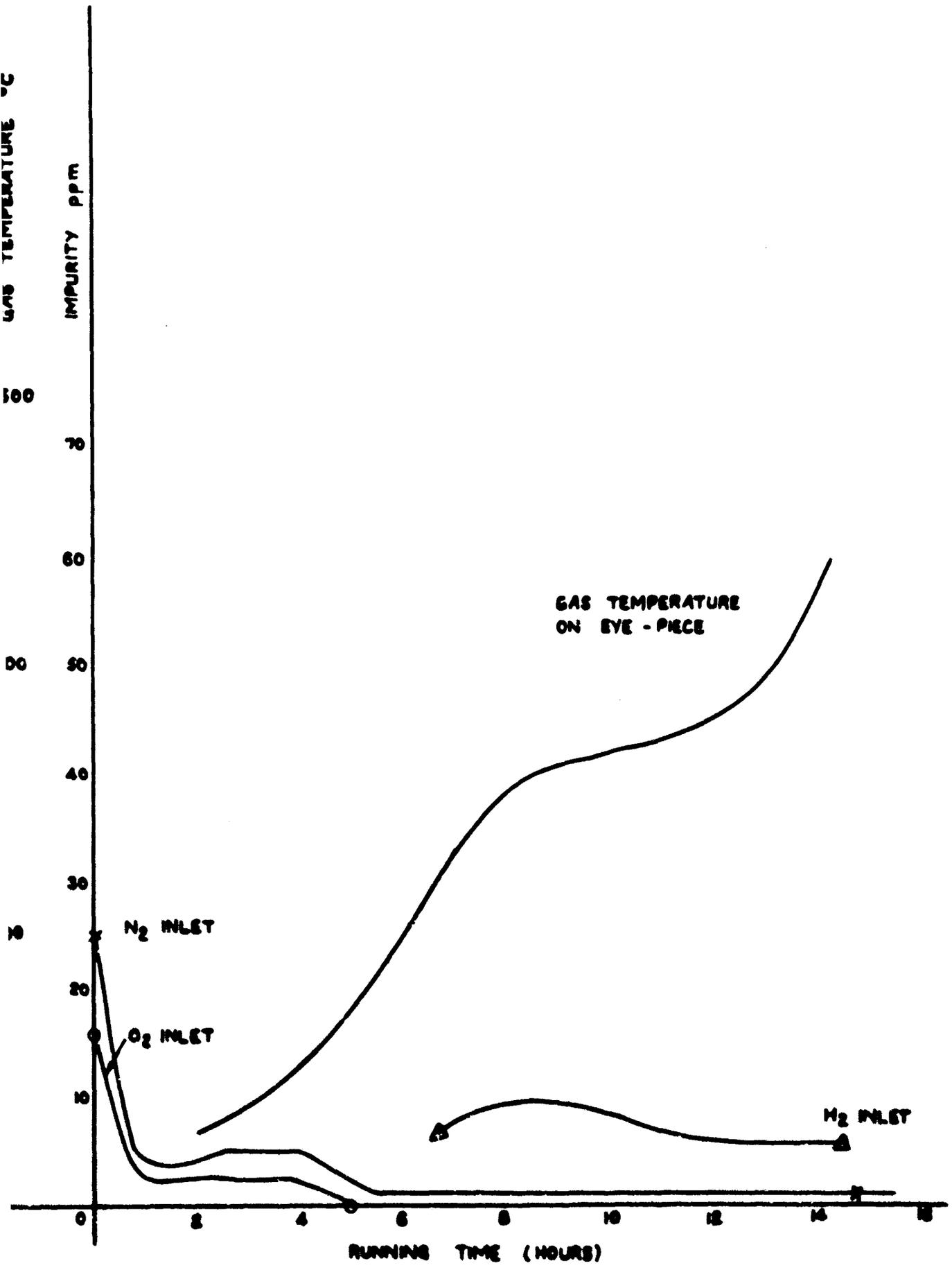

HELIUM PURITY RHT 25

FIG 3·32

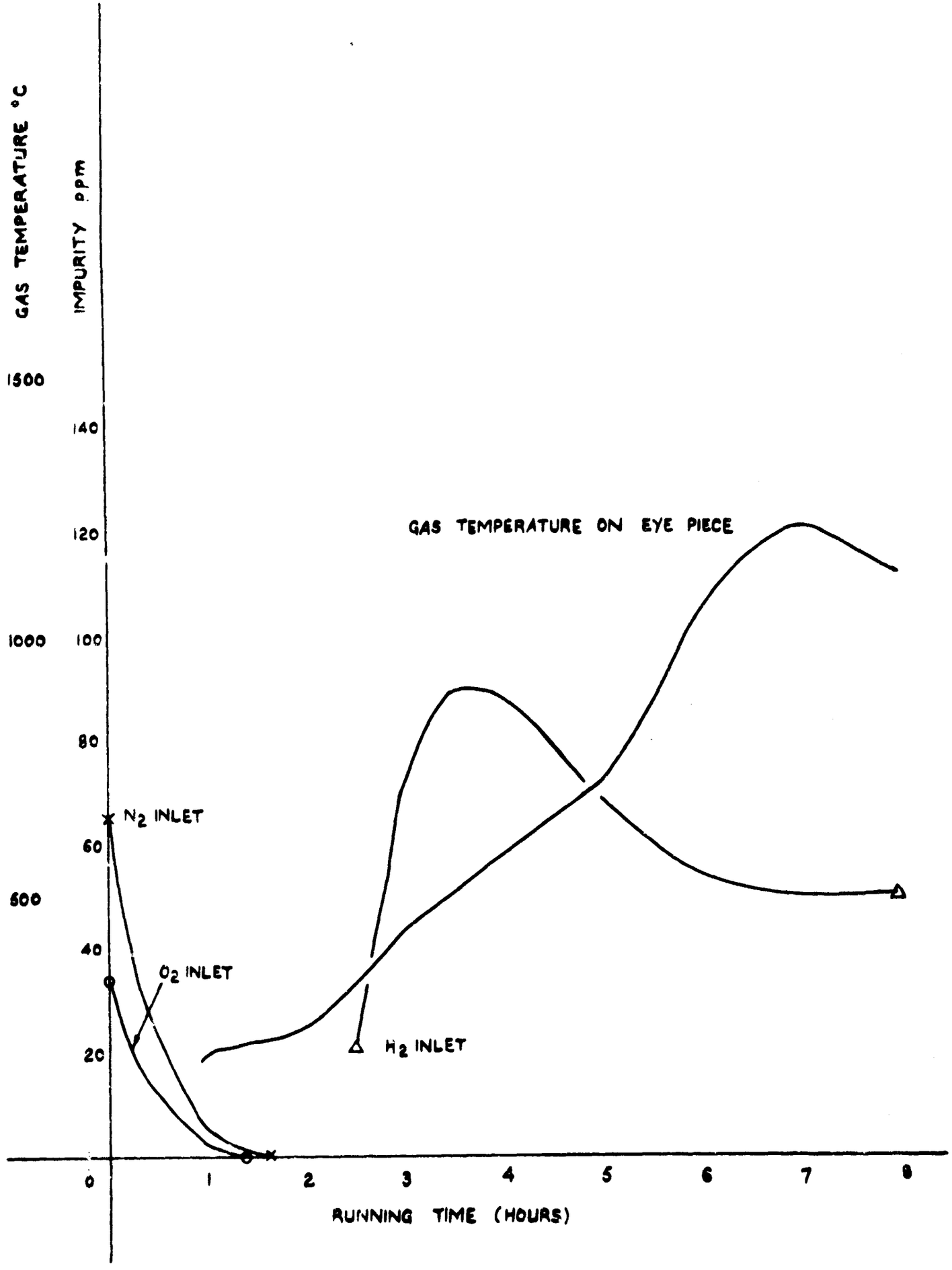

HELIUM PURITY RHT 26

FIG 3·33

ONE INTERFACE SHOWING SEVERE ARCING

FIG 3.34

GAS TEMPERATURE °C

150

100

50

ATTACKED TANTALUM BELLOWS

FIG 3.35

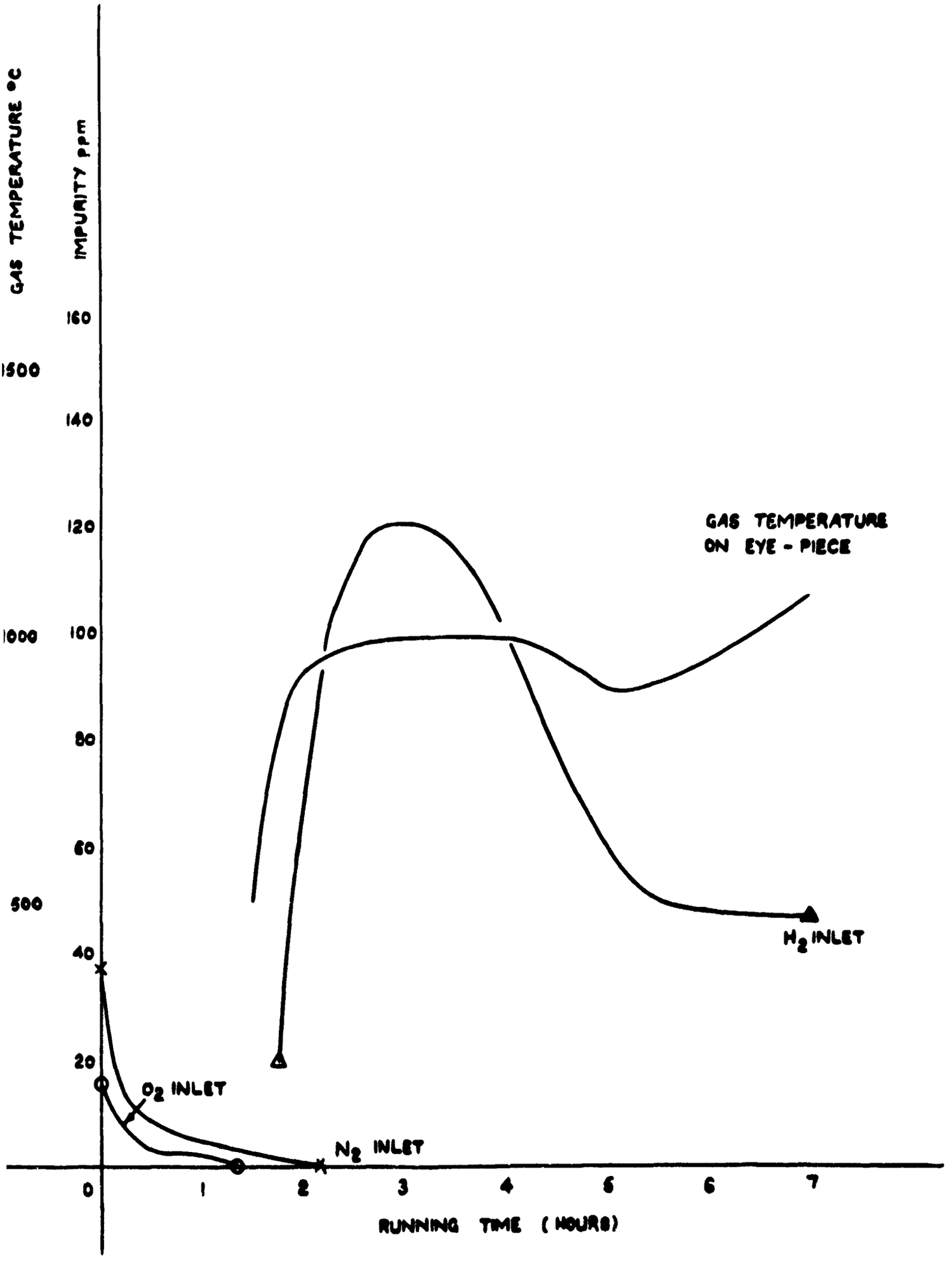

HELIUM PURITY RHT 27

FIG 3·36

OSCILLOGRAPH OF ARC - INITIATION

FIG 3.37

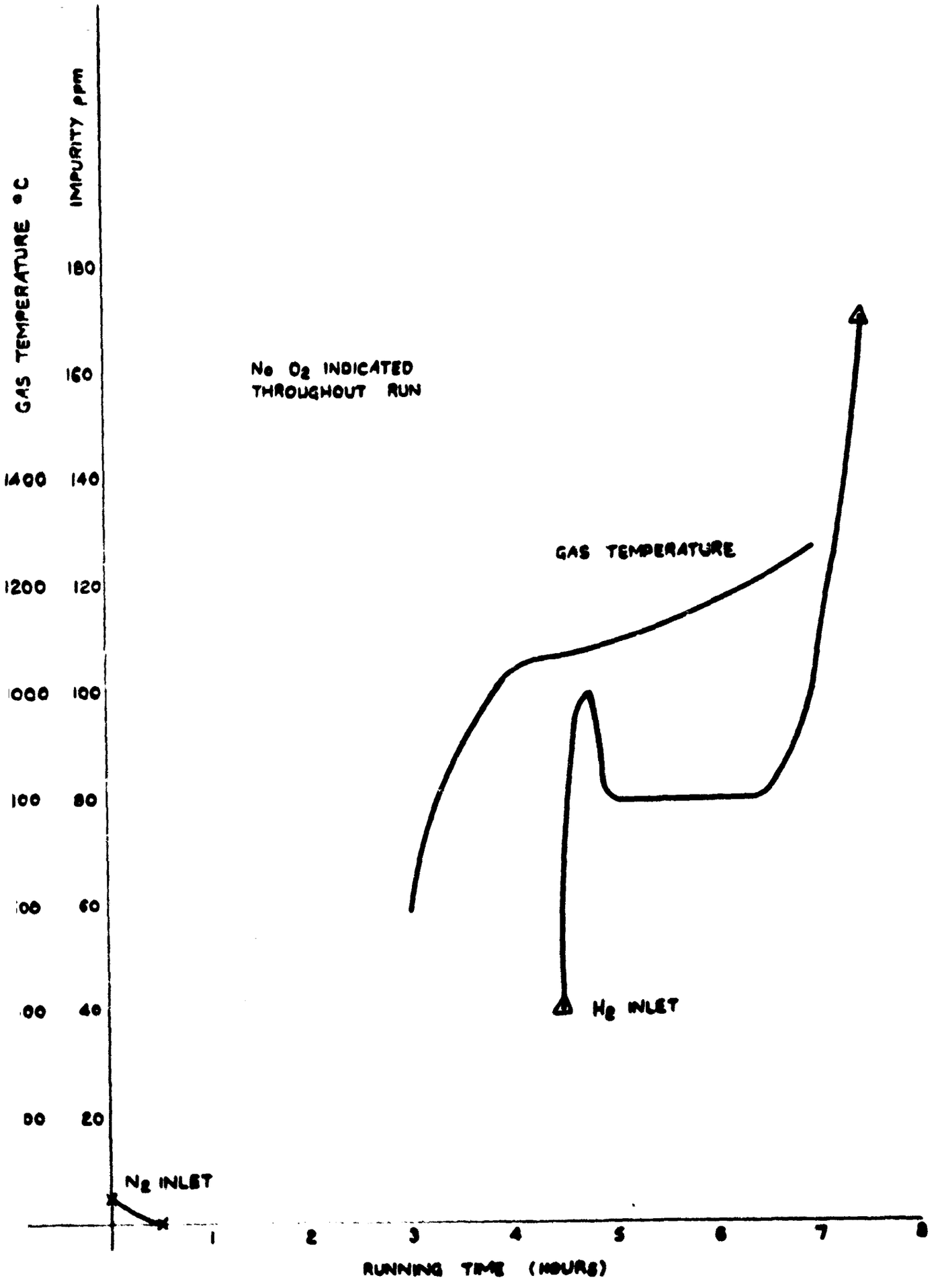

HELIUM PURITY RHT 28

FIG 3-38

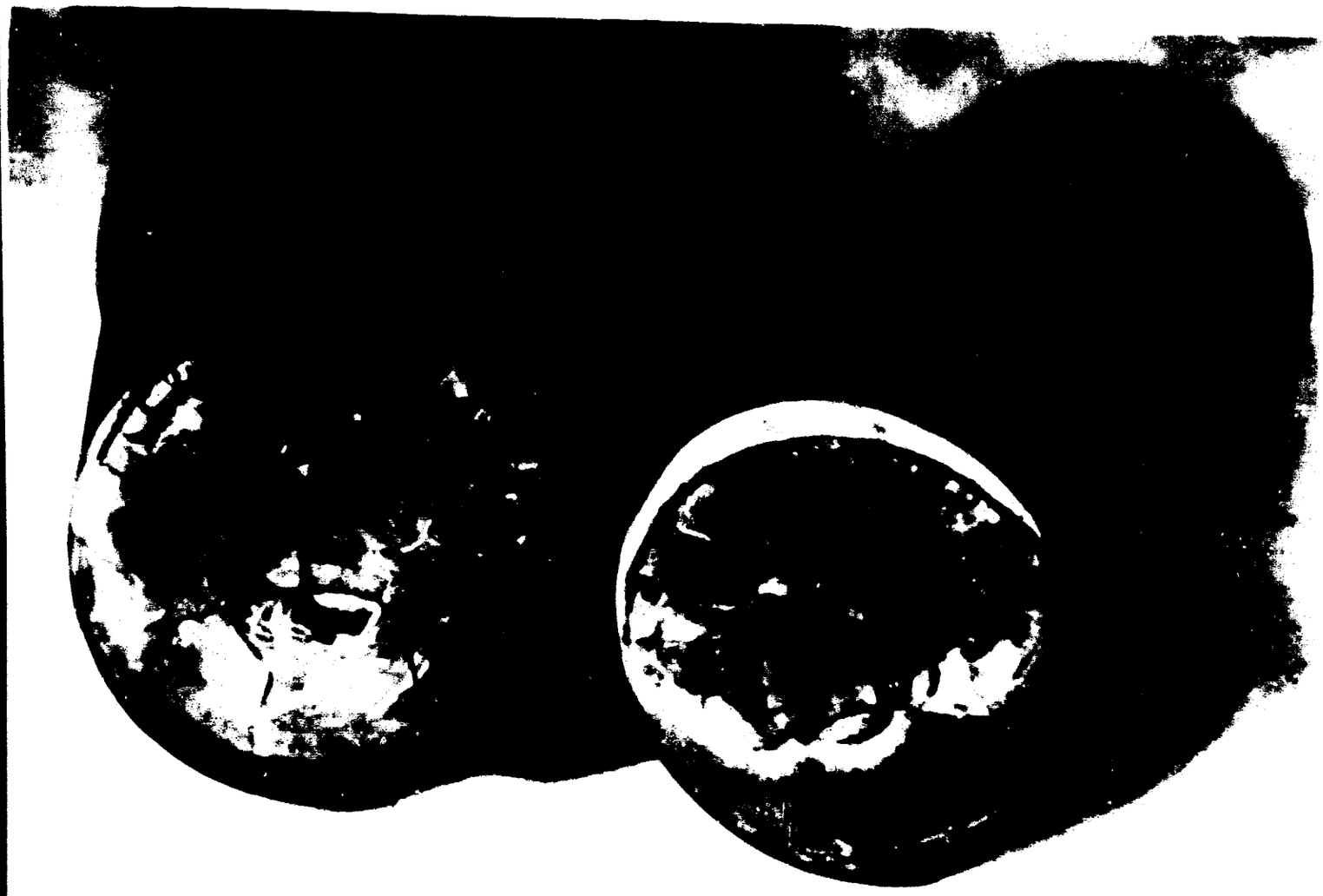

GRAPHITE / GRAPHITE INTERFACE SHOWING EFFECTS OF ARCING

FIG 3.39

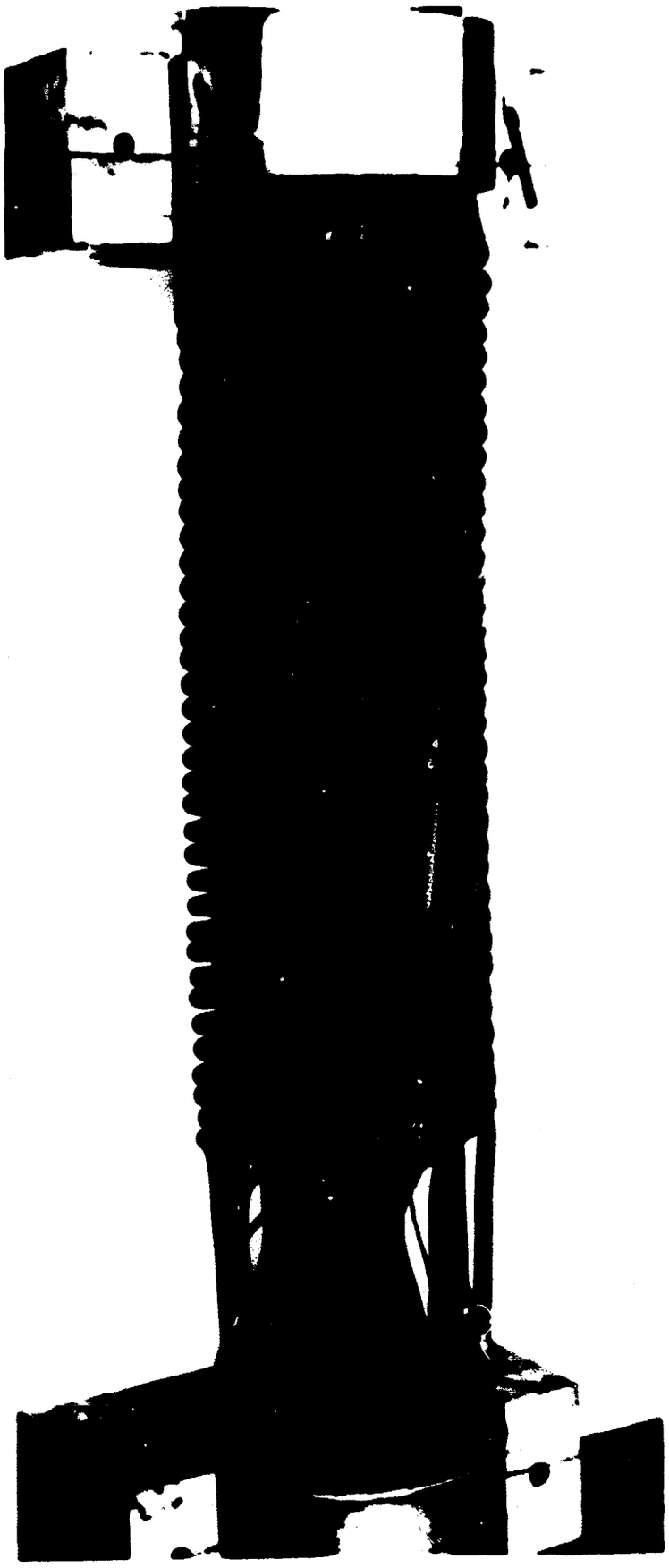

HEAT EXCHANGER COILS AFTER 1800 hr RUNNING TIME

FIG 3.40

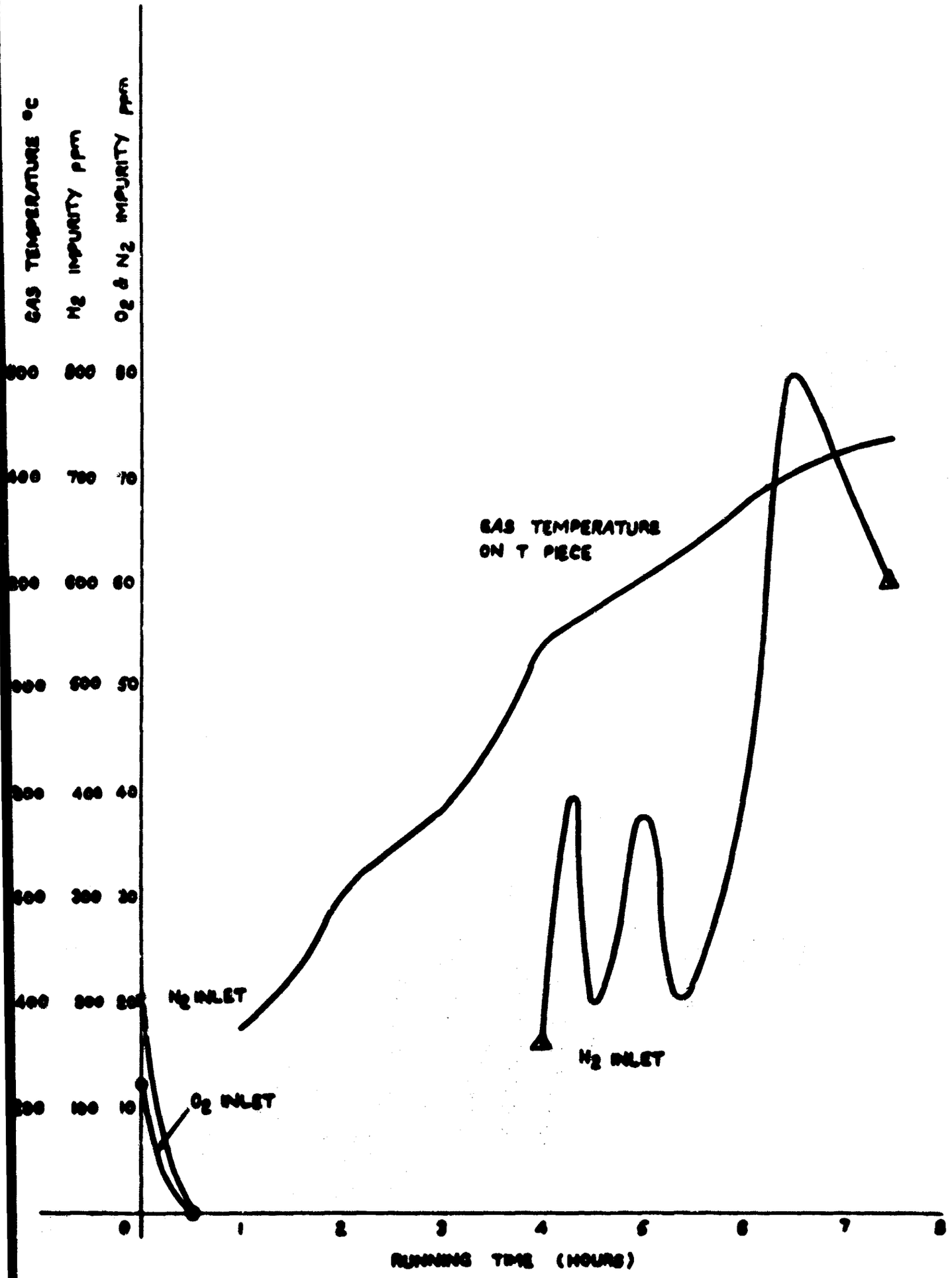

HELIUM PURITY RHT 29

FIG 3·41

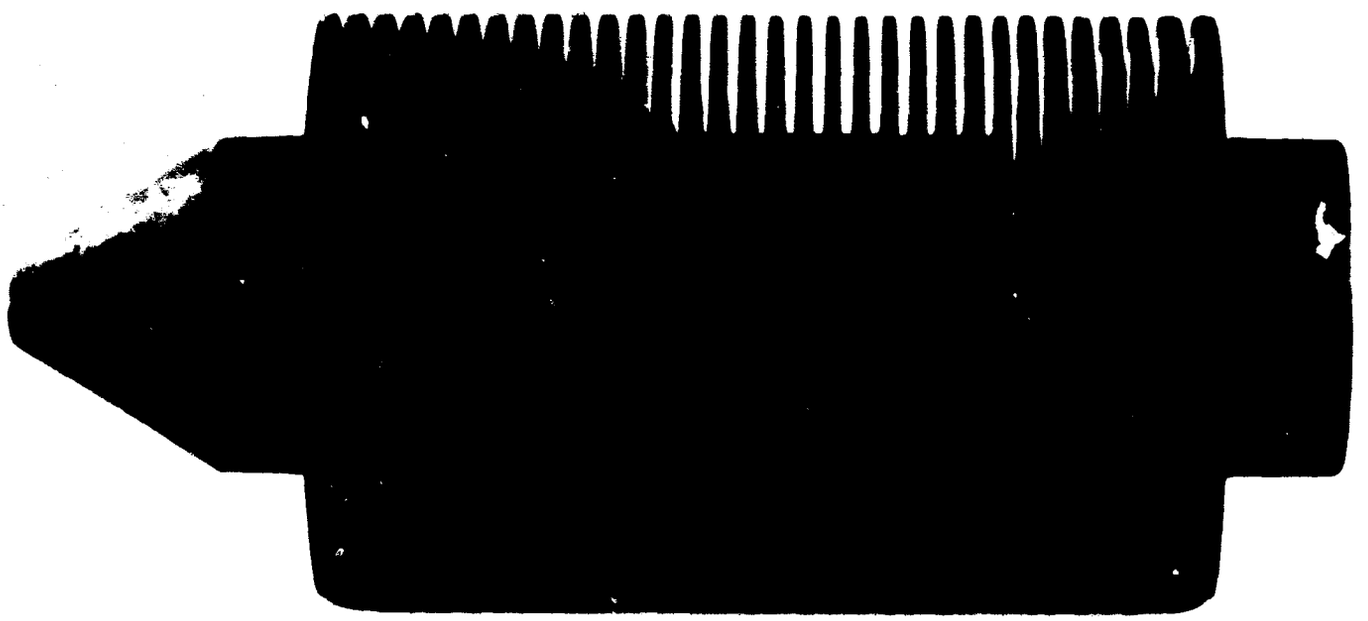

NNED GRAPHITE EXTENSION

FIG 3.42

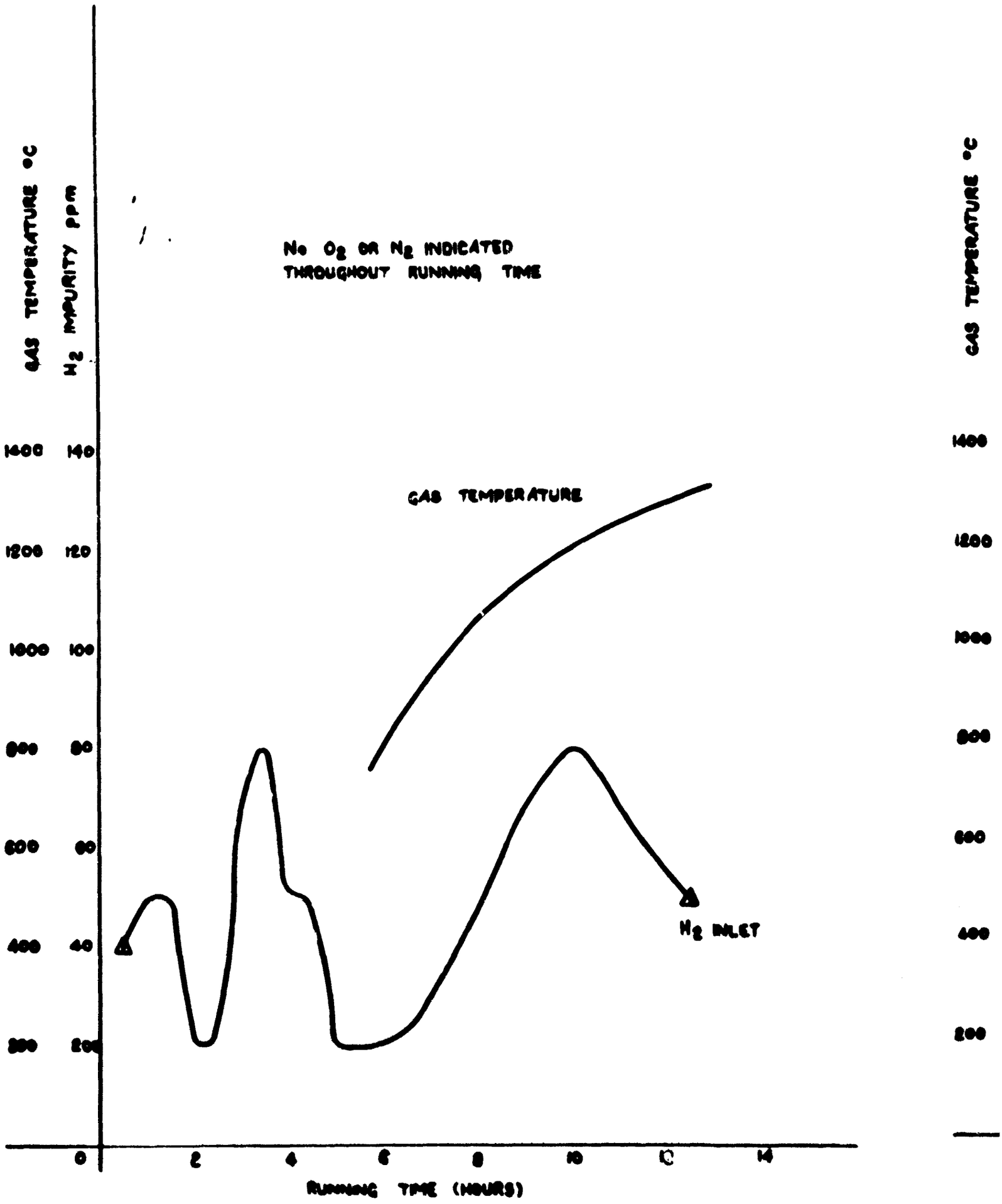

HELIUM PURITY RHT 30

FIG 3·43

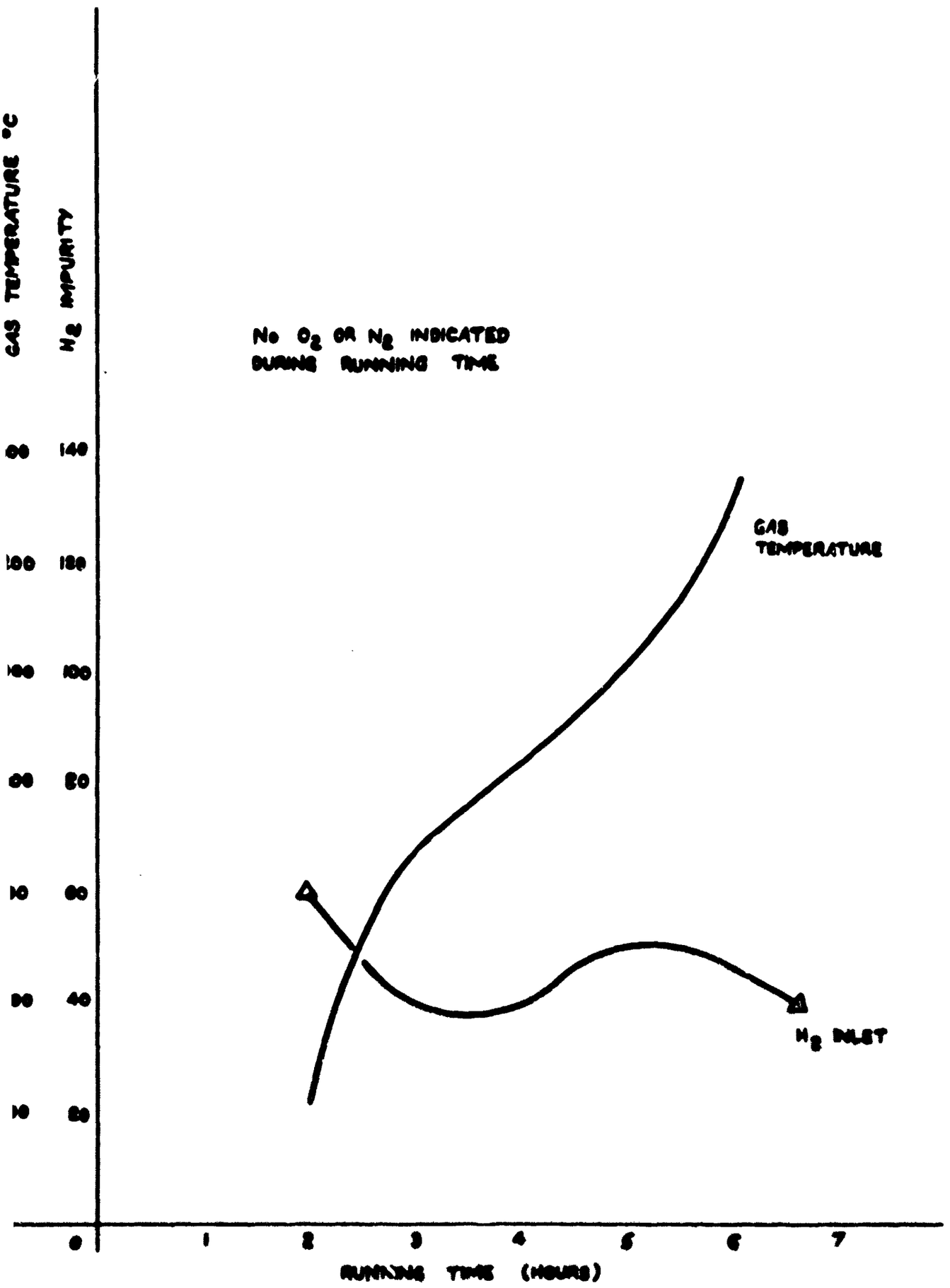

HELIUM PURITY RHT 31

FIG3-44

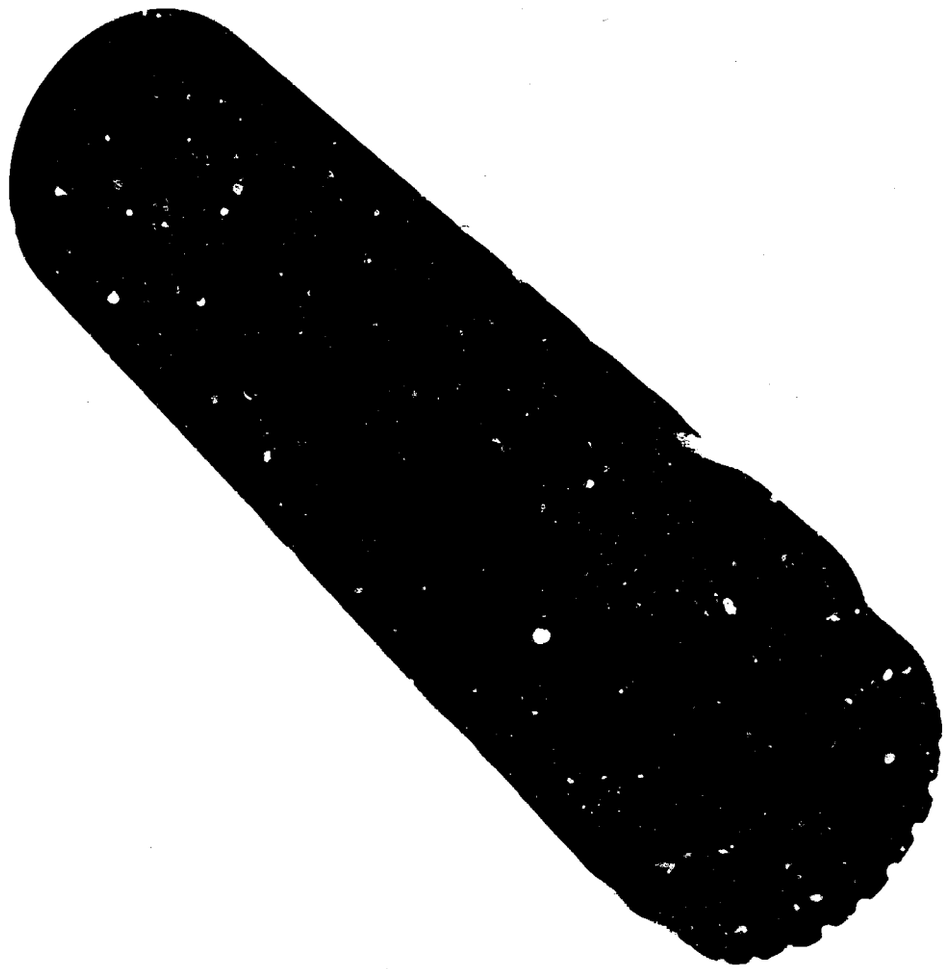

FRACTURED EYX94 ELEMENT SECOND RUN AFTER WATER EROSION

FIG 3·45

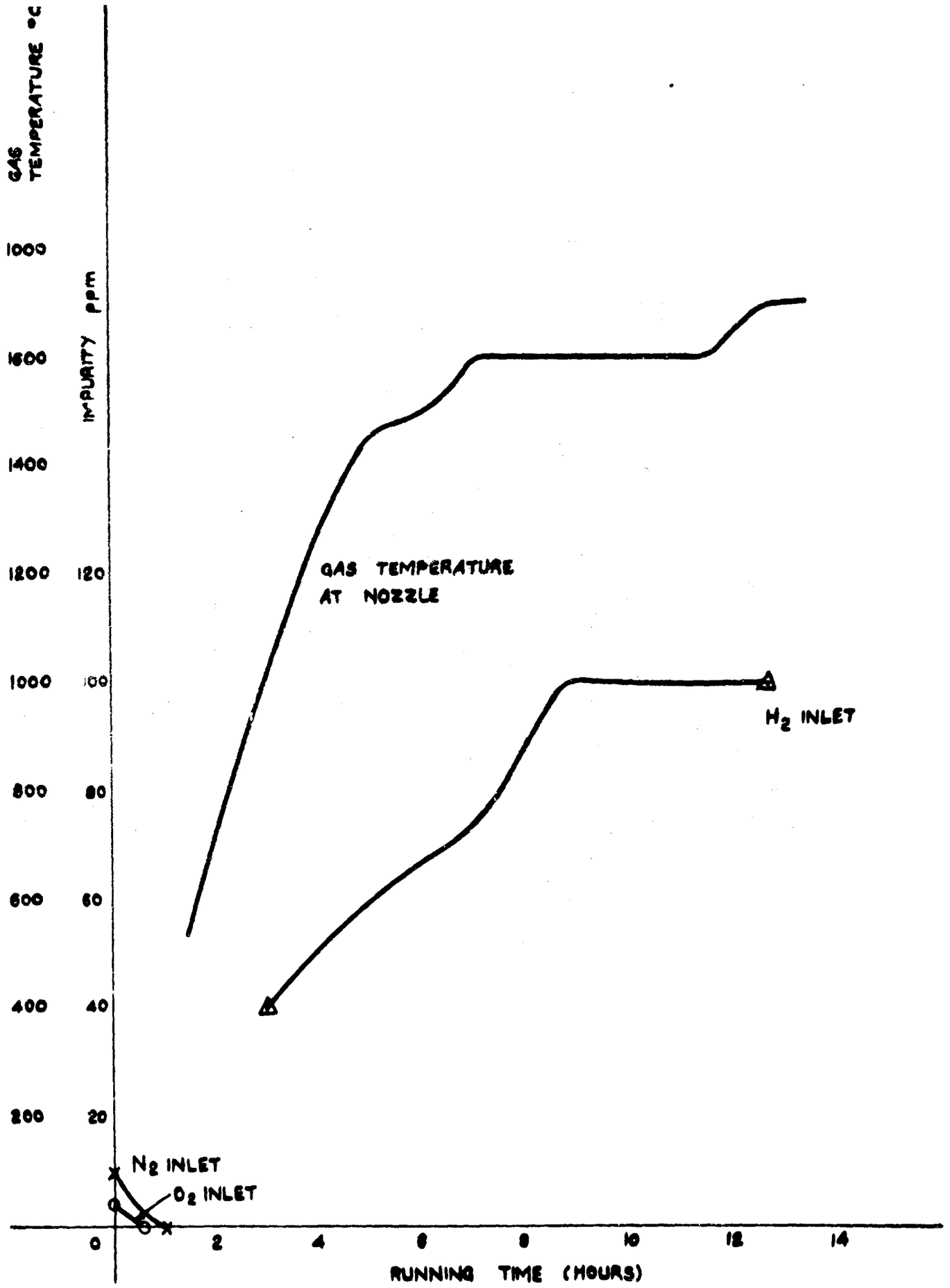

HELIUM PURITY RHT 32

FIG3·46

CHAPTER 4

POWER GENERATION

by

R. Brown, W.J. Slator, V. Brown, K. Cass and J. Davidson

4.1 UNSEEDED OPERATION

With the 2-electrode recrystallized alumina generator duct assembly, during operation at 2200°K (RHT 20), a magnetic field of 1.2 T was applied but no signal obtained fr m a valve voltmeter connected to the electrodes; this indicated an impedance in the channel high compared with that of the leads and voltmeter. At this temperature the gas impurity levels were:

Gas	ppm
H_2	< 30
N_2	< 0.8
O_2	< 0.2
CO	< 0.5
CH_4	< 0.5

4.2 CESIUM-SEEDED OPERATION

Preparations for a cesium-seeded power generation run began on 18 March 1964, with the objective of seeded operation at nozzle inlet temperatures above 1900°K. The heater was previously vacuum-outgassed to about 2500°K, a minor problem being loosening of the copper head clamp connection to the high temperature heater which was retightened.

On start up, cold gas circulation for 45 min gave a total impurity level of less than 3 ppm. At a nozzle inlet temperature of 1100°K the copper head connection loosened again. This was corrected by increasing the diffuser air cooling (thereby reducing the temperature of helium entering the heater) and helium cooling to the head connection, and also an increased heater power input; the combined effect was to re-clamp the connector, clearly indicated by records of

temperatures at the connector interface.

At 1600°K (heater outlet temperature) the hydrogen content had increased to about 100 ppm, necessitating prolonged operation at this temperature; the hydrogen level at purification plant outlet was always less than 2 ppm. At 1810°K (0030 hr on 19 March 1964) choking conditions on the nozzle were gradually achieved (with a mass flow of ~9 gm/sec), by opening the circulator inlet valve. At 0120 hr final preparations for seeding were in progress when the nozzle inlet high temperature thermocouple failed at a gas temperature of 1910°K; temperature indication was re-established shortly afterwards. Cesium lines were purged and the cesium container maintained at between 35° and 38°C.

The power generation runs detailed in Chapter 5 were then carried out over a period of about 5 hr. Full diffuser air cooling was required to achieve a satisfactory operating temperature. The high temperature heater case glowed red, and there was evidence of minor arcing. Difficulty was experienced with blockage of the cesium feed and excess helium pressure was required to clear this. At the final stages the circulator noise characteristic gave some cause for anxiety.

4.3 LOOP CHARACTERISTICS

Extensive measurements of temperatures, pressures, etc. have been made on all runs to characterize the various loop components. A full analysis is in progress and will be presented in the next Technical Summary Report.

CHAPTER 5

MPD EXPERIMENTS WITH A HELIUM-CESIUM LOOP*

by

B.C. Lindley, R. Brown and I.R. McNab

5.1 INTRODUCTION

A broad research programme, based on a pilot-scale closed-loop helium-cesium facility, a series of supporting plasma physics experiments, and theoretical studies, has been undertaken at the IRD laboratories. The work is closely associated with the possibility of utilizing a high temperature nuclear reactor heat source in conjunction with an MPD generator and steam cycle, the overall efficiency of such a system being estimated as up to 60 per cent. The main objectives of the present programme are: to demonstrate the technological feasibility of an MPD direct power generator in a loop closely simulating the ultimate nuclear reactor closed-cycle system; and to establish an understanding of the fundamental processes of power extraction by the MPD technique.

One of the most important aspects of closed-cycle MPD electrical power generation now being studied is the possibility of using non-equilibrium enhanced ionization, particularly when this effect is due to magnetically-induced elevated electron temperature. For thermal equilibrium ionization, temperatures of about 2500°K are considered necessary for useful electrical conductivity and power density; under non-equilibrium conditions, high power densities may be obtained at 1800°K or even lower. Projected performance from very high temperature nuclear reactors of the OECD Dragon type indicates that gas temperatures of 1500° to 1800°K may eventually be achieved. This type of reactor will operate with purified helium as the coolant, as in the helium-cesium MPD loop to be described.

5.2 MPD EXPERIMENT

5.2.1 The closed-cycle loop

In the MPD closed-cycle loop (Figs 5.1 and 5.2), continuously filtered and purified helium passes through an electrical resistance heater (to simulate the nuclear reactor) which is capable of producing gas temperatures up to 2500°K. A metered flow of cesium vapour is introduced before the mixture expands to a high

---

* To be presented at the International Symposium on Magnetohydrodynamic Electrical Power Generation. Paris, July 1964

velocity through a rectangular-section nozzle. In the present arrangement a supersonic flow of helium and ionized cesium passes through the MPD generator duct (alumina or boron nitride) and a subsonic diffuser to a recuperative heat exchanger and final cooler. Cesium is removed in a cold trap before the helium re-enters the circulator. The selected design parameters of the test facility and first generator section ar

helium mass flow, gm/sec	1 - 10
seeding	up to 3 a/o cesium
helium purification	up to 4% of mass flow to reduce the content of impurity gases to less than 5 ppm (by volume)
expansion nozzle inlet temperature, ^{o}K	1500 - 2500
expansion nozzle inlet pressure, atm	1 (variable from 0.2 to 1.2)
expansion pressure ratio	20
Mach number at generator inlet	2.3
velocity at generator inlet, m/sec	3400 - 4000
generator duct cross-section, in^2	0.5 x 1.5
generator duct length (magnetic field region), in.	5
transverse magnetic field, T*	0 - 1.2

* 1 T (Tesla) $\doteq$ 1 Wb/m^2

The power generation experiment will yield data on MPD power processes for a wide range of experimental variables. In particular, closed-cycle steady-state operation allows the investigation of different working fluids (e.g. the various inert gas alkali metal vapour combinations) under controlled purity conditions, and should establish conclusive evidence whether non-eqilibrium ionization can be promoted by elevation of the electron temperature and by other techniques (such as by photoionization, r.f., electron or ion injection, etc.). Additional major variables in the experiment are pressure, pressure ratio, temperature, Mach number, fractional seed concentration, controlled concentration of other gases, generator duct configuration and magnetic field.

In commissioning the power generation experiment about 2000 hours of circuit operation were accomplished, of which 300 hours were at temperatures up to 2500°K with unseeded helium. Several important achievements led to the successful operation. Design and constructional techniques have been established for complex refractory metal (tungsten, tantalum, molybdenum, and tantalum-8 a/o tungsten alloy) duct and heat exchange systems, while a novel high temperature window system will facilitate the application of optical and microwave diagnostics to the plasma region. Other achievements are: the development of a helium circuit, having both static and rotating components, which has an extremely low leakage rate ($<10^{-5}\mu l$/sec); the development of a high-efficiency oil filtration system; advances in techniques for purifying and analyzing helium in flowing systems; and the development of an electrical resistance heater for gas temperatures up to 2500°K, which has demonstrated excellent heat transfer performance and reliability. A cesium injection and handling system, for pumping and accurate metering of pure cesium seed, has been designed and constructed, utilizing an electro-magnetic pump and flowmeter; in initial experiments a positive-feed injection system is being used.

Following the successful seeded operation of the loop the ensuing experimental programme is conveniently divided into two stages: with the present facility and a 1.2 T electromagnet; and with modifications and a 3 T Bitter-type water-cooled copper magnet, which will be built to cover the interim period before the 5 T superconducting magnet (Section 5.2.3) is commissioned.

5.2.2 Experimental programme with present facility

In the first series of runs the inlet pressure and seeding fraction at the nozzle is being kept constant at approximately 1 atm and 0.5 per cent respectively. The inlet temperature will be varied to provide a wide band of thermal ionization levels, and measurements made with 10-electrode and 36-electrode constant area ducts. Before seeding the flow, the accelerating nozzle and generator duct section has been fully characterized for static temperatures and pressures over a range of total head conditions. Having established these values, power generation experiments are being undertaken for a range of nozzle inlet pressure (0.5 to 1.2 atm), nozzle inlet temperature (1500° to 2500°K), cesium seed fraction (up to 3 a/o), electrical load, and magnetic field (up to 1.2 T). The electrical power characteristics will be studied to indicate duct end losses.

Two non-equilibrium ionization effects are anticipated: the first due to 'frozen flow' of electron concentration in rapid acceleration through the nozzle and the second to field-induced ionization in the generator duct. The latter

effect has been demonstrated theoretically to be possible and the present programme is producing experimental evidence in support.

Microwave and spectroscopic techniques are to be used in measuring electron temperatures, concentrations and collision frequencies at the window station upstream of the accelerating nozzle; it is proposed to extend such measurements within the generator duct itself. Later in the programme controlled additions of molecular gases (which inhibit electron motion) and other noble gases (which may assist non-equilibrium ionization) will be made to assess the effect on ionization and electrical conductivity.

5.2.3 Experiments with 3 T electromagnet

Although the low-field magnet will be sufficient for the purpose of the early stages of the experimental programmes, there is a strong incentive to operate at very much higher applied magnetic fields to increase the power density (which is proportional to the square of the magnetic field) and field-induced non-equilibrium ionization effects; in addition, the surface-to-volume ratio of the generator decreases with a consequent lower heat loss through the walls. The Hall number (to which is related the angle by which the electric field and current vectors are displaced from the transverse direction in the plane perpendicular to the magnetic field) increases directly with the magnetic field. The axial pressure gradient in the duct increases with the magnetic field, which may be a disadvantage, and a phenomenon known as ion slip (which gives a reduction in power output) can occur at very high fields. Other problems which may be encountered at high fields are electrical breakdown due to the high electric field in the plasma, inability of electrodes to support the very high current densities which are demanded and transverse pressure gradients in the duct, which could lead to fluid flow instability. In a large-scale system, the fraction of the output power which must be used in conventional copper coils to provide the magnetic field is substantial, so that superconducting field coils (which have no resistive loss and only a small power demand for refrigeration) are attractive. The technical feasibility and capital cost of building large superconducting magnets are uncertain; however, the 5 T superconducting Helmholtz pair, which the UK Department of Scientific and Industrial Research has nominated IRD to construct for operation with this MPD experiment, should contribute significantly to the technology.

To cover the interim period before this 5 T magnet is available, a Bitter-type magnet with water-cooled copper conductors is to be constructed for operation at fields up to 3 T. This will be associated with a re-designed generator duct with modified profile and a construction which will allow a number of alternative

electrode arrangements, based on present knowledge and the data obtained in the first stage (Section 5.2.2). Several expansion nozzles will be used to vary the flow Mach number from the present design level of 2.3 to subsonic values of 0.5 (or possibly less).

The experimental programme will be broadly on the same lines as for the first stage except that generator duct pressure levels will be increased towards those anticipated for a full-scale system and seeding levels will be in the region shown theoretically and by experiment to produce optimum specific power.

5.3 COMMISSIONING

5.3.1 Development problems

In design, construction and commissioning many problems were evident in the materials of construction, assembly techniques, developing a circulator for extremely low helium leak rates, lubricating oil filtration and analysis, eliminating internal contamination, assembly techniques, instrumentation for test conditions, etc. It is beyond the scope of this paper to describe in detail much of this work, but some information is given in the next sections on helium purification, the high temperature heater, cesium injection and recovery, and on materials.

5.3.2 Helium purification

Operation with very low impurity levels in the helium is important for three main reasons:

oxidizing impurities attack components fabricated from graphite and the refractory metals (tantalum, tungsten, etc.);

high cross-section impurities inhibit extra-thermal ionization effects; and

electronegative impurities, by attaching free electrons, also reduce the plasma electrical conductivity.

The purification plant (Fig. 5.3) is designed for a 6 Nm^3/hr continuous flow of helium (about 6 per cent of the main helium flow) at 1 ata and the maximum differential pressure across the circulator (~0.7 ata), and to remove O_2, H_2O, H_2, CO_2, CO, N_2 and A. On entering the purification plant helium is heated electrically to 625°K in catalyst beds to convert CO and H_2 to CO_2 and H_2O respectively, the latter being separated in a trap at liquid nitrogen temperature. The remaining impurities are absorbed in molecular sieve beds held at liquid nitrogen temperature. Residence times for the maximum gas flow are: catalyst

bed, 2 sec; H_2O and CO_2 trap, 2 sec; and molecular sieve beds, 5 sec. The associated chromatographic analysis equipment is capable of resolving concentrations of impurity constituents to levels in the table below:

Minimum delectable concentration in helium

Gas	H_2	O_2	N_2	CH_4	CO	CO_2
ppm (Sr-90 source)	1	0.2	0.8	0.5	1.0	0.5

5.3.3 High temperature heater

Many configurations of high temperature electrical resistance heater have been considered, based on either refractory metal or graphite elements. Following preliminary development of both types, a graphite element was eventually chosen. Inward radial flow through a perforated-wall tubular heater surrounded by a number of radiation shields appeared attractive, but control of radiant losses led to the adoption of a multi-pass axial/radial flow concept (Figs. 5.4 and 5.5). Severe stress and arcing problems were encountered in the end electrical connections, but the present arrangement (tapered cone at lower end and copper clamp at upper end) has proved satisfactory for currents up to 2500 A.

5.3.4 Cesium injection and recovery

The cesium circuit was conceived as a continuous flow system for recovery, filtration, evaporation and injection, utilizing an electromagnetic pump and flowmeter. Difficulties associated with fabrication methods, materials and the small size of components have been encountered and development work is continuing towards a fully-continuous system.

Several alternative semi-continuous systems have been studied, and a mechanical micro-feed cylinder of 1 kg cesium capacity is currently employed (Fig. 5.6). The original provision for cesium removal by condensation on cooled surfaces proved inadequate on the first cesium-seeded operations; precipitation and cyclone separators are being considered.

5.3.5 Materials

All high temperature components of the loop are contained in a 18/8 stainless steel outer casing capable of withstanding vacuum and over-pressure conditions. Pure helium flows from the high temperature heater to the generator duct through a 5 cm diameter tantalum transfer section containing an expansion bellows, a cesium evaporator, a window system, high temperature thermocouples and the accelerating

nozzle. The tantalum sections (0.3 to 1.5 mm thickness) show no significant deterioration after a total of 200 hr operation at temperatures up to 1800°K and with about 30 ppm total gaseous impurity.

Molybdenum has high evaporation losses and will not be used in future. Tantalum 8 a/o tungsten alloy, although amenable to fabrication techniques, has demonstrated brittleness probably associated with non-uniformity of alloying.

Compatibility and vaporization studies of generator duct and electrode materials are in progress; at present, alumina and boron nitride ducts with tantalum electrodes are being operated. After service at temperatures up to 1500°K duct surfaces have been coated with dark grey or black deposits when removed. Fig. 5.7 shows generator duct components (two side walls and an electrode wall) in which the lighter regions are non-electrically-conducting and the dark regions have a relatively low resistance.

5.4 OPERATION

5.4.1 Procedure

Following normal assembly procedure the loop is leak-checked under vacuum. If satisfactory, the high temperature heater is vacuum-outgassed, maintaining a pressure of less than 1 torr up to temperatures greater than 2000°K, the highest temperature being held until a pressure rise of less than 1 torr/min is achieved (usually 2 to 3 hr).

With the high temperature heater cold the helium circulator is started and mineral helium introduced through a purification train. The main bypass purification plant is operated at maximum flow (attained by choking the circulator inlet to produce a high pressure differential across the purification plant) to give clean-up (to less than 5 ppm total gaseous impurity) in about 30 min.

Electrical power input to the high temperature heater is gradually increased over several hours to a gas temperature higher (by 100°K or more) than required in operation. Up to about 1300°K the rate of temperature rise is limited to 200-300°K/hr to minimize thermal stressing of the alumina generator duct; beyond 1300°K the rate of evolution of gaseous impurities is the controlling factor, the most significant, hydrogen, being maintained at less than 50 ppm.

When the tolerable impurity level ($\lesssim$ 30 ppm total) is achieved the temperature is reduced to the operating level. The supersonic accelerating nozzle is gradually choked by opening the valve at circulator inlet. Helium pressure is adjusted by blow-off or introduction of further purified gas. Once steady conditions are attained, power generation experiments with cesium injection can be undertaken.

The loop is shut down under helium pressure above atmospheric and may be dissembled and opened to atmosphere at the expense of some loss of helium.

5.4.2 Results

Twenty separate short duration cesium injection runs were made on 19 March 1964. Details of the observed voltages for runs 9 to 20 are given below, subscripts referring to the five electrode pairs (the second pair were disconnected).

Run No.	U.V. recorder, V				Avo, V		Load, ohm	Field, T
	E_1	E_3	E_4	E_5	E_1	E_3		
9	3.8	3.0	2.5	0			470	10
10		-4.7			-2		470	-5
11	-2.1	-3.8	-1.7	-1.3	-2.5		470	-5
12		4.7(ave) 6.4(max)				5.6	∞	10
13		4.25			5		∞	5
14					2		∞	2
15					2		470	10
16*	5.7	5.1	4.25	4.25		6	470	10
17	6.4	6.4	4.7	4.7		5.8	470	5
18	4.25	4.25	3.8	4.7		4	470	2
19+						2	470	10
20	8.0	6.4	5.5	6.4			470	10
						10		

* indicated nozzle inlet temperature 2000°K (lower than true value)

\+ measured short circuit current 55 mA per electrode pair

Consistently higher voltages were observed for runs 16 to 20 and these will be considered in more detail: in general, overall power outputs of several hundred mWe were observed and reversal of current direction with magnetic polarity was established (runs 10 and 11).

Measurements of temperature, pressure, mass flow and cesium concentrations were made to correlate the observed results with theory. For runs 16 to 20 the indicated pressures at four stations flush with a side wall were sensibly constant (to within ± 5%) at 0.51 ata.

The static gas temperature was estimated at entrance and exit from the duct; for runs 16 to 20 the measured inlet temperature was 1230°K and exit temperature 1190°K. The measured temperatures are subject to considerable error, through conduction down the thermocouple leads, indirectly down the electrode leads and the effects of thermal boundary layers. Correlation experiments resulted in an average (and probably high) correction factor of 1.29 for temperatures of interest. Using this and the observed temperatures gives an average static gas temperature of 1480°K.

From the continuity equation and equation of state, using the mass flow (8.8 g/sec) and duct cross sectional area (0.75 $in.^2$) a flow velocity of 1075 m/sec is obtained fro runs 16 to 20, giving a Mach number of 0.48.

For run 20, the average observed voltage across each 470 ohm load is 6.6; the load current is 14 mA and power output 93 mWe per electrode pair, or 0.46 We for the five electrode pairs. The internal electric field (distance between electrodes 1.5 in.) is 86.5 V/m and the current density (electrode area 0.25 $in.^2$) is 87 A/m^2, yielding an apparent electrical conductivity of about 1 mho/m.

The temporary cesium injection device was designed to give a seeding fraction of 0.5 a/o. The effects of seeding (observed voltage) persisted for much longer than the measured injection time, indicating an evaporation rate much less than the inlet flow; the seeding fraction is probably about 0.1 a/o. Using this seeding fraction, the corrected temperature and measured pressure, the thermal equilibrium electrical conductivity is about 0.05 mho/m^1; thus, the measured conductivity is about twenty times greater than the value for thermal equilibrium. However, it should be noted that the electrical conductivity in this regime is extremely sensitive to temperature, a 100°K change altering the conductivity by a factor of about five.

For run 20, the load factor with a 470 ohm resistor is 0.66; assuming that this factor and the flow velocity remain constant for runs 17 to 20 the observed and calculated (V_{calc} = khUB) voltages are:

Run	Field, T	Calc. voltage, V	Obs. voltage, V	Loading
18	0.2	5.4	4.4	470 ohm load
17	0.5	13.5	5.6	470 ohm load
20	1.0	27	6.6	470 ohm load
20	1.0	41	10	open circuit

The observed voltages are consistently lower than those calculated.

On dissembly of the MPD loop after the power generation runs, a dark deposit (see Section 5.3.5) was found on the alumina duct walls and tantalum electrodes. On test this deposit was found in places to be an extremely good electrical insulator, as shown below (resistances were measured with point electrodes across each side wall, opposite blanked pressure stations (see Fig. 5.7)).

Pressure station no.	1	2	3	4	5	6	7	8	9
	(Resistance, ohm)								
Block A	110	180	350	800	350	2000	300	1800	540
Block B	160	*	440	∞	500	160	600	760	900
A and B in parallel	65	180	194	800	206	148	200	531	340

* side wall cracked

The average resistance of A and B in parallel along the duct (neglecting measurement 2) is 310 ohm. The existence of this deposit throughout runs 9 to 20 could provide an explanation of the low output voltage, although it is possible however that deposition occurred during thermal run down of the loop. In addition to shorting currents through the side walls considerable electrical leakage probably occurred between electrodes on the same wall, down pressure station leads and possibly through the nozzle and diffuser structures (although measured resistances during stand-by operation for the latter were in excess of 1 kilohm); there is also the possibility of internal plasma and end loop leakage.

Assuming that leakage through a conducting deposit on the walls occurs, the electrical conditions have been examined for run 20; a generated voltage of 40 V is assumed. The apparent 'open circuit' and 'on-load' conditions are shown in Fig. 5.8 (R_i is internal plasma resistance, R_w wall resistance, and R_L the load resistance).

From Fig. 5.8 and the conditions of run 20,

$$R_i = 3R_w$$

$$i_1 = i_2 + 0.014$$

$$i_2 R_w = 6.6$$

$$i_1 R_i = 33.4$$

Solution of these equations yields

$$R_i = 970 \text{ ohm}$$

$$R_w = 323 \text{ ohm}$$

$$i_1 = 34.4 \text{ mA}$$

$$i_2 = 20.4 \text{ mA}$$

The calculated wall resistance (R_w) is in good agreement with the average value measured on side walls A and B.

The power dissipated in each external load is about 93 mWe and in the equivalent wall path is about 135 mWe; the total power output in the absence of wall leakage should therefore be about 230 mWe per electrode pair, or for the five electrodes, 1.15 We. The equivalent external load is 190 ohms and the loading factor K = 0.16.

The plasma electrical conductivity may be evaluated from the internal resistance (R_i) calculated above; electrode sheaths have been neglected, their effect being that the calculated electrical conductivity (Fig. 5.8b) for run 20 (0.24 mho/m) is probably substantially less than exists in the volume of the plasma. It has been assumed that the internal plasma resistance is independent of the current drawn.

5.5 CONCLUSIONS

1 The technological feasibility of a closed-cycle high-temperature (up to 2500°K) loop for MPD direct electrical power generation has been demonstrated.

2 Preliminary power generation experiments with cesium-seeded helium indicated electrical outputs at least equivalent to thermal ionization. Magnetically-induced extra-thermal ionization might not occur under the particular conditions which apply, the electron concentration being less ($\sim 5 \times 10^{17}$ m^{-3})[1] than a threshold value ($\sim 3 \times 10^{18}$ m^{-3})[2].

REFERENCES

1 LINDLEY, B.C. Unpublished work at C.A. Parsons and Company. 1959

2 KLEPEIS, J. and ROSA, R.J. Experimental studies of strong Hall effects and V x B induced ionization. Avco-Everett Research Laboratory Report 177, BSD-TDR-64-20. April 1964

MPD CLOSED CYCLE LOOP FLOW DIAGRAM

FIG 5.1

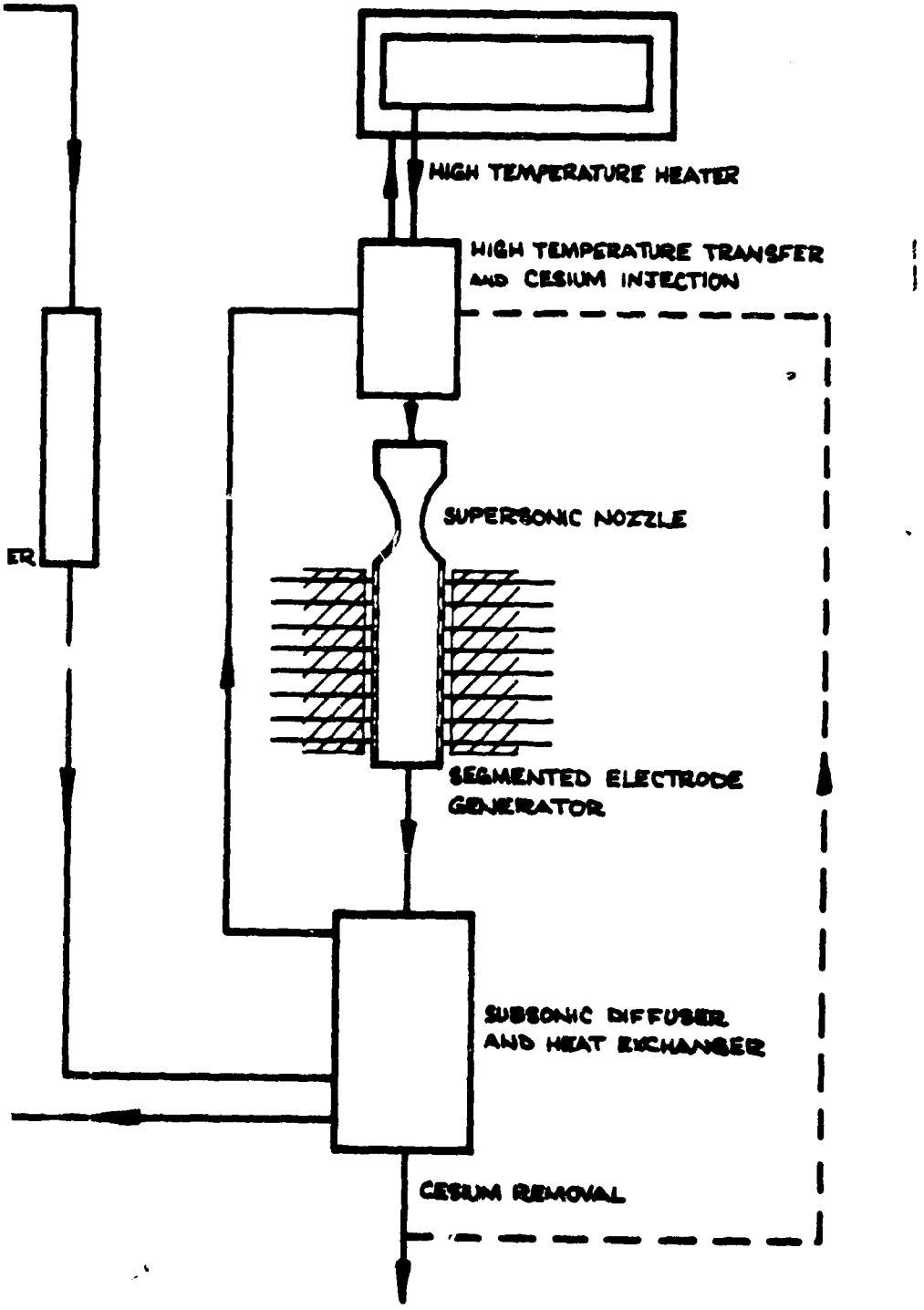
HIGH TEMPERATURE HEATER
HIGH TEMPERATURE TRANSFER
AND CESIUM INJECTION
SUPERSONIC NOZZLE
SEGMENTED ELECTRODE
GENERATOR
SUBSONIC DIFFUSER
AND HEAT EXCHANGER
CESIUM REMOVAL

NERAL VIEW OF MPD CLOSED-CYCLE LOOP

FIG 5-2

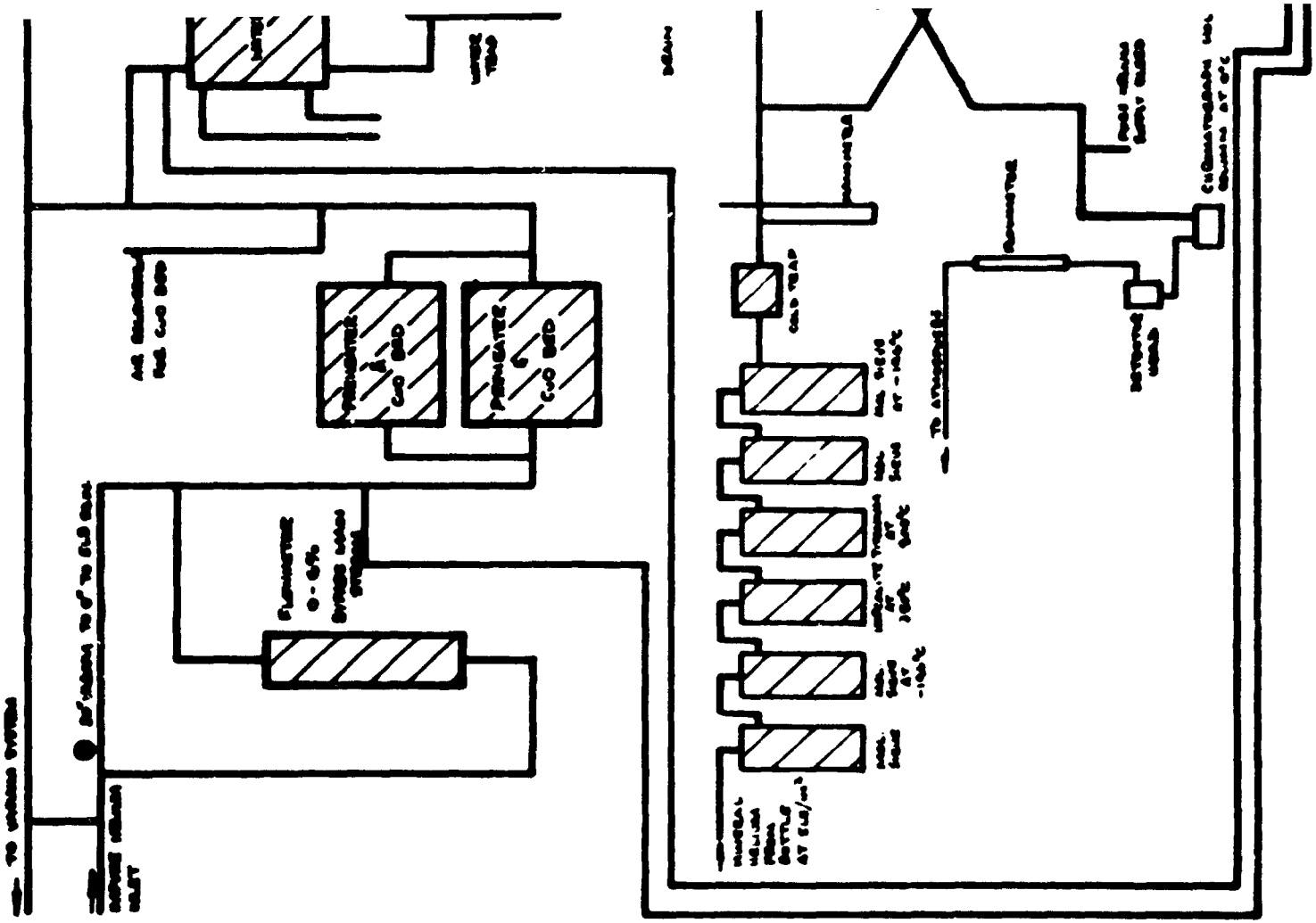

HELIUM PURIFICATION PLANT

FIG 5·3

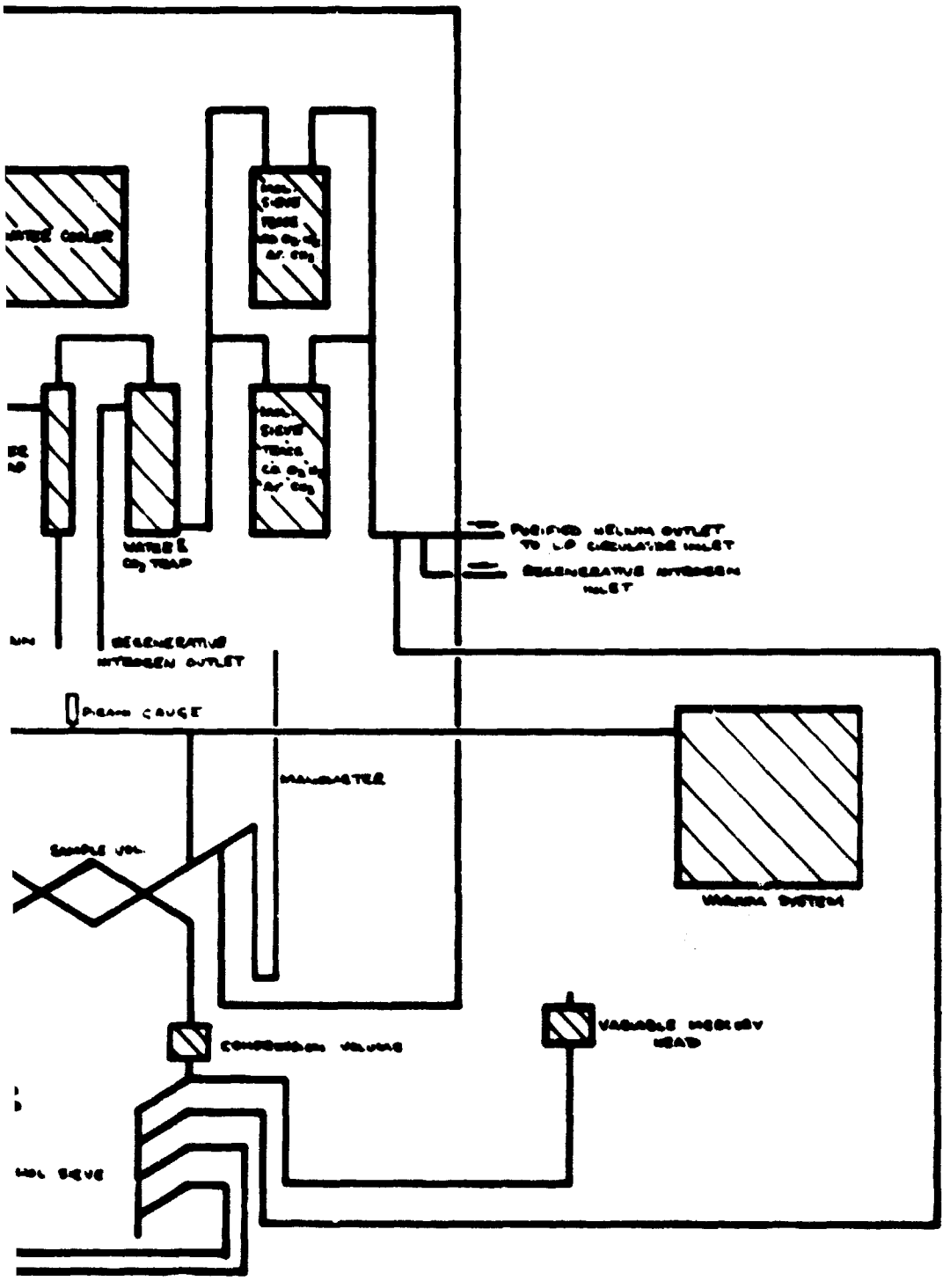
PURIFIED HELIUM OUTLET
TO LIQ CIRCULATING INLET
REGENERATIVE NITROGEN
INLET
REGENERATIVE
NITROGEN OUTLET
MANOMETER
VACUUM SYSTEM
VARIABLE MERCURY
HEAD

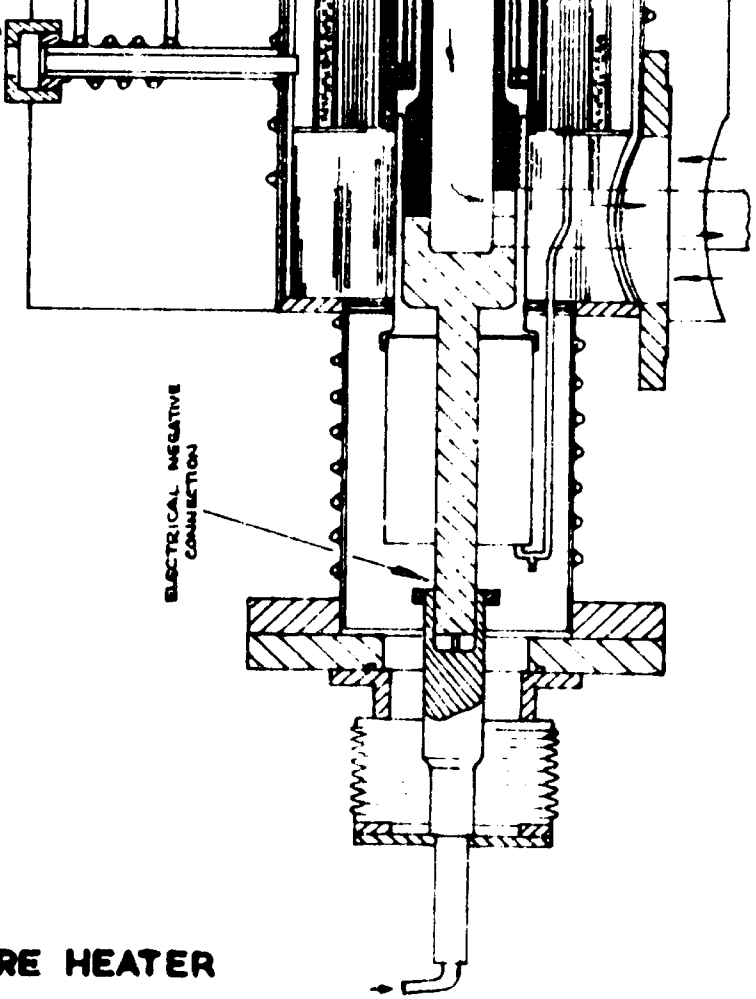

HIGH TEMPERATURE HEATER

FIG 5.4

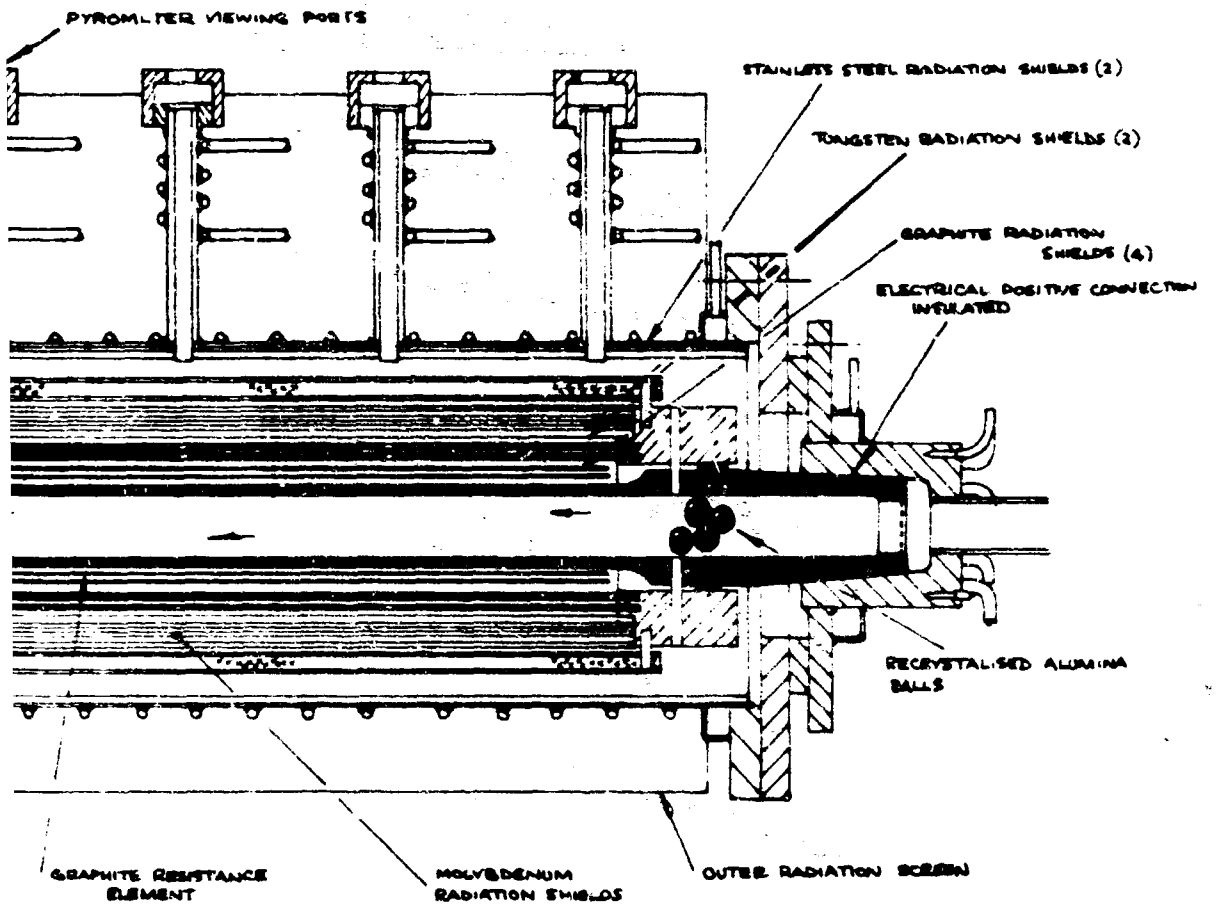
PYROMETER VIEWING PORTS
STAINLESS STEEL RADIATION SHIELDS (2)
TUNGSTEN RADIATION SHIELDS (2)
GRAPHITE RADIATION SHIELDS (4)
ELECTRICAL POSITIVE CONNECTION INSULATED
RECRYSTALISED ALUMINA BALLS
GRAPHITE RESISTANCE ELEMENT
MOLYBDENUM RADIATION SHIELDS
OUTER RADIATION SCREEN

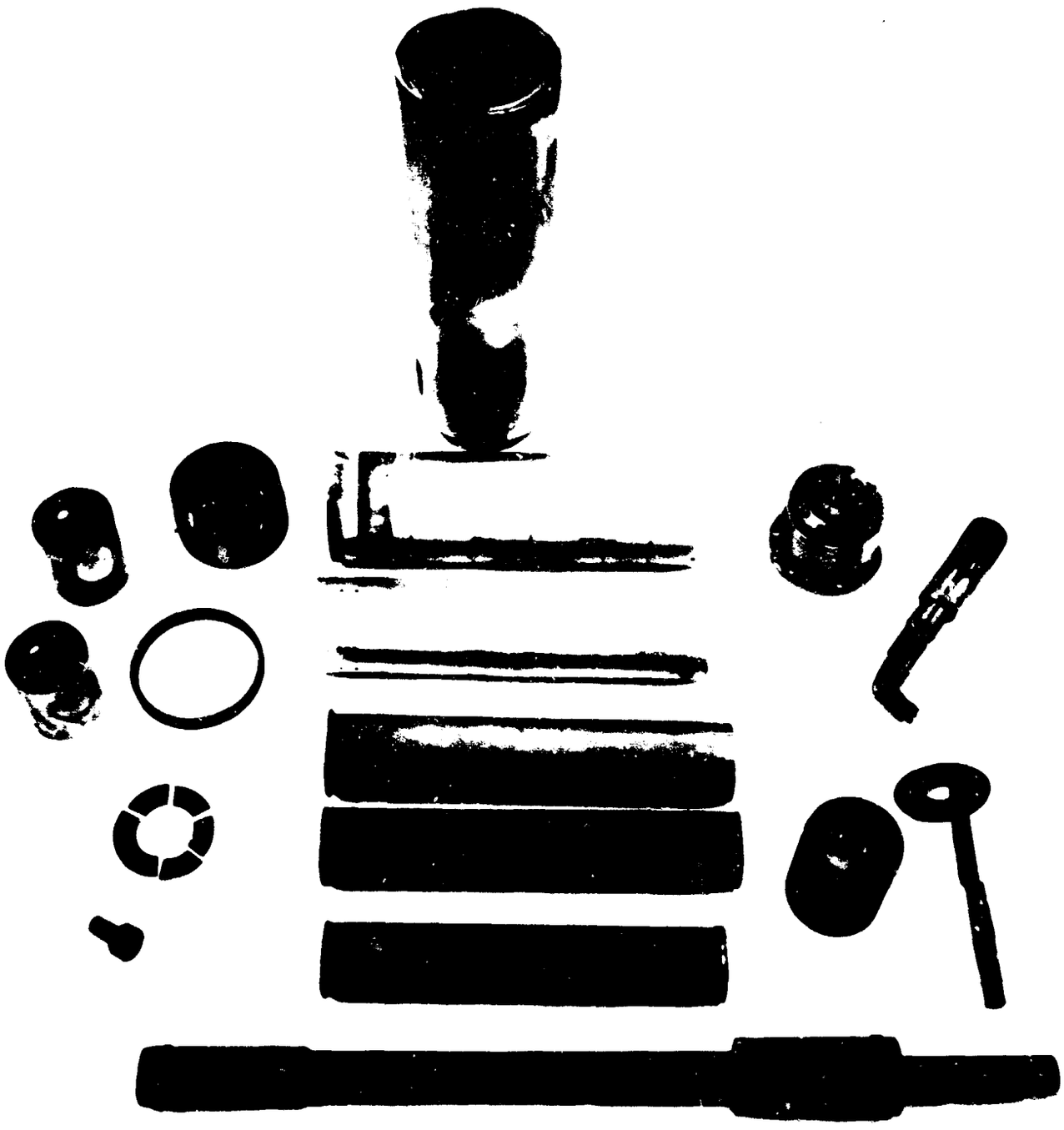

COMPONENTS OF HIGH TEMPERATURE HEATER

FIG 5.5

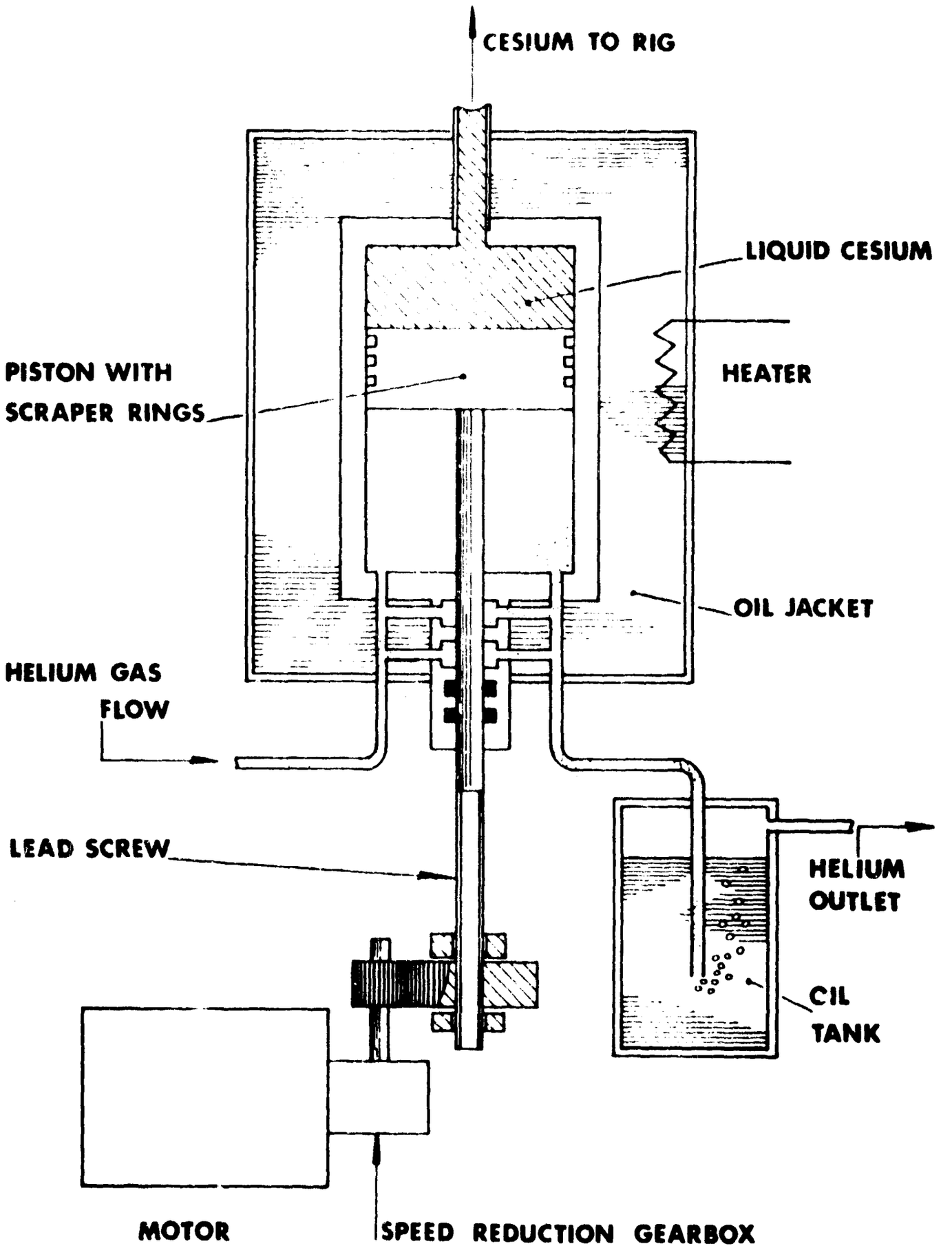

CESIUM INJECTION SYSTEM (schematic)

FIG 5.6

ENERATOR DUCT COMPONENTS

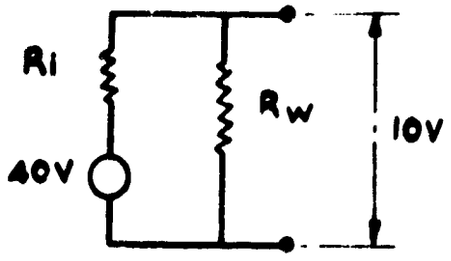

A. 'OPEN CIRCUIT'

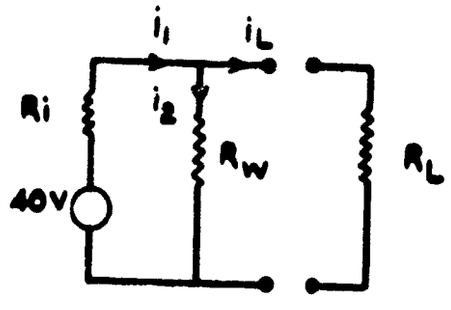

B. 'ON LOAD'

'OPEN CIRCUIT' AND 'ON LOAD' EQUIVALENT CIRCUITS

CHAPTER 6

HIGH TEMPERATURE HEATER

by

R. Brown, W.J. Slator, K. Cass, V. Brown, and J. Davidson

6.1 HEATER DEVELOPMENT

One of the major efforts over a period of three years has been the development of a high temperature heater for the MPD experiment. The programme undertaken with a single element graphite configuration is detailed in Chapter 3. It has resulted in a facility capable of continuously heating helium flows in the range 5 to 10 gm/sec at 1 ata to temperatures approaching 2500°K.

The multi-pass axial/radial flow radiation shield concept adopted during the latter part of the programme has significantly improved the overall heat transfer performance. Control and reduction of high radiant heat losses by more than 60 per cent has been established by the use of an outer concentric thermal insulation pack (zirconia fibre and finely-dispersed cellulose carbon) over the full active length of the resistance element.

Satisfactory vacuum-outgassing techniques have been established for the heater assembly, attaining high temperatures and low pressure rises on isolation conditions, prior to loop start-up. Gaseous impurity contamination from the graphite to the helium under high temperature flow conditions is exceptionally low (<50 ppm) and readily controllable by the helium purification plant. With the heater previously outgassed, top heater outlet temperatures under helium flow conditions can be achieved in under 5 hours.

Figs. 6.1 and 6.2 show the present high temperature heater components without the containment case and the assembled shield and outlet section. The original perforated wall hollow graphite element is unchanged. Electrical end connections are: at the lower end, a reduced graphite cone in contact with a water-cooled stainless steel housing: and at the upper end, a water- gas-cooled copper clamp on to a graphite rod, the latter and an outlet section being screwed to the top end of the graphite element (Fig. 6.4).

Radiation shields (concentrically outwards from element):

- 4 graphite ($\frac{1}{8}$ in. wall with 3/16 in. radial gap)
- 3 tungsten (0.030 in. wall with 3/16 in. radial gap)
- 3 dimpled molybdenum (0.015 in. wall)
- 1 outer thermal insulation pack (inner molybdenum (0.020 in.); outer electropolished stainless steel (0.020 in.); insulating material, cellulose carbon)
- 1 graphite support block

Head radiation shields:

- 2 tungsten (0.030 in. wall $\frac{1}{2}$ in. gap)
- 1 insulation and cooling box (graphite containing chipped recrystallized alumina)

Lower connection internal space:

$\frac{1}{2}$ in. alumina balls

A boron nitride ring is used to electrically insulte the graphite support and element radiation shields from the lower end. The system is arranged for the element to support the shields and their weight to provide the required high electrical contact load pressure on the lower end cone connection.

6.2 TEMPERATURE MEASUREMENT

Although the high temperature thermocouples employed in the MPD loop are capable of measuring up to 2600°K, the tantalum sheath (0.01 in. material) would readily carburize. Over the development period in-line holes through the radiation shield have been viewed using a Leeds Northrup disappearing-filament optical pyrometer, four such viewing stations along the element giving axial temperature profiles under the various operating conditions. Several factors contribute to a significant error in the observed temperature, in particular, the optical pyrometer error. In addition, inflow of cooler helium (<800°K) from the heater outer case impinges on and cools the viewed element area. Minimizing the latter effect by reduction of the in-line hole diameters (at present $\frac{1}{8}$ in.) increases the solid angle and adsorption errors.

The complexity of the viewing configuration and lack of physical information prohibits theoretical analysis for temperature correction. Experience (for example, the melting of refractory metal systems (Chapter 3)) has shown that the observed temperature is approximately 10 per cent lower at 2200°K element temperature.

A large ($\frac{3}{8}$ in. ID) viewing station has been built into the heater outlet head. An $\frac{1}{8}$ in. thick sapphire window is arranged for simultaneous viewing of an $\frac{1}{8}$ in. graphite pin positioned into the central gas outlet region; of the tip of the tantalum thermocouple pocket in the tantalum high temperature transfer; and along the transfer section (to view cesium injection conditions). This arrangement will allow correlation between the heater outlet gas temperature and the tantalum thermocouple indicated temperature, and will establish the accuracy of the theoretical analysis for thermocouple correction (Section 10.2).

6.3 GRAPHITE USED

The heater power supply problems are discussed in Section 10.3. The ideal load resistance requirement of 0.012 ohm introduced difficulties in obtaining graphite with suitable electrical resistance characteristics. Early usage of Acheson CS 20 grade graphite (800 μ ohm.cm) was discontinued (Fig. 6.3) in favour of Morgan EY9, EY110 (2000 μ ohm.cm). Variation in electrical resistance of graphite elements manufactured from nominally the same grade of material required several hot runs to be undertaken to optimize the active element wall thickness.

6.4 CONCLUSION

In general, it may now be concluded that a satisfactory high temperature heater element has been successfully developed; the unit is reliable, robust, has good heat transfer performance and is relatively inexpensive. It is believed that the configuration is suitable for other operating conditions, for example, at higher pressure levels, higher power dissipation and with other inert gases.

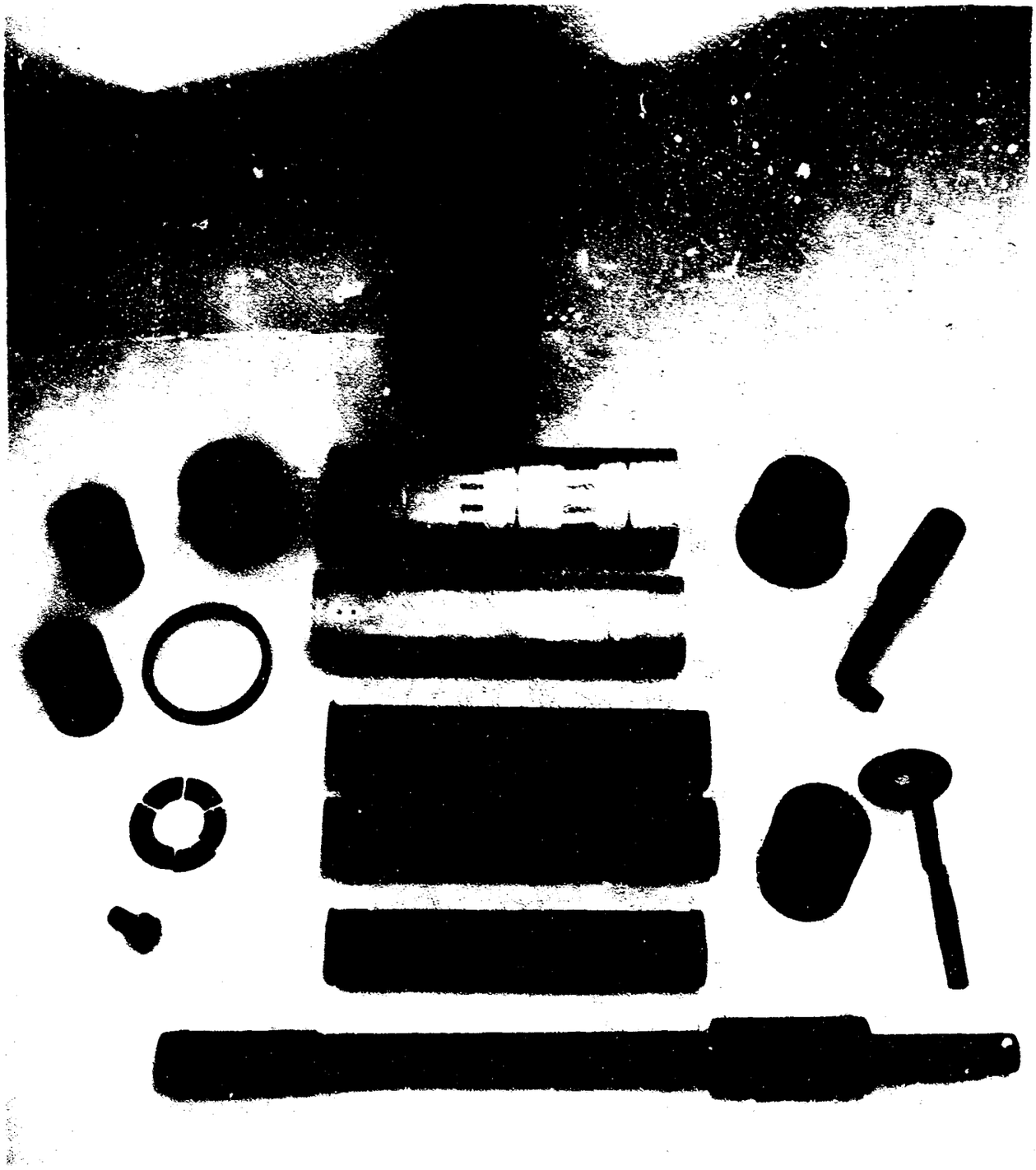

PRESENT HIGH TEMPERATURE HEATER COMPONENTS

FIG 6·1

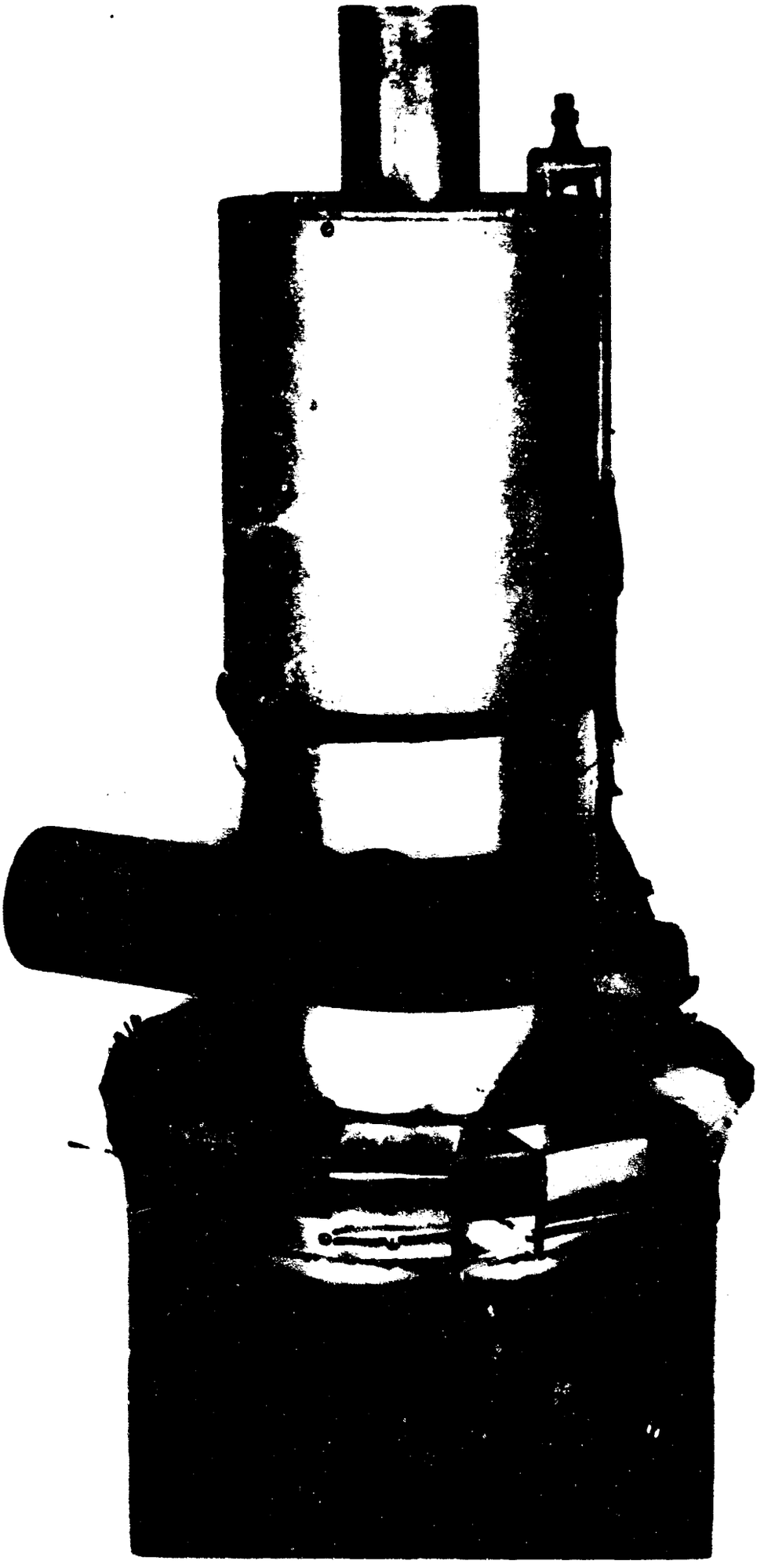

HEATER HEAD ASSEMBLY

·1

FIG 6.2

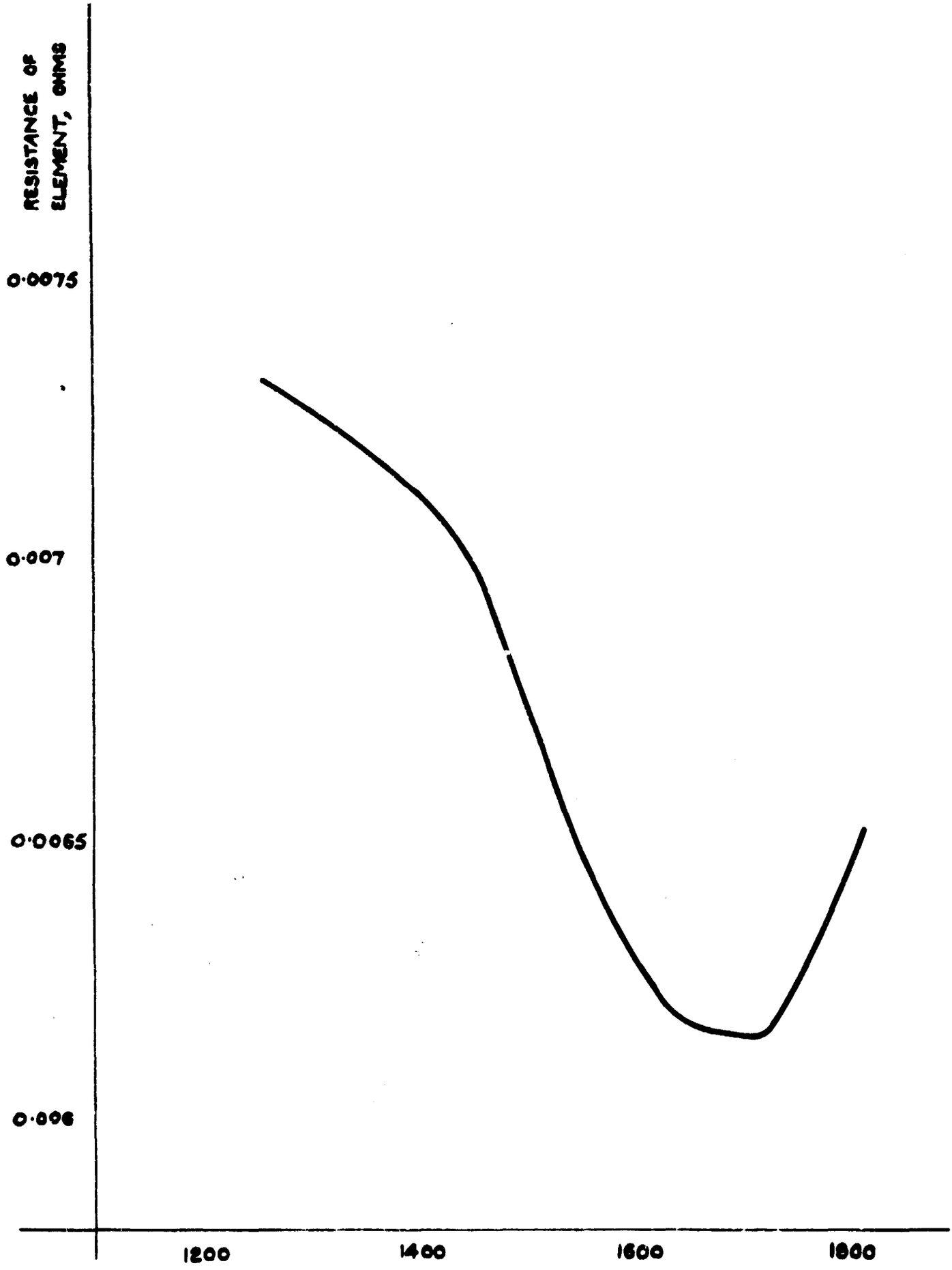

RESISTANCE CHARACTERISTIC OF EY9 GRADE GRAPHITE OBTAINED FROM RHT 13

FIG 63

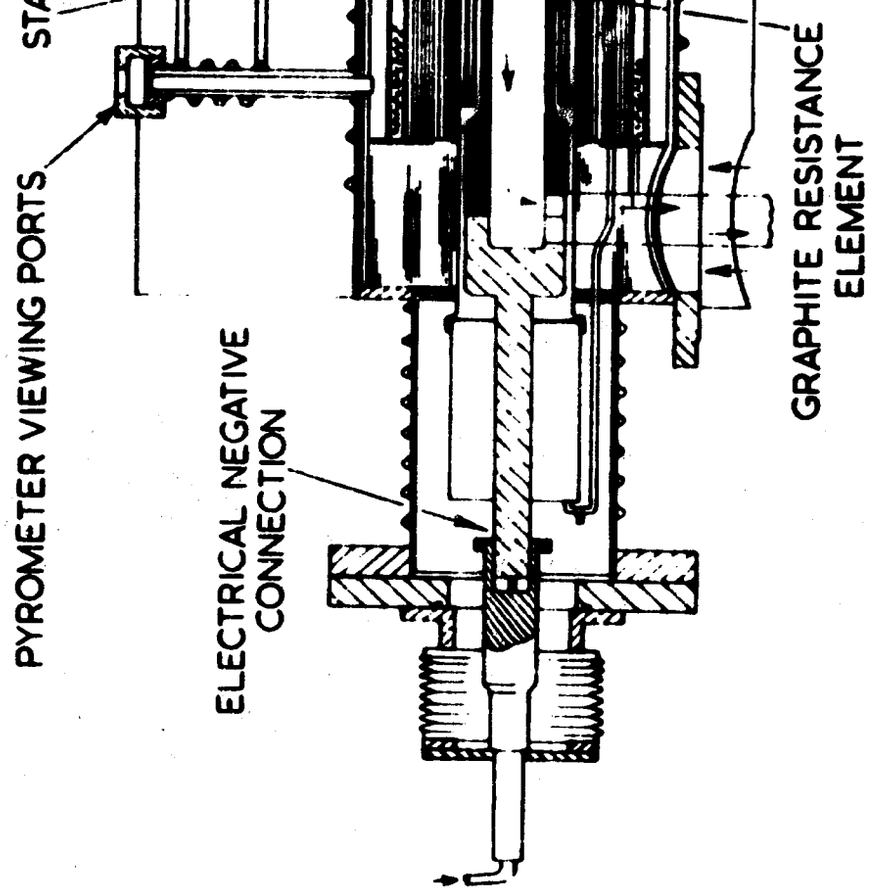

HIGH TEMPERATURE HEATER

FIG 6.4

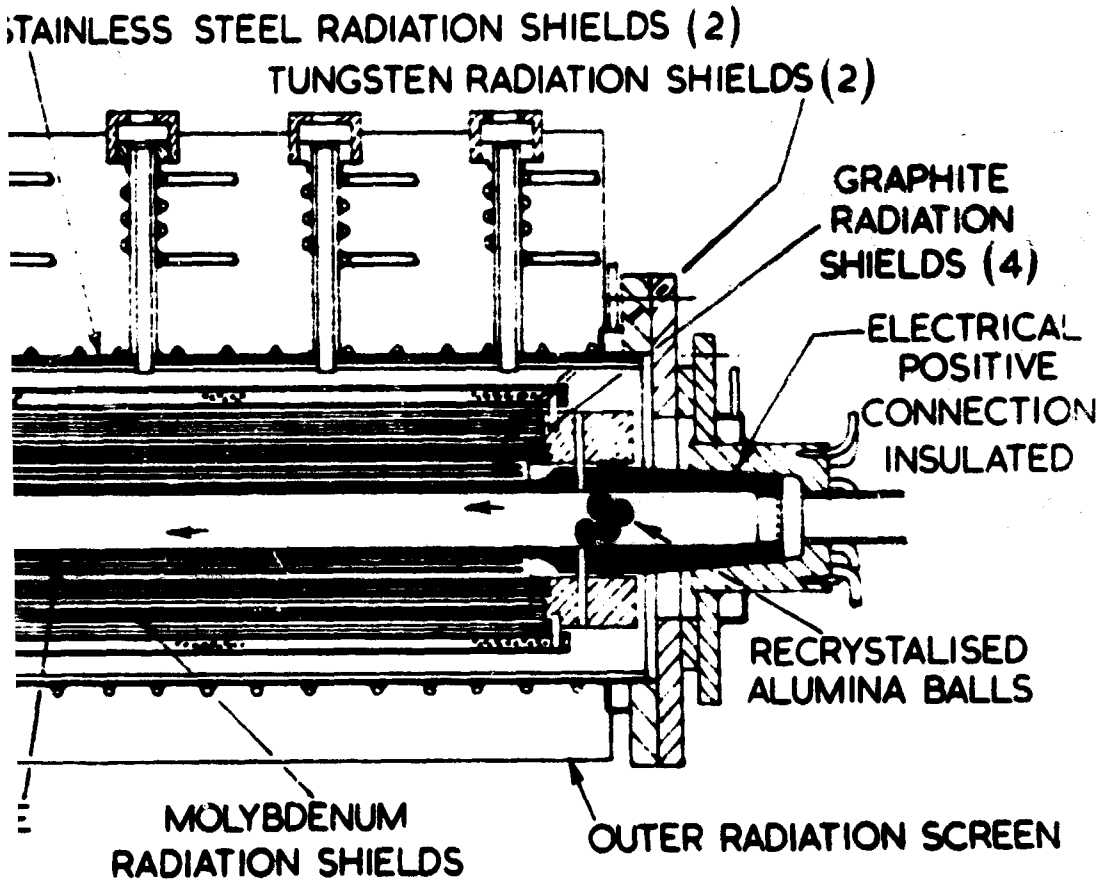
STAINLESS STEEL RADIATION SHIELDS (2)
TUNGSTEN RADIATION SHIELDS (2)
GRAPHITE RADIATION SHIELDS (4)
ELECTRICAL POSITIVE CONNECTION INSULATED
RECRYSTALISED ALUMINA BALLS
MOLYBDENUM RADIATION SHIELDS
OUTER RADIATION SCREEN

CHAPTER 7

HELIUM PURIFICATION ON ANALYSIS

by

R. Brown, J. Davidson, W. Slator, and A. Bottom

Operation with very low impurity levels in the helium is important for three main reasons:

oxidising impurities attack components fabricated from graphite and refractory metals (tantalum, tungsten, etc.);

high cross-section impurities inhibit extra-thermal ionization effects; and

electronegative impurities, by attacking free electrons, also reduce the plasma electrical conductivity.

The presence of other than monatomic gases in the helium and the consequent high inelastic electron energy loss on collision significantly reduces the likelihood of obtaining elevated electron temperature effects. Theoretical investigations on nozzle and channel flow (Chapters 24 and 25) are being extended to investigate these effects in detail. Presence of diatomic gases such as Co_2, N_2 and O_2 even at levels <1 ppm cause the electron to suffer considerable inelastic energy loss through the excitation of rotational and vibrational energy modes. The theoretical investigations will incorporate known inelastic energy transfer coefficients.

The helium purification plant originally supplied by Linde has proved entirely unsatisfactory and has been scrapped. The present operating facility has been designed and built at IRD, (Fig. 7.1).

The purification plant is designed for a 6 Nm^3/hr continuous flow of helium (about 6 per cent of the main helium flow) at 1 ata and the maximum differential pressure across the circulator (~0.7 ata), and to remove O_2, H_2O, H_2, CO_2, CO, N_2 and A. On entering the purification plant helium is heated electrically to 625°K in catalyst beds to convert CO and H_2 to CO_2 and H_2O respectively, the latter being separated in a trap at liquid nitrogen temperature. The remaining impurities are absorbed in molecular sieve beds held at liquid nitrogen temperature. Residence times for the maximum gas flow are: catalyst

bed, 2 sec; H_2O and CO_2 trap, 2 sec; and molecular sieve beds, 5 sec.

The plant is capable of continuous operation by the provision of paralleled catalyst and molecular sieve beds enabling isolation, and reactivation to be undertaken without flow interruption. Large impurity levels (>1000 ppm) can be continuously reduced to undetectable levels at the purification plant outlet (<5 ppm total).

The analysis is carried out using a Pye Argon Chromatograph modified to work with helium as a carrier gas and fitted with additional separating columns to deal with the large number of impurities. The automatic gas analyser uses an ionization detector to determine the impurity concentrations, measuring directly small quantities of impurities. The sampling operation is manual and takes three minutes; the levels of impurity are automatically recorded on a strip chart. Sampling is arranged at the inlet to the purification plant (giving maximum circuit conditions), following the copper oxide bed at the purification plant outlet and at selected stations in the main loop.

The ionization detector head is a standard Pye Instrument (Sr-90 source) used with helium. Gas samples (5ml) are analysed at 0°C on a 40 cm column of Linde molecular sieve 5A (for H_2, O_2, N_2, CH_4 and CO) and a 50 cm column of silica gel (for CO_2). The minimum detectable concentrations of the various gases in helium are shown in the following table.

Gas	H_2	O_2	N_2	CH_4	CO	CO_2
Minimum detectable concentration, ppm (Sr-90 source)	1	0.2	0.6	0.5	1.0	0.5

Detection of the large cross section molecule CO_2 may be necessary as discussed previously. Development is being undertaken on a system for the determination of small amounts of CO_2 in helium (Fig. 7.2). The method is optical, making use of the absorption of infra-red radiation by carbon dioxide, and could be used for the estimation of other infra-red absorbing gases, depending of course on their absorption characteristics. An advantage of the method is that the cell can be built into a side loop of the rig for continuous operation. The optical system is fitted into a gas-tight box which is continuously flushed with pure helium from the helium purification plant outlet.

Radiation from a filament source is split into sample and reference beams. Both beams are brought into focus on a thermocouple detector, the sample beam

adjustable comb, both having already passed through filters to remove unwanted radiation and through a synchronous chopper. The thermocouple signal is amplified and displayed on a millivoltmeter.

Measurement of carbon dioxide content is by a null-point technique. Carbon dioxide-free gas is passed through the cell, and the comb in the reference beam is adjusted by a micrometer screw until a minimum is recorded on the millivoltmeter. The sample gas is passed through the cell, and the new minimum similarly found; the difference in micrometer readings is proportional to the carbon dioxide content. Calibration is necessary. As the amounts of carbon dioxide being estimated are extremely small, long path length cells are required to obtain absorption in the sample beam. A cell of at least 10 in. path-length is probably required for the level sought (<0.01 ppm).

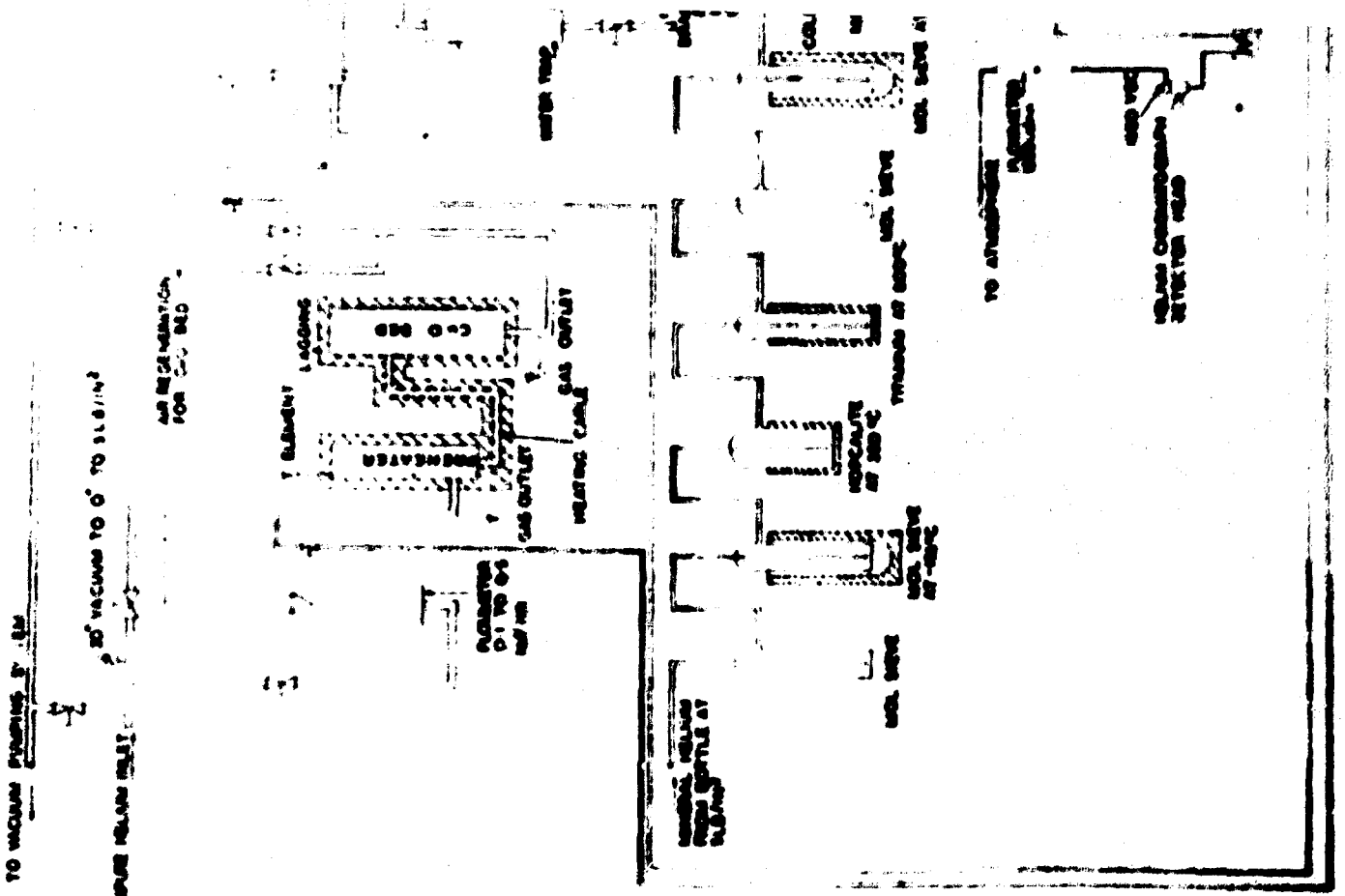

HELIUM PURIFICATION (O TO 15 Nm^3/hr) AND CHROMATOGRAPHIC MANUAL ANALYSIS SYSTEMS

FIG 7·1

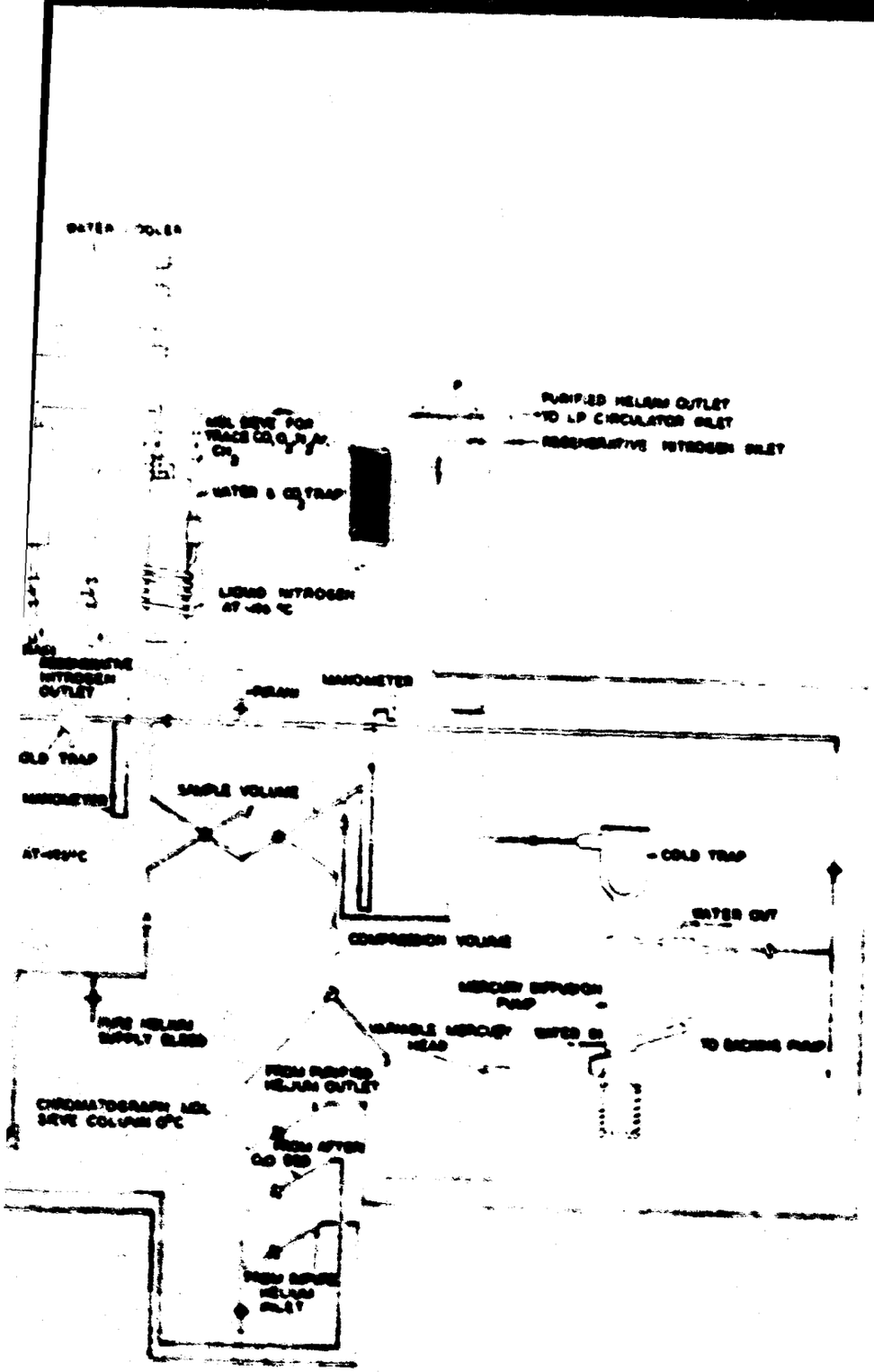
PURIFIED HELIUM OUTLET
TO LP CIRCULATOR INLET
REGENERATIVE NITROGEN INLET
LIQUID NITROGEN
MANOMETER
SAMPLE VOLUME
COLD TRAP
COMPRESSION VOLUME
WATER OUT
MERCURY DIFFUSION PUMP
VARIABLE MERCURY HEAD
TO BACKING PUMP
CHROMATOGRAPH MOL SIEVE COLUMN GPC

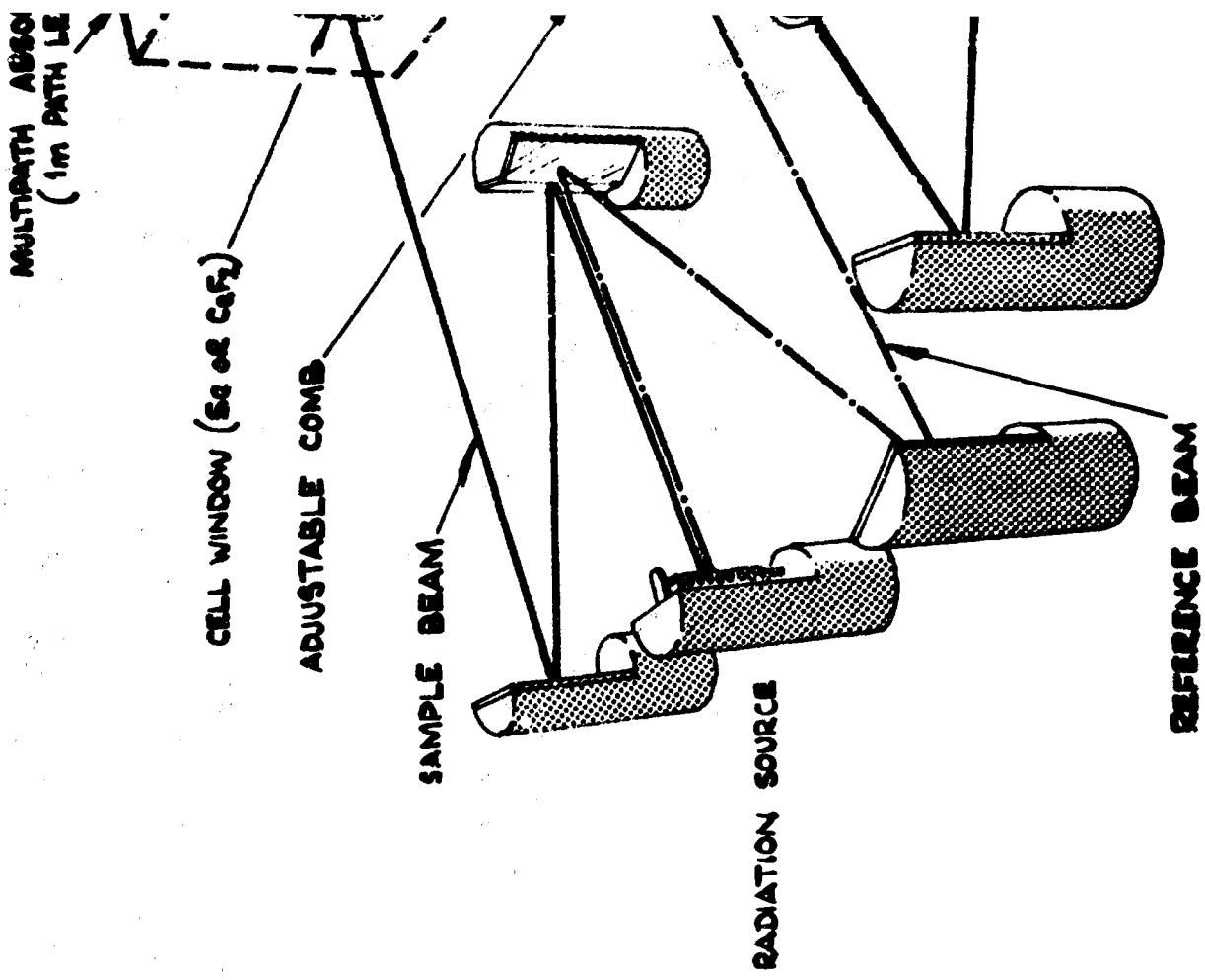

DIAGRAMMATIC RERESENTATION OF TECHNIQUE TO MEASURE VERY SMALL AMOUNTS OF INFRA-RED SENSITIVE GASES IN ION ABSORBING MEDIUM

FIG 72

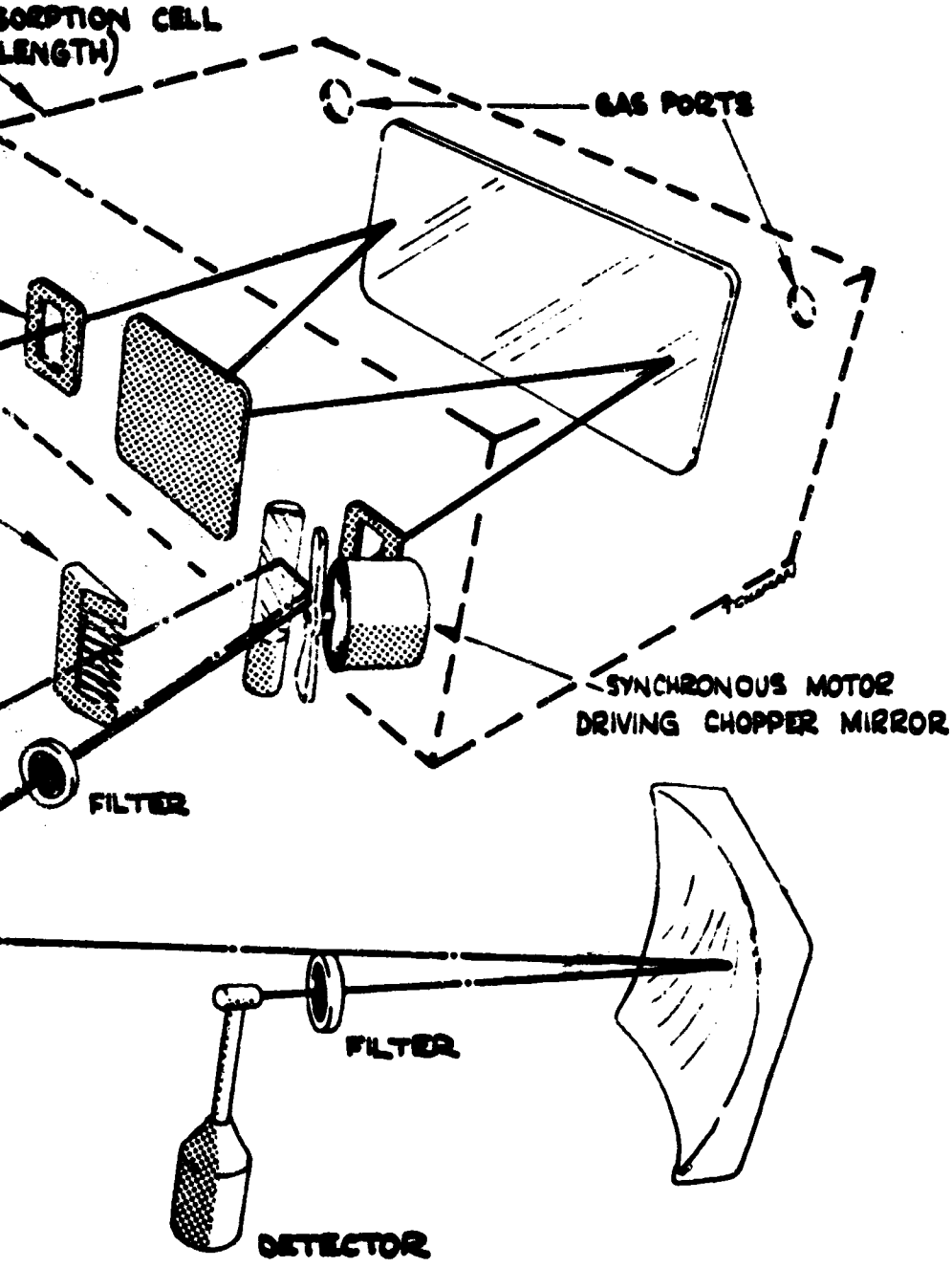
SORPTION CELL
LENGTH)
GAS PORTS
SYNCHRONOUS MOTOR
DRIVING CHOPPER MIRROR
FILTER

FILTER
DETECTOR

CHAPTER 8

CESIUM INJECTION AND RECOVERY

by

R. Brown, W.J. Slator, T. Archbold, V. Brown, K. Cass, and J. Davidson

8.1 INTRODUCTION

Although the major work has been concerned with the main helium loop and its auxilliaries a considerable programme has been required on cesium injection and recovery problems.

8.1.1 Injection

Originally it was envisaged that a metered cesium vapour-flow would be injected continuously into the loop, with efficient recovery and recycling. A design on this concept was sub-contracted for manufacture and, since March 1961, this has been the subject of many development problems at IRD. The difficulties can be attributed mainly to manufacturing errors, to the use of small-bore piping and the supply of impure cesium. Further development of miniature electromagnetic pump channels and flowmeters is in hand and work will continue towards a satisfactory continuous flow facility.

To allow initial seeded runs to be carried out semi-continuous systems have been studied and developed. A constant back pressure cesium feed system employing a hyperdermic needle was used successfully for the twenty seeded runs on 19 March 1964. Seed fractions of ~ 0.5 a/o were maintained over periods of up to 30 sec with a total throughput of ~ 380 gm.

Two further systems are based on the micro-feed piston principle, employing a mechanical piston and a purified paraffin oil piston respectively. Each has a cesium containment of 1 kgm and is capable of metering cesium over a seed fraction range of ≤ 2 a/o. Both systems are in the final stages of commissioning.

8.1.2 Recovery

Efficient removal of the cesium from the main helium flow is desirable for a number of reasons. The helium circuit following the precooler contains materials and components which are adversely affected by cesium. Initial seeded runs are programmed for short duration cesium injection but optical and

microwave plasma diagnostics and materials testing will require steady conditions and prolonged periods of cesium injection. The high investment cost of pure cesium metal and handling difficulties add to the necessity for high efficiency removal and re-injection on a continuous cycle basis.

It was originally arranged for the helium-cesium to pass and cool over the recuperative heat exchanger coils and impinge on a cooled suraface at a low velocity. It was thought the bulk of the cesium would condense part-way down the angled (36^{c}) heat exchanger and, in the cooled lower section, the helium carrying trace cesium and cesium vapour at the appropriate level for the local helium temperature ($<500^{o}K$) would enter the (electropolished) stainless steel precooler. It was thought that complete cesium removal would be effected at this stage before the cooled helium re-entered the circulator.

8.2 OPERATING EXPERIENCE

The requirement for low helium purity under loop operating conditions has been discussed in Chapters 2 and 3. The ultimate condition for purity might result in conditions for super saturation of cesium in the helium, inhibiting the condensation processes.

The twenty seeded runs carried out on 19 March 1964 clearly demonstrated the inefficiency of the removal system. On injection a finely divided cloud of particulate cesium was seen at the window station of the heat exchanger outlet and a change in circulator noise level and quality suggested cesium carry-over through the precooler and circulator. Of the 380 gm injected it is difficult to assess accurately the final distribution in the loop. The unknown adsorption factor of containments and components, the necessity during inspection to isolate the sections using oxidation and alcohol dissolution techniques make quantitative assessments difficult.

It was decided to strip the circuit from the high temperature heater to the oil filter. All units of the loop to be removed were split from the loop under conditions of helium outflow and isolated with blanking flanges. The high temperature heater, transfer and expansion nozzle, generator duct, containment case and subsonic diffuser were cesium free. 5 cm of clean cesium were drained from the heat exchanger, none extracted from the precooler, and 50-70 gm from the precooler outlet (Fig. 8.8). Cesium remaining in the heat exchanger and precooler was allowed to oxidize progressively by flowing argon with increasing concentrations of air. These units were cleaned by circulating methyl alcohol for several hours and draining. Eventually the high temperature heater, generator test section, subsonic diffuser, heat exchanger, precooler, aftercooler,

circulator and activated charcoal filters were removed from the loop. The circulator, aftercooler and filter units were considered safe to dismantle because of lubricating oil coverage. There was evidence that a significant amount of cesium had formed a complex with lubricating oil covering the moving parts of the circulator and aftercooler, and traces of cesium were found in the charcoal filters. The filters were replaced. No permanent damage to the dry part of the loop had occurred.

8.3 CESIUM RECOVERY SYSTEM

The loop was reassembled and leak-checked (leak rate $<10^{-5}$ µl/sec) within ten days of the cesium-seeded operation.

6 in. bore vacuum valves were introduced at the heat exchanger outlet and precooler inlet to allow additional cesium removal systems to be added in series/parallel arrangements.

Three methods for cesium removal have been considered and are at present being developed and prepared for commissioning:

the use of ultrasonics in the heat exchanger region to promote agglomeration and removal of the particulate cesium;

a cyclone separator for the helium-cesium mixture at heat exchanger outlet; and

an electrostatic precipitator.

The first method is at present the subject of a feasibility study but provision for its inclusion in the heat exchanger is being arranged. For both the cyclone and electrostatic precipitator the range of cesium particle size to be removed is so far unknown. However, the tolerable pressure loss of the cyclone separator controls the design parameters and a unit has been constructed and fitted to the loop. Electrostatic precipitation, if feasible, has advantages which include low pressure loss and potentially high efficiency. A single-column unit is being assembled to allow for flow velocities in the region of 1 m/sec at pressures between 1 and 0.3 ata, the operating voltage will probably be between 15 and 30 kV.

Full details of the theoretical and experimental work on cesium recovery will be presented in a subsequent Technical Summary Report.

8.4 DESIGN PARAMETERS FOR THE ORIGINAL CESIUM INJECTION CIRCUIT

8.4.1 Dump tank

Total volume of cesium in circuit:

Connecting pipe work ($\frac{1}{8}$ in. bore say 15 ft)	=	2.2 in.^{3}
Isolating valve No. 8	=	0.4
Flow control valve No. 7	=	1.3
Flow control valve No. 6	=	1.3
Isolating valve No. 5	=	0.4
Dump valve No. 4	=	0.4
Filters	=	0.25
Bypass cooler	=	2.4
Heater - as part of pipe work		
		8.65 in.^{3}
	=	142 cm^3 = 262 gm

Total mass of cesium including 50 gm in injection circuit = 312 gm = 170 cm^3

Tank size say 3.5 in. diameter x 2 in. deep: total volume = 317 cm^3

Heat input to tank and cesium:

temperature rise say 20° to 60° = 40°C

heat input to cesium = 312 x 0.06 x 40	= 750 calories
latent heat of fusion = 312 x 3.77	= 1180 calories
heat input to stainless steel tank = 1000 x 0.11 x 40	= 4400 calories
(based on tank mass of 1000 gm)	6330 calories tote
	= 26,500 joule

(i.e. theoretical 110 watt heater for 4 minute heating time)

Air cooling by nominal air supply to 'canned' metal jacket around dump tank. Jacket will also enclose electrical wound strip heater. Heater coil as a cord heater ($\frac{3}{16}$ in. diameter, 60 watts/ft).

8.4.2 Heater

Maximum throughput = 16 gm/sec

Temperature rise to be 100° - 30% = 70°C approximately

Heat input maximum = 16 x 0.06 x 70 = 67 calories/sec = 280 watt

Electrothermal heating cord $\frac{3}{16}$ in. diameter heat input 60 watt/ft or cord as a 5 ft length wound over $\frac{1}{8}$ in. bore tube (say $\frac{1}{4}$ in. O/D).

12 in. long heat insulated would provide sufficient heating.

8.4.3 Flowmeter

Flow rates to be measured: 0.2 to 6 gm/sec

For calibration purposes:

1 gm/sec cesium = 0.544 cm^3/sec.

Assume magnetic flowmeter with 1 mm bore throat = 0.00784 cm^2

flow velocity at 1 gm/sec = $\frac{0.544}{0.00784}$ = ~ 70 cm/sec

If ceramic, quartz or sapphire flowmeter tube is used, generated voltage ignoring hydraulic losses is as follows, assuming magnet flux of 1 T.

voltage = B.L.V. volt

= 1 x 0.001 x 0.7

generated voltage = 0.7 millivolt per gm/sec

8.4.4 Electromagnetic pump

Flow rate based on constant 16 gm/sec cesium i.e 8.7 cm^3/sec = q, say.
Pressure rise through pump based on 30 psi, i.e. 2020 gm/cm^2 = P.

Assuming that cesium wets fairly well and that stainless steel can be used for the pump channel the following proposal is based on a d.c. conduction pump in which the iron circuit is magnetised from a series connected winding with the channel current source, from a static rectifier set.

resistivity of cesium = 37 microhm. cm
resistivity of
stainless steel = 70 microhm. cm
resistivity of copper = 1.72 microhm. cm

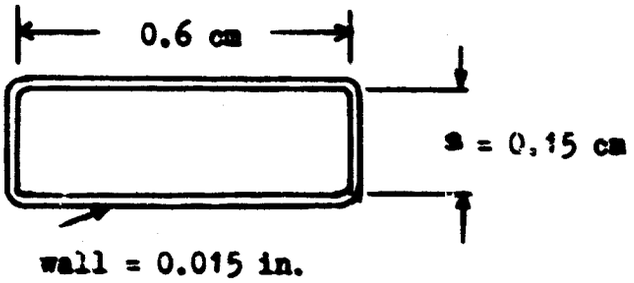

Assume: channel length in concentrated flux as 4 cm long; leakage current bypass length in walls 1 cm each end; and leakage current bypass length in cesium 0.5 cm each end.

resistance of walls:

$$R_w = \frac{70 \times 0.6}{6 \times 2 \times 0.015 \times 2.54} = 92 \text{ microhm}$$

resistance of bypass path in cesium:

$$R_b = \frac{37 \times 0.6}{0.5 \times 2 \times 0.15} = 148 \text{ microhm}$$

resistance of cesium in concentrated flux:

$$R_e = \frac{37 \times 0.6}{4 \times 0.15} = 37 \text{ microhm}$$

From electromagnetic theory:

pressure rise through pump: $p = \frac{B.I_e}{10 \times S}$ dyne/cm^2

or current through cesium in concentrated flux:

$$I_e = \frac{10\ ps}{B} \text{ amp}$$

With a flux density B of 10×10^3 gauss:

$$I_e = \frac{10 \times 2020 \times 981 \times 0.15}{10 \times 10^3}$$

$$\underline{I_e = 296 \text{ amp}}$$

Back emf generated by cesium in pump channel:

$$E_c = \frac{B.q}{10^8 s}$$

$$= \frac{10 \times 10^3 \times 8.7}{10^8 \times 0.15} = 5.8 \times 10^{-3} \text{ volt}$$

Pump channel gap = (0.059 in.) + (0.030 in.) + (0.03 in. insulation) $\simeq$ 0.12 in.
Iron circuit mean length, say, 17 in.
Pole face area = 4 x 0.6 = 2.4 cm^2.
For 0.12 in. gap assume "fringing" loss to increase gap 'plan view' area by 30%, i.e. to 3.12 cm^2.
Also flux leakage for 0.12 in. gap, say, 10%.
If B' is iron flux density at the poles: total iron flux = 2.4 B' gauss; allowing for 10% leakage, total air gap flux = 2.16 B' gauss.

Then gap flux density = $\frac{2.16\ B'}{3.12}$ = 0.69 B' gauss

$\therefore$ 10000 = 0.69 B'

or B' = 14500 line/cm^2.

From standard B/H curves:

For air gap, the amp-turns/in. at flux density 10^4 gauss = 20,000.

For average mild steel, amp-turn/in. at flux density 14500 gauss = 120

or, if general body of iron circuit is 4 cm^2 cross section in "Purefee" iron, amp-turns/in. = 20 .

Then total amp-turns required = 20000 x 0.12 + 20 x 17

= 2740

i.e. at 590 amp, number of turns = 5 approximately.

Power consumed by energizing coil (1.75 in. diameter x 5 turns)

Coil of $\frac{1}{2}$ inch square copper, i.e. 1.61 cm^2 area.

Length of winding and connections on pump but excluding external busbars,

= (1.75 x 3.12x 5) + 8

= 27.5 + 8 = 35.5 in. = 90 cm

Resistance of winding and ends

$$R = 1.72 \times \frac{90}{1.61} = 96 \text{ microhm}$$

Wattage of winding $= I^2.R$

$= 590^2 \times 96 \times 10^{-6}$

= <u>33.5 watt</u>

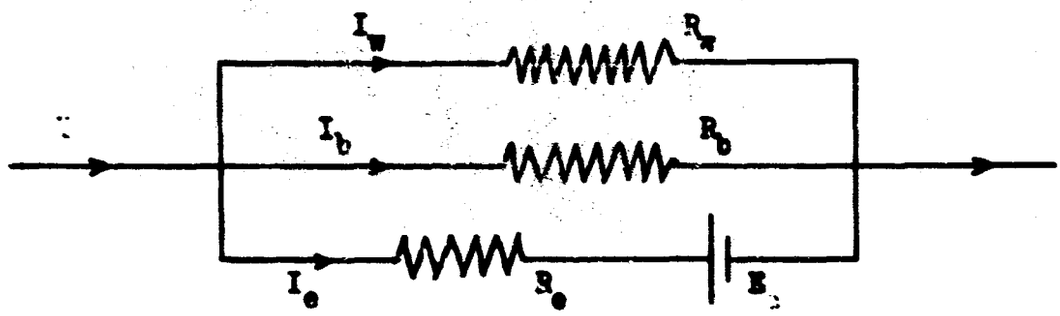

From the above circuit we have the following relationships:

Overall voltage $V = I_e R_e + E_c$ .....(8.1)

$$I = I_w + I_b + I_e$$

$$I_w + I_b = \frac{V}{RB} \qquad \text{where } RB = \frac{R_w.R_b}{R_w + R_b}$$

$$\therefore\ I = \frac{V}{RB} + I_e$$

$$\text{or } V = L.R.B - I_e.RB \qquad \text{.....(8.2)}$$

Equating equations (8.1) and (8.2)

$$I_e.R_e + E_c = I.RB - I_e.R_b$$

or $E_c = I.RB - I_e (RB + R_e)$ .....(8.3)

Now $R_b = \frac{92 \times 148}{92 \times 148} \times 10^{-6} = \frac{13,600}{240} \times 10^{-6} = 56.7$ microhm

From equation (8.3), $5.8 \times 10^{-3} = I \times 56.7 \times 10^{-6} - 296 (56.7 \times 10^{-6} + 37 \times 10^{-6})$

or $I = (5.8 + 296 \times 93.7 \times 10^{-3}) \frac{1}{56.7 \times 10^{-3}}$

$\underline{I = 590 \text{ amp}}$

From equation (8.1) $V = 296 \times 37 \times 10^{-6} + 5.8 \times 10^{-3}$

$\underline{V = 16.8 \text{ millivolt}}$

Power in pump channel = V x I

$\simeq \underline{10 \text{ watt}}$

Mechanical power developed in the cesium:

work done/sec = q.p erg
= $8.7 \times 2020 \times 981 \times 10^{-7}$ watt
= 1.72 watt

Channel theoretical efficiency = $\frac{1.72}{10} \simeq 17$ per cent

Based on series connection with channel duct, winding current is 590 amp, and gap flux density of 10,000 gauss,

Voltage drop of coil = $96 \times 10^{-6} \times 590$
= 56.5 millivolt.

Then voltage drop across pump channel and coil = 73.3 millivolt

8.5 COMMISSIONING TESTS OF ORIGINAL CESIUM INJECTION CIRCUIT

8.5.1 Circuit reclamation

Earlier work has been reported in Technical Summary Report IRD 63-1; Fig. 8.1 shows the continuous cycle cesium injection facility.

The plant was fully reassembled as originally designed with the flowmeter in circuit and a bypass pipe run from the system outlet to the dump tank to make a closed system in which cesium could be circulated. An attempt was then made to clean the system by inserting a pump in this line and circulating a solution of 10% nitric acid and 5% hydrofluoric acid. After about 2 hr the motorised bypass valve developed a leak round the shaft seal. Shortly afterwards one of

the pneumatically operated shut-off valves developed a similar leak. It appeared that this could only have been caused by failure of the stainless steel bellows in the valves which serve as an air-tight seal between cesium and atmosphere. Subsequent stripping down of the valves, which are a welded assembly, proved this to be so, and metallographic examination (Fig. 8.9) of the damaged bellows (Fig. 8.2) showed extensive attack of the grain boundaries and consequent weakening and embrittlement of the 0.005 in. thick stainless steel (En58B) material. The appearance of the material under magnification was similar to some previously examined that had been attacked by cesium.

To establish the precise nature of the attack and the effect of the cleaning solution, a fresh sample of solution was made up and a new bellows immersed in it. Fairly rapid chemical action was seen to take place and the solution rapidly discoloured until the bellows was invisible. After 45 min the bellows were removed and seen to be in a similar state to those attacked in the assembly.

It was concluded after metallographic examination of this bellows and of a bellows in the 'as-received' condition that the material was not to specification and that this type of attack, by both cesium and dilute acid, was due to the material being unstabilized.

Because of the severity of the attack the other valves were dismantled to establish the condition of their bellows. Only one other bellows (the long bellows in the other motorized valve) had suffered attack; the other four were in sound condition and it was probable that these were manufactured from the correct material.

8.5.2 Operation of motorized control valves

The plant had been assembled with both motorized control valves in circuit. The motors are single phase a.c. 50 c/s 250 V and operate the valves via a reduction gear giving 0.25 rpm output and a short lever connected to the valve.

The flow of each valve is controlled by the position of a taper needle in an orifice, and it is intended that the constant output of the pump is metered to the rig in the required amount by adjusting the position of the two taper needles, allowing the proportion of pump output not required by the rig to be returned to the dump tank via the by-pass valve. The valves therefore work in opposition and opening and closing of the two valves is achieved by reversed field windings, changed by means of contactors and micro-switches at the two limit positions of each valve. The valves are thus set up with one in the fully open position and the other in the fully closed position. It is not required that a positive shut-off should be achieved by these valves, this being done by

the pneumatically-operated shut-off valves.

On attempting to operate this system the two valves were found, after being set up as above, to 'creep' on each other until one was on its limit where it was restrained mechanically with considerable stress on the linkage: the proportion of flow was no longer accurately shared between the two valves. This 'creep' would appear to be an inherent feature of a control system of this nature and was due to one or all of the following reasons:

there is a certain degree of 'over-run' after power is cut off to each motor, any difference in this amount of over-run between the two motors (or between the forward and reverse running of each motor) being added into the system as a further positional difference between each valve;

the speed of each motor was not measured, but a difference of only a few rpm would contribute a similar error;

the dead space zone in between the two contact positions on the microswitches might also introduce a similar error; and

there was considerable back-lash in the reduction gears, contributing a positional error between the two valves, although this should be constant.

Measurement of the amount of creep using one valve as datum and running the other on to its limit after several reversals showed that the cumulative error amounted to approximately 0.015 in. per reversal. As frequent reversals take place in attempting to control the flow by this method, this amount is serious. Operation of these valves by two separate motors seems unnecessary in theory and was found to be unsatisfactory in practice. A modification has been arranged for the two valves to be mechanically linked in opposition and operated by one motor, thus obviating all the difficulties listed above.

8.5.3 Re-assembly of system for further attempt to circulate cesium

The system was re-assembled with the motorized valves replaced by hand-operated bellows valves. One pneumatic shut-off valve between the dump tank and filter was omitted from the system because of lack of availability of valves because of damaged bellows.

An attempt was made to fill the circuit with cesium using a single valve cylinder (supplied through Light and Co Ltd) but, on pumping down, the cylinder was found to leak round the (Hoke) valve shaft, which would have resulted in contact of cesium with air had the valve been opened.

A (American Potash and Chemical Co) 1 lb cylinder was substituted. This

is a two-valve cylinder, permitting pressurization of the can by inert gas to evacuate the contents. The Hoke valves on this cylinder also leaked but, after sealing with Araldite, the can could be immersed under oil during the filling operation.

The can was immersed in oil and heated to 60°C and connected to the plant and to a helium line. The whole plant was brought up to 60°C by means of an electric air heater in the enclosing cabinet. It was then evacuated and purged with helium. The cesium cylinder was pressurized, the valves opened to the plant, and about 0.5 lb of cesium was successfully transferred from the can to the plant. An attempt to circulate cesium by means of the electromagnetic pump was not successful despite several attempts and variation of procedure, reversal of pump connections, evacuation and pressurization of the lines. The system was emptied of cesium, with some difficulty, about 0.2 lb of clean cesium being recovered, and stripped down for examination. This established that the cesium has passed right through the system and that the most likely fault lay in the pump itself. The magnetic field of the pump was examined using a Hall type probe and was found to have a strength of only 4 kgauss (Fig. 8.3) compared with a design figure of 10 kgauss, the magnet saturating at 300 amp.

A simple loop was set up containing only the pump with a pipe from inlet to outlet, and filling and evacuating lines. This was filled with cesium recovered from the plant. Again no circulation took place, and this loop was stripped after examination. The flow meter was checked by passing mercury and was found to give an indication of flow.

The pump was then set up in a horizontal position and filled with mercury, a glass tube containing a mercury column being arranged at inlet and outlet. On supplying power at ambient temperature, the pump created a pressure difference equivalent to a column of mercury in 3 mm bore tubing 3.3 cm high. This compares unfavourably with the 35 psi design pressure rise of the pump (with cesium). This test is open to criticism on the grounds that the behaviour of mercury is not necessarily the same as that of cesium under these conditions but, even with the lower magnetic field strength, a better result than this would be expected.

The electromagnetic pump channel was stripped and inspected. The original specification called for a homogeneous layer of copper to be built around the channel for attachment of the current-carrying copper connections; from the appearance of the channel it had been connected by attempting a direct braze between the massive copper leads and the 0.015 in. thick stainless steel channel, promoting oxide filming, the retention apparently being achieved with "lipping"

of the braze material around the channel edges. The pole faces of the magnet were misaligned and one face only was insulated electrically from the channel.

8.5.4 Electromagnetic

Stabilized stainless steel (18/8) has been electropolished and jig-formed to give a channel of longer dimensions, sealed along its axis and ends by electron beam welding. Three channels in the closed capsule form are being built up with electrolytically deposited copper. This is to be machine-profiled and argon arc welded to the copper current carriers.

8.5.5 Magnet

The flux density of the magnet has been rechecked free from the support plate using a Hall probe. Saturation occurred at 4.2 kgauss. A similarly profiled iron circuit in mild steel was formed and checked to give 6.7 kgauss; from this it appears that the original 'Purefee' iron material is faulty.

8.5.6 Further work

Future work with the continuous cesium pumping and metering system is programmed around the electromagnetic pump and flowmeter, existing pneumatic stop valves, linked control valves and 0.25 in. bore piping. An in-line gettering tank running at 1100°K with zirconium will replace the present dump tank.

8.6 SIMPLE INJECTION SYSTEM FOR POWER GENERATION EXPERIMENTS (MARCH, 1964)

To allow seeded operation of the loop a simple constant cesium injection feed system was devised (Fig. 8.4). A small storage tank filled with cesium (filtered and gettered with zirconium at 800°K) was attached to the loop. A variable and metered supply of pure helium allowed for a constant cesium feed from the storage tank to the loop through a hyperdermic needle. The system was previously calibrated with distilled water at 42°C (viscosity approximately equivalent to cesium at this temperature) and with cesium under glove-box conditions. A satisfactory correlation was found between the two. A 0.041 in. bore hyperdermic allowed seeding fractions of the order of 0.5^a/o to be maintained and during the seeded operation of the loop approximately 380 gm of cesium was successfully injected.

8.7 MICRO-FEED CESIUM INJECTION SYSTEM

Two similar systems have been developed from the micro-feed piston displacement concept. Fig. 8.5 shows details of the solid piston system, and Fig. 8.6 the system during commissioning and calibration. Fig. 8.7 is a

schematic arrangement of the oil piston displacement feed system. Both systems are arranged to feed up to 2% cesium seed fraction to the main helium stream. Full design and commissioning details will be given in the subsequent Technical Summary Report.

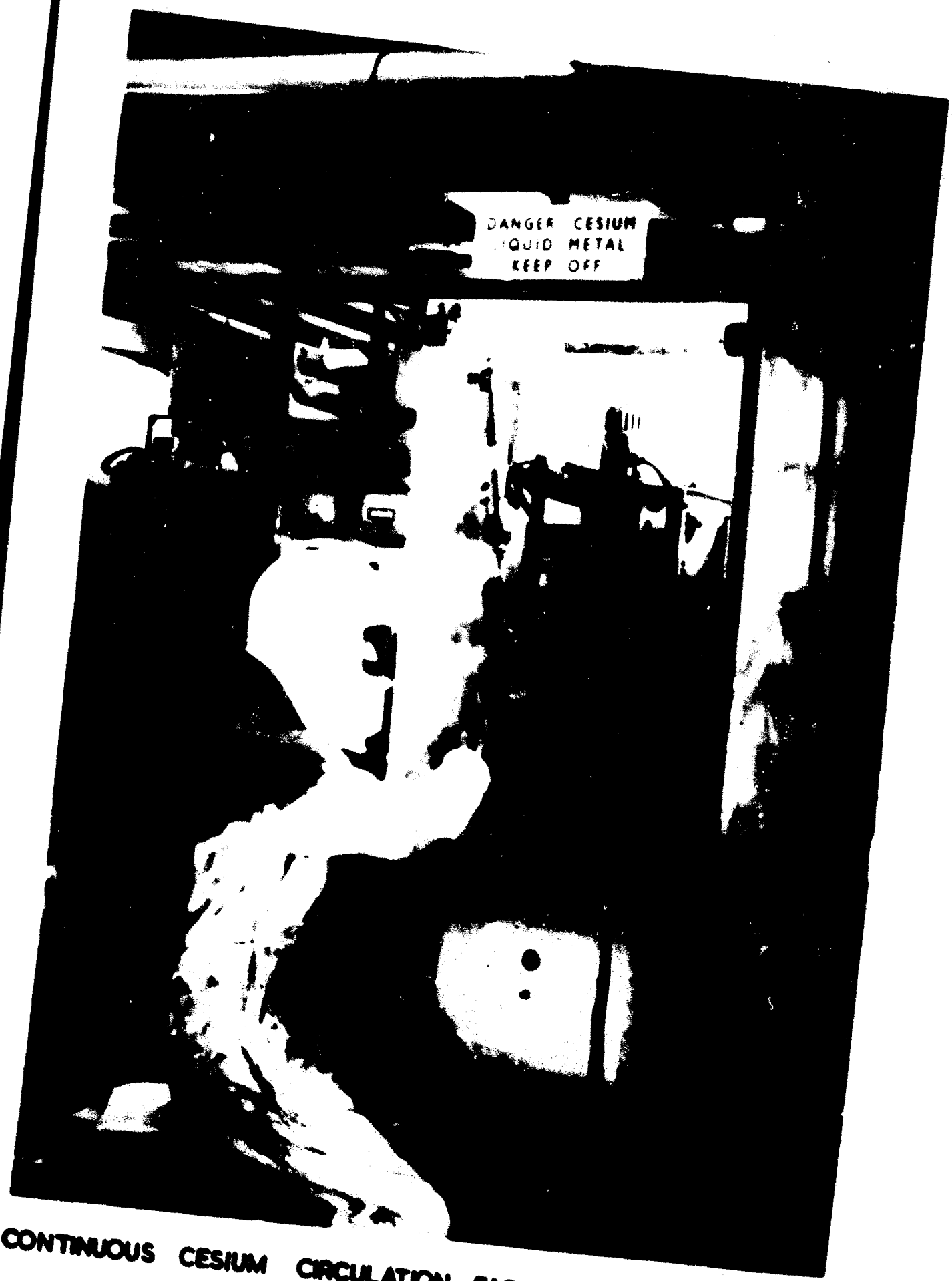

CONTINUOUS CESIUM CIRCULATION FACILITY

FIG 8.1

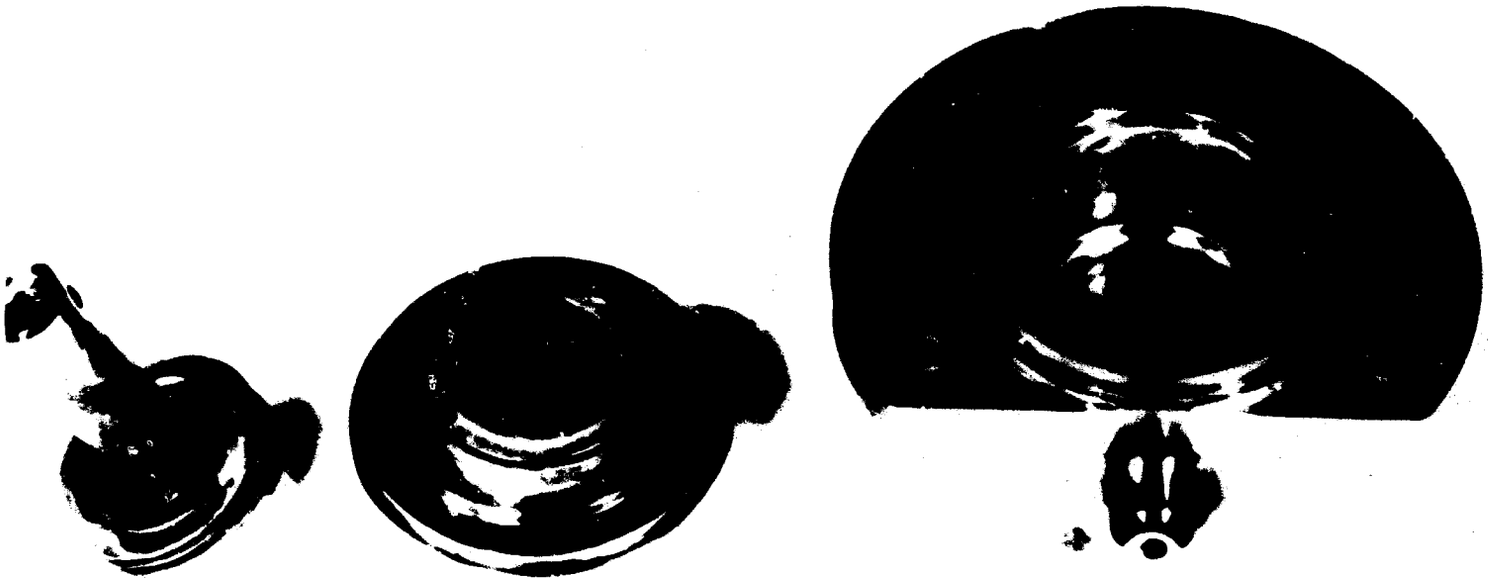

ESIUM ATTACK ON UNSTABILISED STAINLESS STEEL VALVE

FIG 8.3

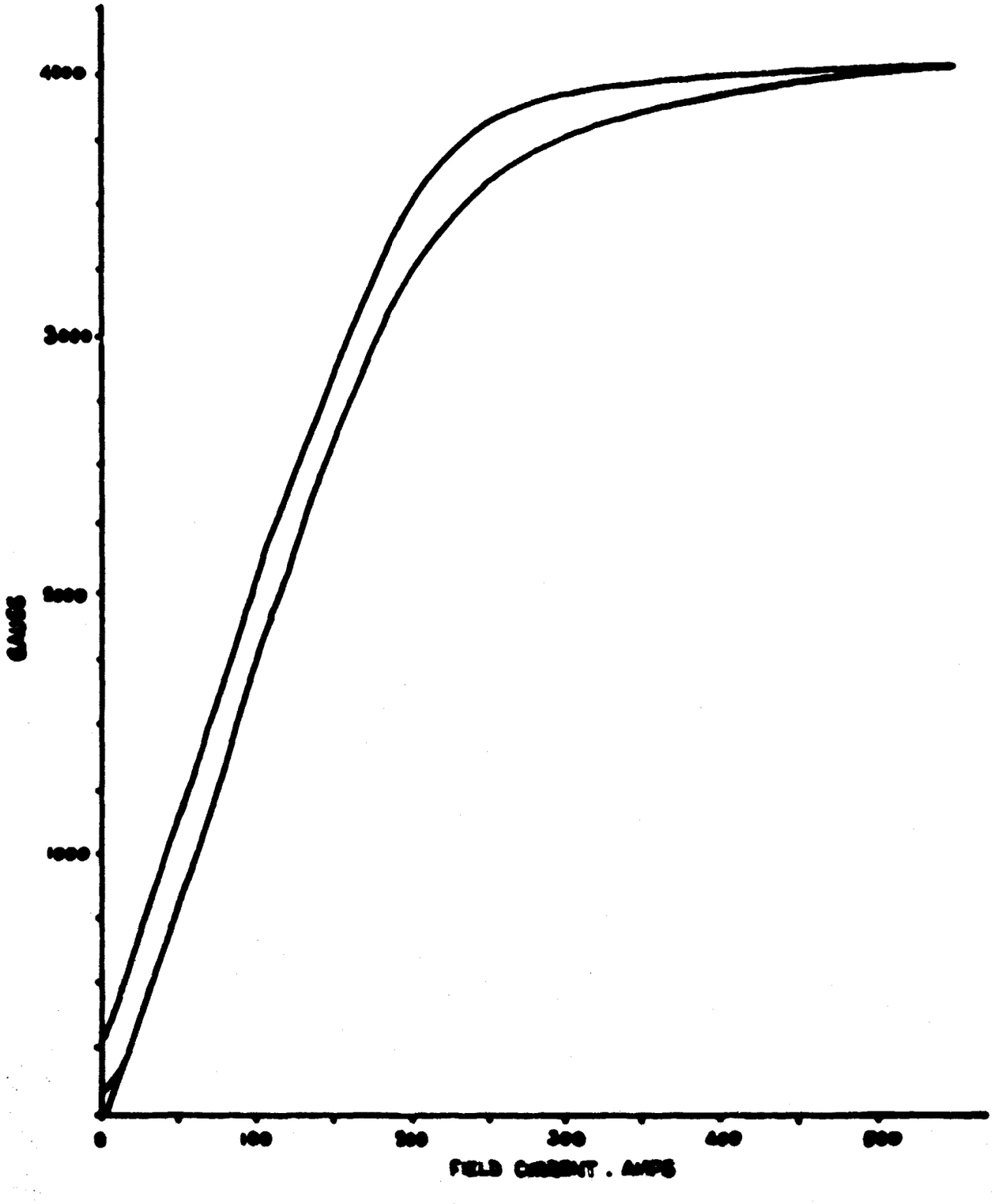

FRAZER NASH ELECTROMAGNETIC CESIUM PUMP
MAGNETISATION CHARACTERISTIC OBTAINED USING
HALL PROBE-TYPE GAUSSMETER

FIG 8.3

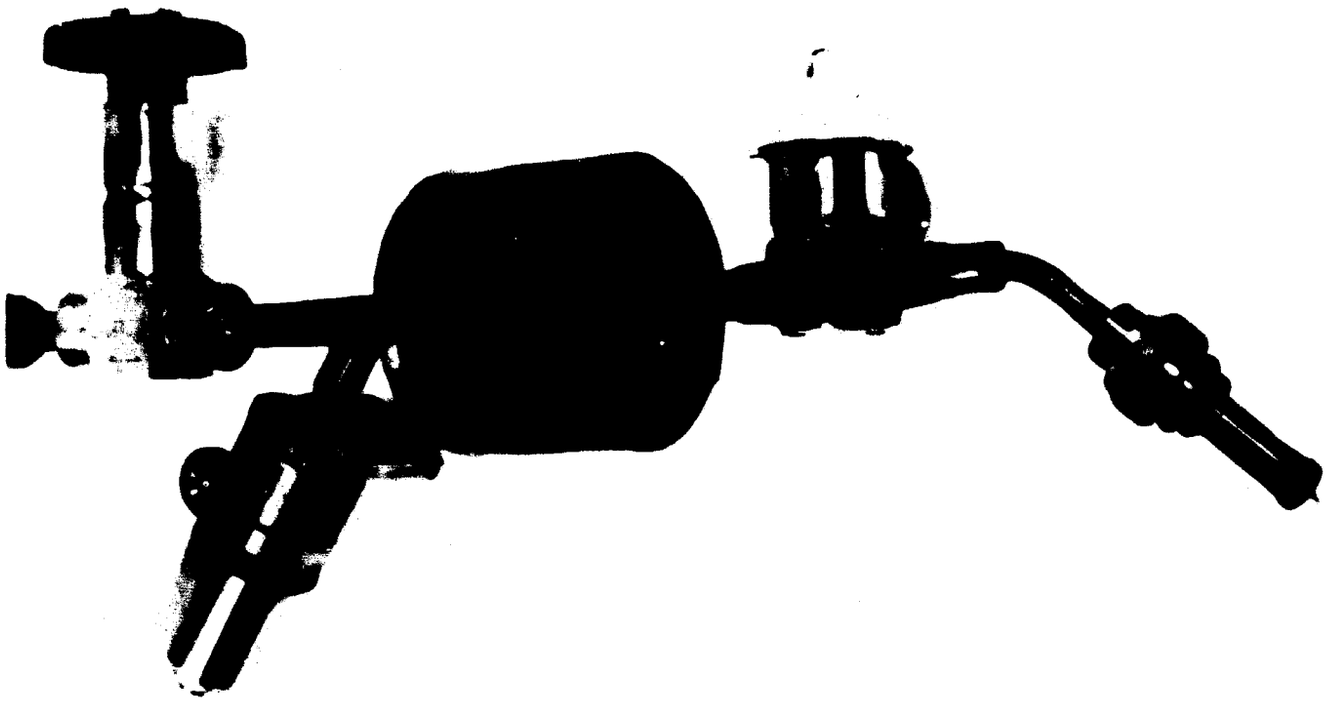

HORT TERM CESIUM INJECTION SYSTEM

FIG 8·4

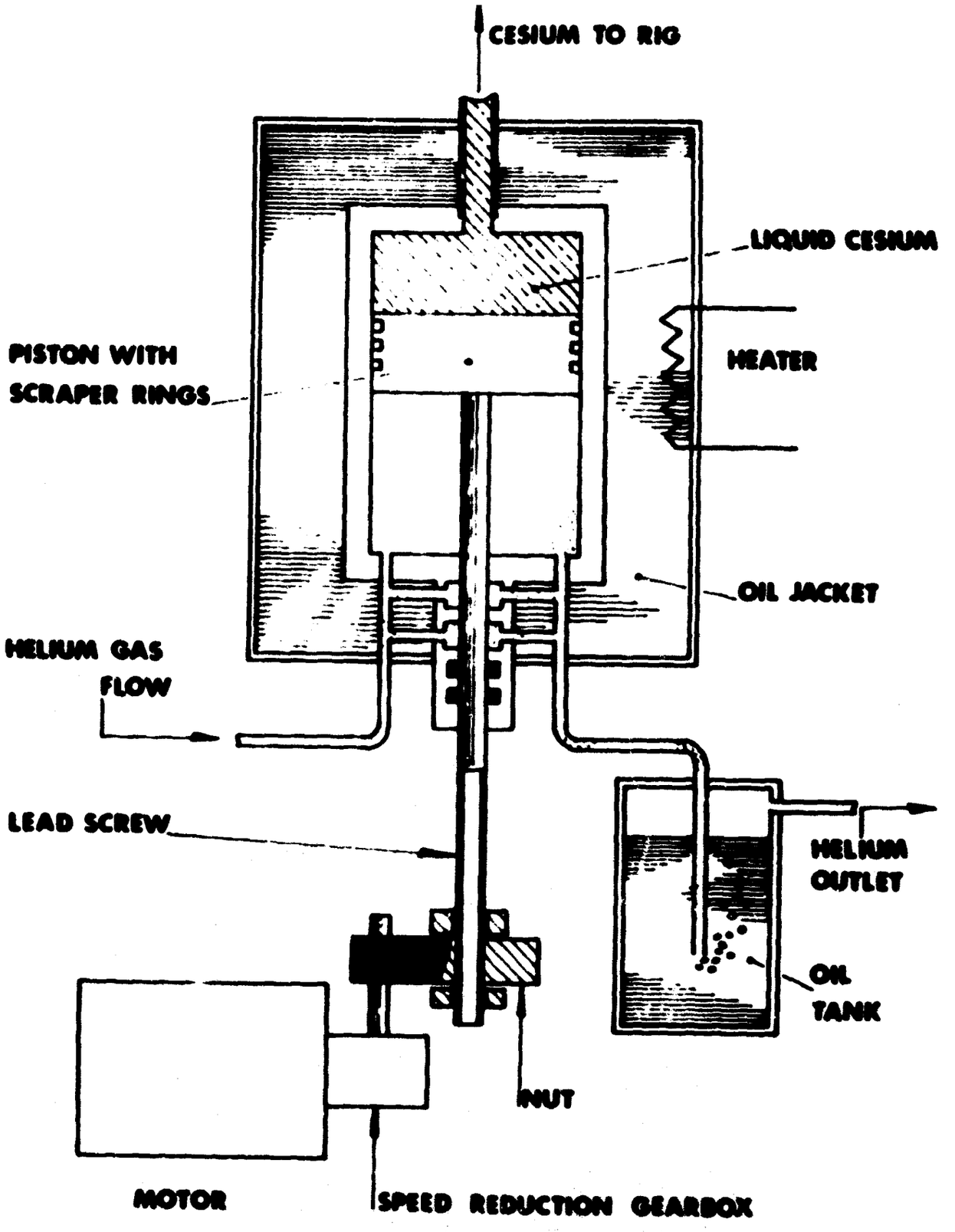

CESIUM INJECTION SYSTEM MECHANICAL PISTON (SCHEMATIC)

FIG 8.5

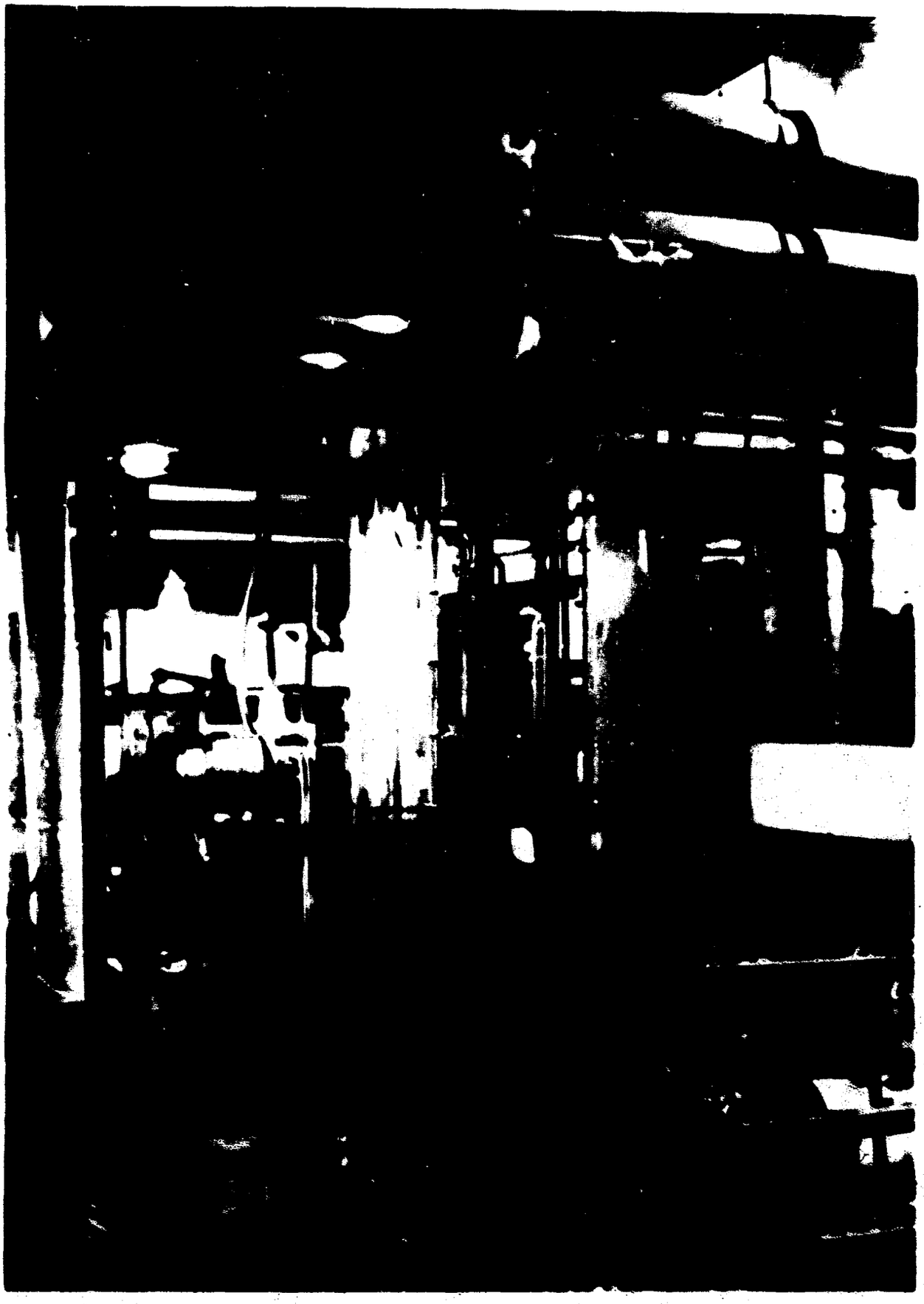

MICRO-FEED CYLINDER UNDER TEST

FIG 8.6

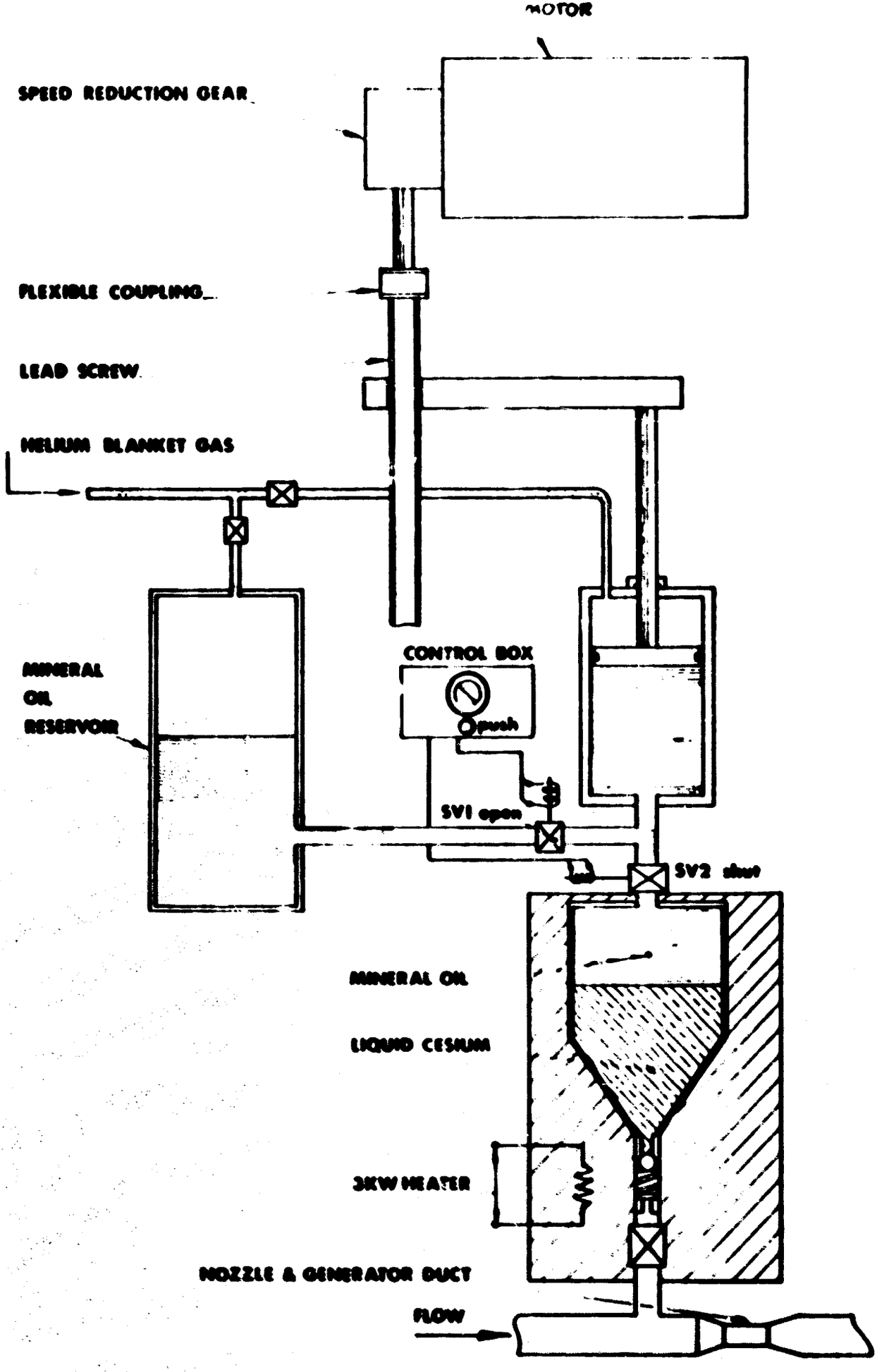

CESIUM INJECTION SYSTEM, OIL PISTON (SCHEMATIC)

FIG 8·7

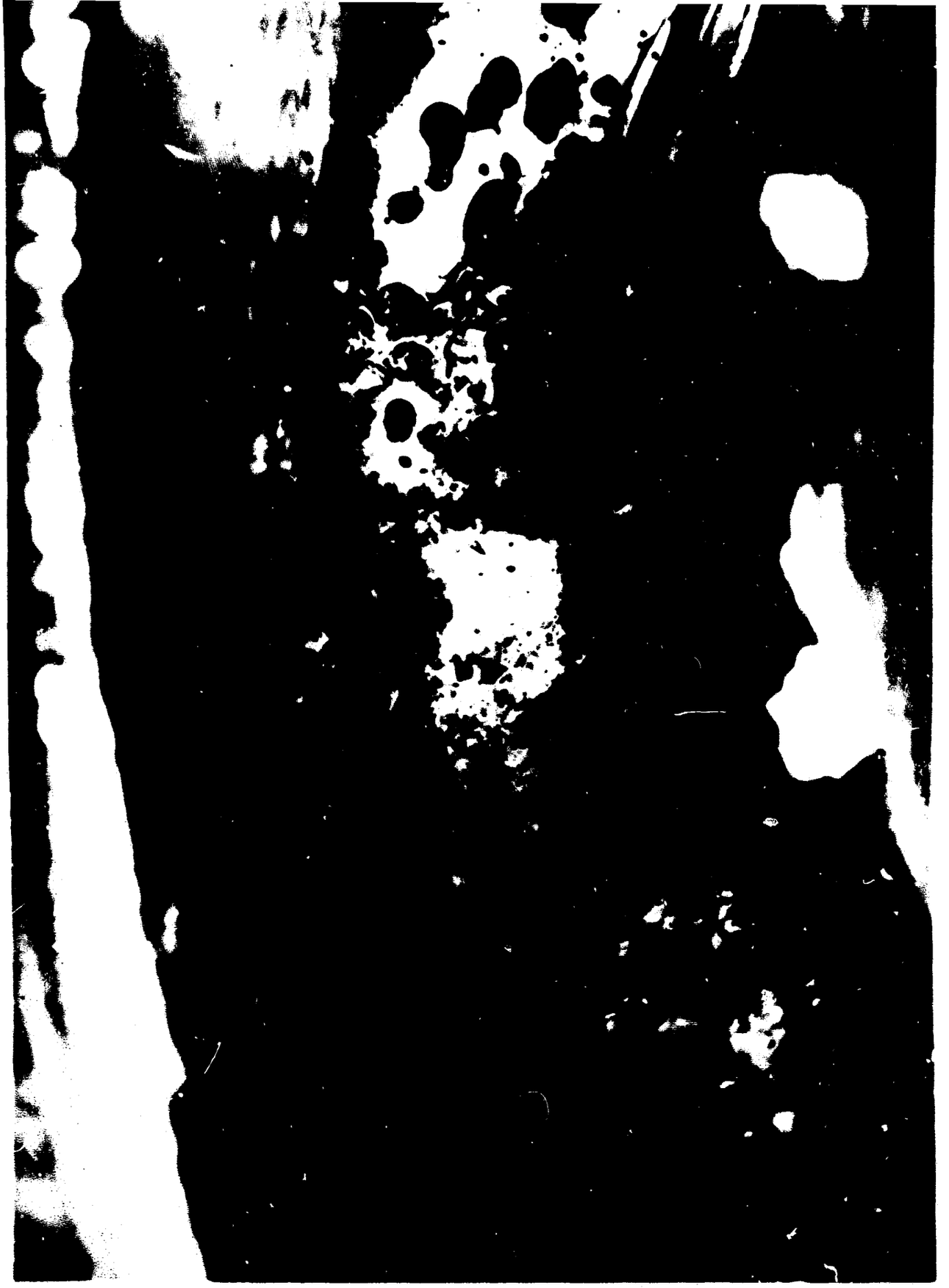

CESIUM DEPOSITION IN PRE-COOLER OUTLET

FIG. 8·8

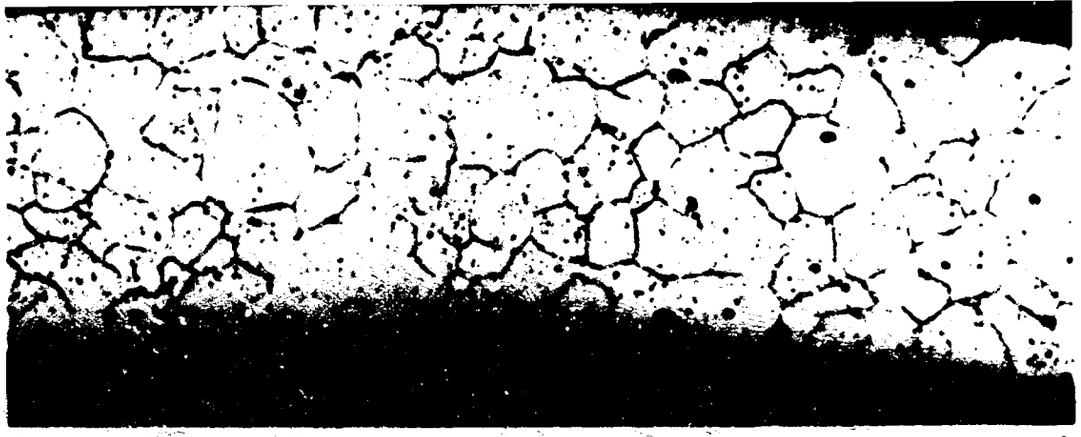

(i) CARBIDE PRECIPITATION IN ORIGINAL MATERIAL (X 300)

(ii) SEVERE INTERGRANULAR ATTACK IN SPECIMEN 2 (X300)

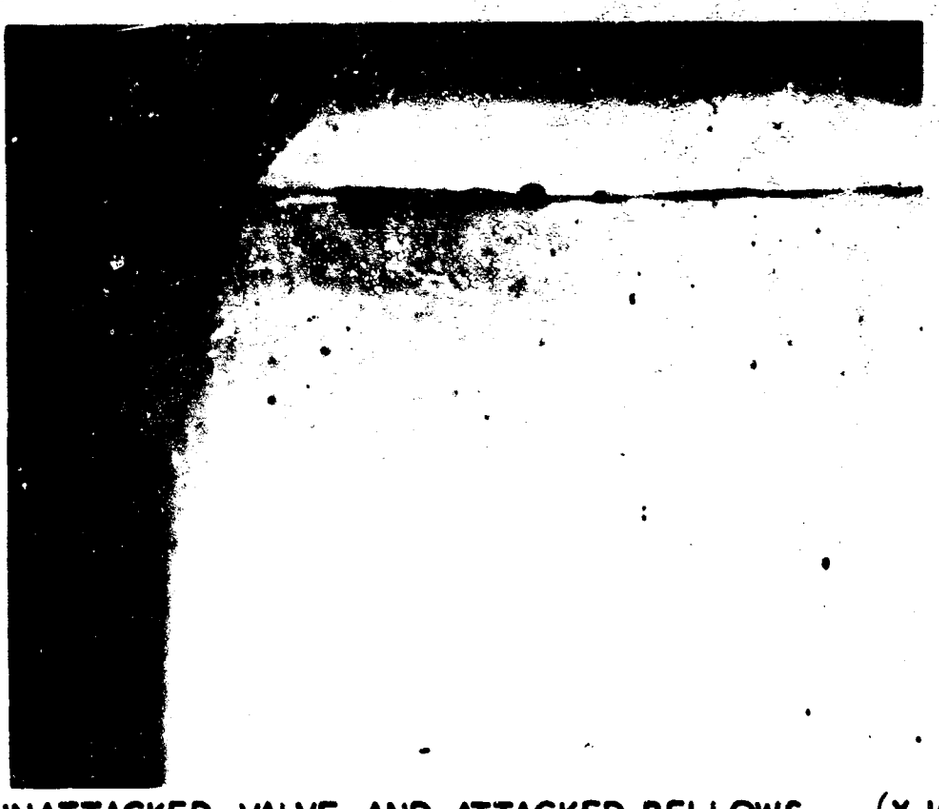

(iii) UNATTACKED VALVE AND ATTACKED BELLOWS (X 100)

METALLOGRAPHIC EXAMINATION OF STOP VALVE BELLOWS

FIG 8·9

CHAPTER 9

GENERATOR DUCT

by

R. Brown

9.1 DEVELOPMENT OF GENERATOR DUCT

The MPD generator test section and its mode of operation under loop conditions has been discussed previously (Technical Summary Report IRD 63-1, Section 6.8). Difficulties experienced with the manufacture of the high-density, high-purity recrystallized alumina channel sections and development problems associated with the high temperature heater precluded its installation in the loop until September 1963.

Initially a simple recrystallized alumina two-electrode (tantalum 0.5 in. diameter) pair rectangular test section (1.5 in. x 0.5 in.) was assembled in the loop (Figs. 9.1 and 9.2). Severe problems were encountered in alignment and location of the ceramic/metal systems and in sealing the rectangular encasement flanges; it is probable that the final assembly was under severe axial and transverse mechanical stress.

After two carefully controlled thermal cycles under loop conditions with helium alone, the duct was stripped and inspected. It appeared that the ceramic section had maintained a smooth gas channel during operation, but all four wall sections were severely fractured, the main cause being mechanical stress. Minor cracks in the side walls were typical of thermal stress patterns (Fig. 9.3 (a and b)).

The support and housing arrangement for the generator section, tantalum transfer duct, cesium injection and supersonic expansion nozzle was redesigned.

During previous high temperature runs with helium, overheating ($\sim 1200^{\circ}K$) of the throat section of the subsonic diffuser (single skin $\frac{1}{8}$ in. stainless steel construction) had occurred. Compatibility tests with stabilized stainless steels and cesium vapour at high temperatures (up to $1150^{\circ}K$) have shown evidence of the possibility of rapid intergranular attack leading to disintegration. The high temperature potential of the IRD closed loop is $2500^{\circ}K$ and for high temperature operation the single skin diffuser was considered a definite hazard.

Consequently the first 14 in. diffuser section was fabricated from tantalum/10% tungsten alloy (0.020 in. section) and integrated as an extension of the redesigned duct and transfer system.

The transfer, generator and diffuser ducts are now supported by a single stainless steel square section beam (Fig. 9.4). The systems can be accurately aligned free from strain, instrumentated, thermally insulated and loaded as a completed unit into a single containment stainless steel case (Fig. 9.5). The rectangular sealing flanges have been scrapped and water cooled (externally); rubber and/or metal O rings in seal flanges have been successfully developed.

Further problems with recrystallised alumina were considered possible and a renewed generator duct materials survey was initiated. As the channel wall temperature conditions appear to be less severe than at first envisaged boron nitride was carefully considered as an alternative generator duct material. Its vapour pressure characteristic permits operation up to 2070°K; the electrical resistivity of boron nitride at this temperature compares favourably with alumina, its resistance to thermal stress is excellent and it is readily machined with conventional equipment. An extended programme of compatability tests between boron nitride and cesium at elevated temperatures has been undertaken (Chapter 12) and it is shown that no significant attack occurs.

A second generator test section was constructed to the original dimensions. The four interlocking pieces comprised:

side wall: high purity, high density recrystallized alumina - (slip cast manufacture);

side wall: high purity, high density recrystallized alumina - (hot pressed manufacture);

bottom wall: high purity, high density recrystallized alumina - nine electrode $\frac{1}{2}$ in. x $\frac{1}{2}$ in. tantalum;

top wall: boron nitride - sapphire insert.

The duct channel was thermally insulated with Zirconia E fibres (Hitco Ltd.) and wa subjected to several thermal cycles during the heater development programme.

Several thermal stress conditions occurred on more than one occasion (cooling at 200°C/min), resulting in minor cracking of the alumina side walls, a single fracture of the bottom wall, and no noticeable damage to the boron nitride wall. Owing to water ingress into the loop under high temperature conditions, embrittlement and fracture of the tantalum 10 per cent tungsten diffuser section occurred (Fig. 9.6) and a replacement finned stainless steel (EN 58B) diffuser

was fitted (Fig. 9.7) and successfully operated.

At this stage extensive repair to the high temperature tantalum transfer duct necessitated its return to the fabricators, Murex Ltd.

As a considerable delay appeared likely, an inert atmosphere, high purity, refractory metal welding facility was constructed. This enabled a temporary replacement thin section(0.015 in.) tantalum transfer duct, cesium injection, and expansion nozzle to be fabricated (Fig. 9.8). The cesium injection and vapourizer section comprised several layers of fine tantalum mesh ($\frac{1}{2}$ in. diameter discs) arranged within a tantalum tube leading into the high temperature gas region of the tantalum transfer duct. The vapourizer efficiency and short residence time of the cesium vapour in the hot helium before expansion into the generator section limited the envisaged cesium seed fraction to 0.5 a/o.

The generator system employed for the twenty seeded runs carried out during March 1964, (Chapters 4 and 5) is shown in Fig. 9.9.

9.2 SPECIFICATION

Channel walls (4) recrystallized, high purity, high density slip cast alumina.

Channel dimensions $1\frac{1}{2}$ in. x $\frac{1}{2}$ in. x 6 in.

5 pressure stations - top wall

2 high temperature thermocouples (flush in top wall)

5 electrode pairs, tantalum $\frac{1}{2}$ in. x $\frac{1}{2}$ in. x 6 in., inter-electrode spacing $\frac{5}{8}$ in.

9.3 CHANNEL SURFACE CONTAMINATION

Previous to seeded operation, after service at up to 1500°K, duct inner surfaces have been coated with dark grey or black deposits when removed. Preliminary metallographic examination of the surfaces showed the presence of tantalum oxide, tantalum carbide and iron. Electrical resistivity measurement showed the surfaces to be non-conducting (1 M ohm. cm). During seeded operation between injection periods measurements showed resistivities of the shortest paths to ground and the interelectrode paths to be >1000 ohm. Inspection afterwards showed the blocks to be again coated with electrically non-conducting black deposit, but lighter regions, in particular on the side walls (Fig. 9.10), were of a relatively low electrical resistance. At present the factors promoting this phenomenon are not understood. Preliminary investigation and analytical work is reported elsewhere (Chapters 4 and 12).

9.4 PRESENT STATUS

The latest generator systems programmed for seeded operation are at present under construction. Electrical end leakage considerations (Chapter 25) have led to an axial extension of the insulating generator duct walls at the subsonic diffuser end. Eighteen tantalum 10% tungsten strip electrode pairs are mounted flush in the channel walls (Fig. 9.11). The channel wall material is boron nitride and the duct internal dimensions are $1\frac{1}{2}$ in. x $\frac{1}{2}$ in. x $7\frac{3}{4}$ in. Inserted refractory metal pins will allow end leakage measurements to ground to be carried out (Chapter 10). The repaired tantalum high temperature transfer duct, modified cesium vapourizer, original nozzle, eighteen electrode pair duct and foreshortened stainless steel subsonic diffuser section are shown under assembly in Fig. 9.12. A stainless steel expansion bellows unit has been incorporated at the diffuser sliding connection to effect a gas seal and accommodate axial differential expansion relative to the outer containment case.

For further investigation into electrical generator duct end leakage problems electrically insulating expansion nozzle systems are being studied. A boron nitride nozzle is under construction for operation up to 2000°K (Fig. 9.13).

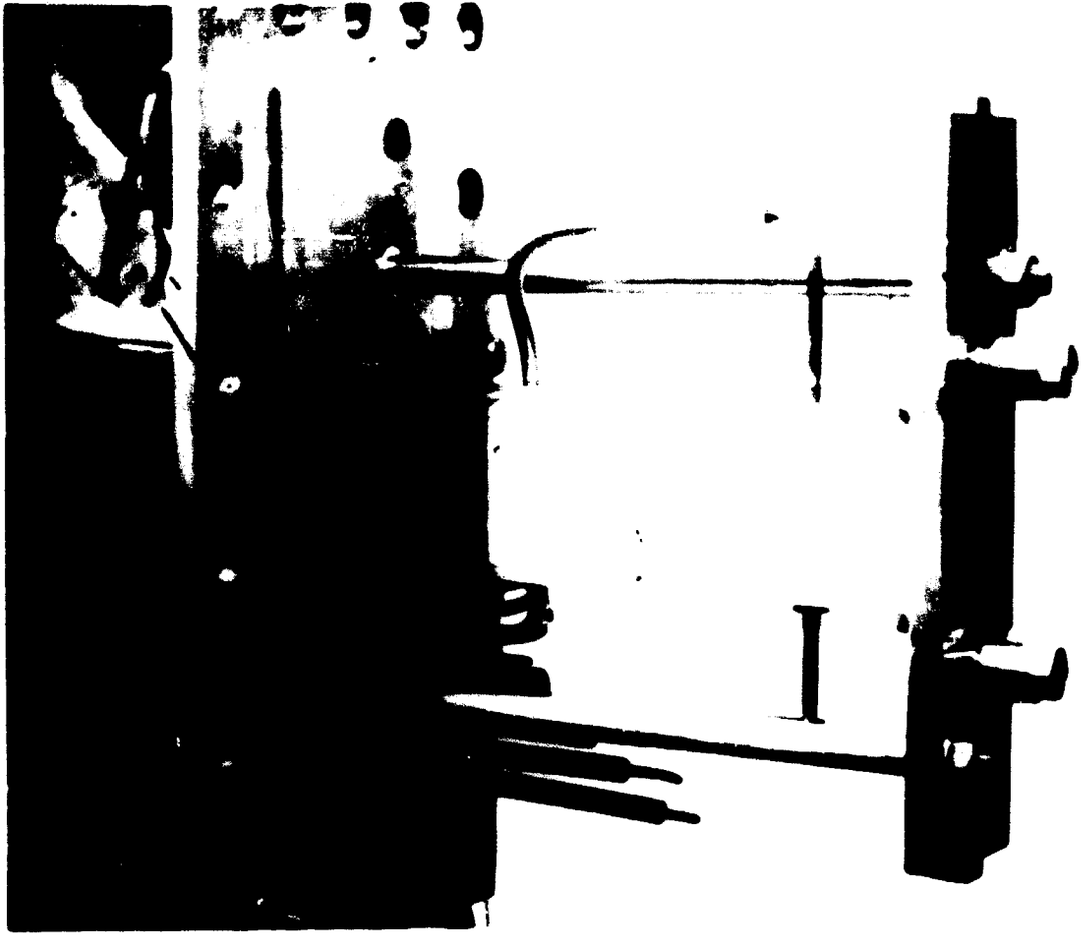

FIG 9.1 TWO-ELECTRODE GENERATOR DUCT ASSEMBLY

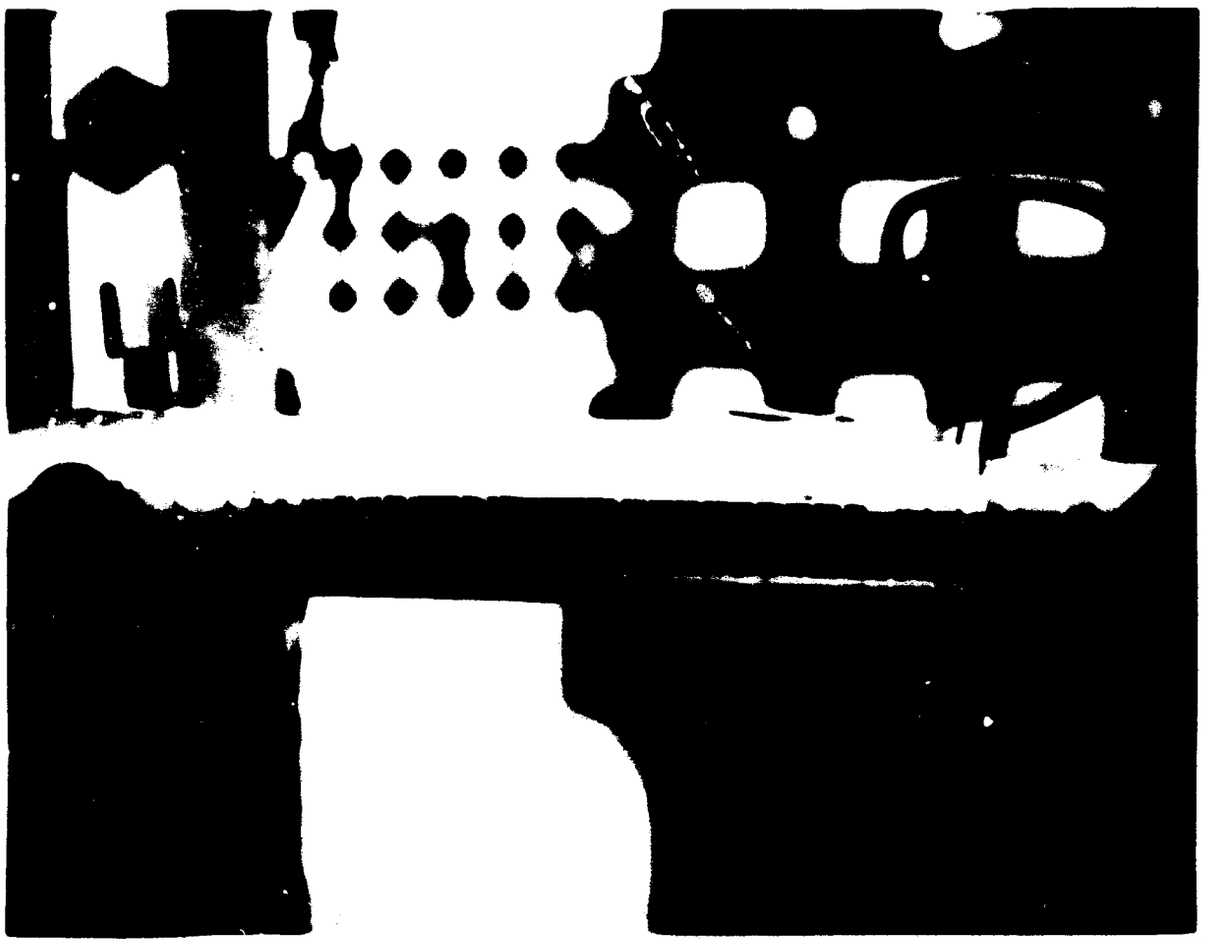

FIG 9.2 THERMALLY-INSULATED TANTALUM TRANSFER DUCT

FIGS 9·1 & 9·2

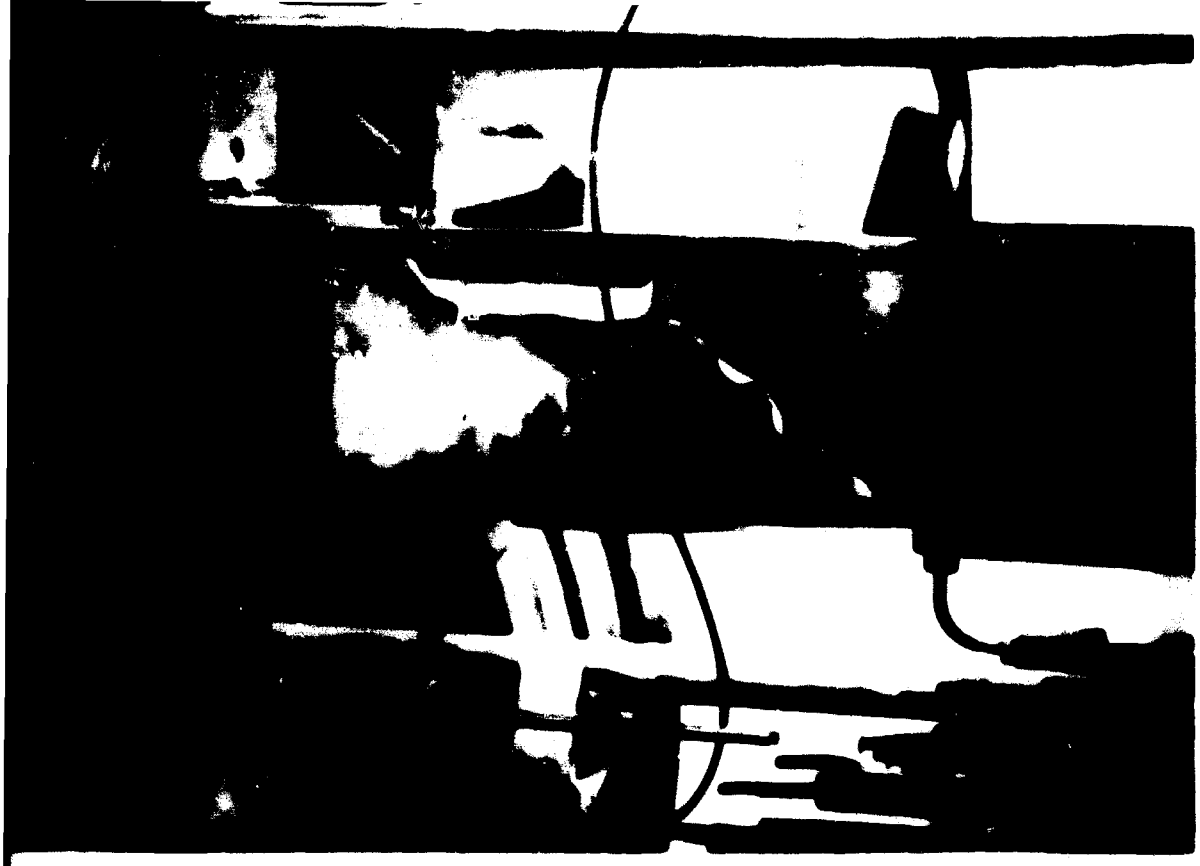

a) PRIOR TO DISSEMBLY

b) DISSEMBLED
TWO ELECTRODE GENERATOR DUCT AFTER THERMAL CYCLE

FIG 9-3(a,b

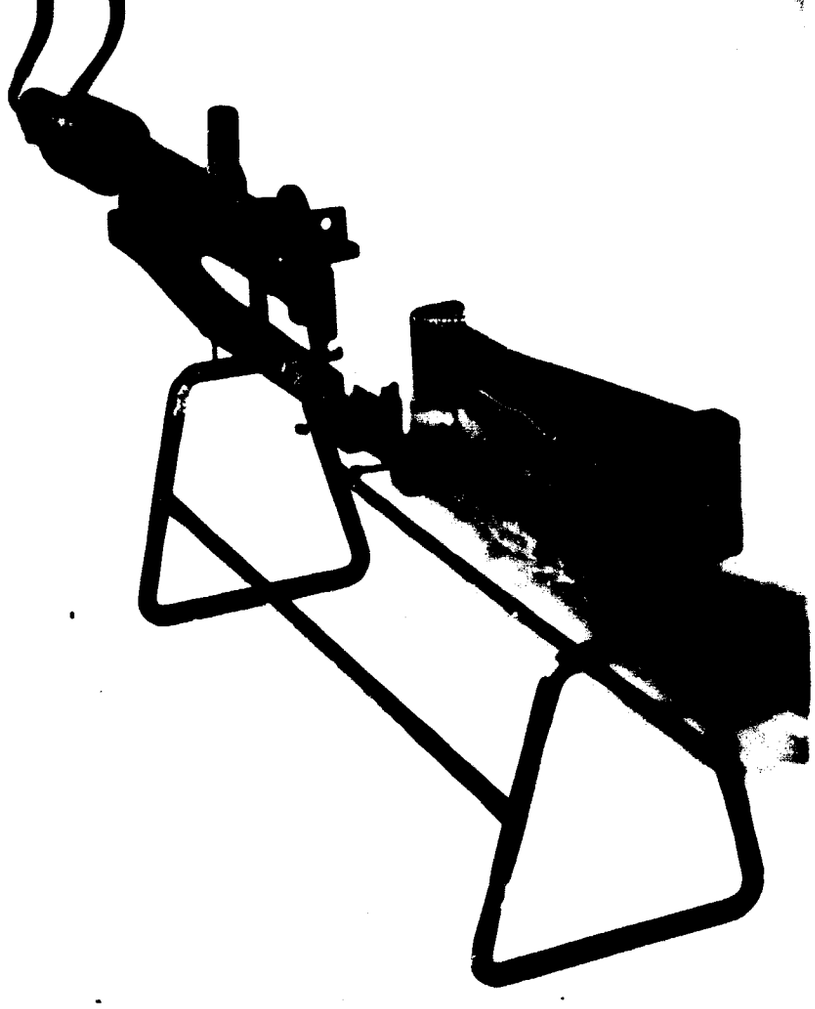

FIG 9.4 MODIFIED SUPPORT SYSTEM FOR TRANSFER DUCT, GENERATOR AND DIFFUSER INLET

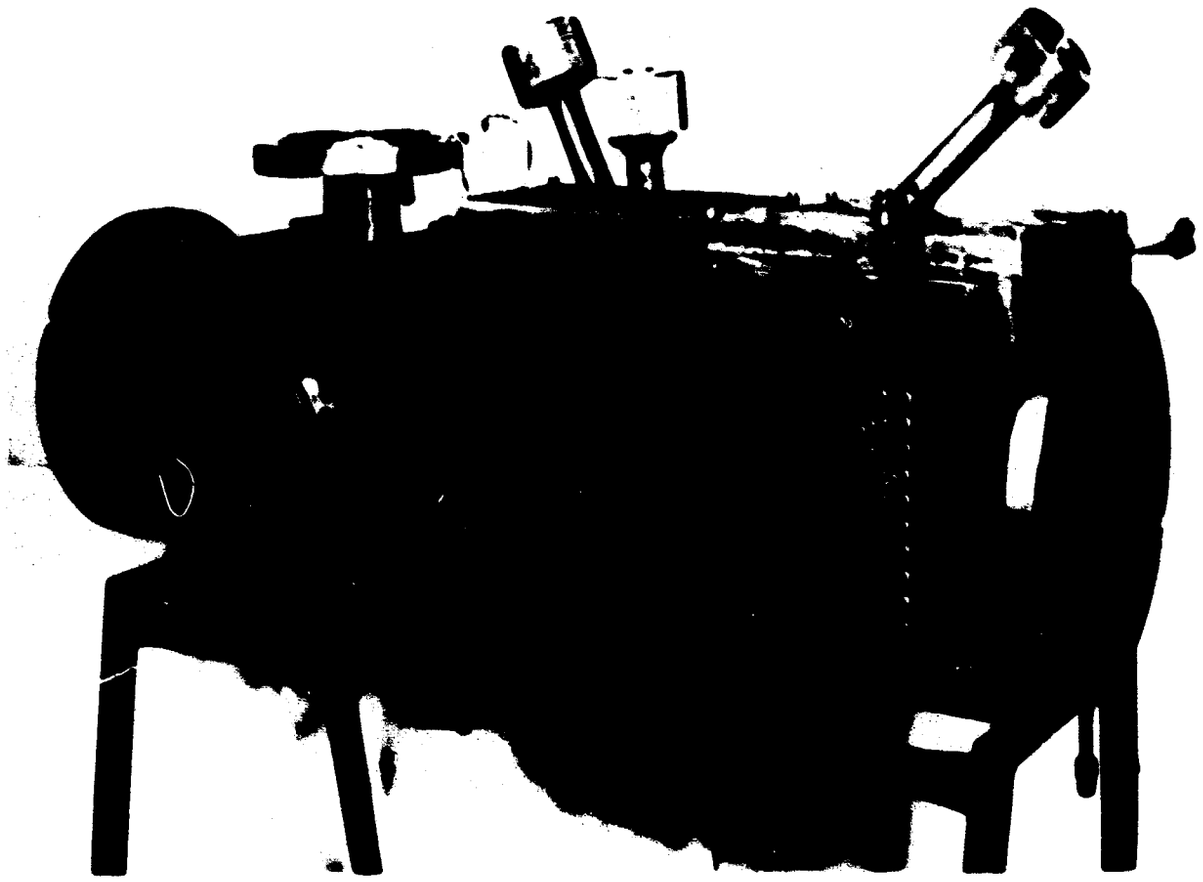

FIG 9.5 GENERATOR DUCT OUTER CASING

b)

FIGS 9·4 & 9·5

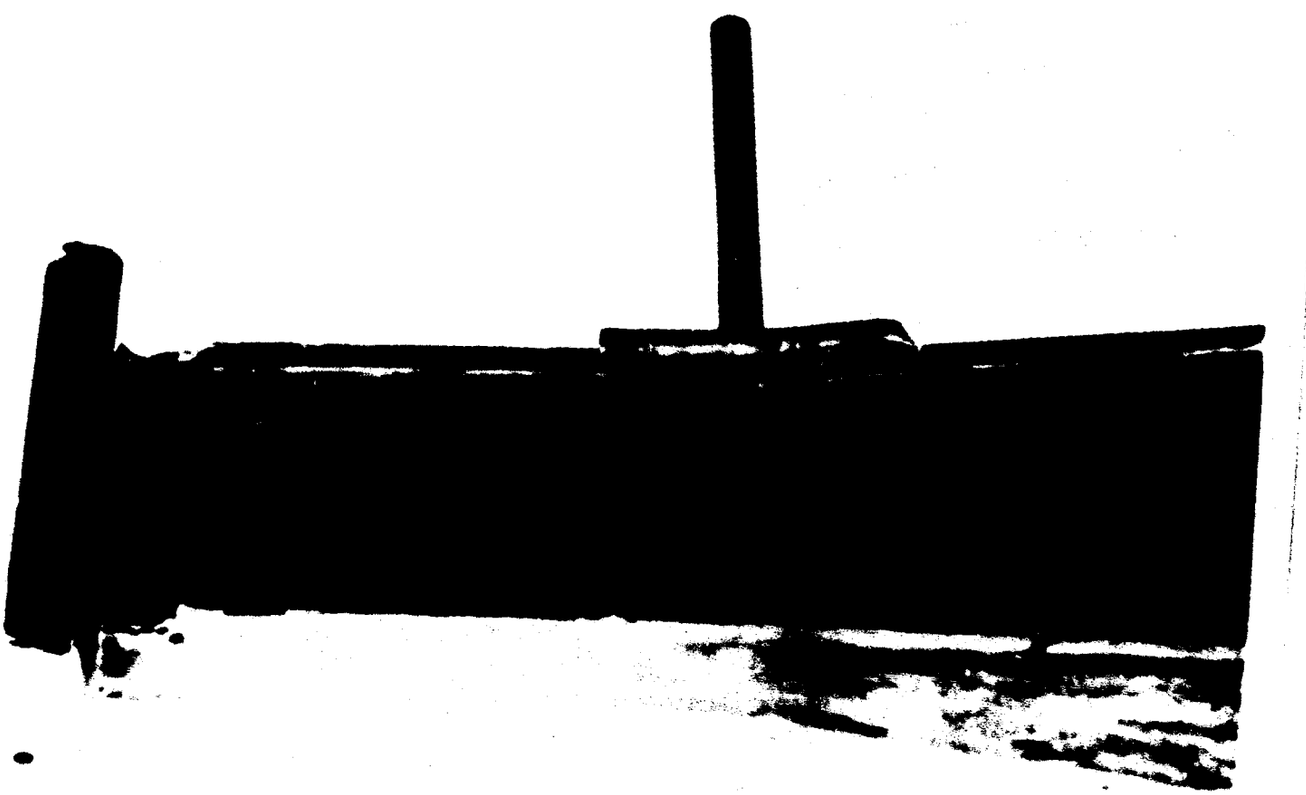

FRACTURED TANTALUM TUNGSTEN ALLOY DIFFUSER SECTION

FIG 9·6

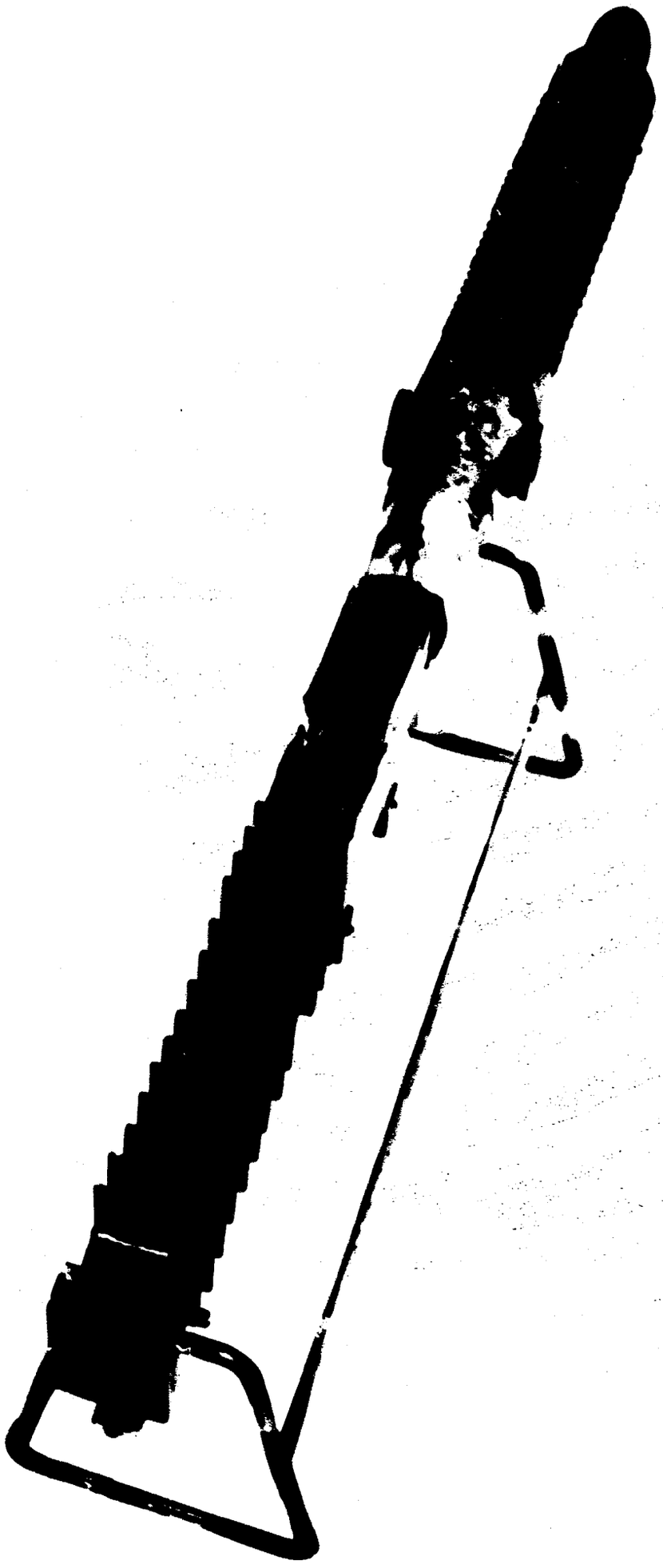

STAINLESS STEEL DIFFUSER INLET SECTION AND INSULATED DUCT ASSEMBLY

FIG 9·7

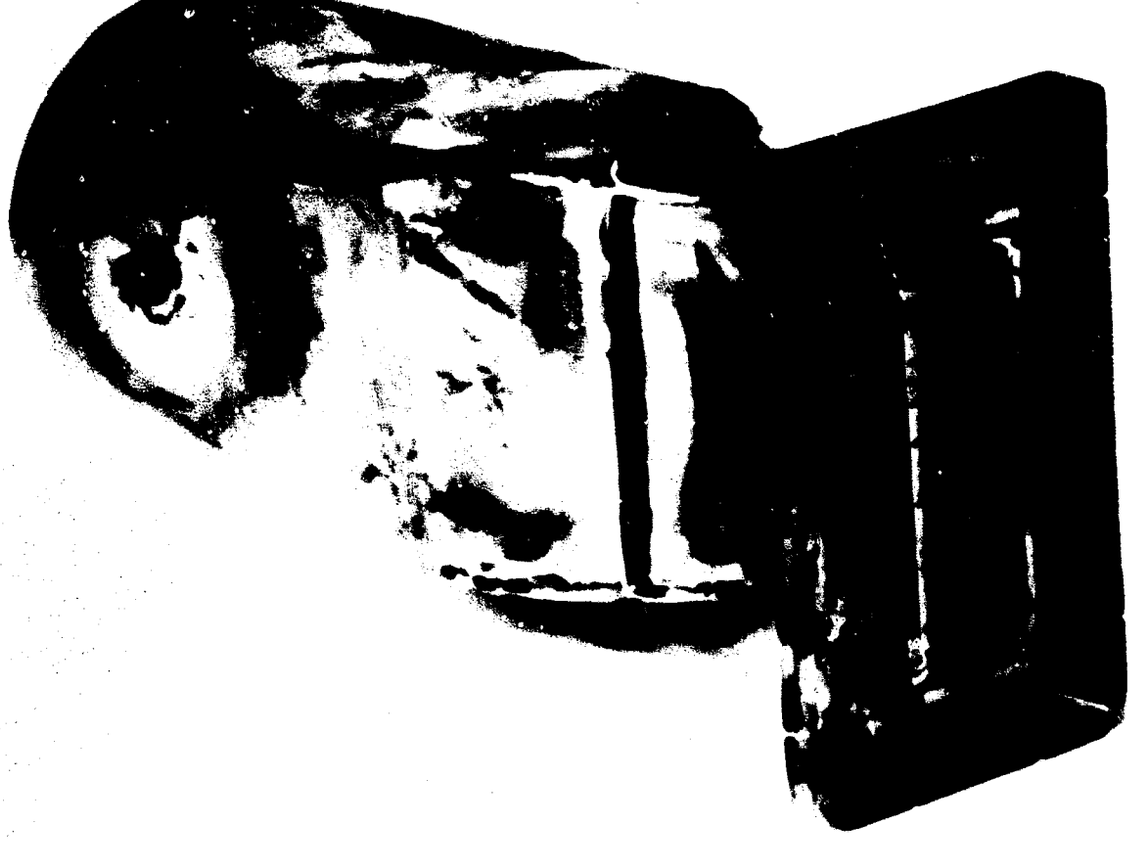

FIG 9.8 TEMPORARY TANTALUM NOZZLE FABRICATION

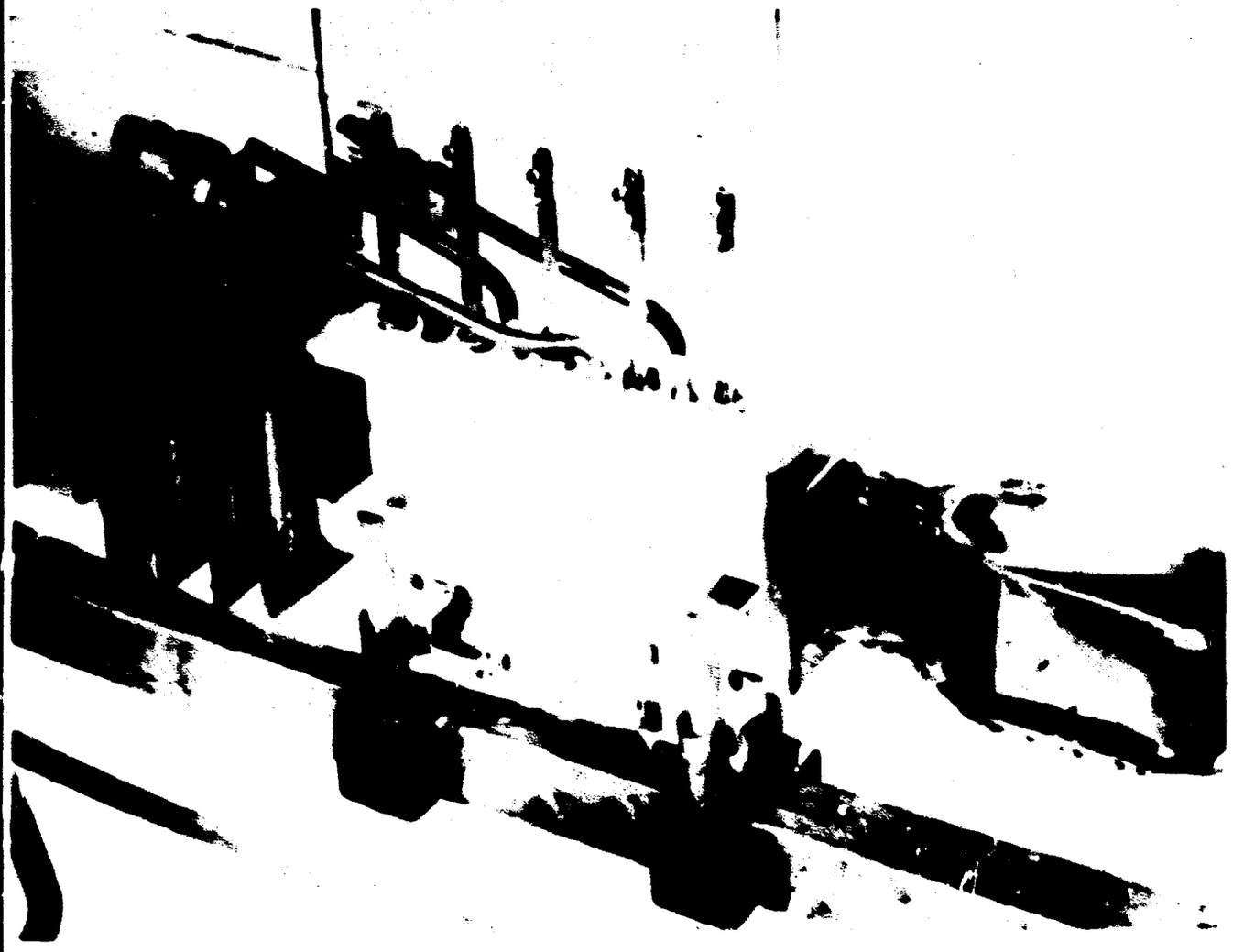

FIG 9.9 FIVE - ELECTRODE GENERATOR DUCT ASSEMBLY

FIGS 9·8 & 9·9

GENERATOR DUCT COMPONENTS AFTER OPERATION

FIG 9-10

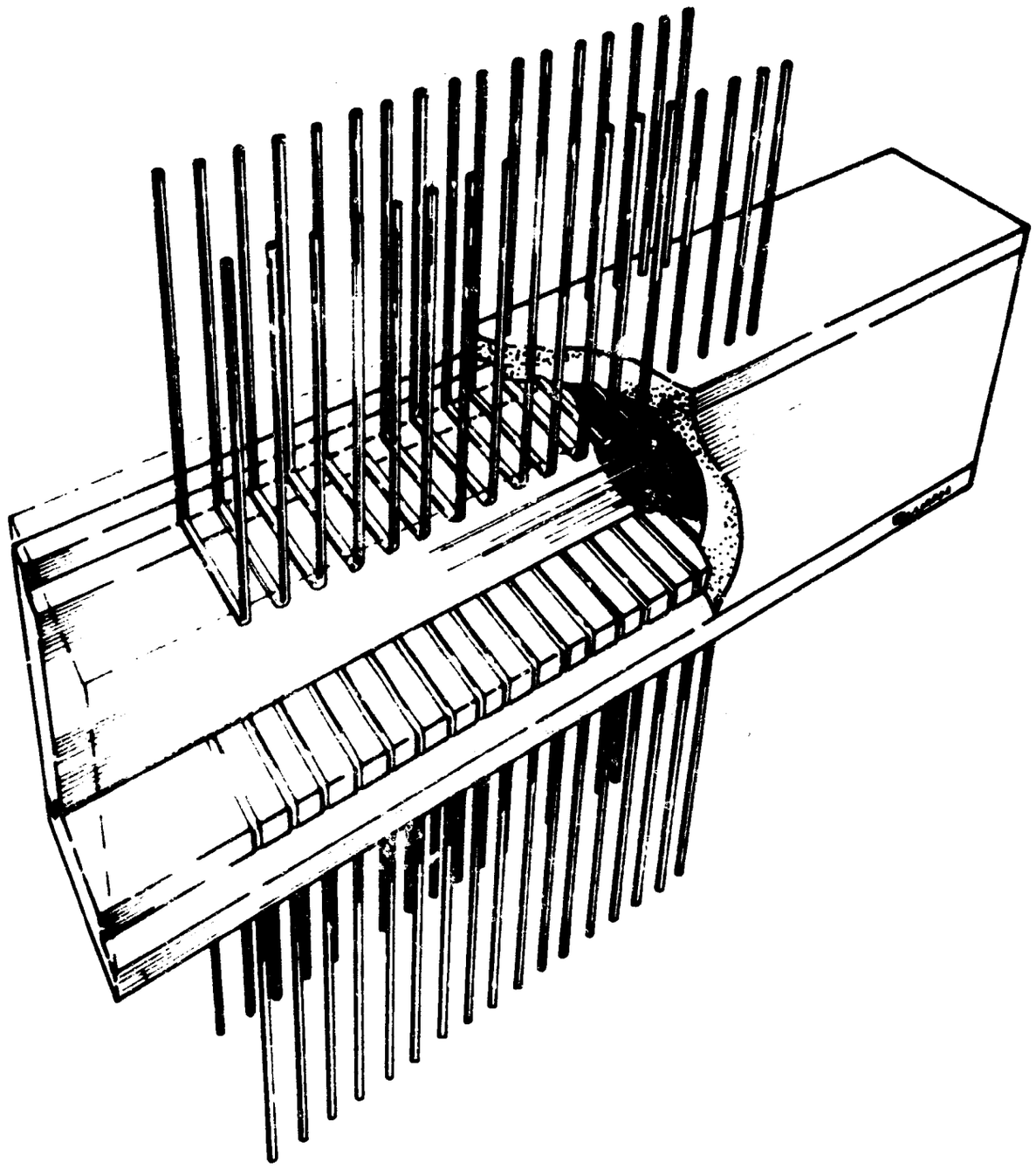

18 ELECTRODE PAIR BORON NITRIDE GENERATOR DUCT

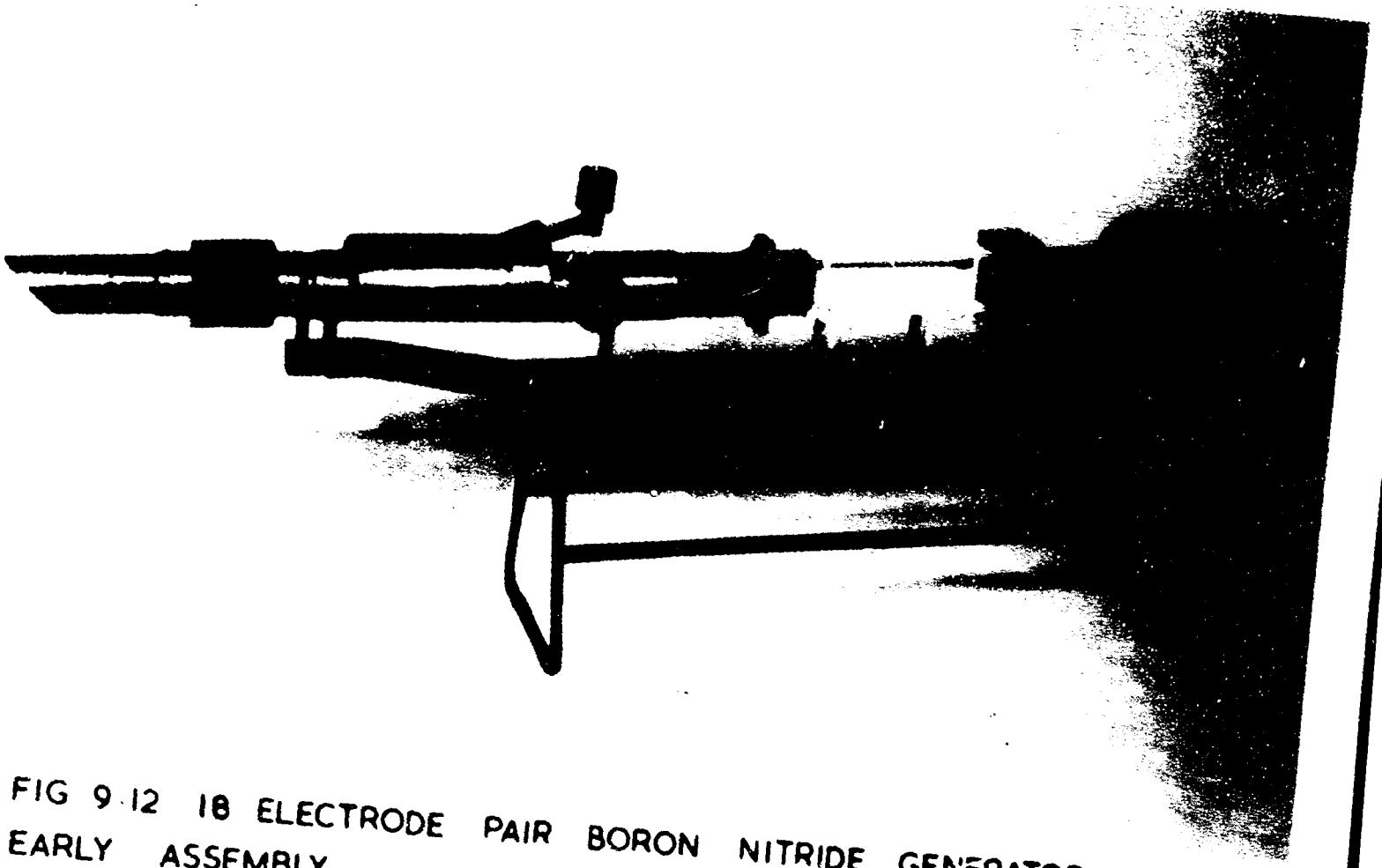

FIG 9.12 18 ELECTRODE PAIR BORON NITRIDE GENERATOR DUCT, EARLY ASSEMBLY

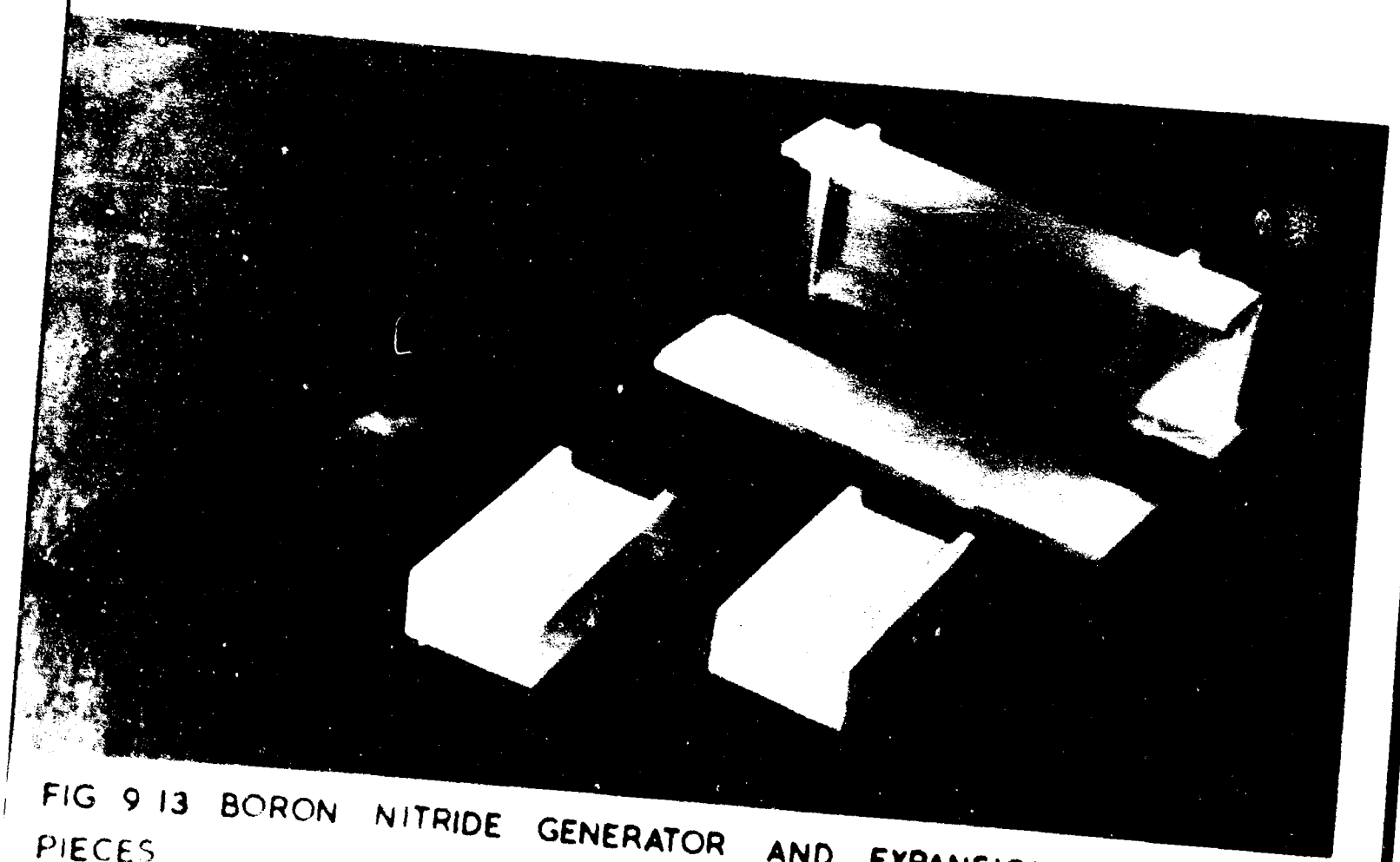

FIG 9 13 BORON NITRIDE GENERATOR AND EXPANSION NOZZLE PIECES

FIGS 9·12 & 9·13

CHAPTER 10

INSTRUMENTATION

by

F.B. Jones, W. Jackson, J. Blunt, R. Brown, and I.R. McNab

10.1 INTRODUCTION

The measurement of a large number of physical parameters in the MPD loop is required to assess the detailed and overall component performances. In addition, physical measurements on the plasma in the nozzle and channel region are required to characterize the plasma state and to compare with theoretical predictions.

The parameter of prime importance insofar as materials problems and plasma properties are concerned is the gas temperature. To date gas temperatures have only been estimated indirectly from corrected thermocouple and radiation pyrometer measurements of appropriate solid body temperatures. The manner in which observed thermocouple temperatures have been corrected to yield the static gas temperature is given in Section 10.2.

During development of the graphite heater assembly considerable difficulty occurred because of inaccurate measurement of the power supplied to the heater. Section 10.3 outlines the investigations carried out to reduce these inaccuracies.

Over the major portion of the contract period the greatest effort has been devoted toward obtaining a reliable, hot, pure gas flow facility. It is only recently, since this facility has been obtained, that power generation with cesium seeding has become possible. From experience gained on the preliminary seeded run a sophisticated power measurement and leakage system has evolved and is described in Section 10.4.

Section 10.5 describes briefly some of the aspects of the future programme on measurement of the plasma properties.

10.2 GAS TEMPERATURE MEASUREMENT BY THERMOCOUPLES

10.2.1 Introduction

One of the temperature measuring stations of particular interest is that in the tantalum transfer section, since, in view of the low Mach number at this point, the static gas temperature is close to the stagnation temperature; that

is, the total enthalpy of the gas at entrance to the nozzle can be found.

In early runs the only means of measuring the gas temperature in the transfer section was by a thermocouple affixed to the transfer wall. In later runs this thermocouple was replaced by a tantalum sheathed tungsten-tungsten-rhenium thermocouple projecting into the centre of the gas stream. The sections below describe the manner in which estimates of the gas to wall temperature drop and corrections to the observed thermocouple temperatures are made, radiation and conduction losses being allowed for.

10.2.2 Transfer section

The tantalum transfer section is circular for most of the length, changing to rectangular where it joins the generator duct. The stainless steel tube surrounding the tantalum tube acts as a radiation shield, the interspace being filled with helium at atmospheric pressure. The helium, in passing to the heater from the heat exchanger, flows between the generator duct case and stainless steel radiation shield, the direction of flow being opposite to that in the transfer section.

To simplify the problem it was assumed that all the tubes were of uniform diameter over the total length and equal to the diameter at the heater exhaust end. Fig. 10.1 shows a diagram of the simplified system.

10.2.3 Estimation of wall temperature

The transfer of heat from the hot to the cold gas is considered to be in thr three stages:

(i) convective heat tranfer from the hot gas to the transfer section;

(ii) conduction and radiation between the tantalum and stainless steel tubes, and

(iii) convective heat transfer from the stainless steel tube to the cold gas.

Conduction through the tube walls is neglected, being small compared with other factors. Convection in the interspace between the tube is also neglected because of the small gap and high conductivity of helium gas.

The convective heat transfer coefficients h_1 and h_4 in both the hot and cold sides of the transfer system are calculated from the formula for laminar heat transfer[1]

$$\frac{hD}{K} = 1.5\left[\frac{WC_p}{KL}\right]^{0.4}$$

where D is the hydraulic diameter of the respective passage, L is the heated length, W the mass flow of helium and K the conductivity.

The radiant heat transfer between the tantalum and stainless steel tubes is expressed as:

$$q_{rad} = \bar{U} \frac{T_2^4 - T_3^4}{\left[\frac{1}{e_2} + \frac{r_2}{r_3}\right]\left[\frac{1}{e_3} - 1\right]} \text{ , cal/cm}^2\text{,}$$

where $\bar{U} = 1.358 \times 10^{-12}$ cal/cm^2 ^oK, and the emissivities of tantalum (e_2) and stainless steel (e_3) are 0.73 and 0.25 respectively. The radiant heat transfer expression may be written as

$$q_{rad} = h_R (T_2^4 - T_3^4)$$

The conduction heat transfer between the tubes is

$$q_{cond} = \frac{K_{23}\left[T_2 - T_3\right]}{r_2 \log(r_3/r_2)} \text{ , cal/cm}^2\text{,}$$

where K_{23} is the mean of K_1 and K_4. This may be written alternatively as

$$q_{cond} = h_c (T_2 - T_3), \text{cal/cm}^2.$$

Therefore if 'q' is the total heat transferred from hot gas to cold gas, then:

$$q/A = h_1 (T_1 - T_2) \quad \ldots\ldots (10.1)$$

$$= h_c (T_2 - T_3) + h_R (T_2^4 - T_3^4) \quad \ldots\ldots (10.2)$$

$$= h_4 (T_3 - T_4) \quad \ldots\ldots (10.3)$$

where A = 585.0 cm^2 is the surface area of the tantalum transfer section.

The mass flow is the same in both streams, the temperature difference between the hot and cold gas streams must be the same at any section along the tube if the effect of temperature on gas properties is ignored.

Hence from Fig. 10.2

$$(T_1 - T_4) = (T_{10} - T_{40}) - \frac{q}{WC_p} \quad \ldots\ldots (10.4)$$

where T_{10} and T_{40} are the hot and cold inlet temperatures Equations (10.1) to (10.4) were solved with a Pegasus Autocode programme.

10.2.4 Correction to the gas thermocouple reading

The thermocouple receives heat from the gas by convective heat transfer, but heat is lost by radiation to the surrounding wall and conduction along its sheath to the wall, thus recording a lower temperature than the true gas temperature.

If T_g, T_c and T_w are the gas, thermocouple and wall temperatures respectively then assuming heat transfer to the whole length of the couple immersed in the gas stream, the tip temperature is given by:

$$T_g - T_c = \frac{T_g - T_w}{\text{Cosh } N}$$

where $N^2 = \dfrac{\pi D_c l_c^2 h}{K_c A_c}$

in which D_c is the outside diameter, l_c the length, A_c the cross section area and K_c the thermal conductivity of the couple sheath.

The nett heat transfer coefficient h between the gas and the couple is given by:

$$h = h_c - \frac{\bar{U} e_2 \left[T_c^4 - T_w^4 \right]}{T_g - T_c}$$

where the emissivity of tantalum is again taken as 0.73.

The convective heat transfer coefficient from the gas to the couple h_c is calculated from:

$$h_c \frac{D_c}{g} = 0.615 \left[\frac{W_g D_c}{A_d g} \right]^{0.466}$$

where A_d is the area of the duct.

The thermocouple reading is obtained from the above equations with a Pegasus Autocode programme.

10.2.5 Thermocouple curves

Fig. 10.3 is a plot of wall temperature against gas temperature. The three curves are for cold side inlet temperatures of 127°, 327° and 527°C (400°, 600° and 800°K). The variation of wall temperature with changing mass flow is very small (10°C maximum over a range of four mass flows, 5.0, 5.5, 6.0 and 6.5 gm/sec); a mean curve has been drawn for each cold side inlet temperature.

The computed wall temperatures are used in the correction of gas thermocouple readings and are plotted in Figs. 10.4 and 10.5.

The above calculations are subjected to the following uncertainties:

(i) choice of the correct convection heat transfer functions;

(ii) property values of helium (the values used are extrapolated from below 1200°C); and

(iii) emissivity values.

10.3 HEATER POWER MEASUREMENT

10.3.1 Introduction

The power to the graphite heater element is supplied from a Sturdy Transductor. In the determination of the heater input power it was found that the measurement systems, particularly those for current measurement, were very inaccurate. Originally the control current was used as a measure of the transductor output current based on the assumption that these were directly proportioned. This is only true for a particular load and voltage setting however, and since several different heaters (with different total resistances) have been used the meter calibration is not generally applicable.

To overcome this difficulty and determine the heater power accurately the measuring technique was changed to that described in the following section.

10.3.2 Power measurement

The input voltage, current and power to the transductor were obtained from voltmeter, ammeter and wattmeter measurements when these instruments had been connected through appropriate current and voltage transformers.

For the heater input power, voltmeter measurements were obtained from oscillograms of the voltage across the heater terminals and current measurements from oscillograms of the voltage drop across a shunt in series with the heater supply busbars. The root mean square values of voltage and current were calculated and are given in Table 10.1. Typical oscillograms are shown in Fig. 10.6 to 10.9. For comparison purposes the readings on the control panel voltmeter and ammeters were noted.

The marked distortion of the current and voltage waveforms is caused by the saturable nature of the transductor. This distortion excludes the use of potential and current transformers and inductive shunts as measuring devices. To measure this current a thermal meter has been constructed in which the temperature of a small oven, which is heated by the heater input current, is measured by a thermocouple; the voltage output of this thermocouple is proportional to the root mean square value of the current. This thermal meter was used to

measure both the heater voltage and current and replaced the control board meters. Since the heater power factor is unity the power can be obtained from the root mean square current and voltages:

$$P = V_{rms} I_{rms}$$

(See Table 10.2).

10.4 GENERATOR POWER AND ASSOCIATED MEASUREMENTS

10.4.1 Introduction

In the preliminary seeded runs (Chapter 4) relatively elementary power measurement techniques were employed, thus all the power measurements were carried out using an external resistance of 470Ω; open circuit voltages were also measured. The voltages across the loads and on open circuit were recorded on a five channel U.V. recorder and with an AVO meter. While these measurements enabled estimates to be made of the plasma electrical conductivity, more reliable measurements require better techniques. An instrumentation system is presently under construction to enable a sophisticated series of measurements to be made on the eighteen electrode pair channel.

Switching over five different loads (4.7, 18, 68, 280, 1000 ohms) is to be provided on each electrode pair and five pins will be inserted in the channel exit region to enable end leakage to be evaluated by voltage measurements. In addition measurements will be made on non-opposite pairs of electrodes with the same set of loads to assess the merits of an angled segmented electrode generator. The characteristics of the generator when working in the Hall mode will be investigated each electrode pair being short circuited and axial voltages and currents measured.

In view of the experience gained in the previous run, where a highly conducting wall deposit was found, measurements of the leakage currents between each pair of electrodes and the pins will be made between seeded runs, the overall loop conditions being identical with those for the power runs.

In addition, resistive measurements on each electrode are to be performed with unseeded gas to enable the temperature profile down the channel to be determined, and to compare these temperatures with those obtained from thermocouple measurements. The resistivity of the tantalum -10% tungsten alloy changes by a factor of seven over the temperature range considered. The voltage-current characteristics of the plasma will also be determined with 110 volt a.c.

Before the eighteen electrode pair channel is used, further preliminary runs with a temporary channel are to be made. In this system three large electrode

pairs (0.25 in.^{2}) and nine pin electrodes are used. This system will be used to investigate the characteristics of the generator when working in a subsonic mode, particularly the effects of boundary layers on power output, thus the pins are no longer flush with the channel wall but extend, by different amounts, into the gas stream.

10.4.2 Measurement system

As outlined above a large number of measurements are to be made with the short available seeding time at present extant. About 300 measurements are required in a few seconds, necessitating a fairly complex system. The system described below has been designed for the eighteen electrode pair channel, but will also be used for the preliminary measurements.

There is no question of supplying 300 separate channels, nor are there sufficient data to warrant an all-electronic multiplexing arrangement feeding a tape recorder. Hence, since in addition many measurements are required free of earth, switching with uniselectors and relays was chosen as the most suitable system. One limitation of the uniselectors, which switch actual load resistors in addition to recorder signals, is their contact rating of 50V, 1A.

A 24 channel U.V. recorder will be available for the tests. Thus with the uniselectors switching at 30 steps per second, 720 readings per second can be taken, although the resistive readings (for the temperature profile) have to be taken singly at a rate of 30 per second. (This is not a drawback since it is not anticipated that any readings will be made until the loop has reached steady state.) Screened cables are used from the channel terminals to the various panels and screening covers are used on the channel terminals.

One end of each electrode pair and any pin connections are brought, using the screened cables, to the following panels:

(i) the temperature measuring panel used to determine the individual electrode resistances and hence the temperature profile in the channel;

(ii) the patch panel which, using stacking plugs, allows flexible connections to the load scanner, so that any generator characteristic mode can be examined: this panel also carries switches and the transistorized uniselector pulser;

(iii) the load scanning panel with 90 load resistors together with range resistors and protective Zener diodes for the galvanometers;

(iv) the leakage measurement panel which has relays for earthing electrodes and the ammeter circuit; and

(v) the voltage-current characteristic panel empolying 110V a.c.

To measure the leakage currents between the eighteen pairs of electrodes, not less than 56 readings are required to establish the equivalent ladder network resistances. Stepped pulses are used to aid the identification of the U.V. recorder traces.

10.5 FUTURE PROGRAMME

Section 10.4 describes the programme of measurement of output powers for the next generating channels.

To obtain reliable gas and plasma temperatures several different measuring systems should be used and the results correlated. The possibility of using sophisticated thermocouple systems (for example of the suction type) and, for the plasma, spectroscopic techniques (such as cesium line reversal) are presently being examined.

In the channel, pressure measurement is currently made at several stations flush with the wall surface. One of the disadvantages of this technique is that rapid fluctuations in pressure cannot be followed. Piezoelectric devices would enable this difficulty to be overcome, although the small scale of the experiment and the relatively high temperatures may necessitate development work.

Provision is made for microwave parts previous to the supersonic nozzle and at inlet to, and exit from, the channel region. The microwave techniques developed in the auxillary plasma physics experiments (Chapter 14) will be used to enable the electron concentrations and electronic collision frequencies to be measured at these positions using phase shift and attenuation methods[2].

The window systems and apparatus required for plasma temperature measurement could also be adopted for spectroscopic investigations of the electron concentration and collision frequencies[2].

When the generator is operated in a subsonic mode useful information on plasma properties (on electron temperatures and concentrations) could be obtained from probes inserted in the stream. However, supersonic operation of the generator makes the interpretation of the probe characteristics difficult.

REFERENCES

1 McADAMS, W.H. 'Heat transmission' McGraw-Hill Book Co. 1954

2 McNAB, I.R. 'The electrical properties of cesium-helium plasmas'. C.A. Parsons, NRC Report 61-12. 1961

TABLE 10.1

RESULTS OF TEST FOR OBTAINING OSCILLOGRAMS

Transductor Input				Heater Input				
V, volts	I, amps	P, watts	cos ϕ	V meter, volts	I meter, amps	V_{osc}, volts	I_{osc}, amps	Power V.I, watts
247	52.5	3000	0.231	3.5	0.1	3.84	442	1700
247	90.0	7800	0.35	6.0	0.5	5.5	720	3980
244	122.5	13700	0.486	8.0	1.0	8.22	930	7690
244	144.0	18900	0.537	9.5	1.15	9.32	1146	10720
242	72.5	25000	0.618	11.5	1.5	11.5	1425	16400

TABLE 10.2

RESULTS OF TESTS TO CHECK THERMAL METER

Transductor Input				Heater Input				
V, volts	I, amps	P, watts	cos ϕ	V meter, volts	I meter, amps	V thermal, volts	I thermal	Power V.I, watts
238	322.5	42400	0.525	21.0	-	20	2131	42620
237.8	352.5	51200	0.613	-	-	22.4	2268	50080
240	271.5	30600	0.47	-	-	16.4	1600	26250
239.6	273.0	29400	0.45	-	-	15.8	1600	24000
241	248.3	21300	0.355	12.8	-	15.2	1200	18240
244	150.0	8700	0.237	7.5	-	8.4	666	5600
245.4	61.5	5610	0.371	6.0	-	5.8	400	[illegible]0
247.0	41.3	3000	0.294	4.0	-	4.0	133	534

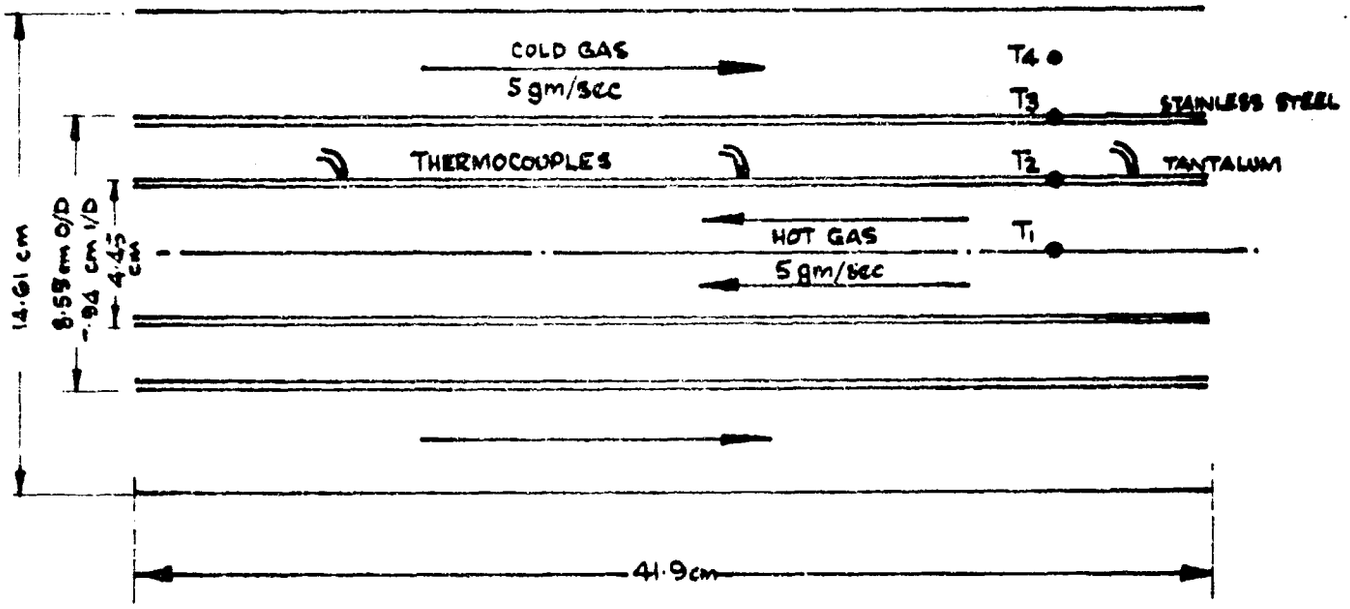

FIG 10.1 TEMPORARY HIGH TEMPERATURE TRANSFER (SECTION)

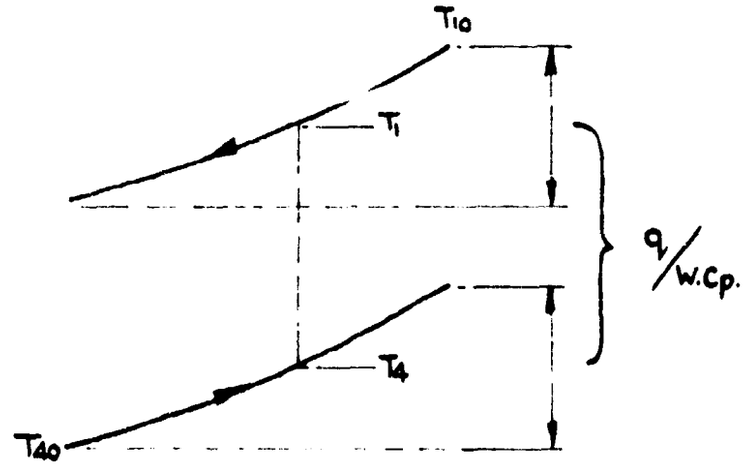

FIG 10.2

FIGS 10.1 & 10.2

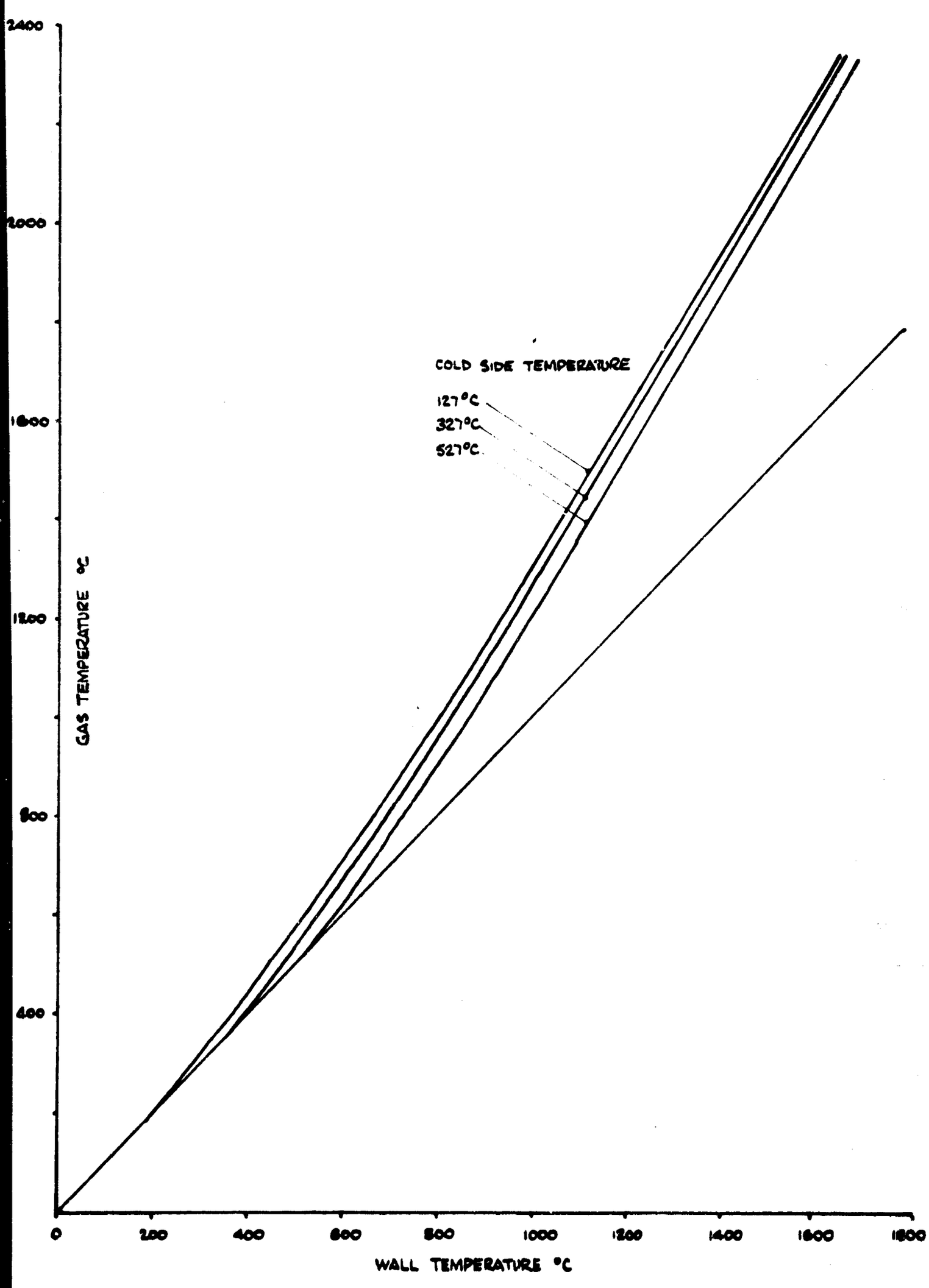

WALL TEMPERATURE ESTIMATION IN TANTALUM TRANSFER SYSTEM (TEMPORARY)
MASS FLOW 5·0-6·5 GM/SEC.

FIG 10.3

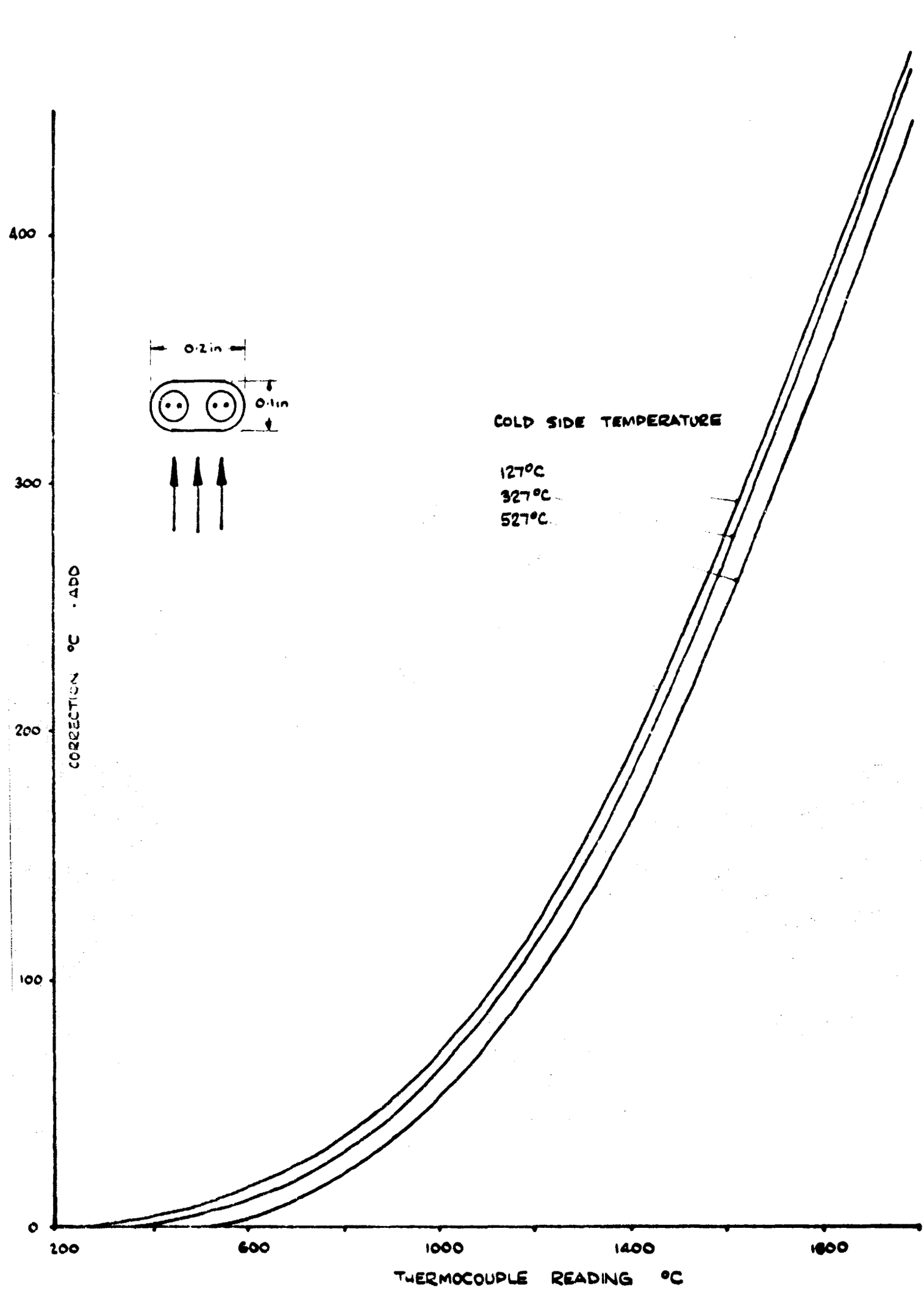

TEMPORARY GAS T/C CORRECTION IN TANTALUM TRANSFER SYSTEM
MASS FLOW 5·0 GM/SEC 2 T/CS IN ·0005 IN. SHEATH

FIG 10.4

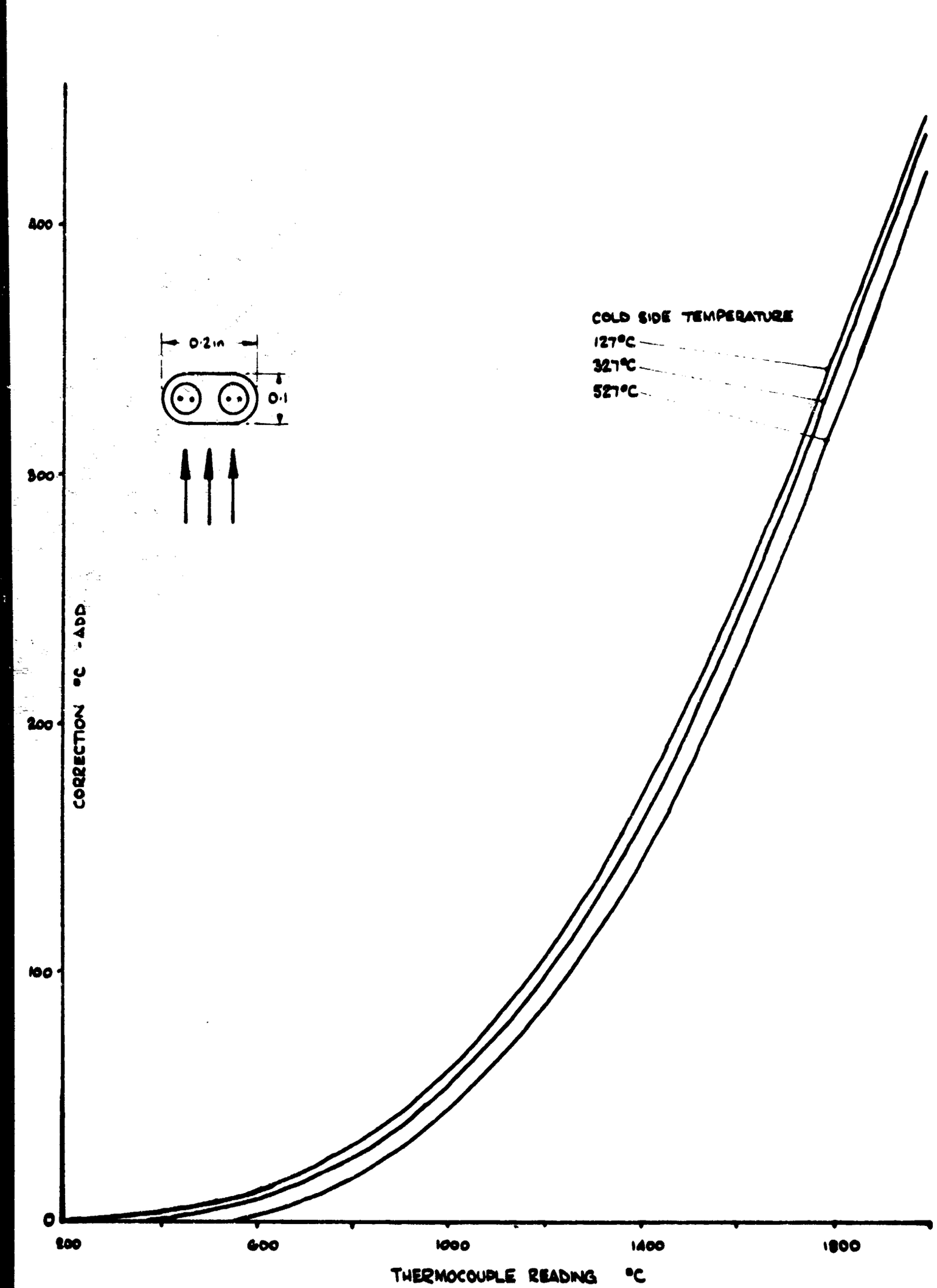

TEMPORARY GAS T/C CORRECTION IN TANTALUM TRANSFER SYSTEM
MASS FLOW 6·5 GM/SEC 2 T/CS IN ·0005 IN. SHEATH

FIG 10.5

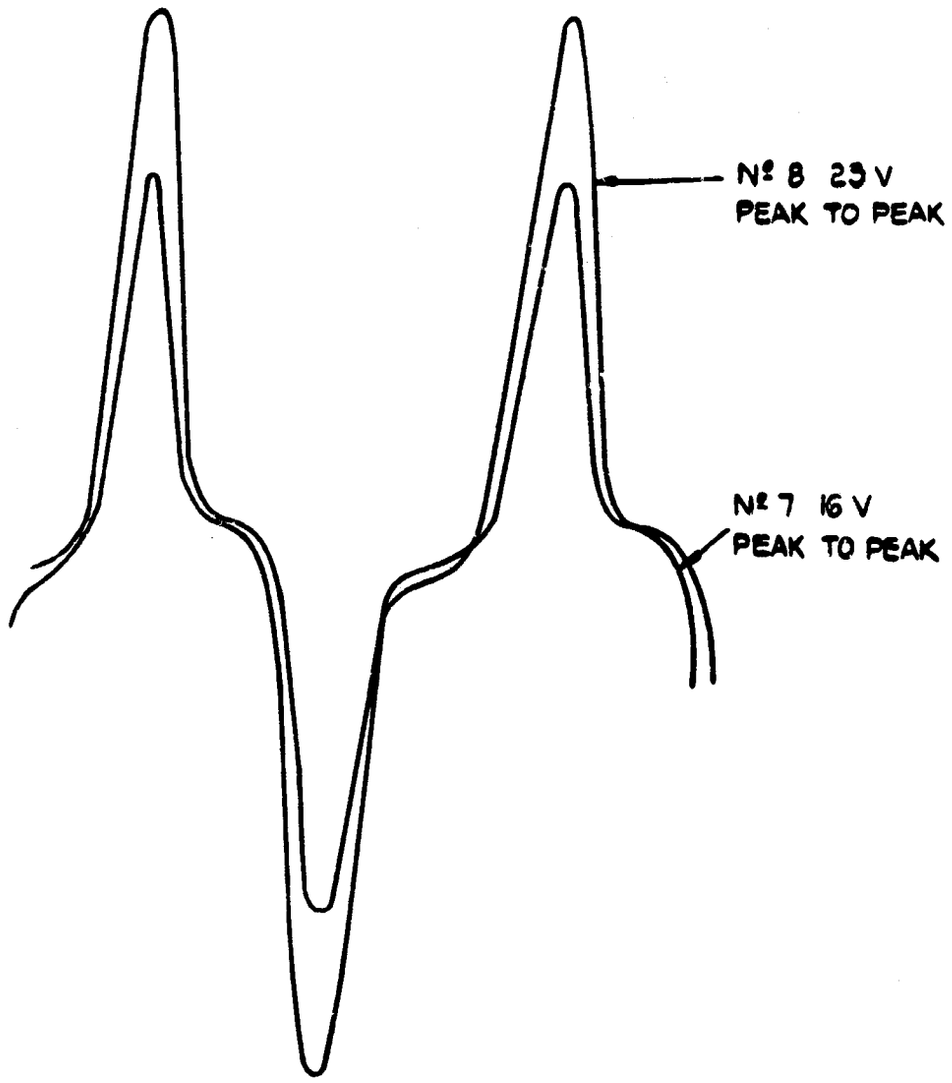

TRANSDUCTER OUTPUT WAVE FORM

FIG 10·6

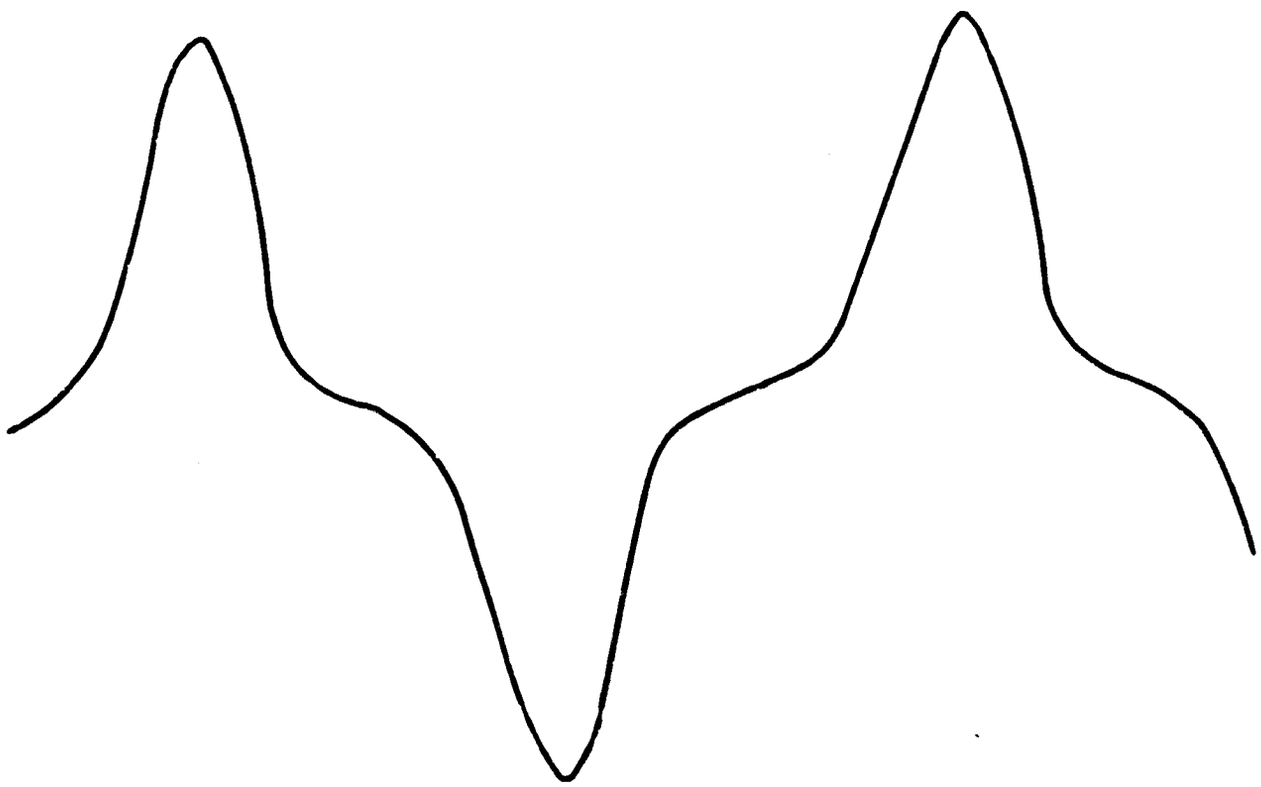

SHUNT p d PEAK TO PEAK 9·1 mV ON OUTPUT CURRENT

FIG10·7

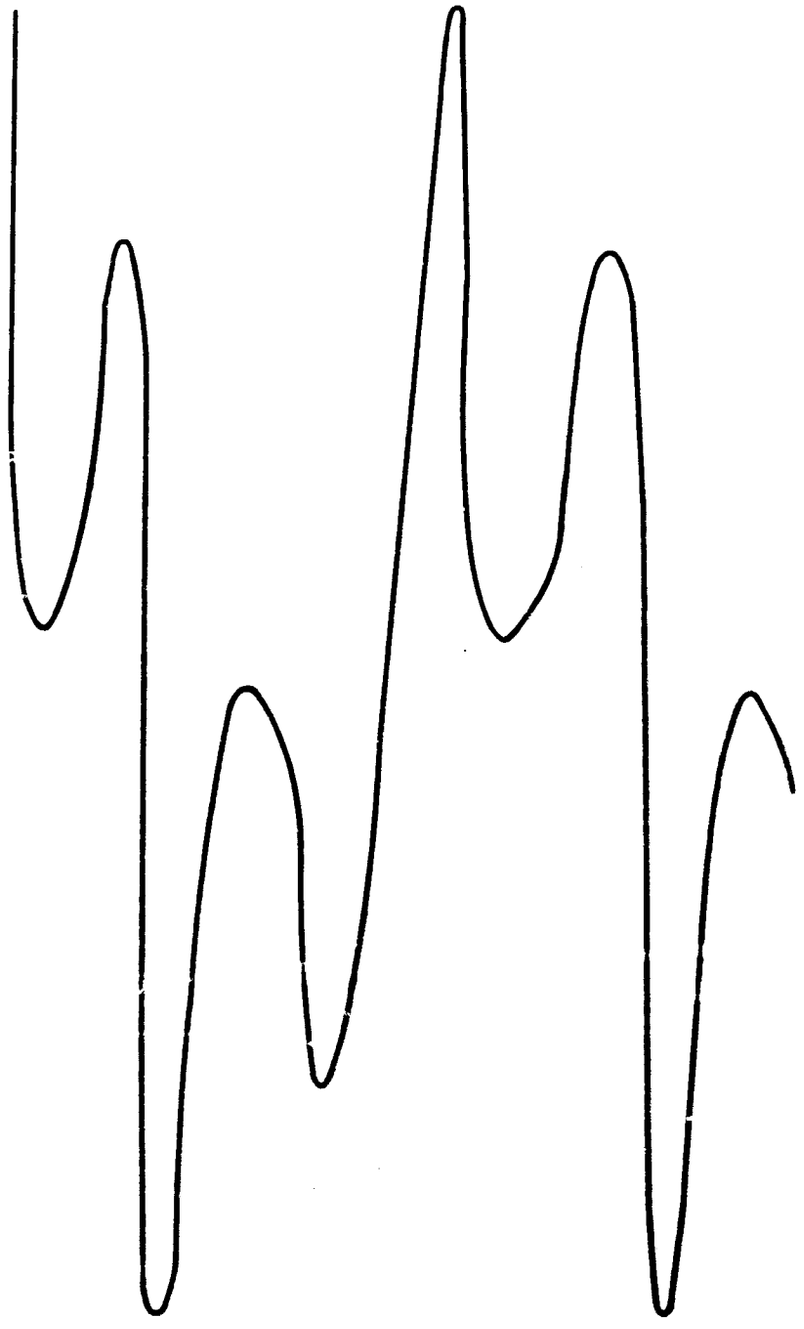

VOLTS ACROSS 4 ft BAR SECTION, 0·8 V PEAK TO PEAK

FIG 10·8

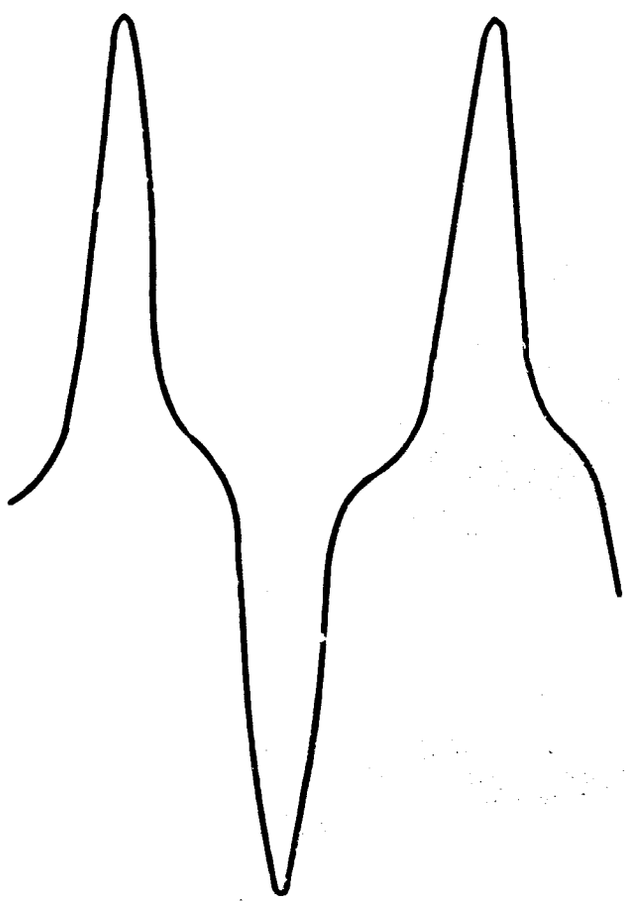

HEATER VOLTS, PEAK TO PEAK 21.5V

FIG 10.9

CHAPTER 11

MATERIALS

11.1 INTRODUCTION

A number of investigations into materials problems under the operating conditions of the loop have been undertaken in an effort to understand ultra-high-temperature loop technology. Some of the main topics have been: the behaviour of tantalum under dynamic conditions of impure helium flow; compatibility and physical properties of electrode and duct wall materials; compatibility of metals, ceramics and other materials with cesium liquid and cesium vapour; and nature of the dark deposit on generator duct walls after operation.

It is hoped to present a more complete analysis and review of some of the materials problems in a subsequent Technical Summary Report; in the present report the results of some of the tests are presented in the belief that the findings may be of value to other workers.

11.2 EXAMINATION OF A TEMPORARY TANTALUM TRANSFER DUCT (RHT 2)

by

N. McCormick, A. Taylor and C.C. Robinson

11.2.1 Introduction

A temporary tantalum transfer duct from the MPD loop was received for metallographic examination to determine the cause of embrittlement which had led to the failure of the tube. Helium gas, heated by a graphite heater to ~1400°K, had been passed through the duct. The impurity level of the helium gas (nitrogen and oxygen) was estimated to be <50 ppm.

11.2.2 Visual examination

The mouth of the duct had completely fractured (Fig. 11.1) and fine cracks had developed along the duct which was extremely brittle, particularly near the inlet area, and two gauzes which had been mounted in the duct had disintegrated. A black deposit lined the inner walls of the duct, being most dense at the inlet region.

11.2.3 Specimen preparation

Six transverse sections were taken from the tube wall (Fig. 11.2):

1 section through wall and gauze at the duct inlet,
2 section through region of visible cracking,
3 section through wall to include thermocouple strap,
4 section through spot welded area of duct,
5 section as indicated in diagram
6 section through wall and gauze at the exhaust end of duct.

The sections were mounted in black bakelite, ground on 180 and 600 grit SiC papers and polished on 14μ, 6μ and 1μ diamond paste. They were then etched in a solution of 40 cc conc H_2SO_4, 20 cc conc HNO_3 and 20 cc aqueous HF.

11.2.4 Metallographic examination

A discontinuous layer of tantalum carbide had formed along the wall of the duct, having maximum thicknesses of 0.004 in. and 0.0015 in. at the inlet and exhaust ends respectively (Figs. 11.3 and 11.4).

Islands of massive Ta_2O_5 phase were observed in the carbide layer and in some areas had penetrated into the grain boundaries of the tantalum (Fig. 11.3).

Platelets of a second phase precipitate, which was anisotropic (Fig. 11.5), extended across the duct wall. The occurrence of this precipitate was more pronounced at the inlet end of the duct (compare Figs. 11.3 and 11.4).

Sections taken through fragments of the gauzes exhibited similar corrosion phenomena to those found in the duct wall (Fig. 11.6).

11.2.5 X-ray analysis

Standard Debye Scherrer photographs and X-ray diffractometer traces were obtained from samples of the deposit and metallic debris.

Comparison with the ASTM index showed these samples to consist mainly of tantalum carbide (TaC) together with tantalum pentoxide (Ta_2O_5) in either the α or β form. Since nitrogen is soluble up to 1% in tantalum oxide it cannot be detected by X-ray crystallography below this concentration. At concentrations greater than 1% of the nitride is formed, but none was detected.

11.2.6 Comments

1 Embrittlement which had caused the failure of the duct was due primarily to severe oxidation followed by carburization.

2 The surface oxide, Ta_2O_5, is reported to have no protective properties[1].

3 The platelets of second phase precipitate appear to be similar to a suboxide phase observed by previous investigators. However, X-ray analysis gave no evidence to confirm the presence of this phase[1,2].

4 The fine matrix precipitate is thought to be impurities inherent in the original material.

REFERENCES

1 NORMAN, N., KOFSTAD, P., and KRUDTAA, O.J. Metallic oxide phases of Nb and Ta. Journal of the Less Common Metals, Vol. 4. April 1962

2 KOFSTAD, P. Oxidation of Ta in temp. range 500-700°C. J.I.M. March 1962

11.3 EXAMINATION OF TANTALUM TEST STRIPS (RHT14)

by

Mrs. S. Beale and A. Taylor

11.3.1 Introduction

Two tantalum test strips were held within a tantalum transfer duct in a helium atmosphere for 1½ hr to study the effect of impurities in the gas stream. The position of the specimens within the duct and the atmospheric conditions are indicated in Fig. 11.7. After testing, the clamps and pieces of original material from which these were made were examined as follows.

11.3.2 Specimen preparation

Longitudinal sections were taken through the clamps, leading edges of the test strips and "as-received" material: these were mounted in black bakelite, ground on SiC papers down to 600 and finally polished with 1 μ diamond paste on a vibratory polisher. Specimens were then electrolytically etched in lactic acid/sulphuric acid/hydrofluoric acid mixture to reveal general structure and sulphuric acid/nitric acid/hydrofluoric acid mixture for grain boundary definition.

11.3.3 X-ray examination

Diffractometer traces were obtained from all the samples using Copper K α radiation.

Samples A and B were found to be similar and consisted of free Ta with TaC. Large amounts of Ta_2C, Ta-N, or β-TaH were also present. Ta_2C, β-TaH and Ta-N have similar structures and it would be difficult to state which was present in this case.

Sample C consisted mainly of Ta with small amounts of the previously

mentioned compounds. No evidence of oxides of tantalum was found. Two control samples received consisted of Ta only.

11.3.4 **Metallographic examination**

Surface attack in specimens A and B could be resolved into three layers (Fig. 11.8) whereas in specimen C only two layers were observed (Fig. 11.9). Measurements of the layers are given in table below. The centre layer in specimens A and B occurred as a precipitate separating the white inner and pink outer layers. The two layers in specimen C occurred (a) as a very thin pink outer layer and (b) as a precipitate sometimes needle shaped and penetrating into the strip (Fig. 11.10).

Very fine inter and transgranular precipitates similar to those found in the test strips and clamps (Figs. 11.8 and 11.10) also appeared in the original material (Figs. 11.11 and 11.12).

Hardness measurements and grain size determinations are reported in the following table.

Specimen code	Overall layer thickness, μ		Ave. grain size, μ	K.M. Hardness No.			
	Max	Ave		Outer layer	Inner layer	Area between surface layers	Random
A	35	15	11	1120-1250	450-520	210-225	-
B	21	17	11	*	810-1150	320-385	-
C	<4	<4	16	*	*	385-440	-
As-received (0.002 in.)	-	-	18	-	-	-	130-135
As-received (0.015 in.)	-	-	12	-	-	-	130-135

* area not large enough to accommodate hardness impression

Impressions were made both across and along the length of the strips between the surface layers and within these layers wherever there was an area large enough to accommodate an impression. Random hardness tests were carried out on the as-received material.

Grain sizes were uniform in all specimens except in specimen A (Fig. 11.13) where an area of larger grains (average grain size 31 μ) was found at the end of the strip remote from the clamp.

11.3.5 Conclusions

The embrittlement of the samples was caused by the penetration by surrounding gases which comprised carbon, hydrogen and nitrogen.

11.4 EXAMINATION OF TANTALUM THERMOCOUPLE SHEATH (RHT 11)

by

A. Taylor

11.4.1 Introduction

A tungsten-tungsten/rhenium thermocouple packed with BeO was examined to ascertain the nature of embrittlement in the tantalum sheath.

11.4.2 Specimen preparation

Longitudinal sections were taken adjacent to the fracture, and behind the fracture within and outside the helium gas stream. All precautions relating to BeO laid down by IRD Health Physics Department were followed. Grinding was carried out on SiC papers down to 600 and diamond polishing down to 1μ. Etching procedure was carried out as described in Section 11.3.

11.4.3 Micro-examination

Precipitation of the type illustrated in Fig. 11.14 was found in the area of the fracture. In the section taken behind the fracture in the gas stream precipitation occurred mainly at the outside edge of the sheath (Fig. 11.15) whereas outside the gas stream uniform precipitation occurred (Fig. 11.16). Results of hardness and grain size determinations are given in the following table .

Area	Ave. grain size	R.M. hardness No.
In gas stream	45μ	400 - 445
Outside gas stream	cold worked structure (Fig. 11.17)	230 - 235

The thermocouple sheath within the gas stream was harder than the sheath outside the gas stream and grain size was largest in the fracture area. (Figs. 11.15 and 11.17). Fig. 11.18 illustrates the change in the original cold worked structure which occurred in an area about 0.5 in. behind the fracture.

11.4.4 Conclusion

Precipitation in and immediately behind the fracture area, occurring mainly at the outside edge of the thermocouple sheath, suggests that embrittlement had

been caused by pick up of some impurity present in the helium gas stream.

11.5 EXAMINATION OF EMBRITTLED TANTALUM BELLOWS (RHT 12)

by

A. Taylor and Mrs. S. Devine

11.5.1 Introduction

A tantalum bellows from the MPD loop was examined to investigate the reason for its embrittlement.

11.5.2 Specimen preparation

Longitudinal sections were taken through the bellows and prepared in the manner described in Section 11.3.

11.5.3 Micro-examination

Extensive corrosion occurred on the inside walls of the bellows, maximum overall thickness 132 μ. This attack could be distinguished as three separate layers (Fig. 11.19). An intergranular phase similar to the inner layer on the surface extended right across the wall (Fig. 11.20).

A precipitate in the form of platelets was found along the outside edge of the bellows wall and in regions where cracking has occurred (Figs. 11.21 and 11.22).

R.M. Hardness impressions were attempted in the surface layers but were unsatisfactory because: the particles in the outside layer were too brittle; the centre layer appeared to be too porous; and the inner layer was too small. Impressions made across and down the centre of the tantalum wall were in the range 400-420.

A uniform grain size of 19 μ was measured.

11.5.4 X-ray analysis

From the diffraction patterns produced, the deposit was found to consist of TaC and either Ta_2C, TaN, β TaH or a mixture of these. Some extra peaks were observed but could not be identified. The scale consisted of TaC and a trace of graphite.

11.5.5 Comments

Embrittlement is thought to be due primarily to severe carbonization. The possible presence of nitrogen, hydrogen or both would also be a contributary factor.

11.6 EXAMINATION OF TANTALUM TEST STRIPS (RHT 14)

by

A. Taylor

11.6.1 Introduction

Further tantalum test strips and clamps were received to study the effect of environmental conditions. These conditions together with the position of the test pieces within the transfer tube are given in Section 11.3.

11.6.2 Specimen preparation

As in Section 11.3

11.6.3 Micro-examination

Surface attack in specimens A and B occurred mainly as a single layer (Fig. 11.23). There were, however, areas where more than one layer was present (Fig. 11.24) but these were difficult to resolve. Measurements of the layers are given in the following table.

Specimen code	Overall layer thickness, μ		Ave. grain size, μ	R.M. Hardness No.		
	Maximum	Average		Outer layer+	Area between surface layers	Random
A	10	8	11	500 - 550	155 - 185	-
B	8	6	10	*	115 - 145	-
C	-	-	15	-	-	170-185

* area not large enough to accommodate hardness impression. + outer layer as shown in Fig.11.23

No surface attack was observed in specimen C. Fine inter- and transgranular precipitates similar to those found in the original material were present in all test specimens (Figs. 11.23 and 11.25).

Hardness measurements and grain size determinations are given in the table.

Impressions were made both across and along the length of the strips A and B, between the surface layers and within these layers wherever there was an area large enough to accommodate an impression. Random impressions were made in specimen C.

Grain sizes were uniform in all specimens except in specimen A where an area of larger grains (average grain size 45 μ) was found at the end of the strip remote from the clamp.

11.6.4 Comments

1 Surface attack was less severe in these specimens than in the previous ones (section 11.3).

2 Whereas in the previous specimens surface attack could be resolved into three distinct layers, it was difficult to decide whether the "centre layer" in the present specimens was

(a) the boundary between inner and outer layers or

(b) a fine precipitate separating two layers.

11.7 EXAMINATION OF TANTALUM TEST STRIPS (A RHT 15, B RHT 19)

by

A. Taylor

11.7.1 Introduction

Further tantalum test strips were received to study the effect of environmenta conditions and temperature. Apart from test strip B which had been subjected to a maximum temperature of 2200°K, the other conditions of environment, temperature and the position of the test pieces within the transfer tube were the same as those given previously in Section 11.3.

11.7.2 Specimen preparation

As in Section 11.3.

11.7.3 Micro-examination

Surface attack in specimen A was confined to a very thin single layer of not more than 2 μ thick. A fine precipitate similar to that found in the original material (Section 11.3) was present throughout the strip.

In specimen B, surface attack appeared as two separate layers Figs. 11.26, 11.27 and 11.28. A white intergranular phase (Fig. 11.26) similar in appearance to the inner surface layer and a fine needle-like precipitate (Fig. 11.27) were both found within the strip. Hardness measurements and grain size determinations are given in the following table:

Specimen code	Overall layer thickness, μ		Average grain size, μ	R.M. Hardness no.		
	Max.	Ave.		Outer surface layer	Inner surface layer	Area between surface layers
A	< 2	-	14	Layers too thin to accommodate impressions		275 - 315
B	10	7	16			310 - 365

Impressions were made both across and along the lengths of the strips between the surface layers.

The grain size in specimen A was uniform but in specimen B large grains (max. 540 μ) were found along one edge (Fig. 11.28).

11.7.4 Comments

Test strip B has been the only specimen to date in which the white grain boundary phase or the needle-like precipitate has been observed.

11.8 EXAMINATION OF BLACK COATING ON ALUMINA DUCT COMPONENT (RHT 20)

by

S. Maxwell

Diffractometer traces obtained from the sample using copper K α radiation showed mainly α-alumina but small amounts of TaC and either Ta_2C, TaH or TaN or a mixture of these were found from the surface layer.

11.9 EXAMINATION OF TANTALUM TEST STRIPS (RHT 24)

by

A. Taylor

11.9.1 Introduction

Two tantalum test strips (0.010 in. and 0.020 in. thick) from the MPD loop were received for metallographic examination.

11.9.2 Specimen preparation

As in Section 11.5.

11.9.3 Micro-examination

The results of micro-examination are recorded in the following table.

Specimen	Overall layer thickness, μ		Average grain size, μ	R.M. hardness no.	
	Max.	Ave.		Surface layer	Area between surface layers
1 (0.010 in.)	12	5-7	39	layers too thin to accommodate impressions	200 - 245
2 (0.020 in.)	7	5	39		185 - 200

Corrosion in both test strips occurred mainly as a thin surface layer. A white intergranular phase similar in appearance to the surface layer was also found within the strip. The surface layer and intergranular precipitates resembled those illustrated in Fig. 11.26 although the intergranular precipitates occurred to a much lesser degree. A uniform grain size was observed in both specimens.

11.10 EXAMINATION OF TANTALUM PRESSURE PIPE WELD (RHT 25)

by

A. Taylor

11.10.1 Introduction

A tantalum pressure pipe weld was received to investigate the reason for its failure.

11.10.2 Specimen preparation

A section was taken through the assembly so as to give a transverse section through the weld and a longitudinal section through the tube insert (Fig. 11.29). The preparation was the same as that described in Section 11.3.

11.10.3 Micro-examination

The formation of a hard white surface layer occurred along the inside of the high temperature transfer duct at the base of the weld (Fig. 11.30). This layer was also apparent on the small tube insert and extended for at least 0.5 in. up the tube wall (Figs. 11.31 and 11.32). A white grain boundary phase and intragranular precipitate was found in the weld metal itself but was most dominant in the tube insert region of the weld (Fig. 11.33). Penetration of the surface layer occurred in tube inserts, outer and inner walls remote from the weld (Fig. 11.32). The general form of the weld was not good, there being a bulging of the weld into the tube insert wall and extensive porosity. Results of R.M. Hardness Impressions are reported in the following table:

Area	R.M.H. No.
Surface layer	1200 - 1350
Weld metal (Ta)	430 - 480
Ta insert tube remote from weld	320
Grain boundary phase	Too small to accommodate impression

11.10.4 Comments

Although the weld itself was not good, failure is thought to be due to embrittlement caused by pickup of impurities in the helium gas stream.

11.11 ANALYTICAL EXAMINATION OF GENERATOR SIDE WALL SECTIONS AFTER SERVICE (RHT 32)

by

A. Robertshaw

11.11.1 Introduction

The re-crystallised alumina side walls were tiles of approximate dimensions: 6 in. x 2 in. x 3/8 in., coated with an adherent, dark grey to black layer which proved resistant to mineral acids.

Two tiles were available for examination: (I) where the deposit appeared non-uniform and contained electrically-conducting areas which, in general, were darker in colour than the non-conducting areas on the same surface; and (II) where the deposit was more uniform in colour (grey) and found to be wholly non-conducting by the Avometer test as applied to tile I.

11.11.2 Preliminary examination of tile I (conducting area)

(1) X-ray diffraction crystallography showed the presence of tantalum carbide and α iron. Other unidentified elements were present in smaller amount.

(2) Chemical spot tests indicated iron and tantalum present.
Surface iron concentration ~ 150 $\mu gm/cm^2$
Surface carbon concentration ~ 200 $\mu gm/cm^2$

11.11.3 X-ray fluorescence examination of tiles I and II

Two samples A and B, 1 cm square, were prepared from Tile I.

Sample A was from an electrically-conducting area.

Sample B was from an electrically non-conducting area.

Two further samples C and D, of similar size, were prepared from Tiles I and II.

Sample C was from an electrically conducting area of Tile I (and therefore identical to Sample A).

Sample D was from Tile II (where the whole area was non-conducting).

The X-ray fluorescence analysis report is summarized in the table overleaf (and see also Figs. 11.34 and 11.35).

Element	Sample A	Sample B	Sample C	Sample D
W	Trace	Trace	Trace	Major
Ta	Major	Major	Major	Trace
Mo	N.D.	Trace	Trace	Minor
Zr	Trace	Trace	Minor	Trace
Fe	Major	Trace	Major	Major
Ni	Trace	Minor	Trace	Minor
Cu	Trace	Trace	Trace	Minor
Zn	Trace	Trace	Trace	Trace
Cr	Minor	Minor	Minor	Minor
Mn	N.D.	Trace	Trace	Minor
Ti	Trace	Trace	Trace	Trace
Ca	Trace	Trace	Trace	Trace
Cs	Minor	Trace	Minor	Trace

Note: Trace <0.1%
Minor 0.2 - 2%
Major >2%
N.D. none detectable (probably <0.01)

11.11.4 Summary

(1) With regard to the electrically conducting areas of deposit found in one instance on a generator side wall section, the analytical data gathered to date points to either one of the alternatives, below, or a combination of them.

(a) The build up of a continuous layer of metal and/or carbide containing Fe, Ta, Cr. etc.

(b) Deposition of cesium on the alumina surface.

(2) In analytical studies of this nature, it is clear that the conventional wet chemical techniques are of limited value, and methods such as X-ray fluorescence, micro-probe analysis and possibly emission spectrography may all be required to establish quantitatively the nature of such deposits on alumina. Future planned MPD experiments should therefore make an account for this, so that earlier arrangements can be made with outside authorities for the service techniques mentioned.

11.11.5 Sample preparation

Four samples were received, these were labelled as follows:-

A 3/4/64 Conductive

B 3/4/64 Non-conductive

C 10/4/64 Conductive

D 10/4/64 Non-conductive

For the purposes of this report these samples will be called A, B, C and D.

Samples were placed directly into sample cups fitted with 6.25μ mylar windows.

11.11.6 Operating conditions

A full list of operating conditions is given on each of the individual chart records (Figs. 11.34 and 11.35). The following points should be noted:

1 The scintillation counter was used up to 61° 2θ at which point it was replaced by the gas flow proportional counter.

2 All chart records were made under identical conditions such that direct comparison of relative intensities can be made. It must be realized, however, that as the deposit layer was not in excess of critical thickness and that the samples only partially covered the cell windows, absolute comparison between samples is subject to large error.

3 R.M. refers to rate meter and represents the sensitivity of the recorder. At RM = 1 full scale deflection is equivalent to 50 c/s, thus at RM = 64 full scale deflection is equivalent to 50 x 64 c/s. In all cases the R.M. settings were changed at 61° 2θ (i.e. at the change point of the detectors).

4 In the case of sample B the scan above 61° 2θ was repeated at higher sensitivity as peak intensities from this sample were particularly low.

5 A tungsten target x-ray tube was used for the majority of the work. As tungsten itself was being sought in the samples and as, due to scatter, the spectra from an irradiated sample will always contain primary lines, the spectra in the area of the tungsten lines were repeated with a gold target tube.

11.11.7 Results and discussion

The elements detected include W, Ta, Mo, Zr, Fe, Ni, Cu, Zn, Cr, Mn, Ti, Ca and Cs (Figs. 11.34 and 11.35). Under the conditions of scan, all elements present at concentration levels in excess of about 100 ppm will have given detectable responses.

11.12 ANALYSIS OF OXYGEN IN CESIUM

by

V. Cullen

The method currently used for analysis of oxygen in cesium is based on heating cesium with a known excess of sodium under vacuum, and as the cesium oxides break down then the liberated oxygen will be readsorbed until all the cesium metal is removed by distillation. Alternatively the more stable sodium monoxide will be slowly formed until eventually only free cesium is present.

A two-stage distillation removes firstly the cesium and then the sodium until finally only sodium monoxide is left. This is then dissolved in water and titrated to a phenolphthalein end point with standard acid. A separate sodium-only distillation gives a 'blank' for the sodium used hence any oxide in excess of this amount must be from the cesium, and thus the concentration of oxygen in the cesium is known.

When first proposing this method the stabilities of various common cesium oxides were considered, and all were found to decompose at or below 650°C, with the exception of the trioxide Cs_2O_3, which was known to melt at 400°C. Since then more data on decomposition of the more common oxides has been obtained. All decompose below 880°C when the most stable of these, the superoxide, CsO_2, decomposes. This information is in agreement with IRD findings since, in accordance with the first proposal[2], several distillations of cesium alone were carried out without detecting any residual alkalinity. As a continuation, cesium was then added to sodium and a vacuum distillation carried out; again no residual alkalinity was detected. Finally the Cs/Na alloy was raised to 400°C, sealed under vacuum and heated for an hour to allow the cesium oxides to decompose and the oxygen to be finally absorbed by the sodium, when the temperature was raised to 700°C and the two-stage distillation completed.

This presents the method in its most recent and modified form, and it has produced results of a reasonable order particularly in the 300 - 700 ppm oxygen range on samples of glass-encapsulated cesium, for which the makers claim a purity of about 99.9%.

REFERENCES

1 Cesium and rubidium (supplement to bulletin No. TD - Cs/Rb) American Potash and Chemical Corporation.

2 Tech. Memo. IRD/IR/VC/MK. 22/1/63. A proposed method for the determination of oxygen in cesium.

11.13 COMPATIBILITY OF CESIUM WITH 'GASCO' AND SILICON RUBBER O-RINGS

by

V. Brown

Stainless steel containers were cleaned chemically (pickle: 5 per cent hydrofluoric acid; 10 per cent nitric acid) and then washed with Inhibisol. Unused O-rings were weighed, inserted into containers with a 1 gm cesium ampoule, and evacuated to 4×10^{-3} torr at a temperature of 80°C. The ampoule was then broken to immerse the O-ring under cesium at 85-95°C for 10 hr. Weight losses of about 1 per cent, attributed to outgassing, were obtained.

Fig. 11.36 shows the attack on silicon rubber; the 'Gasco' rubber was unaffected.

SEVERE EMBRITTLEMENT AT INLET END OF TUBE (X1)

FIG 11·1

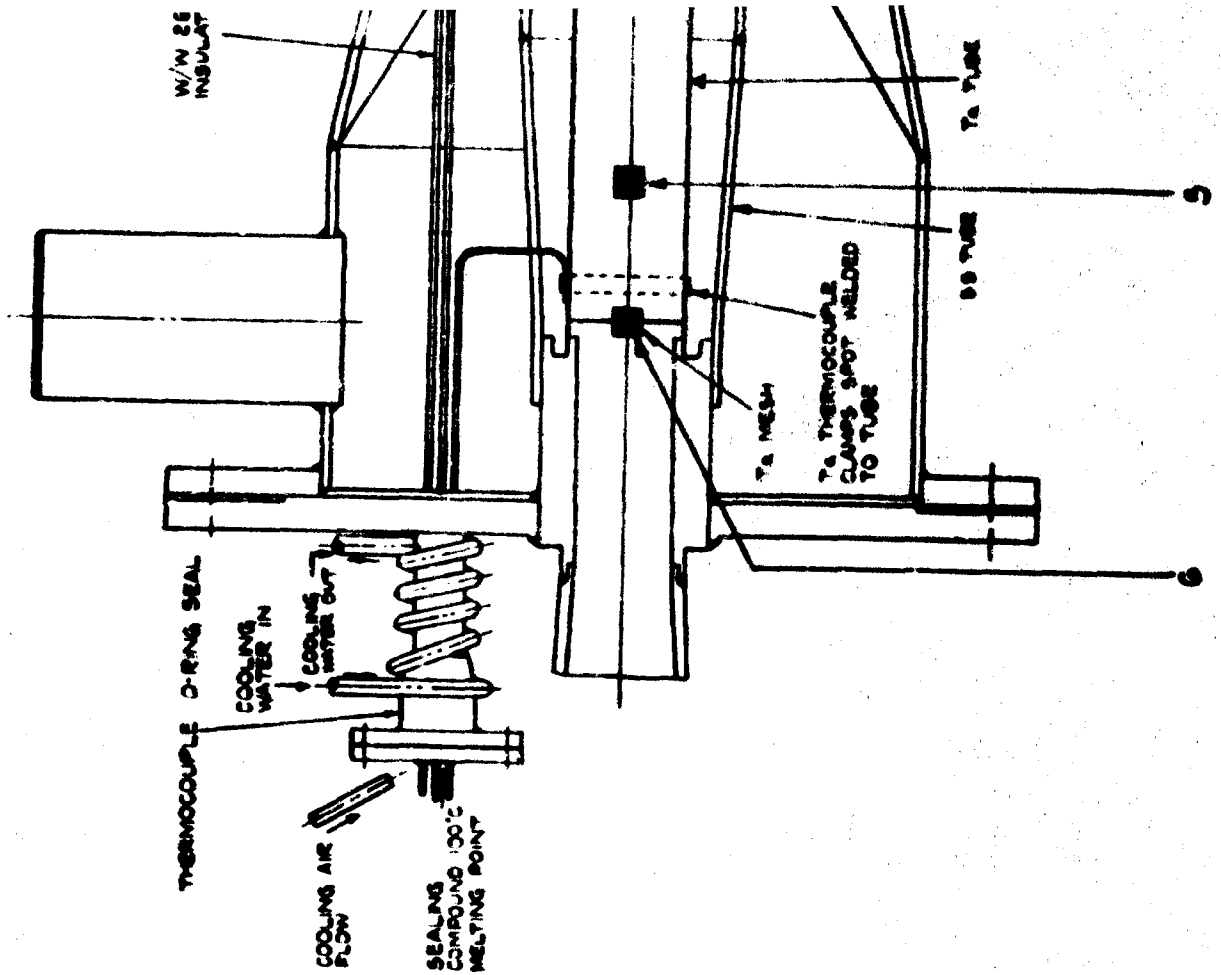

LOCATION OF SECTIONS ON TEMPORARY TANTALUM TRANSFER DUCT

FIG 11·2

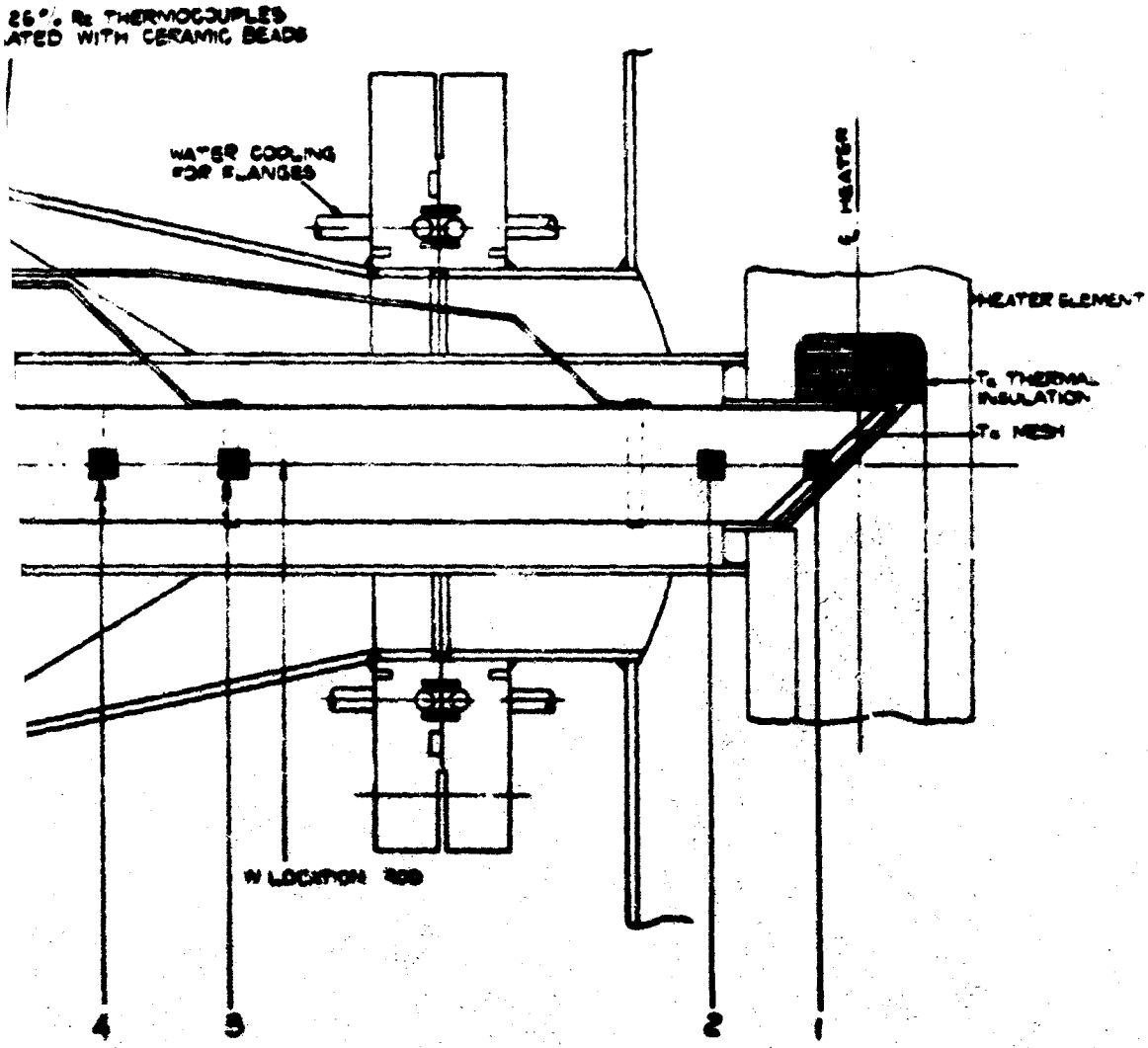
ATED WITH CERAMIC BEADS
WATER COOLING FOR FLANGES
HEATER ELEMENT
To THERMAL INSULATION
To MESH
4
3
2
1

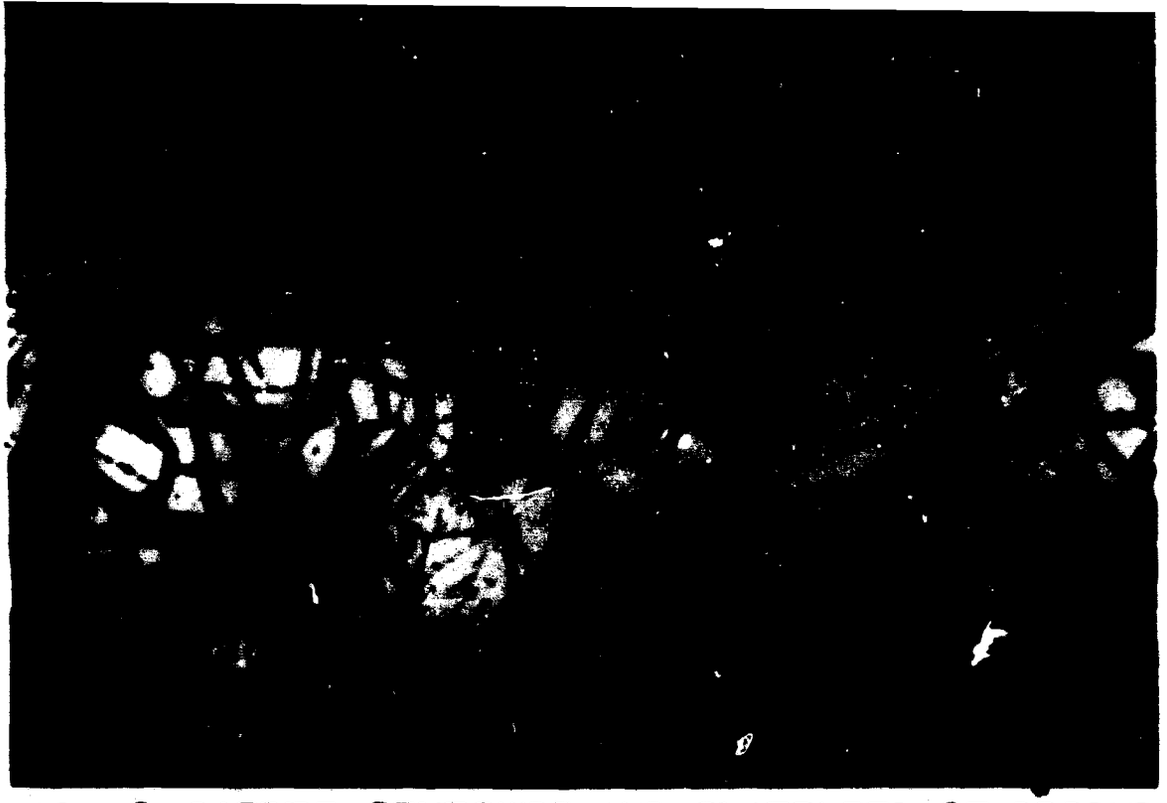

FIG 11·3 CARBIDE, PENTOXIDE AND PLATELETS OF SECOND PHASE PRECIPITATE IN SECTION 1 (X 400)

FIG 11·4 CARBIDE, PENTOXIDE AND PLATELETS OF SECOND PHASE PRECIPITATE IN SECTION 6 (X 400)

FIG 11·3 & 11·4

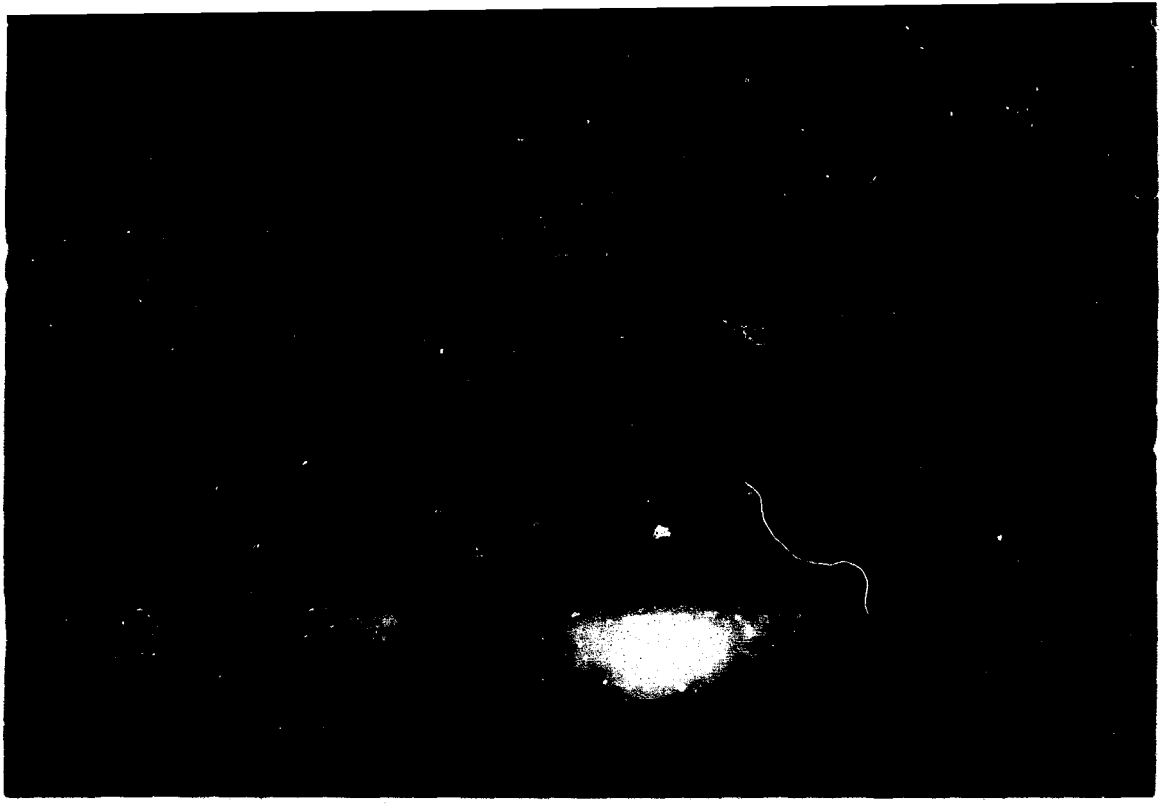

FIG 11·5 PLATELETS OF SECOND PHASE PRECIPITATE (POLARISED LIGHT) (X 400)

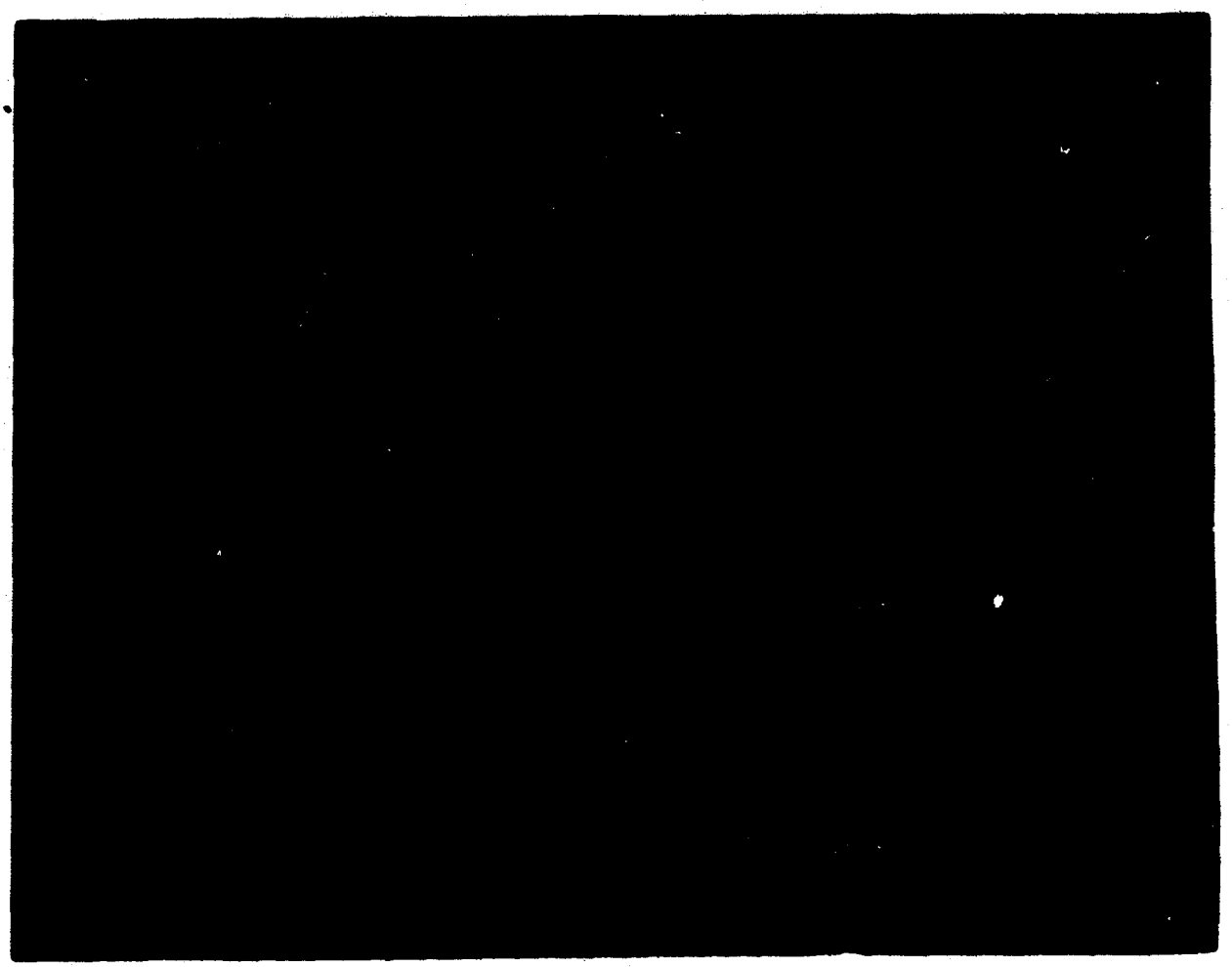

FIG 11·6 CARBIDE, PENTOXIDE AND PLATELETS OF SECOND PHASE PRECIPITATE IN A FRAGMENT OF GAUZE (X 400)

FIGS 11·5 & 11·6

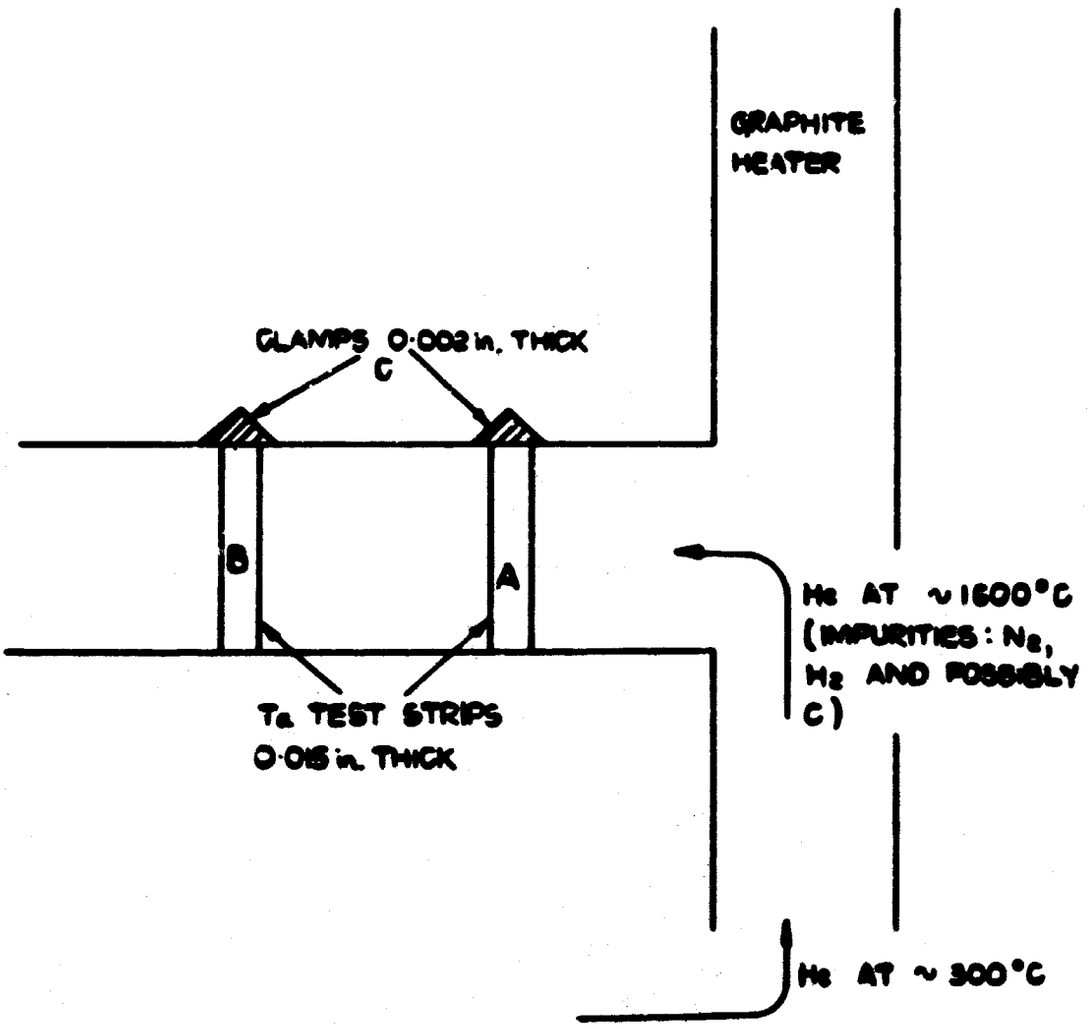

POSITION OF TANTALUM SPECIMENS IN TRANSFER DUCT

FIG 11·7

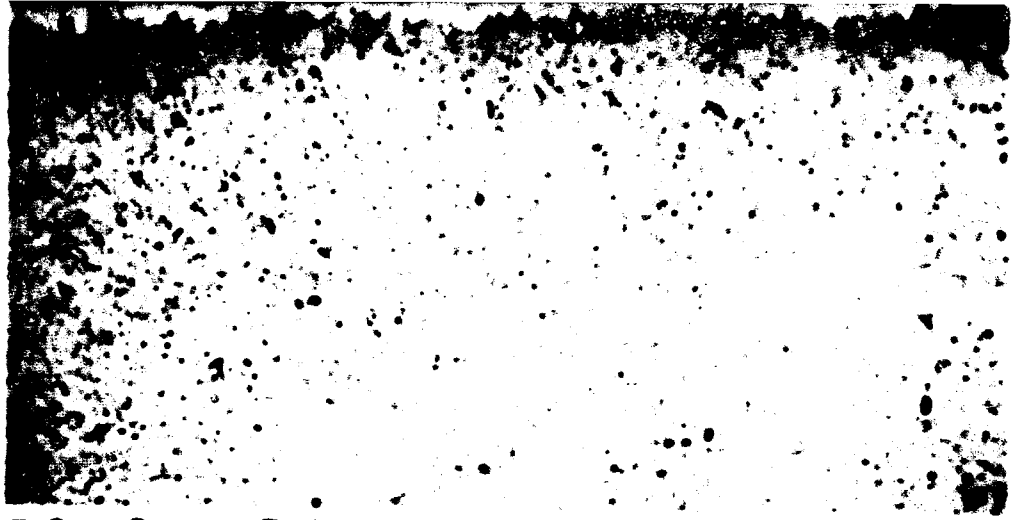

FIG 11·8 SURFACE ATTACK AND FINE PRECIPITATION IN SPECIMEN A (X400)

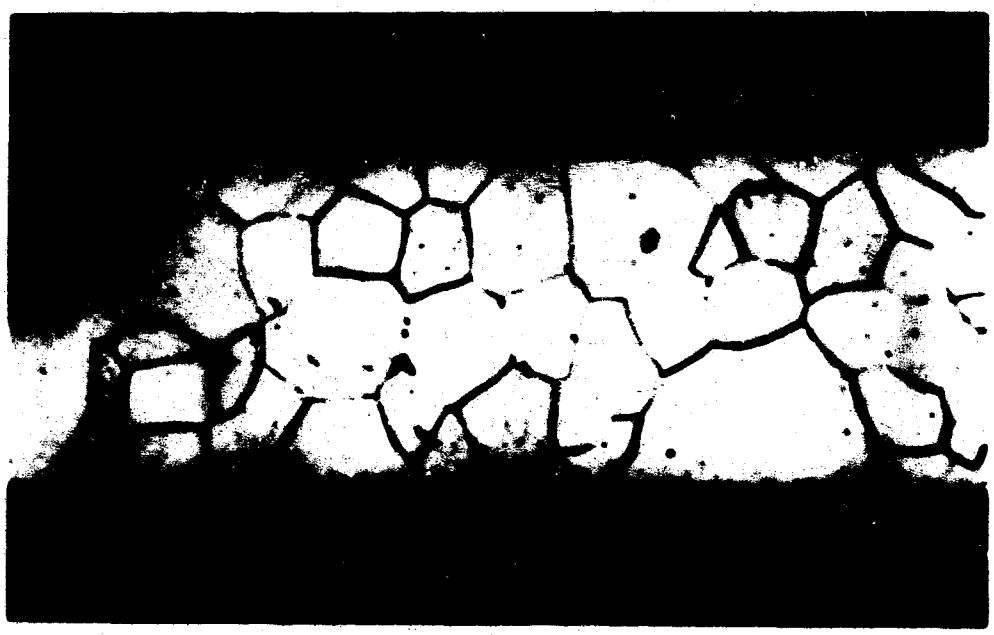

FIG 11·9 SURFACE ATTACK IN SPECIMEN C (X500)

FIG 11·10 INTER AND TRANSGRANULAR PRECIPITATION IN SPECIMEN C (X400)

FIGS 11·8, 11·9 & 11·10

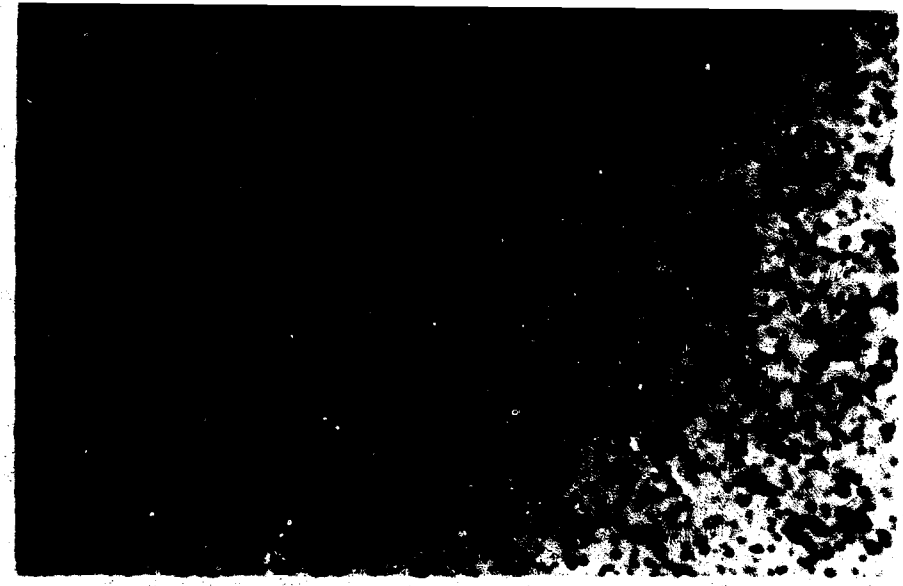

FIG 11·11 FINE PRECIPITATION IN 0·015 in. THICK AS-RECEIVED MATERIAL (X 400)

FIG 11·12 FINE PRECIPITATION IN 0·002 in. THICK AS-RECEIVED MATERIAL (X 400)

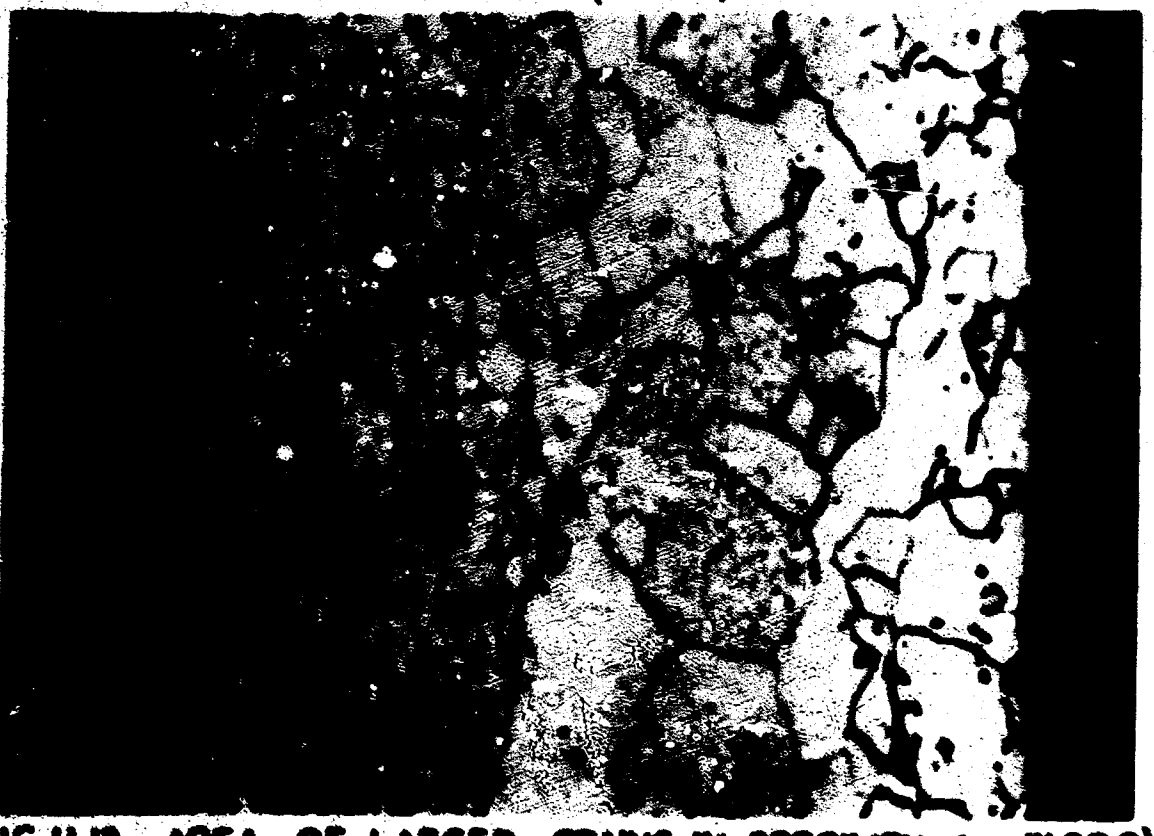

FIG 11·13 AREA OF LARGER GRAINS IN SPECIMEN A (X 300)

FIGS 11·11, 11·12 & 11·13

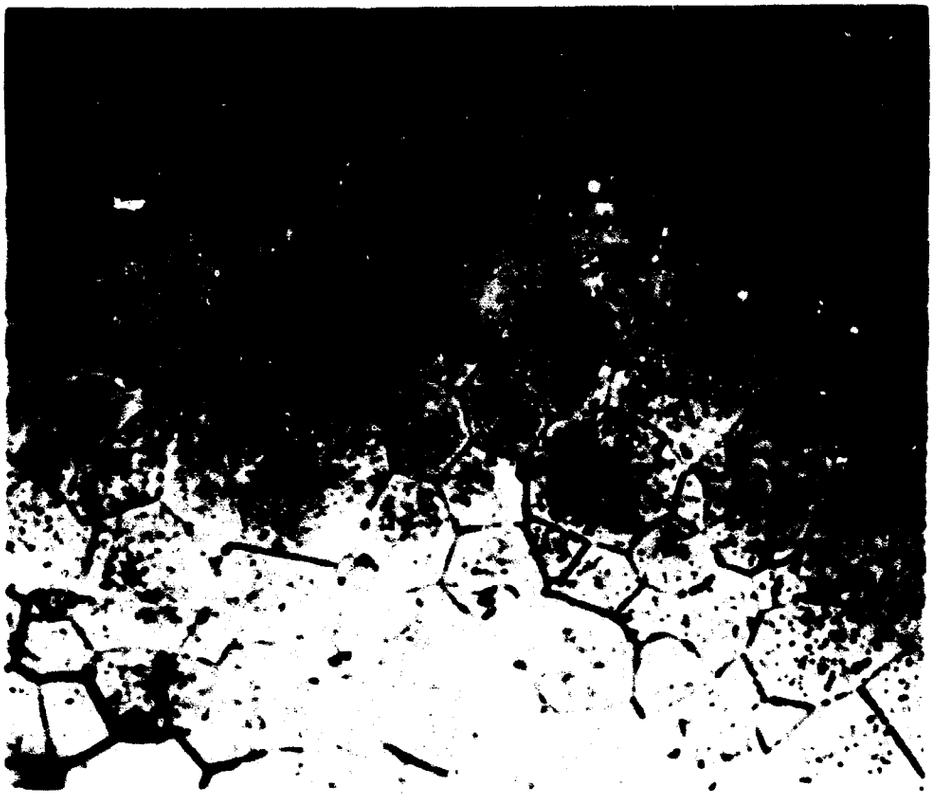

FIG 11·14 PRECIPITATE IN FRACTURE AREA (X400)

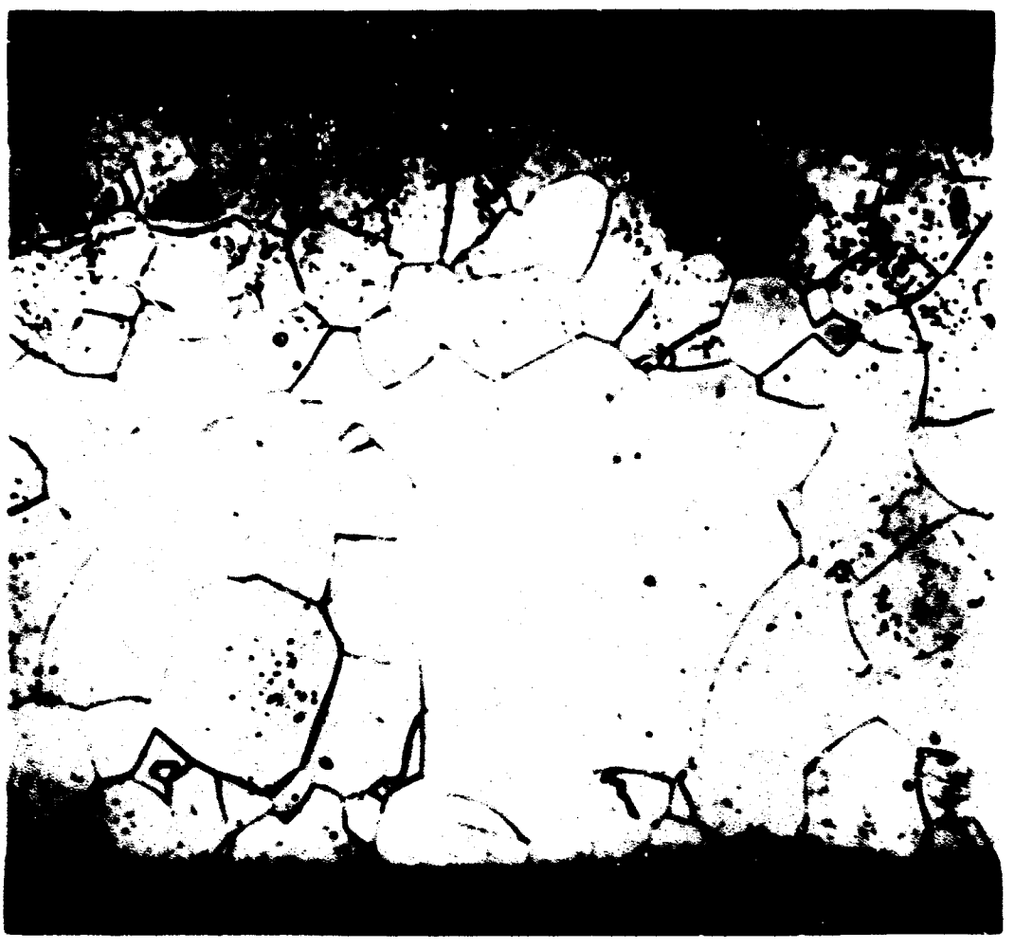

FIG 11·15 BULK OF PRECIPITATE AT OUTSIDE EDGE OF SHEATH (X 300)

FIGS 11.14 & 11.15

FIG 11.16 UNIFORM PRECIPITATION IN SHEATH (x300)

FIG 11.17 COLD WORKED STRUCTURE OF SHEATH (x300)

FIG 11.18 CHANGE IN ORIGINAL COLD WORKED STRUCTURE

FIGS 11.16 11.17 11.18

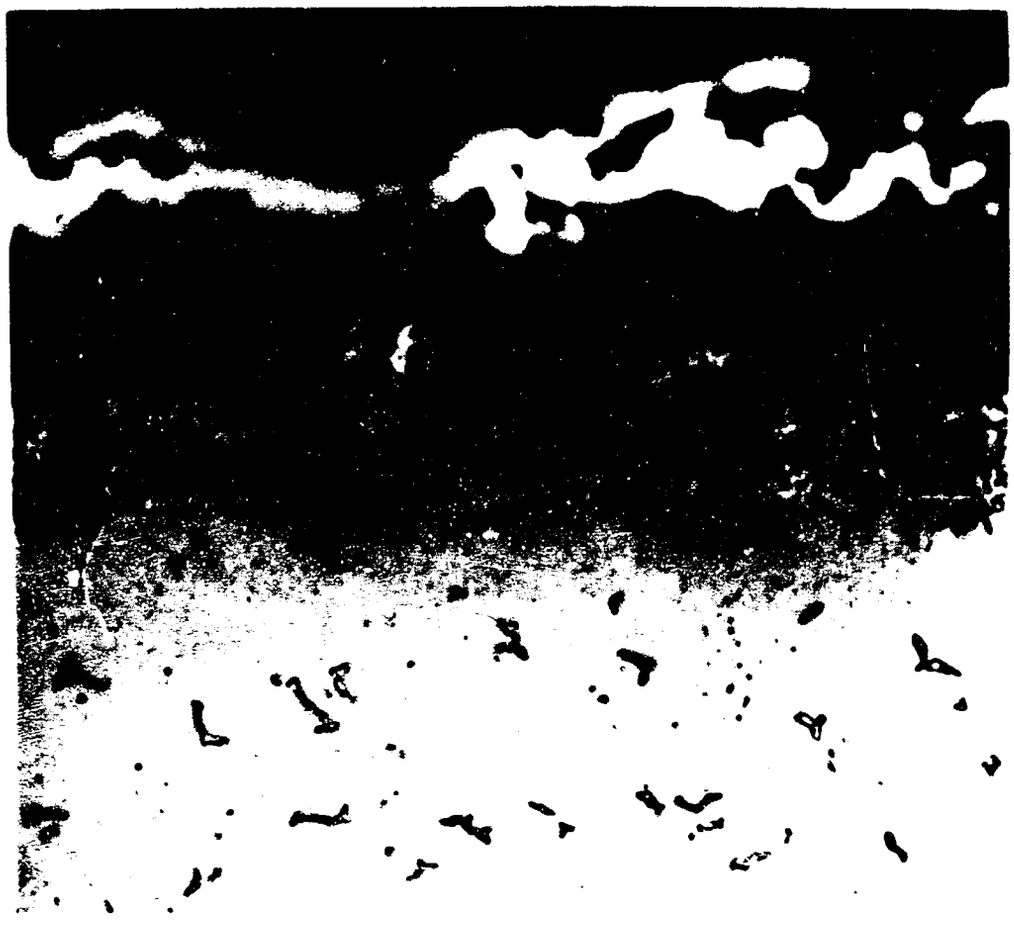

FIG 11·19 SURFACE LAYERS X 400

FIG 11·20 INTERGRANULAR PRECIPITATION ACROSS WALL X150

FIGS 11·19 & 11·20

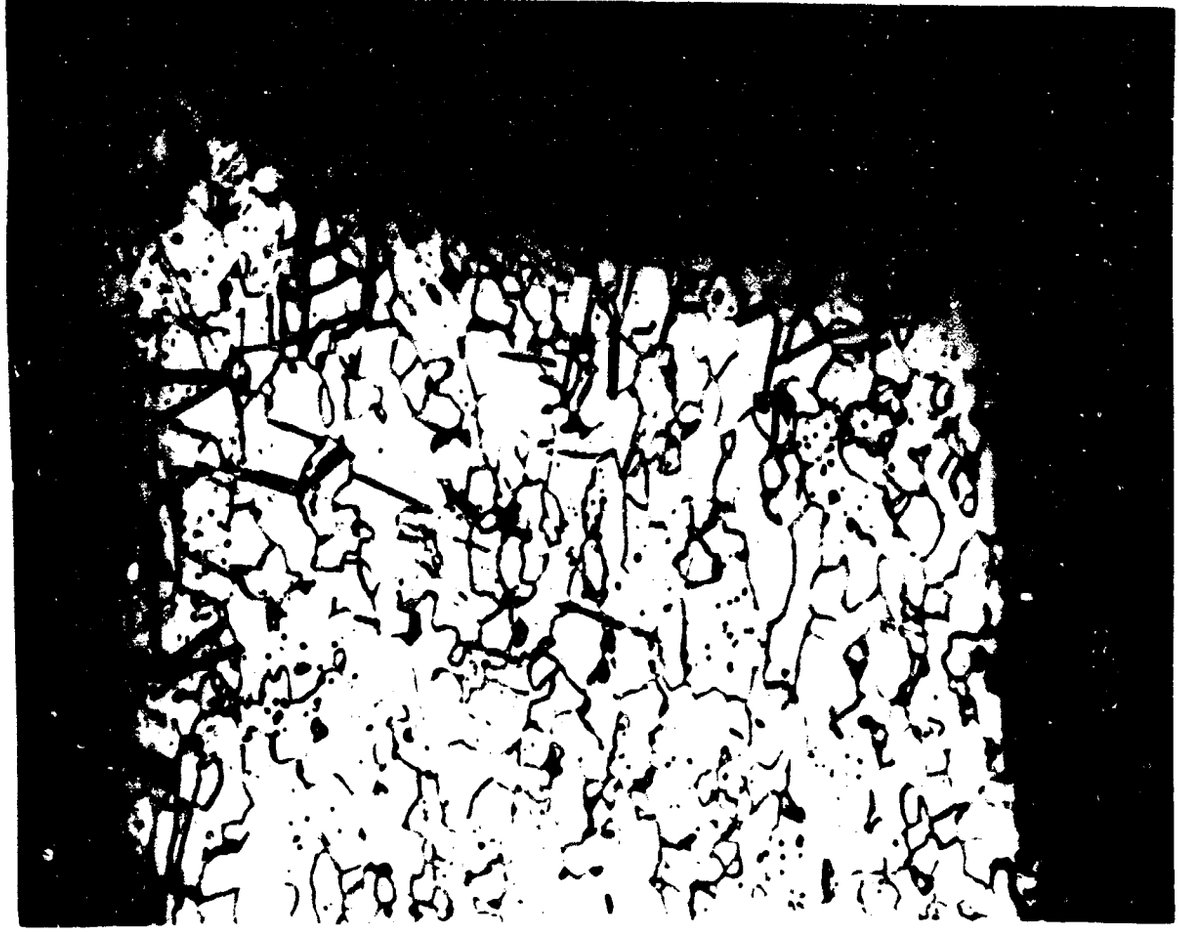

G 11·21 PLATELETS IN BELLOWS WALL (X 250)

G 11·22 PLATELETS IN BELLOWS WALL (X 300)

FIGS 11·21 & 11·22

FIG II.23 SURFACE ATTACK AND FINE PRECIPITATION IN SPECIMEN A (× 400)

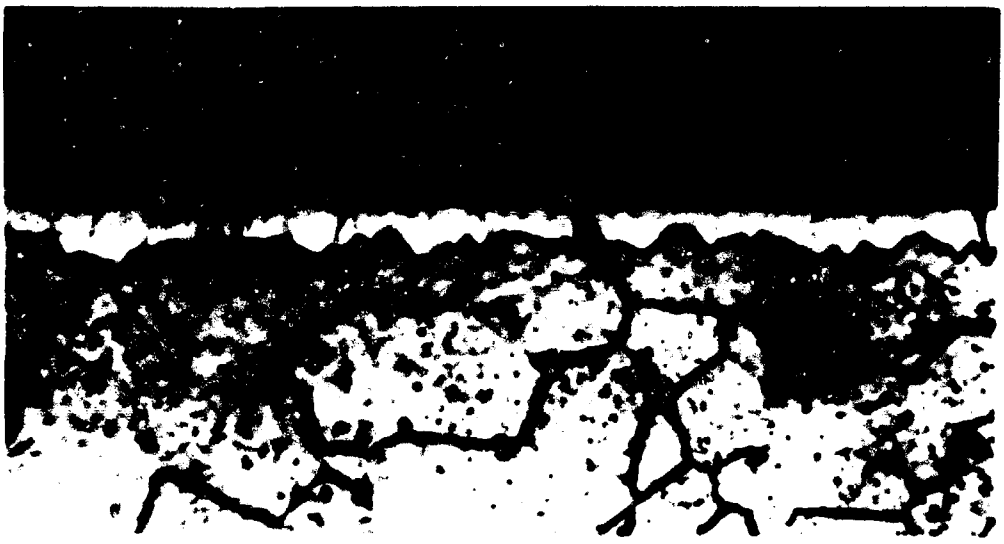

FIG II.24 SURFACE LAYERS ON SPECIMEN A (×750)

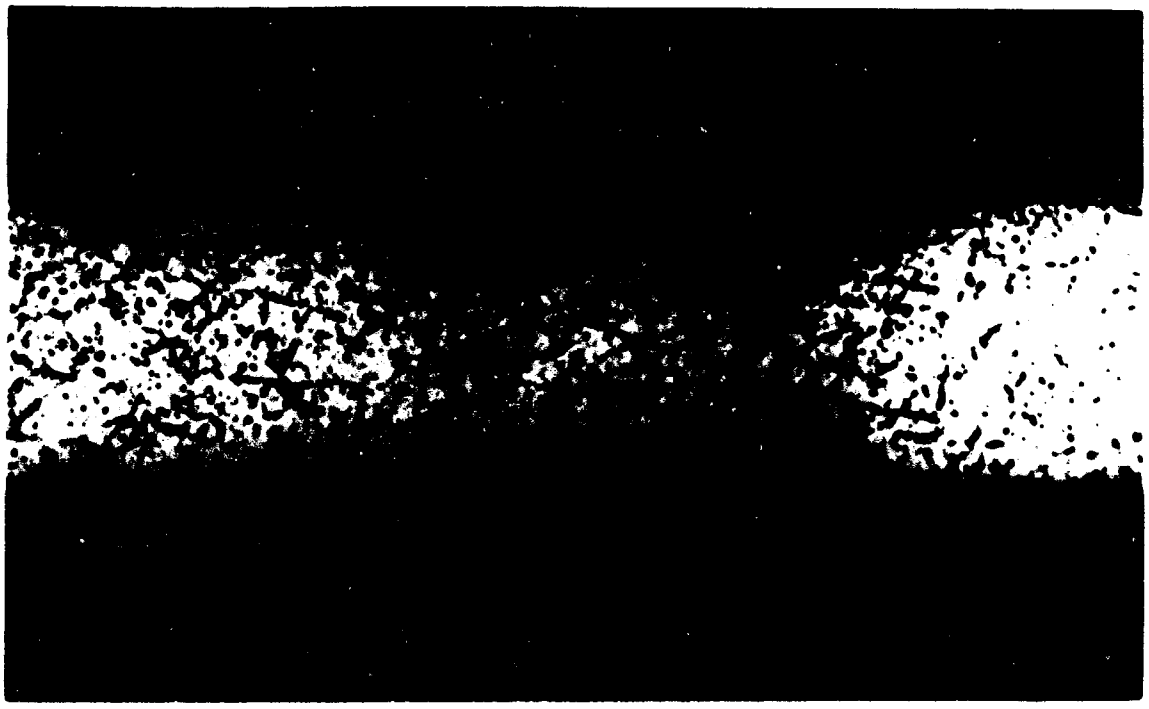

FIG II.25 FINE INTER AND TRANSGRANULAR PRECIPITATION IN SPECIMEN C (× 400)

FIGS II.23 II.24 II.25

FIG 11.26 SURFACE LAYER AND GRAIN BOUNDARY PHASE IN SPECIMEN B (.400)

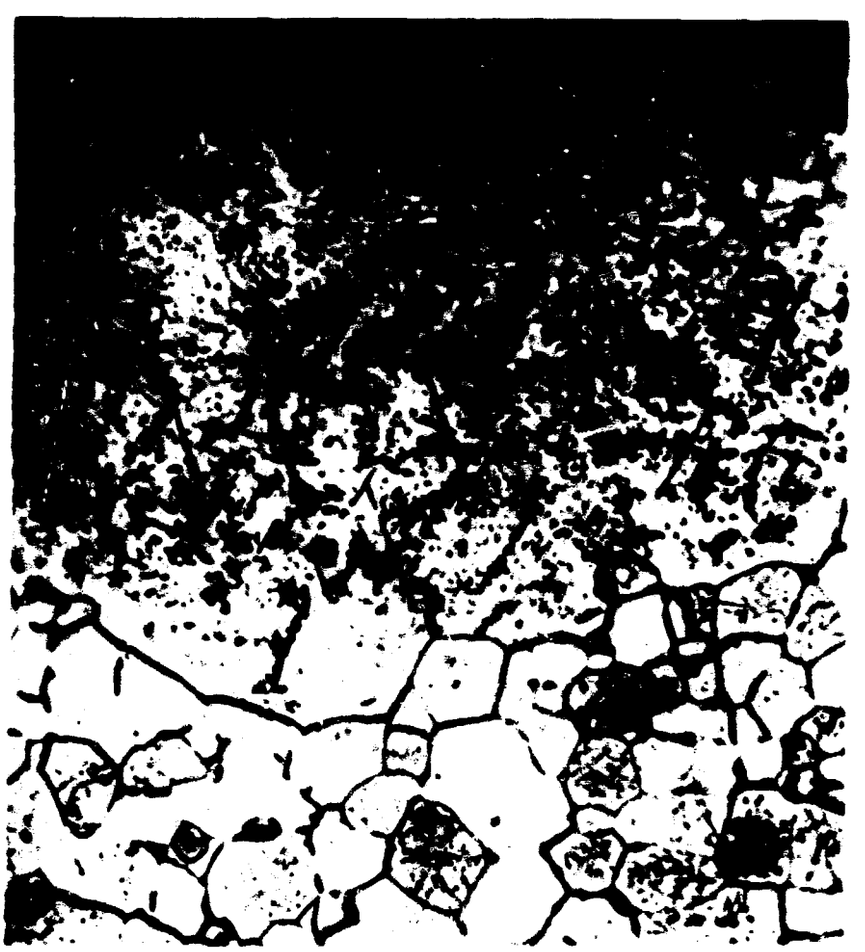

FIG 11.27 SURFACE LAYER AND NEEDLE-LIKE PRECIPITATE IN SPECIMEN B (x400)

FIGS 11.26 11.27

LARGE SURFACE GRAINS IN SPECIMEN B (X 300)

FIG 11·28

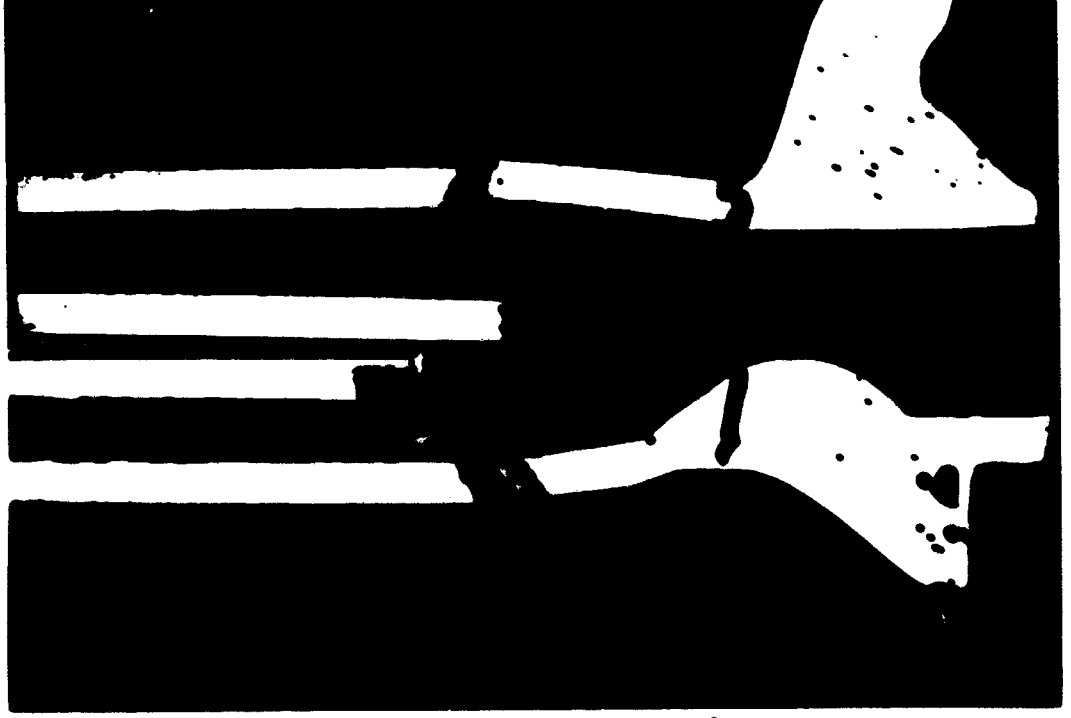

G 11·29 SECTION THROUGH WELD (X 8)

G 11·30 SURFACE LAYER ON TUBE (X100)

FIGS 11·29 & 11·30

FIG 11.31 SURFACE LAYER DISTRIBUTION OF GRAI
WELD AREA (×40)

FIG 11.32 SURFACE CORROSION
WELD (×400)

FIGS 11.31 11.32

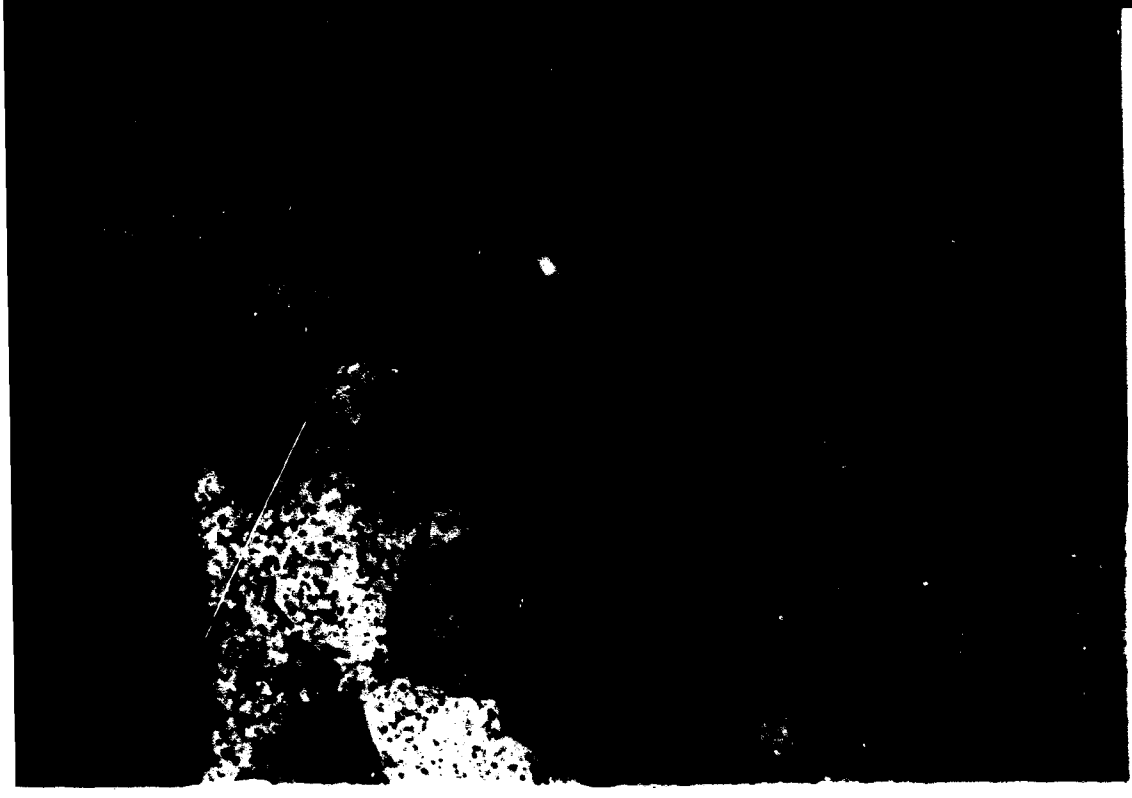

IN BOUNDARY PHASE AND INTRAGRANULAR PRECIPITATE IN

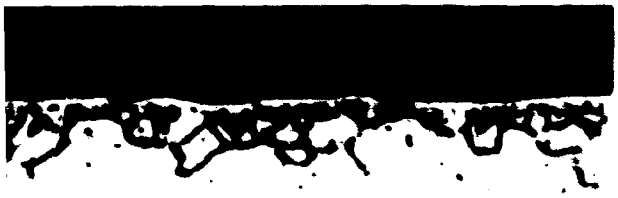

ON INSERT TUBE REMOTE FROM

DEGREE OF CORROSION ON INSERT TUBE STU

FIG 11-33

DS (X100)

X - RAY FLUORESCENCE RECORDINGS, I

FIG 11·34

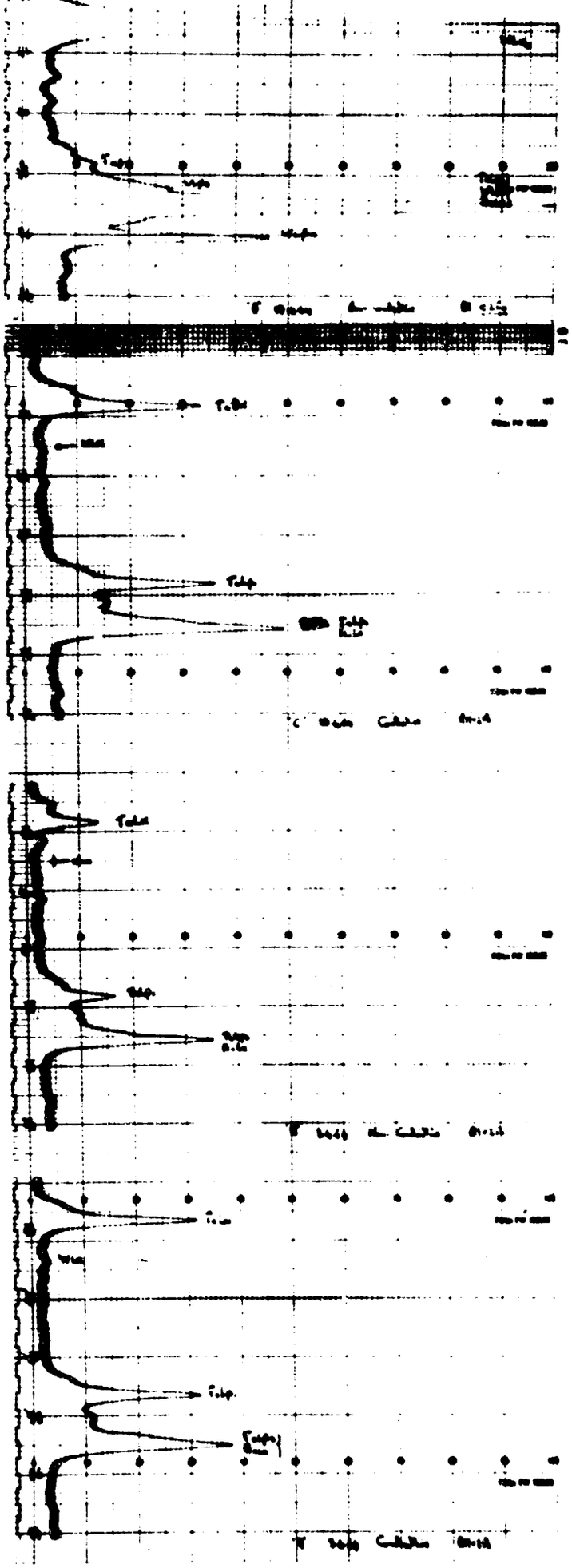

X - RAY FLUORESCENCE RECORDINGS, II

FIG 11·35

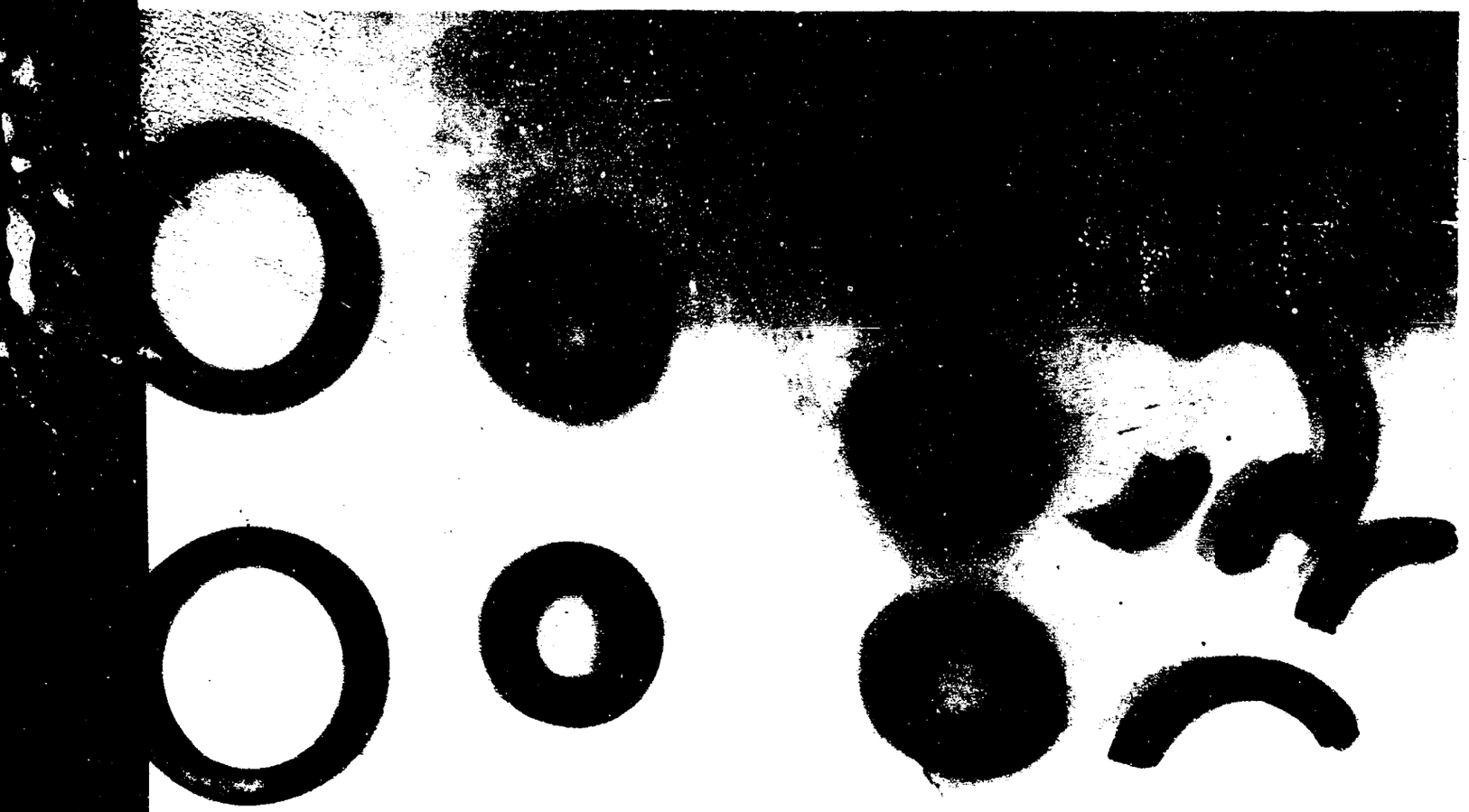

ATTACK ON SILICON RUBBER

FIG 11·36

CHAPTER 12

COMPATIBILITY OF MPD REFRACTORY MATERIALS WITH CESIUM VAPOUR*

by

G. Arthur

12.1 INTRODUCTION

This paper describes some of the materials work being carried out in support of the closed cycle MPD power generation project at IRD.

In the closed cycle MPD system a high velocity stream of helium containing a small amount of cesium is passed through a duct containing a series of electrodes insulated from each other. The minimum temperatures of operation are at present not established but will probably be in the range 1500 - 2200°C.

In a previous paper[1] the stability of various refractory insulating materials to vaporization were discussed and it was concluded that for operating temperatures in the region of 2200°C only hafnia and thoria would be suitable insulants and tungsten a suitable electrode material. However, it is now thought[2] that lower temperatures of operation (~1500°C) are possible and this considerably widens the choice of both insulating and electrode materials. For example, boron nitride, which has a high electrical resistivity, good thermal shock resistance and is easily machined, can now be considered as an insulant.

However, it still remains to determine whether these electrode and insulant materials are resistant to cesium vapour and this is the purpose of the present work.

Considerable information is already available on the reactions of alkali metals, especially sodium and potassium, with various materials at low temperatures (~300°C)[3,4], but many of the results are complicated by the presence of alkali oxides. Smith et al[5] and Slivka[6] have investigated the compatibility of some metallic and non-metallic thermionic converter materials with cesium up to 600° and 900°C respectively. They found, among other things, that high purity alumina was not attacked in contrast to alumina of lower purity. Wagner and Corriell[7] studied the effect of cesium vapour on several of the more stable oxides at temperatures up to 1475°C. In the short time (~10 min) of their experiments no marked effects were found.

---

* To be presented at the International Symposium on Magnetohydrodynamic Power Generation. Paris, July 1964

12.2 THERMODYNAMIC PROPERTIES OF CESIUM AND ITS OXIDES

The vapour pressure of cesium in torr is given by

$$\log p = 11.0531 - 1.35 \log \left(-\frac{4041}{T}\right) \quad \ldots\ldots (12.1)$$

at 300° and 375°C, the cesium reservoir temperatures used in the present work, the corresponding pressures are 1.9 and 10 torr.

The free energies of formation of Cs_2O, Cs_2O_2, Cs_2O_3 and CsO_2 have been given by Coughlin[8]. Cs_2O is the most stable and the other oxides decompose to give Cs_2O with increasing temperature and decreasing partial pressure of oxygen.

The free energy of formation of Cs_2O is given by

$$2Cs_{(g)} + \tfrac{1}{2}O_{2(g)} = Cs_2O_{(\ell)} \quad \Delta G = -101,730 + 64.51\ T \quad \ldots\ldots (12.2)$$

Brewer[9] states that none of the cesium oxides are volatile and that volatilization takes place by decomposition to oxygen and monatomic cesium. Thus, irrespective of the oxygen content of liquid cesium there are no oxides in the vapour. Systems containing cesium vapour are thus considerably simpler than those with liquid cesium.

Calculation[1] shows that at no temperature would cesium react with the more stable refractory oxides (such as Al_2O_3, ZrO_2, MgO) by reactions of the form

$$2Cs + MO = Cs_2O + M.$$

No thermodynamic information can be found on compounds of Cs_2O with other oxides but it is unlikely that they would have sufficient stability to allow reactions of the form

$$2Cs + 2MO = Cs_2O.MO + M$$

to proceed at high temperatures where the stability of Cs_2O is lowest. At low temperatures it is possible that cesium oxide-alumina-silica compounds similar to the felspars could form and thus account for the observed attack[5] of liquid cesium on impure aluminas.

12.3 EXPERIMENTAL WORK

12.3.1 Apparatus

The apparatus is shown in Fig. 12.1. The outer vessel was of austenitic stainless steel closed at one end by a flange seating on a copper ring of diamond cross section. This ring was replaced after each run. The heating element was a 5 cm long spiral of 8 turns of 2 mm molybdenum wire, one end of which was connecte directly to the case and the other to a ceramic-metal seal brazed to the detachable

flange. The molybdenum power leads inside the vessel were sleeved with alumina tubes to prevent arcing to the case in the presence of cesium vapour. The element was surrounded by radiation shields, the inner three of which were molybdenum and the outer two stainless steel. A small sheet of zirconium was also inserted between the molybdenum and the stainless steel to act as a getter.

The vessel was evacuated through a 1.5 cm diameter stainless steel tube fitted with an all metal vacuum valve suitable for use up to 400°C. This 1.5 cm tube was fitted with a side arm to which was welded another stainless steel tube into which had been inserted a glass capsule containing 1 gm of cesium.

Eight chromel-alumel thermocouples were fitted to what were known from preliminary experiments to be the coldest spots on the outer vessel. The temperature of these spots was controlled by lagging with refrasil heating tapes.

Temperature measurement of the specimen was by a Kodial window fitted to the stainless steel vessel by flanges seating on a small copper O-ring. This window was maintained at the same temperature on the rest of the vessel by a small hot air heater not shown in Fig. 12.1.

12.3.2 Test procedure

The test samples consisted of small cylinders approximately 3 mm diameter and 5 mm long held in the molybdenum heater by small molybdenum clips. After insertion of the specimen, the observation window and end flanges were fitted and the side arm containing the cesium phial was welded in position. The assembly was then evacuated and leak-tested by means of a helium mass spectrometer sensitive to a leak rate of 10^{-10} litre-torr-seconds. When this leak rate had been achieved the specimen was slowly heated to the test temperature to outgas and to calibrate the optical temperature with power input. That black-body conditions were approximately achieved was confirmed by the insertion of graphite specimens which, for a given power input, gave the same temperature as the other specimens tested. The specimen was then cooled, the stainless steel bellows valve closed and the cesium capsule broken by compressing the stainless steel side arm. The cesium was then driven from the side arm by the application of a gas burner and the side arm sealed by compression in a vice. The specimen was then reheated to the test temperature by adjustment of the power input to the previously-determined level. This procedure was necessary because of the discoloration of the glass window by cesium which made accurate optical temperature measurement impossible. The brown discoloration was, however, easily removed by water at the completion of the run.

The vapour pressure of cesium was determined by the minimum temperature of the enclosing vacuum vessel. This was controlled by power adjustment of the

external heating tapes at either 300° or 375°C corresponding to 1.9 and 10 torr respectively.

The presence of cesium vapour in the vessel was checked periodically by cooling the observation window below the minimum vessel temperature when globules of cesium could be seen condensing.

The test runs were of four hours duration. Concurrently duplicate specimens were heated in vacuum without cesium so that the effects of temperature and cesium could be separated. The maximum specimen temperature in the experiments done in cesium was 1800°C.

12.3.3 Examination of specimens

All specimens were weighed and measured before and after exposure to cesium. Most specimens were also examined microscopically and some by X-ray diffraction. The cesium content of some of the specimens was also estimated.

12.4 RESULTS

The materials which have been tested to date are boron nitride, graphite, hot-pressed silicon carbide, alumina, hafnia, zirconia, tungsten, tantalum and molybdenum. Graphite was included in the programme so that its behaviour could be compared with that of boron nitride under similar experimental conditions.

12.4.1 Boron nitride

The boron nitride was hot-pressed material obtained from the Carborundum Co. The boric oxide content was determined by chemical analysis to be 2.70% and only trace quantities of other elements could be found. The density of the as-received material was 2.04 gm/cm^3.

The results of the tests in both cesium and in vacuum are summarized in the following table.

CHANGES IN SIZE AND WEIGHT OF BORON NITRIDE SPECIMENS HEATED IN CESIUM VAPOUR AND IN VACUUM

Spec. No.	Temp, °C	Vapour pressure of cesium, torr	Percentage weight change in 4 hr		Percentage volume change in 4 hr	
			with cesium	without cesium	with cesium	without cesium
1	375	10.0	nil	nil	nil	nil
2	600	10.0	+1.5	nil	nil	nil
3	1600	1.9	-2.1	-5.4	+2.3	+1.5
4	1600	10.0	-5.0	-5.4	+2.3	+1.5
5	1700	1.9	-4.8	-12.0	+4.5	+3.5
6	1700	10.0	-5.5	-12.0	+1.5	+3.5
7*	1800	10.0	-15.0	-14.6	-	+3.34
8	1800	10.0	-7.6	-14.6	+1.5	+3.34
9	1900	nil	-	-27.0‡	-	not done

* specimen cracked ‡ 1 hr run

Specimen No. 7, which was cracked both radially and longitudinally, was the only one showing any gross attack by cesium. A repeat of this, test no. 8, however, showed no cracking. In all cases the weight loss in cesium was less than in vacuum. This was probably partly due to suppression of volatilization by the pressure of cesium and partly to the pick-up of cesium by the boron nitride. A small expansion occurred in all the specimens whether heated in vacuum or in cesium. This expansion may in both cases be caused by the volatilization of boric oxide from the interior of the specimen. Some support for this hypothesis is given by the results of a previous investigation[10] which found larger expansions (9-10%) at 1800°C for material containing higher oxide contents (~15%).

Photomicrographs of some of the specimens heated in cesium are shown in Fig. 12.2. The specimens heated for 4 hr at 1600°, 1700° and 1800°C all showed an outer rim of close-textured material and an inner core which also differed in appearance from the original. None of the specimens heated in vacuum to these temperatures showed a rim and core effect. The specimen heated to 375°C in cesium was unchanged from the original but that heated at 600°C also showed a rim (Fig. 12.2) but examination at higher magnification (Fig. 12.3) showed no difference in microstructure between the inner and outer areas. X-ray examination of the rim and core of specimens treated at 1600° and 1800°C showed that the core contained less B_2O_3 than the rim but otherwise the patterns were identical.

12.4.2 Graphite

Morgan EY9 graphite was tested at 600°, 1000° and 1800°C. A summary of the results is given in the following table.

EFFECT OF HEATING GRAPHITE SPECIMENS FOR 4 HR IN CESIUM VAPOUR AT 10 TORR PRESSURE

Specimen No.	Temp, °C	Comments
10	600	Specimen disintegrated
11	600	Specimen disintegrated
12	1000	Specimen badly cracked
13	1800	No apparent attack

Photographs of the specimens after treatment are shown in Fig. 12.4. The specimen tested at 1800°C showed no change in appearance, weight or size.

12.4.3 Silicon carbide

A sample of silicon carbide hot-pressed from β silicon carbide containing 4% Al_2O_3 to a density of 3.10 gm/cm^3 was tested in cesium at 1800°C for 4 hr. A

weight loss of 4% was measured which was approximately the same as found in the thermal history run. Microscopic examination showed no evidence of attack by cesium.

12.4.4 Oxides

Samples of alumina, hafnia and zirconia (magnesia stabilized) were also tested for 4 hr at 1800°C. In none of these specimens was there any change in weight, dimensions or microstructure.

12.4.5 Metals

(i) Molybdenum

The molybdenum heaters used remained ductile and uncorroded by the cesium. One of these after being at approximately 1900°C (the heater was noticeably hotter than the specimens which were at 1800°C) for 30 hr was examined microscopically and showed an even equiaxed grain structure with no evidence of attack by cesium.

(ii) Tantalum

Small pieces of tantalum foil heated to 1800°C in cesium were invariably embrittled. No change was, however, apparent in the microstructure. The embrittlement may have been due to reaction of the tantalum with oxygen or nitrogen which had leaked into the vessel during the course of the experiment. Further work is being done to elucidate this point.

(iii) Tungsten

A piece of tungsten wire heated for 4 hr in cesium at 1800°C was neither embrittled nor corroded.

12.5 DISCUSSION OF RESULTS

Of the materials tested in cesium, the most marked changes were found in graphite and tantalum, the former disintegrating or showing gross cracking at temperatures up to at least 1000°C and the latter being embrittled at 1800°C. This embrittlement may, however, be due to oxygen or nitrogen and not cesium.

Graphite is known[11] to form interlamellar compounds with the alkali metals of types C_8M, $C_{24}M$ and $C_{40}M$. These compounds are believed to be ionic in character, electrons being transferred from the metal to the graphite to give structures such as $C_8^-M^+$. The stability of the compounds increases with the atomic number of the metal, reflecting the increasing ease with which electrons can be removed. It is doubtful if Li and Na (having higher ionization potentials) form any compounds at all. Most of the studies of these compounds have been done at comparatively low temperatures (<300°C) and at these temperatures the insertion of the alkali metal

ions between the graphite layers causes an expansion in the c direction and specimen disintegration. It is probable that a similar reaction caused disintegration of the specimens at 600° and 1000°C in this work. At 1800°C the decomposition pressure of any graphite-cesium compound has presumably exceeded the cesium pressure inside the reaction vessel.

It is of interest that boron nitride, having a layer lattice almost identical to that of graphite, does not disintegrate in cesium vapour even at temperatures as low of 375°C. However, boron nitride, unlike graphite, is a good electrical insulator with a band gap of 4.6 eV between the uppermost filled molecular orbital and the next higher level. For this reason boron nitride would be unlikely to either accept or donate electrons to form ionic interlamellar compounds.

The effect which cesium has on boron nitride (Fig. 12.2 and 12.3) is not reflected in any change in the lattice parameters. It is possible that the cesium reacts with the small amount of boric oxide present in the boron nitride to form a cesium borate glass.

Cesium vapour has been shown to have no effect on the oxides, alumina, hafnia and zirconia at 1800°C, in agreement with the known thermodynamic properties of these materials.

12.6 CONCLUSIONS

1 Alumina and hafnia are suitable closed cycle MPD duct materials up to 1800°C.

2 Boron nitride, although altered by cesium at 1800°C, is not severely damaged and the limitation on life would be the high rate of evaporation. It should be noted that after 4 hr at 1800°C boron nitride undergoes a 1% linear increase in size and provision may have to be made for this in design.

3 Of the electrode materials tested, molybdenum and tungsten were unaffected by heating in cesium to 1800°C. Tantalum was embrittled but this may be due to oxygen and nitrogen pick-up and not to cesium.

ACKNOWLEDGEMENTS

The author would like to acknowledge the help of Mr. C.P. Dale who carried out most of the experimental work.

REFERENCES

1 ARTHUR, G, and HEPWORTH, M.A. I.E.E. Symposium on Magnetoplasmadynamics. Newcastle upon Tyne, (1962)

2 LINDLEY, B.C. Private communication

3 Liquid Metals Handbook. U.S.A.E.C. T.I.D. 5277, (1955)

4 TAYLOR, J.W., and WARD, A.G. Nuclear Power, Vol. 3, p.101, (1958) and Nuclear Power, vol. 3, p.50, (1958)

5 SMITH, R.G. et al. Jnl. Nucl. Matls. Vol. 10, No. 3, p.191, (1963)

6 SLIVKA, M.J. Advanced Energy Conversion, Vol. 3, p.157, (1963)

7 WAGNER, P., and CORRIELL, S.R. Review Sci. Instr. Vol. 30, No. 10, p.937, (1959)

8 COUGHLIN, J.P. U.S. Bur. Min. Bull, 542. (1954)

9 BREWER, L. Chem. Rev., Vol. 52, No. 1, p.1, (1953)

10 INGLES, T.A., and POPPER, P. B.C.R.A. report 452, (19')

11 HENNIG, G.H. Prog. in Inorg. Chem. Vol, 1, p.125, (1959)

IGH TEMPERATURE CESIUM COMPATIBILITY APPARATUS

FIG. 12.1

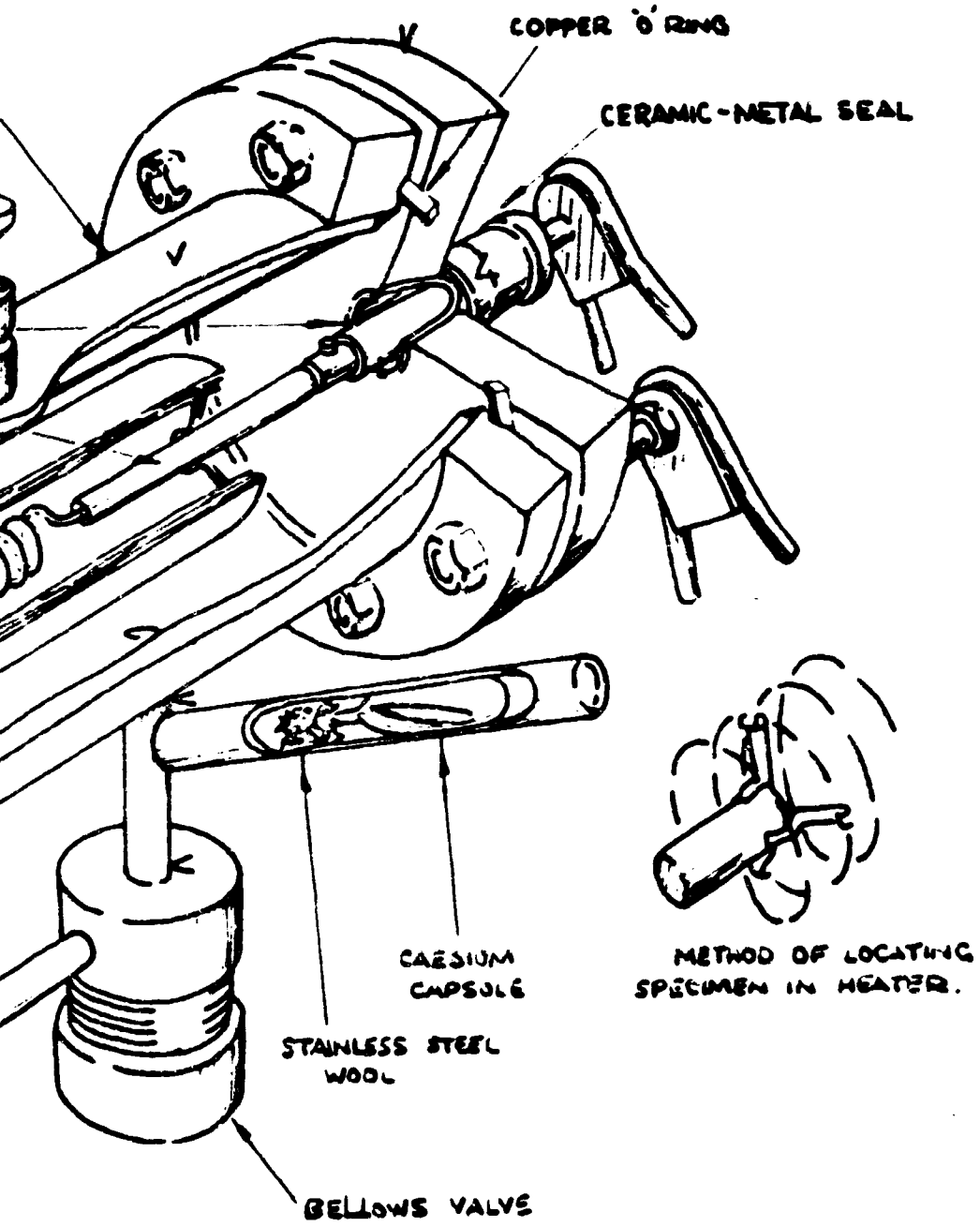

METHOD OF LOCATING SPECIMEN IN HEATER.

600°C (X50)

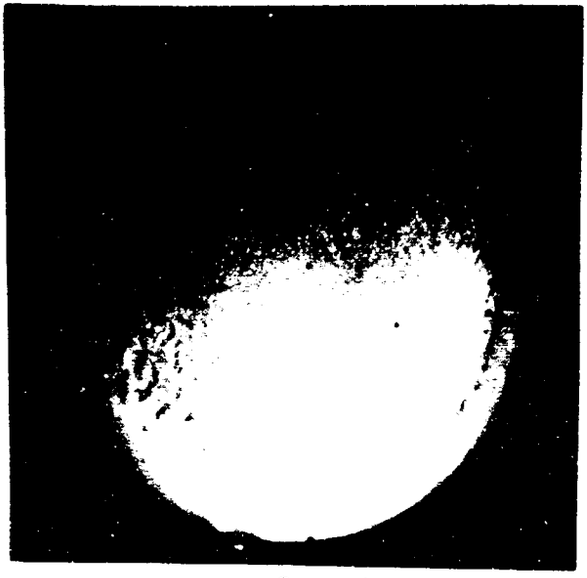

1600°C (X50)

1700°C (X50)

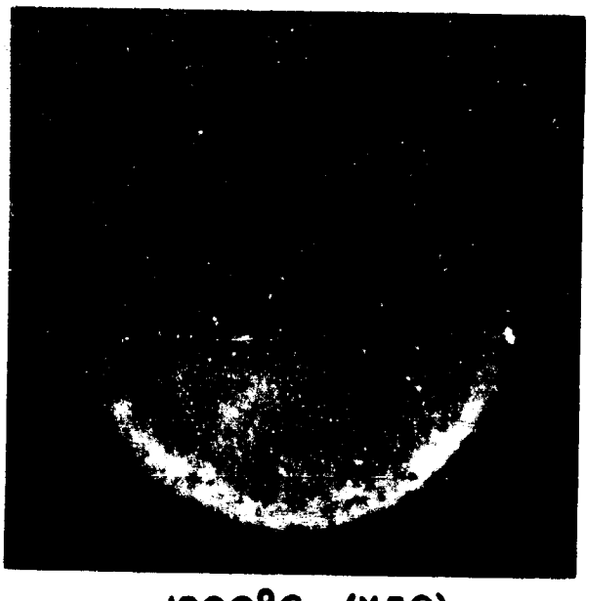

1800°C (X50)

BORON NITRIDE HEATED TO VARIOUS TEMPERATURES IN CESIUM VAPOUR FOR 4 hr

FIG 12.2

AS RECEIVED
(X 450)

RIM OF SPECIMEN
HEATED TO 1800°C
(X 450)

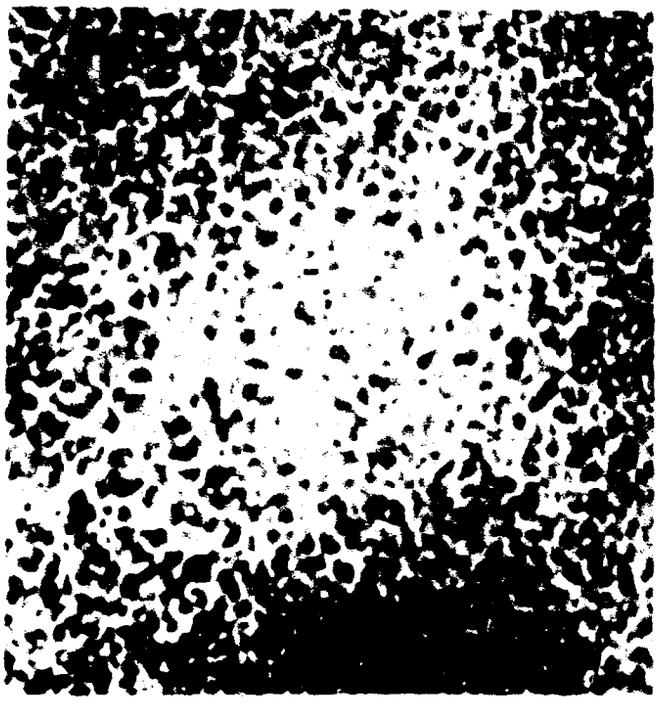

CORE OF SPECIMEN
HEATED TO 1800°C
(X 450)

BORON NITRIDE HEATED TO 1800°C IN CESIUM VAPOUR (10 mm)
FOR 4 hr

FIG 12·3

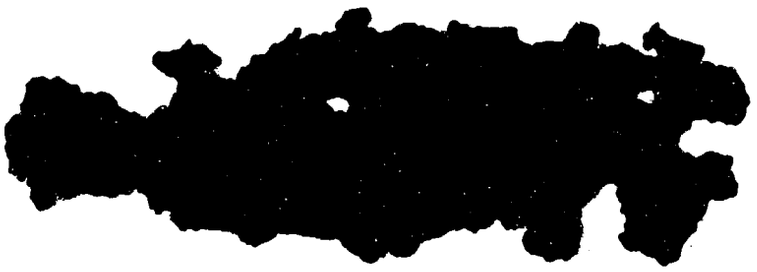

600°C

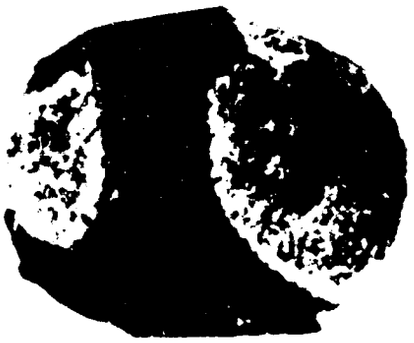

1000°C

1800°C

GRAPHITE AFTER HEATING TO VARIOUS TEMPERATURES FOR 4hr IN CESIUM VAPOUR (10mm)

FIG 12.4

CHAPTER 13

FUTURE PROGRAMME

by

B.C. Lindley

Descriptions of proposed future experiments (over a two-year period) scheduled for the IRD closed-loop facility are given in Section 1.2 and in Chapter 5, detailing the very wide ranges of operating parameters over which data on plasma behaviour and MPD power extraction are required.

In the immediate future (that is, until the termination in July 1964 of the present ARPA contract) the main aspects receiving attention are: the electrically-conducting layer which appears during service on the generator duct walls; and the recovery of cesium from the helium-cesium mixture. (End leakage in the plasma itself is thought to be substantial.) Before the next series of power generation runs, the insulated regions of the duct will be extended by several inches on each side of the active duct region; a ceramic (boron nitride) expansion nozzle (already manufactured) may also be adopted.

A preliminary run is scheduled in May, followed in June by a series of runs with a 36-electrode generator duct; fully automatic recording of a comprehensive range of electrical performance parameters is planned. For these and subsequent runs a modified electromagnet will provide fields of about 2T maximum.